Repairing and Strengthening of Reinforced Concrete Beam with Web Opening using Alkali activated Geopolymeric Material

A Thesis Submitted in
Partial Fulfilment of the Requirements
for the Degree

DOCTOR OF PHILOSOPHY

by

Arnab Kumar Sinha

Roll No. 166104032

DEPARTMENT OF CIVIL ENGINEERING
INDIAN INSTITUTE OF TECHNOLOGY GUWAHATI
GUWAHATI-781039, INDIA
AUGUST, 2022

Dedicated

To

My Parents

Mrs. Gita Mullick Sinha

and

Mr. Ananta Kumar Sinha

Certificate

It is certified that the work contained in the thesis entitled **Repairing and Strengthening of Reinforced Concrete Beam with Web Opening using Alkali activated Geopolymeric Material** by Arnab Kumar Sinha (Roll No.: 166104032), a student of the Department of Civil Engineering, Indian Institute of Technology Guwahati, submitted for the award of the degree of Doctor of Philosophy, has been carried out under my supervision and that this work has not been submitted elsewhere for a degree.

August, 2022

Dr. S. Talukdar
Professor
Department of Civil Engineering
Indian Institute of Technology Guwahati
Assam, India

Acknowledgement

At the onset, I would like to express my sincere gratitude to my supervisor, Prof. S. Talukdar, for his constant guidance and valuable advices throughout my research work. His continuous encouragement, suggestions and effusive cooperation have been a great driving force for me while carrying out my work. I will remain grateful to him throughout my life for the knowledge he imparted from his vast experience in the field of research.

Besides my supervisor, I would like to thank the rest of my Doctoral committee members: Prof. K. D. Singh, Prof. R. Ganesh Narayan and Dr. A. Shelke for their encouragement and valuable suggestions. I would like to thank Head of Civil Engineering Department for providing the financial grant for purchasing materials for conducting laboratory experiments. I am also thankful to Counto Microfine Products Private Limited, India and Fosroc Chemicals India Private Limited, India for providing materials free of cost for the research work.

I am grateful to Central Library, IITG, for offering such a vast resource of research material and making it easily accessible.

I would also like to thank my colleagues Biswajit chand, Sulaem Laskar, Anjaly Pilllai, G. Shekhar, Luptesh and all the laboratory staff of the Structural engineering laboratory for helping me in conducting my laboratory experiments.

I also acknowledge the good times shared with my friends Siddhart, Saroj, Chandan, Shubra, Argha, Prasanta and other friends at this institute. They have been a source of great help and co-operation at times of need. Last but not least, I extend my gratitude to my parents, Gita Mullick and Ananta Kumar Sinha, for their endless support and sacrifices. They have also stood behind me and motivated me for my research work. Thank you for your love and for constantly reminding me of the end goal. Their prayer is what sustained me so far and in the future too.

August, 2022 Arnab Kumar Sinha

Abstract

Transverse opening in the web of RC beam is a source of weakness which leads to early and wider cracks in the beam, when subjected to its service load or any accidental load. This gives rise to excessive deflection and beam may collapse before its service life. Such situation can be avoided in beams with pre-planned opening by internal strengthening. But if the opening is post planned then repairing and external strengthening are the only way to restore the structural integrity of such beams. So far, several techniques have been implemented for retrofitting and strengthening RC structures like epoxy resin, CFRP, steel plates, reinforced concrete jacketing etc. However, such method is having their own short coming and also costly in nature.

Recently alkali-activated geopolymeric binder has emerged as a new binder, which has gained a significant research interest due to their cost effectiveness and environmental benefits. The term Geopolymer is generically used to describe a polymer that can be synthesized from industrial waste such as Fly Ash and Slag. When these minerals come in contact with an alkaline environment, an exothermic polycondensation reaction takes place, which gives rise to a three-dimensional chain-like structure known as Geopolymer. This reaction is very fast, as compared to the hydration of cement, and hence the product formed hardens faster, which gives rise to high compressive strength of Geopolymer at a very early stage. Numerous research articles are published on the fresh and hardened stage of Geopolymer, where it is revealed that Slag-based Geopolymer gives rise to better strength properties and can be cured at ambient temperature. Such Geopolymer being able to offer early strength needs further study for its application as a repair material for damaged reinforced concrete structures.

Hence, the present research work deals with the development of ultrafine slag-based Geopolymer mortar (GM) and Fiber reinforced geopolymer concrete (FRGC) and assess their efficiency as a repairing material and jacketing agent by repairing and strengthening of damaged web opened beam.

Ultrafine blast furnace slag (UBFS), partially replaced by Fly Ash (FA), has been used in the synthesis of Geopolymer by activating it with sodium hydroxide (SH) and a combined solution of sodium hydroxide and Sodium silicate (SHSS). A total 28 number of GM mixes are prepared where the effect of FA content, the molar concentration (M) alkali, alkali to binder ratio (a/b), mass ratio of SHSS solution and the dosage of retarder are studied. Test results

indicate that GM containing a high volume of UBFS exhibits prompt setting and is capable of attaining 79 % of the 28th day strength in one day when activated by the SHSS solution. High molar concentration (M) of SH within 12M largely enhances the strength of GM, and a good correlation between flexural strength and compressive strength is obtained for a mass ratio of 1.5. The application of Borate greatly enhances the setting time and also assists in retaining the fluidity of GM for a longer time. The optimal retarder dose of 4 % produces a densely packed microstructure, resulting in improved mechanical properties.

Before preparing the FRGC, geopolymer concrete (GPC) was initially developed to investigate the effect of varying alkali content, fine aggregate to the total aggregate ratio (*s/a*) and molarity of SH, including their bond strength with Portland cement concrete (PCC). A suitable mix proportion of GPC are then incorporated by various volume fraction (V_f) of steel fiber, and their effect on the fresh and hardened properties were assessed. The test result showed that the *s/a* ratio is a crucial factor in controlling segregation and bleeding in GPC. However, an ideal GPC mix with a *s/a* ratio of 0.41 provides a better packing resulting in improved mechanical properties. Application of a high volume of UBFS exhibits better microstructure and strength properties at a relatively lower alkali concentration. The GPC mix exhibits a superior bond strength with the old PCC substrate; however, the molarity of SH significantly affects the adhesion property of GPC. The addition of steel 1.3 % V_f of fiber significantly improved the compressive strength and flexural strength by 12 % and 59 %, respectively.

To carry out the repairing work 8 numbers of RC beams with opening in the flexure (BMS) and in the shear zone (BSS) are tested, and their behaviour is compared with that of a solid beam (SB). The damaged beams are then repaired using GM, followed by local strengthening using welded wire mesh. The repaired specimens are tested again on the 3rd day and the 28th day of repairing. The test result shows that the presence of an opening reduced the load carrying capacity of the beam and significantly effects the post-peak behaviour of the beam. GM as a repair material exhibits a good adherence with the damaged beam at all ages. Due to the early strength gain property of GM and the better adhesion property, the repaired beam could attain an appreciable load even on the 3rd day of testing. The repaired beam not only exhibits full restoration of the structural integrity but also enhances the cracking load, load carrying capacity and post-peak responses of the beam.

To examine the efficiency of the jacketing material, further 8 numbers of RC beam of similar types are also taken in the strengthening scheme. The damaged beams with opening are initially repaired by GM and then strengthened by a three-side jacketing layer of thickness 40 mm with FRGC material. The test results indicate that FRGC material can effectively restore the structure to its functional use at the earliest possible time. The Jacketed beam of BMS types exhibits improved stiffness and with enhanced load carrying capacity of 1.3 times higher than the original beam. However, the effect of FRGC jacketing is found to be more effective in enhancing the load carrying capacity of the BSS type by 1.75 times higher than the original specimen. All the jacketed specimens exhibit improved deformation capacity leading to improved ductility.

Content

	Abstract	i-iii
	Contents	v-x
	List of Tables	xi-xii
	List of Figures	xiii-xvi
	Nomenclature	xvii-xx
1	**Introduction**	**1-34**
	1.1 Overview	1
	1.2 Geopolymer	4
	1.3 Sources of Geopolymer	6
	1.3.1 Blast Furnace Slag	6
	1.3.2 Fly Ash	6
	1.3.3 Metakaolin	7
	1.3.4 Rice Husk Ash	8
	1.4 Deterioration of Reinforced Concrete Structural Members	8
	1.5 Literature Review	10
	1.5.1 Geopolymer and geopolymeric materials	10
	1.5.2 Characteristics of Geopolymer in Fresh and Hardened state	10
	1.5.3 Durability of Geopolymer	13
	1.5.4 Bond strength of Geopolymer	14
	1.5.5 Fiber reinforced geopolymer concrete	17
	1.5.6 Geopolymer as repairing agent	19
	1.5.7 Transverse Opening in RC beam	20
	1.5.8 Retrofitting and Strengthening of RC structures	24
	1.6 Critical comment on existing Literature	31

1.7 Scope of the Present study 32
1.8 Objective of the present work 33
1.9 Organization of Thesis 33
1.10 Closure 34

2 Material Characterization 35-45

2.1 Introduction 35
2.2 Materials 35
2.2.1 Portland Cement 35
2.2.2 Ultrafine Blast Furnace Slag 36
2.2.3 Fly Ash 37
2.2.4 Alkali Activators 38
2.2.5 Aggregate 40
2.2.6 Admixture 41
2.2.7 Steel reinforcement rebar 41
2.2.8 Welded Wire-mesh 41
2.2.9 Drop bolt anchor 42
2.2.10 Hooked end steel fiber 43
2.3 Mix Design 43
2.4 Design of Reinforced Concrete beam 44
2.5 Closure 45

3 Development of Silicate activated UBFS based Geopolymer Mortar as Repair material 47-81

3.1 Introduction 47
3.2 Experimental Investigation 49
3.2.1 Material 49
3.2.1.1 Geopolymer Mortar 49
3.2.1.2 Portland Cement Mortar 50
3.2.2 Mix proportion 50
3.2.3 Specimen preparation and Curing 53
3.2.4 Experiments 55
3.3 Experimental Observations 57
3.3.1 Geopolymer mortar 57
3.3.1.1 Effect of FA content in UBFS based GM 57
3.3.1.2 Effect of Sodium Hydroxide solution 60
3.3.1.3 Effect of combined activator solution 63

3.3.1.4 Relation between compressive strength and flexural strength 71
3.3.1.5 Effect of Retarder in the properties of Geopolymer mortar 72
3.3.2 Portland cement mortar 77
3.4 FESEM analysis 77
3.5 Statistical analysis of Test results 79
3.6 Closure 80
4 Development and Testing of Geopolymer Concrete and Fiber Reinforced Geopolymer Concrete 83-122
4.1 Introduction 83
4.2 Experimental Investigation 84
4.2.1 Materials 85
4.2.1.1 Geopolymer concrete and Fiber reinforced geopolymer concrete 85
4.2.1.2 Portland cement concrete and Fiber reinforced cement concrete 85
4.2.2 Mix proportion 85
4.2.2.1 Mix proportion of Geopolymer concrete 86
4.2.2.2 Mix proportion of Fiber reinforced geopolymer concrete 88
4.2.2.3 Mix proportion of controlled mix using Ordinary Portland cement 88
4.2.3 Specimen preparation 89
4.2.3.1 Preparation of specimen for Concrete mixes 89
4.2.3.2 Preparation of specimen for Fiber reinforced concrete mixes 92
4.2.4 Experimental Program 94
4.2.4.1 Geopolymer concrete 94
4.2.4.2 Fiber reinforced geopolymer concrete 94
4.3 Experimental Observation 95
4.3.1 Results and discussion of Geopolymer concrete 95
4.3.1.1 Workability 95
4.3.1.2 Compressive strength 98
4.3.1.3 Split tensile strength 104
4.3.1.4 Bond strength 106
4.3.2 Result and discussion of Fiber reinforced geopolymer concrete 110

4.3.2.1 Workability 110
4.3.2.2 Mechanical Properties 111
4.4 Microstructure 116
4.5 Statistical analysis 118
4.6 Correlation between the mechanical properties 119
4.6.1 Relationship between Tensile strength and Bond strength and Compressive strength in GPC 119
4.6.2 Relationship between Flexural strength and Compressive strength in FRGC 121
4.7 Closure 122
5 Repairing of Web opened RC beam using Geopolymer Mortar 123-159
5.1 Introduction 123
5.2 Experimental Program 126
5.2.1 Test Matrix 126
5.2.2 Materials 128
5.2.2.1 Geopolymer paste 128
5.2.2.2 Portland cement paste 130
5.2.2.3 Geopolymer Mortar 131
5.2.2.4 Portland Cement Mortar 132
5.2.2.5 Portland Cement Concrete 132
5.2.2.6 Reinforcement 133
5.2.2.7 Welded wire mesh and Drop bolt anchor 133
5.2.3 Preparation of Controlled beam 133
5.2.4 Experimental setup and Instrument 135
5.2.5 Method of beam preparation for Repairing work 135
5.2.6 Preliminary investigation of Repairing technique 140
5.3 Experimental Observation 141
5.3.1 Test result of repaired prismatic beam 141
5.3.2 Behaviour of Reinforced concrete beam with web opening 143
5.3.3 Experimental observation of repaired beam with web opening 146
5.3.3.1 Behaviour of repaired beam with web opening in the Flexure zone 146
5.3.3.2 Behaviour of repaired beam with web opening in the Shear zone 152
5.4 Closure 158

6 Jacketing of Web opened RC beam using Fiber Reinforced Geopolymer Concrete **161-190**

6.1 Introduction 161

6.2 Experimental Program 163

6.2.1 Test Matrix 163

6.2.2 Materials 165

6.2.2.1 Geopolymer paste 165

6.2.2.2 Portland cement paste 166

6.2.2.3 Geopolymer Mortar 166

6.2.2.4 Portland Cement Mortar 166

6.2.2.5 Portland Cement Concrete 166

6.2.2.6 Fiber Reinforced Geopolymer Concrete 167

6.2.2.7 Fiber Reinforced Cement Concrete 168

6.2.2.8 Reinforcement 169

6.2.3 Experimental setup and Instrument 169

6.2.4 Method of beam Jacketing 170

6.2.4.1 Repairing of Controlled beam 170

6.2.4.2 Surface preparation and Jacketing 171

6.2.5 Preliminary investigation of Jacketing technique 176

6.3 Result and Discussion 178

6.3.1 Test result of Jacketed prismatic beam 178

6.3.2 Experimental observation of Jacketed beam with web opening 179

6.3.2.1 Behaviour of Jacketed beam with web opening in the Flexure zone 179

6.3.2.2 Behaviour of Jacketed beam with web opening in the Shear zone 184

6.4 Closure 190

7 Summary and Conclusions **191-197**

7.1 Introduction 191

7.2 Major conclusions and recommendations 193

7.2.1 Properties of GM, GPC and FRGC 193

7.2.2 Repairing of Web opened RC beam using GM 195

7.2.3 Jacketing of Web opened RC beam using FRGC 196

7.3 Significant contribution 196

7.4 Scope of Future Work 197

7.5 Closure 197

Appendix **199-210**

Appendix A: Mix Design of PCC mix and GPC mix 199

Appendix B: Design of Reinforced Concrete beam 207

References **211-228**

List of Publication **229**

List of Tables

Table 2.1	Properties of Ordinary Portland cement	36
Table 2.2	Properties of Ultrafine blast furnace slag	37
Table 2.3	Properties of Fly Ash	38
Table 2.4	Sieve analysis of Fine Aggregate	40
Table 2.5	Sieve analysis of Coarse Aggregate	40
Table 2.6	Tensile properties of Steel rebar	41
Table 2.7	Properties of MS wire mesh	42
Table 2.8	Properties of hooked end steel fiber	43
Table 2.9	Mix proportion of PCC mix	44
Table 2.10	Load carrying capacity of Solid beam	45
Table 3.1	Mixes with different parameters of GM	51
Table 3.2	Mix proportion of PCM	52
Table 3.3	Flexural strength of GM mix activated by SH (Group II)	63
Table 3.4	Flexural strength of GM mix activated by SHSS (Group III)	67
Table 3.5	Compressive strength of PCM	77
Table 3.6	Statistical data of compressive strength of GM	80
Table 3.7	Statistical data of flexural strength of GM	80
Table 4.1	Mix proportion of GPC	87
Table 4.2	Mix proportion of FRGC	88
Table 4.3	Mix proportion of the controlled mixes with OPC	89
Table 4.4	Statistical data of the strength parameters of GPC and PCC	118
Table 4.5	Statistical data of FRGC and FRCC	119
Table 5.1	Experimental test matrix for Repairing work	128

Table 5.2	Mixes of Geopolymer Paste	129
Table 5.3	Properties of Geopolymer paste	130
Table 5.4	Properties of cement paste	130
Table 5.5	Mix proportion of GM used in Repairing	131
Table 5.6	Test results of GM used in Repairing	131
Table 5.7	Properties of PCM	132
Table 5.8	Properties of mix CM1	132
Table 5.9	Test result repaired prismatic beam	142
Table 5.10	Test result of controlled beam with opening	143
Table 5.11	Test result of controlled and repaired beam with mid-span opening	149
Table 5.12	Test result of controlled and repaired beam with shear opening	155
Table 6.1	Experimental test matrix for Jacketing work	164
Table 6.2	Mix proportion of FRGC used for Jacketing	168
Table 6.3	Fresh and hardened test results of FRGC mix	168
Table 6.4	Mix proportion of FRCC mix used for Jacketing	169
Table 6.5	Fresh and hardened test results of FRCC mix	169
Table 6.6	Compressive strength properties of Jacketing Material	177
Table 6.7	Test result of the prismatic beam after Jacketing	178
Table 6.8	Test result of controlled and Jacketed beam with mid-span opening	179
Table 6.9	Test result of controlled and Jacketed beam with shear opening	187

List of Figures

Figure 1.1	Worldwide cement production of major countries in 2021	2
Figure 1.2	Production of Portland cement in India, 2012-2022	2
Figure 1.3	Molecular structure of Geopolymer	4
Figure 1.4	Prismatic specimen containing interlayer of Geopolymer	15
Figure 1.5	Slant shear test specimen	16
Figure 1.6	Bond strength test a) Concrete pull of test b) Rebar pull out test	17
Figure 1.7	Transverse Opening in beams	21
Figure 1.8	Different strengthening Schemes	25
Figure 1.9	Strengthening scheme with CFRP Laminates	26
Figure 1.10	Externally bonded a) CFRP plates and b) Steel plates	27
Figure 1.11	Jacketing methodology used in damaged RC beams	30
Figure 2.1	Ultra-fine blast furnace slag	36
Figure 2.2	Fly Ash	37
Figure 2.3	Alkali activator	39
Figure 2.4	Mild steel welded wire mesh	42
Figure 2.5	Drop bolt anchor	42
Figure 2.6	Hooked end steel fiber	43
Figure 3.1	Preparation of GM mix	53
Figure 3.2	Preparation of mortar specimen	54
Figure 3.3	Setting time test using Vicat apparatus	55
Figure 3.4	Flow table Test apparatus	56
Figure 3.5	Flexural Test of GM prism	56
Figure 3.6	Effect FA content on Setting time and Workability of GM	58
Figure 3.7	Effect of FA content on Compressive strength of GM	59

Figure 3.8	Effect of SH on Setting Time and Workability of GM	61
Figure 3.9	Effect of SH on Compressive strength of GM	62
Figure 3.10	Effect of SHSS in the Setting Time and Flow index of mixes with a/b-0.6	64
Figure 3.11	Effect of SHSS in the Setting Time and Flow index of mixes with a/b-0.65	66
Figure 3.12	Effect of SHSS solution in the compressive strength of GM with a/b-0.6	68
Figure 3.13	Effect of SHSS solution in the compressive strength of GM with a/b-0.65	69
Figure 3.14	Crushed cube specimen of GM	70
Figure 3.15	Relationship between Flexural strength and Compressive strength of GM	71
Figure 3.16	Effect of retarder on the setting time of Geopolymer paste	73
Figure 3.17	Effect of retarder on Workability of GM	74
Figure 3.18	Effect of Borate in the spread of GM: (a) GM17 (b) GM17_2R (c) GM17_4R (d) GM17_6R	75
Figure 3.19	Effect of retarder on the Compressive strength and Flexural strength of GM	76
Figure 3.20	FESEM images of the geopolymer mixes on 7^{th} and 28^{th} day	78
Figure 4.1	Freshly prepared GPC mix	90
Figure 4.2	Demoulded specimen cast with GPC	90
Figure 4.3	Preparation of substrate part of Slant shear specimen	91
Figure 4.4	Preparation of Slant shear specimen	92
Figure 4.5	Casting and preparation of FRGC specimen	93
Figure 4.6	Types of slump	96
Figure 4.7	Slump value of GPC mixes	97
Figure 4.8	Effect of alkali content in GPC mixes	99
Figure 4.9	Effect of molar concentration on compressive strength with *s/a* = 0.33 in GPC	100
Figure 4.10	Effect of molar concentration on compressive strength with *s/a* = 0.41 in GPC	101
Figure 4.11	Effect of molar concentration on compressive strength with *s/a* = 0.49 in GPC	102
Figure 4.12	Split tensile strength of GPC mixes	105
Figure 4.13	Bond strength property of GPC mixes at the 3^{rd} and 28^{th} day	106
Figure 4.14	Different modes of failure in slant shear specimens of GPC	107
Figure 4.15	Mode of failure in slant shear specimens of PCC	109
Figure 4.16	Workability of FRGC mixes	110

Figure 4.17	Testing of FRGC specimen	112
Figure 4.18	Compressive strength and flexural strength for *s/a* = 0.33 and 8M solution in FRGC mixes	113
Figure 4.19	Compressive strength and flexural strength for *s/a* =0.41 and 6M solution in FRGC mixes	114
Figure 4.20	Compressive strength and flexural strength for *s/a* = 0.49 and 6M solution in FRGC mixes	115
Figure 4.21	FESEM image of GPC mixes: (a) 4M,5kX, (b) 4M, 20kX, (c) 6M, 5kX and (d) 6M, 20kX	116
Figure 4.21	FESEM image of GPC mixes: (e) 8M, 5kX, (f) 8M, 20kX, (g) 10M, 5kX, (h) 10M, 20kX, (i) 12M, 5kX and (j) 12M, 20kX	117
Figure 4.22	Relationship between split tensile and compressive strength of GPC	120
Figure 4.23	Relationship between bond strength and compressive strength of GPC	120
Figure 4.24	Relationship between bond strength and compressive strength of FRGC	121
Figure 5.1	Deterioration of concrete in the structural member	124
Figure 5.2	Reinforcement detailing of Beam specimen	127
Figure 5.3	Compressive strength test of GP	129
Figure 5.4	Preparation of Beam specimen	134
Figure 5.5	Curing of specimen	134
Figure 5.6	Test setup of Four-point bending for repairing work	135
Figure 5.7	Surface preparation and initial repairing	137
Figure 5.8	Wrapping of wire mesh and final repairing	139
Figure 5.9	Detailing of the Prismatic beam	140
Figure 5.10	Detail of repairing using wire mesh	141
Figure 5.11	Crack pattern in different types of beam a) SB b) BMS c) BSS	144
Figure 5.12	Load Displacement curve of tested beam with and without opening	145
Figure 5.13	Crack pattern of controlled and repaired beam with mid-span opening (3^{rd} Day)	147
Figure 5.14	Load deflection curve of controlled and repaired beam with mid span opening (3^{rd} Day)	148
Figure 5.15	Crack pattern of controlled and repaired beam with mid-span opening (28^{th} Day)	150
Figure 5.16	Load deflection curve of controlled and repaired beam with mid-span opening (28^{th} Day)	151
Figure 5.17	Crack pattern of controlled and repaired beam with shear opening (3^{rd} Day)	153

Figure 5.18	Load deflection curve of controlled and repaired beam with shear opening (3rd Day)	154
Figure 5.19	Crack pattern of controlled and repaired beam with shear opening (28th Day)	156
Figure 5.20	Load deflection curve of controlled and repaired beam with shear opening (28th Day)	157
Figure 6.1	Detail of the Reinforced concrete specimen for Jacketing work	163
Figure 6.2	Test setup of Four-point bending for Jacketing work	170
Figure 6.3	Repairing process of damaged beam	171
Figure 6.4	Repaired beam with opening in the flexure zone	172
Figure 6.5	(a): Typical sectional details of the FRGC Jacketing	173
Figure 6.5	(b): Isometric view of the Jacketed beam	173
Figure 6.6	Form work for Jacketing	174
Figure 6.7	Pre-installed wooden box	174
Figure 6.8	Jacketing of specimen	175
Figure 6.9	Section of Jacketed specimen	176
Figure 6.10	Jacketing of small prismatic beam	177
Figure 6.11	Failed Jacketed prismatic beam specimen	178
Figure 6.12	Crack patters of tested beam with opening in flexure (3rd Day)	180
Figure 6.13	Load deflection curve of controlled and Jacketed beam with mid-span opening (3rd Day)	181
Figure 6.14	Crack patters of tested beam with opening in flexure (28th Days)	183
Figure 6.15	Load deflection curve of controlled and Jacketed beam with mid-span opening (28th Day)	184
Figure 6.16	Crack patters of tested beam with shear-span opening (3rd Days)	185
Figure 6.17	Load deflection curve of controlled and Jacketed beam with shear span opening (3rd Day)	186
Figure 6.18	Crack patters of tested beam with shear-span opening (28th Days)	188
Figure 6.19	Load deflection curve of controlled and Jacketed beam with shear span opening (3rd Day)	189
Figure B1	Reinforcement detailing of Beam	210

Nomenclature

An overview of the most important symbols and abbreviations used in the present thesis:

Symbols

A_{st}	Area of Tension steel
A_{sc}	Area of compression steel
A_{sv}	Area of steel in shear reinforcement
A_c	Area of the bonded surface
B	Breadth of beam
B_{sc}	Bond strength
C_{uc}	Resultant compressive force in concrete
C_{us}	Resultant compressive force in compressive steel
D_o	Over all depth of beam
L/D	Aspect ratio
E_s	Modulus of elasticity of steel
F_c	Load carried by the slant shear specimen
L	Span of beam
M_{CA}	Mass of Coarse aggregate
M_{FA}	Mass of Fine aggregate
M_a	Mass of alkali activator
M_w	Mass of water
M_c	Mass of cement
M_{TB}	Mass of Total binder
M_F	Mass of FA
M_S	Mass of UBFS
M_u	Moment carrying capacity of the beam specimen
R^2	Coefficient of determination
S_r	Flexural strength of mortar prism
SG_c	Specific gravity of cement

SG_{FA}	Specific gravity of Fine aggregate
SG_{CA}	Specific gravity of Coarse aggregate
SG_S	Specific gravity of UBFS
SG_F	Specific gravity of FA
T_u	Resultant tensile force in tension steel
V_{CA}	Volume of Coarse aggregate
V_{FA}	Volume of Fine aggregate
V_f	Volume fraction
V_u	Shear force
V_{us}	Shear resistance of steel
V_c	Shear resistance of concrete
W_u	Ultimate load carrying capacity of beam specimen
a/b	Alkali to binder ratio
P_t	Percentage of tensile steel
s/a	Fine aggregate to total aggregate ratio
d	Effective depth
d'	Effective cover
d_c	Clear cover of beam
f_b	Flexural strength of Concrete
f_{ck}	Characteristic compressive strength
f'_{ck}	Target strength of concrete
f_y	Yield stress of steel
f'_y	$f_y/0.87$
w/c	Water to cement ratio
w/s	Water to solid ratio
x	Neutral axis depth of beam
μ	Mean
σ	Standard deviation
ρ	Coefficient of variation
β	Dip angles
ε_{s1}	Strain in compression steel
τ_v	Nominal shear stress
τ_c	Shear strength of concrete

Abbreviations

Al	Aluminium
ASTM	American Society for Testing and Materials
BMS	Beam with Mid-span opening
BSS	Beam with Shear-span opening
C-A-S-H	Calcium alumina-silicate hydrate

CFRP	Carbon fiber reinforced polymer
CP	Cement paste
C-S-H	Calcium silicate hydrate
CTM	Compression Testing Machine
DFRGC	Ductile fiber reinforced geopolymer concrete
DR	Ductility ratio
EGC	Engineered geopolymer composite
ESPs	Electrostatic precipitators
FA	Fly Ash
FESEM	Field emission scanning electron microscope
FI	Flow index
FM	Fineness modulus
FRCC	Fiber Reinforced Cement Concrete
FRG	Fiber reinforced geopolymer composite
FRGC	Fiber Reinforced Geopolymer Concrete
FRP	Fiber reinforced polymer
FWSS	Flexural weakening shear strengthening
GFRP	Glass fiber reinforced polymer
GGBS	Ground granulated blast furnace slag
GM	Geopolymer Mortar
GP	Geopolymer paste
IS	Indian Standard
ITZ	Interfacial transition zone
KOH	Potassium hydroxide
LVDT	Linear variable differential transducer
M	Molar concentration
MCC	Moment Carrying Capacity
MS	Mild steel
N-A-S-H	Sodium alumina-silicate hydrate
OPC	Ordinary Portland Cement
PC	Portland cement
PCC	Portland Cement Concrete
PCM	Portland Cement Mortar
PVA	Polyvinyl alcohol
RC	Reinforced Concrete
RC	Reinforced concrete
RHA	Rise husk ash
RM	Repair materials
SB	Solid beam
SD	Super Ductile
SER	Strength enhancement ratio

SF	Silica Fume
SFRC	Steel fiber reinforced concrete
SH	Sodium Hydroxide
SHCC	Strain hardening cementitious composite
SHSS	Combined Sodium Hydroxide and Sodium Silicate
Si	Silicon
SP	Super plasticizer
SS	Sodium Silicate
UBFS	Ultrafine blast furnace slag
UHPC	Ultra high performance concrete
UHPFRC	Ultra high performance fiber reinforced concrete
UHPGC	Ultra high performance geopolymer concrete
UTM	Universal Testing Machine
XRF	X-Ray Fluorescence Spectrometer

Chapter 1

Introduction

1.1 Overview

Building materials in construction industry and construction methodologies have been developed through ages and numerous engineering materials and technologies have evolved time to time. Several kind of construction materials have been in use since the ancient time and a continuous developments and innovation in the building materials is seen. However, it is seen that infrastructure development has been in great boom from the time when Portland cement (PC) emerged as the material of choice for modern infrastructure in the 20th century. Concrete is the most widely used building material in the world, and it is well known that the concrete industry consumes the most natural resources such as water, sand, gravel, and rock. The growing industrialization and urbanisation of emerging countries such as India creates a steady need for new construction materials. Constant research is consequently being conducted around the world to improvise construction materials for humanity, yet economy and material longevity are often a priority.

At present, the production of PC has risen from less than 1.4 billion metric tonnes in 1995 to 4.4 billion metric tonnes in the year 2021 (Statista, the statistics portal, www.statista.com) and the demand of the PC is expected to rise 8 to 9 billion tonnes by 2050 (Mehta 2002). India ranks the second largest manufacturer of cement among all the countries in the world. With the rise in the infrastructure development and the economy of India, the consumption of Portland cement is increased to 297 million metric tonne in the current year. Fig. 1.1 shows the latest trend of cement production by the top leading countries, whereas the

production of cement in India from the year 2012 to 2022 respectively is presented in Fig. 1.2. (Statista, the statistics portal, www.statista.com).

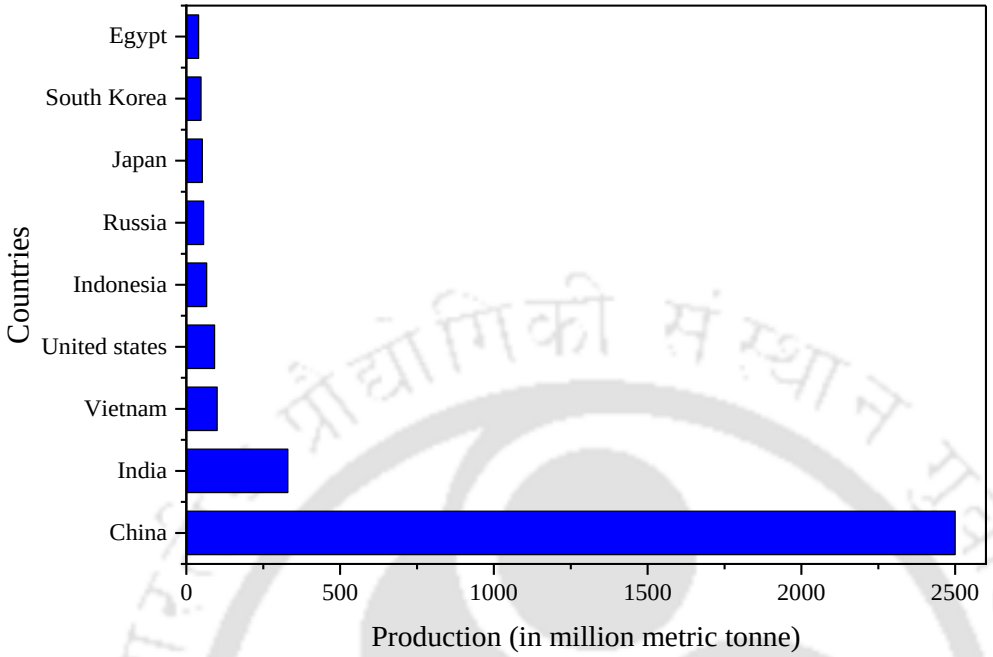

Figure 1.1: World-wide cement production of major countries in 2021 (Data source: Statista, the statistics portal, www.statista.com)

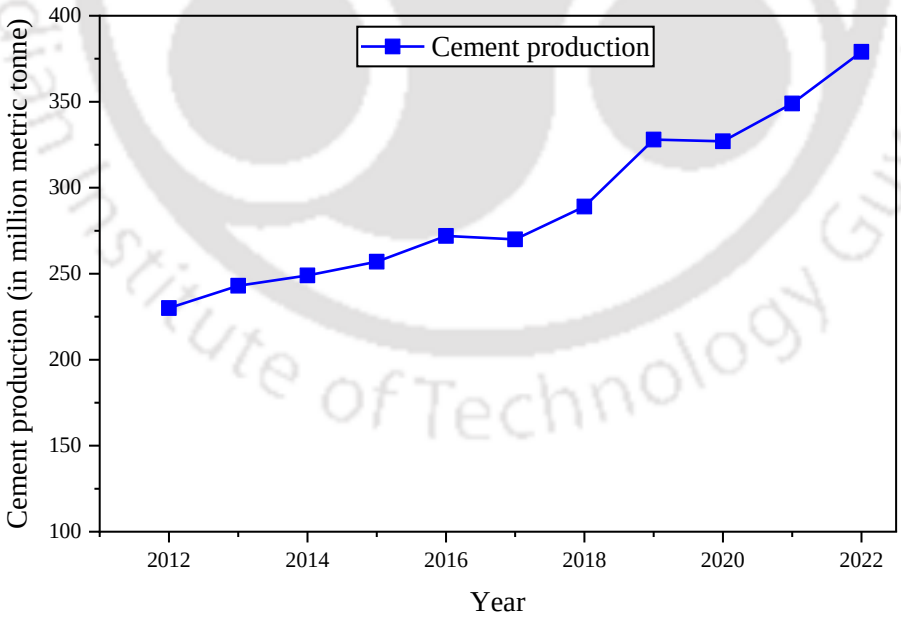

Figure 1.2: Production of Portland cement in India, 2012-2022 (Data source: Statista, the statistics portal, www.statista.com)

The production of PC necessarily involves the calcination of calcium carbonate into Lime, and during this process, carbon dioxide (CO_2) is emitted due to the combustion of fossil fuel along with other greenhouse gases (Mehta, 2002). Besides other raw materials, each tonne of PC requires approximately 1.5 tonnes of limestone along with a huge amount of electrical energy. Every year approximately 13500 tonnes of CO_2 is released into the earth's atmosphere during the production of cement, which is around 7 % of the total CO_2 emitted into the environment from various sources.

Recently, there has been a rapid growth in public awareness regarding the climate change and its impact on society. One of the main reason of this is the increase in the depletion of natural resources and the intensity and diversity of hazardous solid waste generation. It may not be possible to cease the formation of this hazardous industrial waste completely. However, if these issues are not addressed, they will constitute a clear threat to our way of life as well as the entire system of life support that our planet relies on.

Today a majority of the industrial waste is disposed of in the landfill, which is again not economic moreover, from these landfills, the toxic substance from the waste infiltrates the soil and comes in contact with water causing groundwater contamination. The rising concerns of climate change and the economic condition have compelled the industrial sector to consider waste material recycling as a superior alternative to landfilling and dumping.

In order to keep a balance between the growing industrialization and the environment, reuse of this industrial waste to create newer materials is found to be the best way. One way to achieve this goal of managing hazardous industrial waste or by-products is to use such material as an alternative to the existing building materials. In order to achieve the goal, researchers have developed a highly effective strategy by consuming the waste product of industry such as Fly Ash (FA), Blast furnace slag (BFS), Rice husk ash (RHA), etc. as an alternative binding material in concrete. These by-products possess cementitious property and can be used by blending with the PC to produce mortar or concrete. However, when these mortar or concrete are produced by replacing the entire cement with these by-products, then the product formed is known as Geopolymer mortar (GM) or Geopolymer concrete (GPC). Replacement of the traditional cement is the most effective solution to solve the problem of solid waste management. Apart from this, it indirectly reduces the amount of cement clinker responsible for the carbon footprint in the cement industry (Ruan et al., 2022).

1.2 Geopolymer

Geopolymer is a patented technology which is first developed by Joseph Davidovits in the year 1978 (Davidovits, 1994). Geopolymer is considered as the third generation cement after lime and Ordinary Portland cement. The term geopolymer is generically used to describe an amorphous alkali alumino-silicate polymer, synthesized from minerals of geological origin like kaolinite, feldspar or industrial by-products such as FA, metallurgical Slag, Rice husk, mining wastes etc. that are rich in silicon (Si) and aluminium (Al). These materials are also known as allumino-silicate material (AS), which are being used as a solid material in geopolymerization technology.

The reaction mechanism in geopolymer mainly includes three main steps Dissolution, Depolymerization and Reconstruction as explained by Palomo et al. (2015). The process is activated when these AS material comes in contact with an alkali component. Under the high alkali condition, the chemical bond in the AS material destroys and decomposes into silicon-oxygen tetrahedral units $[SiO_4]^-$ and alumina-oxygen tetrahedral units $[AlO_4]^-$. These tetrahedral units are also called monomers which have a tendency to unite with another monomer molecule to form dimers. This process continues with the dissociation of AS material, and the dimers again link to another monomer to produce a trimer; finally, a large chain or three-dimensional network-like structure consisting of Si-O-Al-O bonds is produced. This process is known as polymerization, which is an exothermic process, and the final product is known as Geopolymer. The geopolymer consisting of silicon (Si) and aluminium (Al) tetrahedrally linked by sharing oxygen (O) atoms, shown in Fig. 1.3.

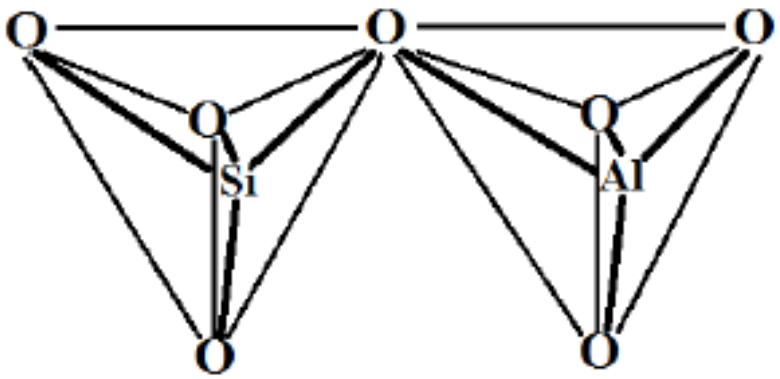

Figure 1.3: Molecular structure of Geopolymer (Davidovits, 1994)

When slag is introduced as the binding material in the synthesis of geopolymer, the main geopolymeric product that forms consist of a linear chain of Calcium Silicate Hydrate (C-S-H) gel along with Calcium Alumino-silicate Hydrate (C-A-S-H) gel. The reaction that takes place during the geopolymerization is as follows:

$$(Si_2O_5.Al_2O_2)_n + H_2O + OH^- \longrightarrow Si(OH)_4 + Al(OH)^{4-} \quad (1.1)$$

$$Si(OH)_4 + Al(OH)^{4-} \longrightarrow \left(\text{-Si-O-AL-O-}\right)_n + 4H_2O \quad (1.2)$$

Based on the structure of geopolymer Davidovits (1991), classified Geopolymer in to three different types- Poly sialate type (-Si-O-Al-), Poly sialate-siloxo type (-Si-OAl-O-Si-) and Poly sialate-disiloxo (-Si-O-Al-O-Si-O-Si-). Based on this structure, Davidovits has presented a molecular formula (Zhao et al., 2021) which is expressed as:

$$M_n\left\{\text{-}\left(SiO_2\right)_z\text{-}ALO_2\text{-}\right\}_n .wH_2O \quad (1.3)$$

where M is the metal cation (Na^+ or K^+), z is 1, 2 or 3 respectively, for different types of geopolymer and n is the degree of polymerization.

The products formed during the geopolymerization significantly depend on the physical features of the source materials. A highly amorphous with sufficient reactive glassy content in the source material leads to a better leeching of Al and Si ions, which results to better geopolymeric products. The alkaline activators required in the geopolymerization include sodium hydroxide (NaOH), potassium hydroxide (KOH), sodium silicate (Na_2SiO_3) and potassium silicate (K_2SiO_3). However, NaOH produces better dissociation of Al^{3+} and Si^{4+} ions, which are required for condensation polymerization reactions in geopolymer synthesis (Singh et al., 2015).

The reaction process in geopolymer greatly differs from the reaction mechanism of PC as it uses a completely different reaction route to achieve structural integrity. The strength of PC-based concrete is mainly governed by the formation of C-S-H gel. Whereas, in geopolymer, prepared with slag and FA, the main reaction product governing the strength is C-A-S-H gel produced by the high calcium Slag and Sodium alumina-silicate hydrate (N-A-S-H) gel. In addition, various other products are generated during the synthesis of Geopolymer, which participate to the strength and durability.

1.3 Sources of Geopolymer

The main key component of geopolymeric material is the Al and Si content present in the material. Several industrial by-products which contain Al and Si in the form of oxides can be used to synthesize geopolymer. Apart from this, naturally occurring materials like volcanic ash, Metakaolin etc., are also used to prepare geopolymer. The strength of geopolymer products is mainly governed by the chemical composition of the source material. Better geopolymeric products depend on the Al/Si atomic ratio and the amorphous content in the raw material. The various alumina-silicate materials that are often used in the synthesis of geopolymer are as follows

1.3.1 Blast Furnace Slag

Blast furnace slag is a waste product generated in steel mills during the production of steel from iron. Iron scrap, coal, coke, and fluxes (limestone or dolomite) are fused together in a blast furnace during the manufacturing of iron. After the metallurgical smelting process is completed, the lime in the flux chemically interacts with the iron ore's aluminates and silicates, as well as the coke ash, to generate a non-metallic product (slag). These molten slag floats on top of the iron (Suresh and Nagaraju. 2015), which is regularly tapped out during the process, and quickly cooled in vast amounts of water, leading to the production of Ground granulated blast furnace slag (GGBS). The quenching improves the cementitious characteristics and creates coarse sand-like granules. This granulated slag is then dried and ground to a fine powder.

GGBS has a chemical composition that changes depending on the nature of the raw materials used in the iron-making process. The main components of blast furnace slag are CaO (30 – 50 %), SiO_2 (28 – 38 %), Al_2O_3 (8 – 24 %), and MgO (1 – 18 %). Increasing the CaO content of the slag results in raised slag basicity, which also contributes in increasing the compressive strength. As per the latest record available (Statista, the statistics portal, www.statista.com), the total volume of iron ore generated in India was around 250.02 million metric tons latest by 2021.

1.3.2 Fly Ash

FA is a toxic waste material that is generated in the Thermal power plant during the combustion of pulverised coal to produce electricity. During combustion of pulverised coal in the boiler, it gets converted into the molten mineral residue. The boiler tubes extract heat generated in the

boiler, and simultaneously, the flue gases get cool. The molten residue cools and solidifies to form ashes. The coarser component of this residue, known as bottom ash, settles in the bottom of the combustion chamber. On the other hand, the smaller ash particles rise with the flue gas, which is then collected by electrostatic precipitators (ESPs). These collected finer particles of ashes are known as FA.

FA primarily contains oxides of silicon (SiO_2) and aluminium (Al_2O_3), and calcium (CaO) along with other chemical oxides. Based on their chemical composition, FA is classified as either Class C or Class F, as per ASTM C618 - 17a (2013). Class C FA is generally obtained after burning bituminous coals. Such FA contains more than 20 % of free lime (CaO) and does not require any activator to form a cementitious compound. On the other hand, Class F FA is generated by the combustion of bituminous and anthracite coals. In class F FA, the CaO content is less than 10 % and hence is also called low calcium FA. Such fly ash needs an activator for the formation of a cementitious compound (Yousuf et al., 2020).

At present, India ranks as the second largest producer of coal in the world, followed by the United States and Russia (Assi et al., 2020). The average coal production in 2021-22 is expected to be at 777.31 metric tonnes, representing an increase of 8.55 % (Ministry of Coal, GOI). Despite a large amount of fly ash produced, only around 53 % of the total fly ash products are used globally.

1.3.3 Metakaolin

Metakaolin is a clay mineral kaolinite in form of anhydrous calcined clay. Traditionally, china clay is used as the raw material for the production of metakaolin since such materials are rich in kaolinite. Metakaolin is produced by heating the kaolin between 600 to 850^0 C (Assi et al. 2020). The average particle size of Metakaolin is between (1-2) µm, smaller than Portland cement particles and larger than silica fume particles. Its quality is controlled during manufacture, resulting in a much less variable material than other pozzolanic by products. Due to its pozzolanic and highly reactive nature it is used in the development of concrete composites, and it is used as an admixture to enhance the mechanical and chemical performance of concretes and other cementitious products or as a substitute to Portland cement (Rashad 2013). Metakaolin possesses significant amount of alumina and silica and hence it has a strong potential to be used in the production of geopolymer concrete.

1.3.4 Rice Husk Ash

Rice husks are the firm protective covering of rice grains, this is obtained during the milling process. It is a waste product that is widely accessible in all rice-producing nations. The husks are removed from the raw grain during a normal milling operation, revealing complete brown rice, which is subsequently milled to remove the bran layer, yielding white rice. Rice husk ash (RHA) is the product of combustion of rice husk. RHA contains a huge quantity (85 – 90 %) of amorphous silica (Hossain et al., 2018), especially when it is burned at temperatures between 500^0 C - 700^0 C. Due to the presence of high reactive silica and its pozzolanic property several research work has been under taken in the last few decades, where RHA has been used as a supplementary component of sand and Portland cement for preparing mortar or concrete. In addition to this it is also been used as a binding material and filler in synthesizing geopolymer concrete (Jauberthie et al., 2000).

1.4 Deterioration of Reinforced Concrete Structural Members

Cracks in concrete is the most common phenomena in the Reinforced concrete (RC) structural members. Cracks in concrete may occur both in the plastic stage as well as in the hardened stage. Cracks which appears in the concrete at the plastic stage of concrete i.e. when they are freshly placed, are referred as the plastic shrinkage cracks. These cracks are mainly governed by the rapid loss of water due to drying, which leads to a volume change in the concrete leading to cracks in the concrete surface (Ruacho Mora et al. 2009). While in the hardened state the concrete cracks due to drying shrinkage, thermal stresses, weathering, corrosion of reinforcement etc.

The cracks can be categorised in to two types namely: Non-structural cracks and Structural cracks. Non-structural cracks occur due to internally induced stresses in the building materials. Cracks in wall, parapet wall, drive way are non-structural cracks. Such cracks do not endanger safety of the structures. While structural cracks are the consequences of incorrect design, faulty construction, earthquake, overloading in structures etc. Cracks in the beam, column, slab and footing are considered structural cracks. Such cracks may endanger safety of the structures. When these cracks penetrate and widens beyond a certain limit, it not only destroys the serviceability of the structure but also provide pathway for intrusion of moisture and harmful ions in it leading to further enlargement of the cracks. The presence of cracks leads to a reduction in the strength of the concrete and the member fails at load lower than that for which it was initially designed.

Cracks in the RC members if not addressed in the initial stage, may lead to serious damage in the structure. Repair of deteriorated concrete of the structural members is essential not only to use them for their intended service life but also to assure the safety and serviceability of the associated components so that they meet the same requirements of the structures built today and in future. Repairing enhances the functionality of the structure, by restoring and/or enhancing the structural integrity and it also upgrade the aesthetic beauty of damaged surface. In addition to this it also inhibits the entry of moisture, harmful chemical, carbon dioxide etc. to the reinforcement bar, which ultimately enhances the longevity of the structure.

An effective repairing of cracked concrete depends on proper identification of the cause and then come up with the most suitable and sustainable solution. Repairing is sometimes followed by retrofitting and strengthening or rehabilitation of the damaged structure. Repair, retrofitting, and rehabilitation are all referred to as strengthening. These terminologies differ in terms of their roles and characteristics (Ganesh and Murthy, 2019). Repair is often a technique in which the structure's performance is little improved over its original performance or to match the aesthetic appearance without enhancing the performance. Typical repair works include filling of cracks, re-plastering etc. While Retrofitting is a process used to increase structural performance such as flexure, shear, ductility, service life and fatigue life. On the other hand, Rehabilitation is the process which is intended for restitution and restoration of strength or performance lost in the structures due to various distressing factors. Strengthening of structural components by means of repair, retrofitting, and rehabilitation is essential throughout its service life for which the members were designed.

Some of the repairing and strengthening materials found in the previous literature are: Epoxy resin, Carbon nanotubes, OPC grouting, OPC mortar, Shrinkage compensating mortar, Free flow micro concrete, Fiber reinforced polymer (FRP), Steel plates jacketing, Reinforced jacketing, External pre-stressing or external bar reinforcement technique, overlay of ultra-high performance concrete (UHPC) etc. Among them, the most conventional and widely used retrofitting materials are reinforced concrete jacketing, wrapping of FRP laminates and epoxy resin. Although epoxy resin is useful for crack sealing but such material is not favourable in all condition as it is expensive, required modern equipment and skilled labour and cannot be used in wet condition.

1.5 Literature Review

1.5.1 Geopolymer and geopolymeric materials

Davidovits (1982), was first who patented Geopolymer and described the polycondensation method of creating synthetic polymer. Since then, several academic studies have been published on the synthesis and hardening processes of geopolymer. The potential use of geopolymer as a binder in concrete was highlighted by the application of geopolymer in several sectors. The compressive strength tests performed on concretes made from blended geopolymer and Portland cement showed that these types of concrete can achieve high compressive strengths and can also maintain such strengths when subjected to high temperatures in the order of 600^0 C to 1100^0 C.

1.5.2 Characteristics of Geopolymer in Fresh and Hardened state.

Douglas et al. (1991) carried out investigation on the alkali activated Geopolymer concrete (GPC) prepared with GGBS activated by silicate based alkali solution (Na_2SiO_3). The test matrix includes five different mixes of GPC which differ from each other in their water to binder ratio. Based on the findings, the author reported that GGBS can be utilized to make concrete possessing considerable fluidity and mechanical properties. For all five concrete mixes, a significant gain in strength occurred at 7^{th} day compared to strength attained at the later age. The addition of lime slurry and air entertainer, intended to act as a retarder effectively increased the workability.

The strength and crystalline phased of GGBS and FA based geopolymer concrete was investigated by Oh et al. (2010). The author reported that major reaction products that contribute to the strength of geopolymer are sodium-aluminate-hydrate-silicate gel (N-A-S-H) generated from FA and calcium-aluminosilicate-hydrate gel (C-A-S-H); derived from slag. Whereas, geopolymer matrix containing both Slag and FA is mostly dominated by C-A-S-H gel with a considerable degree of alumina and crystalline phases of Mullite and Quartz.

Hardjito et al. (2004) studied GPC prepared with low calcium FA, activated by NaOH and Na_2SiO_3. The author claimed that increasing the concentration of NaOH improved compressive strength. However, even when cured at an increased temperature, the mixture shows no appreciable strength at 1 day, although curing duration has a favourable influence on strength enhancement. It was also stated that the GPC had little drying shrinkage and creep.

Chindraprasirt et al. (2012) investigated the influence silica and Allumina content on setting time, microstructure and strength of geopolymeric binder rich in calcium content. The study takes into account a range of SiO_2/Al_2O_3 concentrations ranging from 2.57 to 4. 79. The author reported that rapid setting property of the geopolymer systems is primarily attributed to the formation of C-S-H and C-A-S-H gel. Considerable improvement in setting property can be achieved by keeping the SiO_2/ Al_2O_3 within a range of 3.20 to 3.70, which also leads to a higher strength in the geopolymer than the other ratio of SiO_2/Al_2O_3. A higher SiO_2/Al_2O_3 ratio leads to a decrease in both the rate of strength development and also the strength characteristics.

John et al. (2021) reviewed the various source materials that are adopted for the development of geopolymer. From their study, it is revealed that low calcareous content in FA demands an elevated temperature for development of strength. However, the mechanical properties are also dependent on the particle size and the presence of glassy content. While on the other hand, GGBS is one of such additives which has given promising results in terms of strength and durability. Puligilla (2011) studied the effect of GGBS in the hardening stage of geopolymer. The study reveals that calcium in GGBS plays a very significant role in the formation of geopolymeric gel. The formation of these C-S-H gel in geopolymer occurs as a result of the reaction between the free calcium species supplied by the calcium source with the soluble silicate species in the alkali solution. The formation of the C-S-H gel depends on the type and nature of the calcium source, the alkali activator and the mass ratio of the binders used in the synthesis.

Manjunatha et al. (2014) conducted experimental investigation on FA and GGBS based GPC, in terms of their mechanical properties, and found it to be superior in comparison to conventional concrete. FA is replaced in different proportion with slag and different mix proportions were obtained for the test. With increase in GGBS content from GC1 (FA/GGBS: 100/0) to GC6 (FA/GGBS: 0/100) specifically enhance the compressive strength and tensile strength at all ages. Even at low percentage of GGBS, the mechanical strength of geopolymer mix was found to be higher than that of conventional concrete (100% OPC). A similar trend is also seen for the flexural strength, where the Geopolymer mix showed an enhance strength compared to conventional concrete and found to be very rapid in GC5 and GC6 which possess high GGBS content. But an opposite behaviour is also seen in case of the shear strength where all shear strength of GPC mixes are found to be less than the reference concrete.

As calcium content plays a major role in the strength of geopolymer concrete several calcium additives are often used in Metakaoline or FA based geopolymer to enhance the mechanical properties. Qian and Song (2015) used lime stone powder as a filler to geopolymer which is prepared with Metakaoiline as the main binding material. The author observed a delayed formation of amorphous product with dominated calcite and compacted micro structure. While, Yip (2004), reported that minerals like Calcite used in geopolymerization is moderate in forming geopolymeric products due to their limited solubility in alkaline solution but acts as a filler which results in enhancing the strength of geopolymer. However, such additive has an adverse effect in long-term durability, as reported by Elchalakani et al. (2018). The ingress of moisture and CO_2 reacts with calcium carbonate ($CaCO_3$) and forms soluble bicarbonates of calcium, which ultimately increases the porosity leading to degradation in strength at a later age.

The use of ultrafine binder has shown several promising results than the coarser material. Teng et al. (2013) investigate the effect of low volume ultrafine GGBS on the strength development and durability aspects of GPC. Their study reveals that fineness of the binding material provides an increased surface area which accelerates the pozzolanic reactions, thereby enhances the early strength. The ultrafine nature of the material also contributes as a filler leading to better packing, reduces porosity and also improves the interfacial transition zone (ITZ), which enhances the strength and homogeneity of the concrete (Sengul and Tasdemir, 2009). In another study, Li et al (2021) reported that the Ultrafine AS material can accelerate the dissociation rate of Al^{3+} and Si^{4+} ions in the alkali solution. This led to the early formation of geopolymeric products leading to fast setting and improves the rate of gain in strength of geopolymer. As high fineness increases the pozzolanic activity, it helps in early development of reaction products, which gives rise to early setting and loss in workability.

The effect of various chemical admixtures on Slag or FA-based geopolymer properties has been extensively studied in the past several years. Nemathollohi and Sanjayan (2014) investigated the effect of different types of commercially available plasticizers, on the fresh and hardened properties of FA based geopolymer. The various plasticizer that have been used are naphthalene, melamine and modified Polycarboxylate, which are used in GPC activated by sodium hydroxide and a combine solution of sodium hydroxide (NaOH) and sodium silicate (Na_2SiO_3). The addition of Naphthalene-based superplasticizer (SP) and Polycarboxylate

ether-based SP exhibits adequate workability when activated with SH and SS solution. Nevertheless, such SP simultaneously causes a strength reduction in geopolymer.

In another study, Sasaki et al. (2019) tested various chelators to deaccelerate the fast setting in geopolymer. HIDS chelator (chemical name: Tetrasodium 3-Hydroxy-2,2'-Iminodisuccinate) is a chelating ligand that has a strong ability in formation of water-soluble complexes in an alkaline solution of wide range of pH. During the process of chelation, HIDS chelating ligand traps the Ca^{2+} ions to form stable complexes. This phenomenon effectively slows down the formation of geopolymeric structure, which ultimately prolongs the setting time of the geopolymer. Another admixture, sodium tetraborate, which is well documented as a retarder for cementitious material, is also helpful in retarding the setting time in alkali-activated cement (Nicholson et al., 2005). In the work published by Zang et al. (2019), the author reported that borate is capable of deaccelerating the setting time and simultaneously speed up the hardening in ordinary cement. Participation of borate in Class C FA activated with both sodium hydroxide and silicate significantly delays N-A-S-H gel formation, resulting in prolonged setting time.

1.5.3 Durability of Geopolymer

Durability is one of the primary problems in Portland-based concrete, which is associated with it in an aggressive environment. The deterioration of concrete is mainly assessed by its resistance to sulphate attack, chloride-induced corrosion, atmospheric carbonation, alkali-silica reaction and freeze-thaw attack.

The durability of FA-based geopolymer paste against sulphate attack was studied by Fernandez Jimenez et al. (2007). The author reported no significant deterioration of FA-based paste under the influence of sodium sulphate and the ASTM seawater compared to Portland-based mortar. However, some fluctuations in flexural strength were reported between the 7^{th} day and three months of exposure.

Ren et al. (2020) studied the efficiency of FA/Slag based geopolymer paste when exposed to a high concentration of phosphoric acid. Such an environment is very common in the case of Portland cement-based concrete (PCC) in a sewer line or drainage system. The degradation of different geopolymer-based paste and Portland cement-based paste are studied at different pH levels of phosphoric acid. Degradation depth measurement, which indicated the deterioration of the concrete, was conducted to check the severity of the damages in the

concrete. The test result showed that alkali-activated cement is more resistant to phosphoric acid, regardless of the concentration, than Portland cement. Their study also predicted that even after 50 Years of exposure, geopolymer pastes would have a degradation depth around 70 % – 80 % less than that of the PCC.

High calcium geopolymeric binder and FA were assessed in terms of chloride diffusivity and chloride threshold by Babaee and Castel (2018). The study reveals that an increase in the calcium content plays a significant role in reducing chloride diffusivity. High calcium also leads to better production of C-A-S-H gel, which reduces permeability and chloride diffusivity. While in another study, Humad et al. (2019) investigated high Blast furnace slag with high MgO partially replaced by the different weight of FA. The author reported that the quantity of FA and lower alkali modulus of silicate solution mainly influence the autogenous shrinkage, whereas no significant drying shrinkage could be noticed with the variation of FA.

GGBS and FA-based GM cured in ambient temperature and at an elevated temperate (up to 200^0 C) was studied by Chithambaram et al. (2019). GM with 100 % FA is required to be cured at an elevated temperature of 60^0 C to yield high compressive strength. However, GM with 30 % of FA substituted by GGBS exhibits the maximum compressive strength even when cured at an ambient temperature. Their study reveals that GM is capable of withstanding high temperatures up to 600^0 C, however, the geopolymeric gel changes from a crystalline phase to amorphous phases, which leads to a marginal reduction in the mechanical strength.

1.5.4 Bond strength of Geopolymer

Bond strength is one of the main concern in any concrete, which is responsible to the monolithic action between an old concrete and a newly placed concrete over it. The bond behaviour of two different concretes is fundamental when there is a need of extending the structure, retrofitting, or repair.

Over the past decades, several test method has been developed to obtain the shear bond response of monolithic and cold joint concrete. Ueng et al. (2012) investigated the adhesion property at the interface of cement mortar and geopolymer by conducting several laboratory tests. To determine the strength attributes, failure modes and deformational moduli, a simple mechanical model was created considering the factors impacting various components at the interface. The typical prism sample utilised for the interface adhesion investigation is shown

in Fig. 1.4. The tests are performed by selecting numerous dip angles (β) of the geopolymer interlayer sandwiched between the cement mortar. The test was performed by uniaxial and tri-axial loading applied to the prismatic specimen. The stress-strain curve of the specimen subjected to uniaxial loading shows a brittle failure due to tensile splitting.

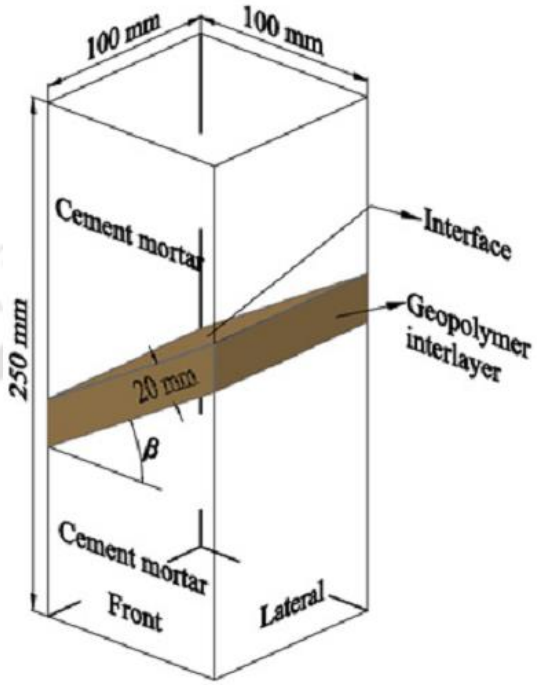

Figure 1.4: Prismatic specimen containing interlayer of Geopolymer (Ueng et al., 2012)

However, the specimen showed a ductile behaviour when the specimen was subjected to an increased confining pressure under triaxial loading. The author reported that all the prismatic specimens failed due to the shearing at the interface between the cement mortar and the geopolymer. Their study reveals that adhesion at the interface between the cement mortar and the geopolymer interlayer was 34-43 % stronger than the cohesion of the cement mortar and the geopolymer.

The bond strength of GPC with smooth and deformed reinforcing bar was studied by Castel and Foster (2015) immediately from 24 hours to 28th days of curing. Their GPC mix was composed of 85.2 % of FA and 14.8 % of GGBFS. Their study revealed that minimum 48 hours of heat curing at 80 °C is required to obtain a significant bond strength like that of PCC concrete of 45 MPa.

The bond strength of GM and PC based mortar modified by different volume fraction (V_f) of Polyvinyl alcohol (PVA) fiber with the conventional PCC material was studied by

Zanotti et al. (2017). The study was conducted by several nonstandard slant shear specimen possessing variable inclination of bonding plane. Where the concrete to geopolymer shear bond strength under different combinations of normal and shear stresses at the concrete-geopolymer interface was studied, considering different slant angles as shown in Fig. 1.5. From their work it is understood that interfacial cohesion and friction coefficients are the two inherent mechanical properties of the substrate-repair interface. The author concluded that cohesion in GM is significantly improved by the addition of PVA fibers. Effective performance was obtained by incorporating a 0.5 % V_f of PVA fibers to the plain matrix, which results in a 65 % increase of cohesion, however the effect is more promising when cured in elevated temperature. The author also reported that variation in interfacial friction angle undergoes only minimal variations.

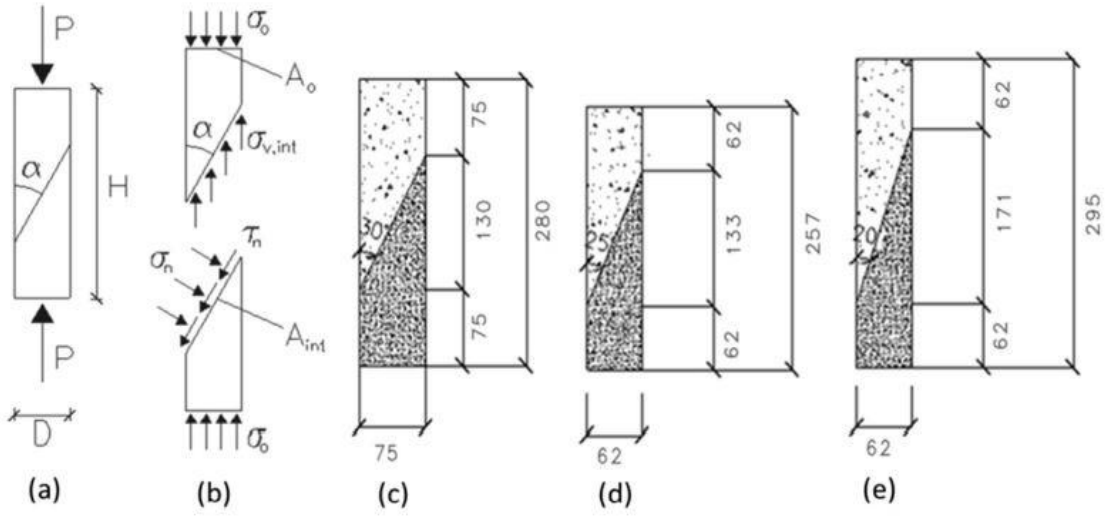

Figure 1.5: Slant shear test specimen (Zanotti et al., 2017).

In another study, Tan et al. (2022) investigated the effect of aggressive chemical environment and several other environments like freeze-thaw cycles, wet-dry cycles on the bond strength of geopolymer. Their results revealed that geopolymer shows negligible degradation in all the harsh environment like freeze-thaw, wet-dry and heat-cool cycles including the change of moisture and temperature variations. However, in the case of acid attack, fracture of Si–O–Al bonds took place, leading to increasing the amount of Al–OH and Si–OH groups in the acid solution, which leads to a significant loss in the mass of geopolymer. The effect of efflorescence on the mortar leads to a considerable bond strength drop (up to 20 %). However, the samples containing higher amount of GGBS exhibits the lower bond strength loss caused by efflorescence.

The effectiveness of different sand to binder ratio (s/b) ranging between 0.3 to 1, in Engineered geopolymer composite (EGC) towards bond strength with substrate concrete and steel rebar was studied by Kumar et al. (2022). The aforementioned EGC was prepared to be used as a repair material and composed of both FA and GGBS and also incorporated with short polyethylene and steel fiber. The bond strength test of EGC with the concrete substrate and the rebar was carried out as per the test setup presented in Fig. 1.6 (a) and (b).

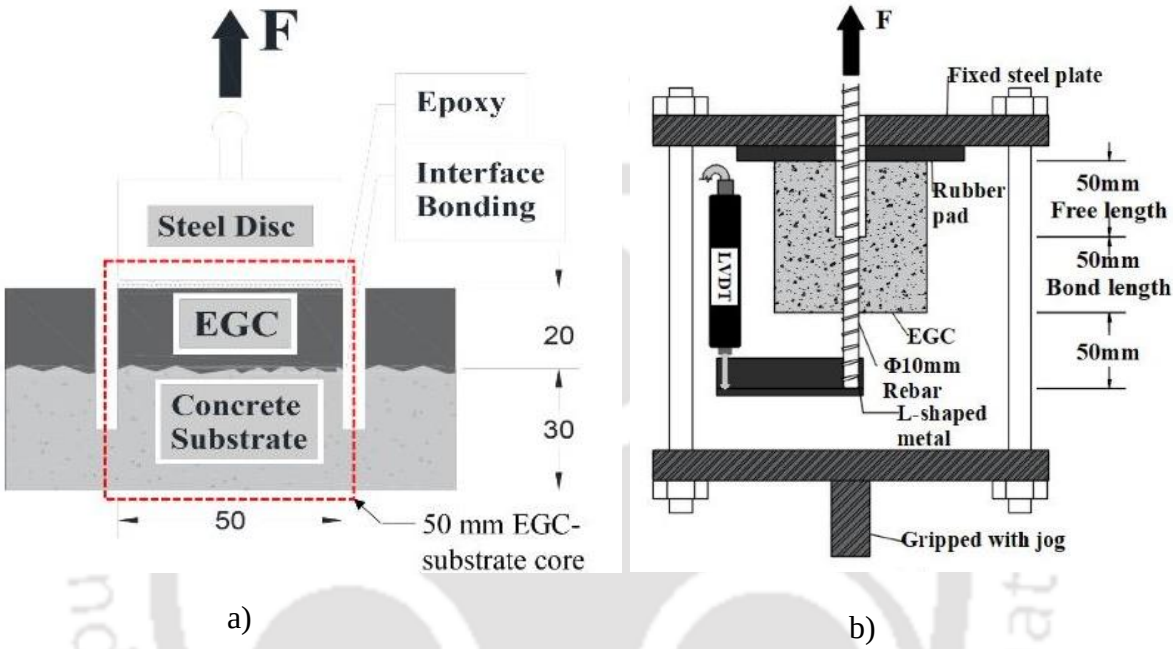

Figure 1.6: Bond strength test: a) Concrete pull of test b) Rebar pull out test (Kumar et al., 2022).

It was reported that the minimum bond strength which was achieved between the EGC and concrete substrate is higher than that bond strength required for repair purpose. Higher amount of s/b ratio decreases the micro cracks resulting in increase of the elastic modulus of the EGC, which is found to be in direct relation to bond strength of EGC with the concrete and rebar. The peak pull-out strength follows the same trends as that of the compressive strength of EGC. The fibers on the EGC matrix effectively bridged the cracks and prevented radial cracks, thereby resist the pull out mechanism.

1.5.5 Fiber Reinforced Geopolymer Concrete

The most undesirable feature of concrete is its low tensile strength and brittle behaviour however this can be improved by incorporating short fibers, randomly distributed in the

concrete matrix thereby known as fiber reinforced concrete. Fibers that are usually used in concrete are steel, glass, and polymer or derived from natural materials. It is revealed that the compressive strength of GPC mix is significantly high, which varies in a wide range due to varying nature of the source material. However, their tensile strength is comparatively low when estimated by the standard code of Portland cement (Ranjbar and Zhang 2020). Thus, fibers in the different forms of threads, filaments, whiskers or nanoparticles are often used as reinforcement in geopolymer composites to increase the tensile strength, flexural strength and energy absorption capacity.

Bernal et al. (2010) investigated the effect of different quantity of steel fiber on the strength parameters of FRGC. They reported that inclusion of fiber leads to a marginal reduction in the compressive strength however the flexural strength can largely be improved using fiber. Shaikh (2013) developed a ductile fiber reinforced geopolymer concrete (DFRGC) by employing both steel fiber and polyvinyl alcohol fiber (PVA) in Flyash based geopolymer. The DFRGC materials exhibited a significant deflection hardening behaviour thereby enhanced the ductility of material when compared to conventional concrete with same fiber. On the other hand, different types of steel fiber (length deformed, end deformed, straight) and polypropylene fiber (length deformed) of higher aspect ratio were used by Bhutta et al. (2017) to prepare FA based fiber reinforced geopolymer composites (FRG) with an optimum V_f of 0.5 %. The effect of the different shape of the fiber under different curing condition (i.e. ambient temperature and 60^0C temperature) was studied based on the first peak strength, modulus of rapture and toughness. It is seen that heat curing increases the first peak load for all types of FRG composites. Moreover, the end deformed fiber exhibit better performance in enhancing the average compressive strength, split tensile strength and flexural response as compared to other fiber irrespective of the curing condition.

Yazici et al. (2007) carried out experimental study on properties of steel fiber reinforced concrete (SFRC). In their study the influence of steel fiber with varying aspect ratio (L/D: 45, 65, 80) and volume fraction (V_f 0.5%, 1%, 1.5%) has been studied. Their result shows that inclusion of steel fibers significantly affects the properties of concrete like decrease in workability, increases in weight and increase in compressive strength, but it also depends on aspect ratio and V_f. Flexural strength and tensile strength both increase with the inclusion of steel fiber however it also depends on the optimum value of L/D ratio and V_f. Similar study with steel fiber was also reported by Rao and Seshu (2003), who investigated the behaviour of

SFRC beam under torsion. Four groups of RCC beams are casted with four different grades of concrete (M_{20} to M_{50}) with volume fraction (V_f = 0, .3, .6, .9, 1.2 %). Where the same L/D equal to 75 was considered. The result shows that Steel fiber improves the ultimate torsional strength, torsional toughness and torsional stiffness of the beams. The author recommended that a minimum volume fraction of 0.9 % is required to impart noticeable ductility to the SFRC beams under torsion. However, addition of steel is needed for High strength concrete as they are brittle in nature.

In another study, Liu et al. (2020) develop ultra-high performance geopolymer concrete (UHPGC) and studied the effect of aspect ratio by incorporating different sizer of steel fiber. The inclusion of steel fiber enhances the mechanical property by delaying the crack initiation and their propagation. The author reported that inclusion of steel fiber in geopolymer is more effective than that in the Portland based concrete, owing to the high bond strength between geopolymer matrix and steel fiber. Higher aspect ratio affects the workability and first crack load and also helps in improving the mechanical properties. Hooked end steel fiber exhibits highest toughness index than straight steel fiber due to mechanical interlock. But above all, the mechanical properties are significantly dependent on the curing conditions and fiber dosages.

1.5.6 Geopolymer as repairing agent

Several researchers have employed GM and GPC for restoration and/or strengthening of damaged structural members. Phoo-ngernkham et al. (2015) investigated the application of FA and Portland cement based alkali activated GM as a repair material. The repair mortar exhibits a much better bond strength with the PCC substrate in comparison to commercially available repair material (RM). The bending strength of notched concrete beam filled with GM provided high bending strengths compared with the use of RM. Alanazi et al. (2016) investigated MK based GM as repair material for pavement. They reported that interface bonding was significantly affected by the curing time however significant bond strength and tensile strength could be achieved at 3 days. It is also reported in the literatures that geopolymer developed from MK and steel slag are susceptible to shrinkage (Fahin et al. 2017) but shrinkage properties of the geopolymer can be minimised by incorporating some percentage FA.

Recently, research on GPC has gained a huge momentum due to its superior mechanical properties, durability, sustainability and early hardening of the geopolymer matrix, which widens its application in the engineering field. Sarkar (2011), conducted pull out test to

evaluate the bond strength between FA based GPC and steel reinforcement. The author concluded that GPC possess a higher bond strength with the steel rebar that the conventional concrete (OPC based concrete), which is attributed to the higher splitting tensile strength in the GPC. The high splitting tensile strength in GPC is also reported by Zhang et al. (2005), who studied the hydration process of the ITZ between the coarse aggregate and the geopolymer matrix. The strong ITZ in the GPC is found to be much stronger which contributed to greater split tensile strength than the OPC based concrete.

Hu et al. (2008) intended to establish an efficient repair material by examining the properties of geopolymer prepared from types of binders. The different binder that has been taken into account by the author was Portland cement, metakaolin and steel slag. The assess the effect of the binder, several tests like compressive strength, abrasion resistance and bond strength tests were performed. However, the strength attributed were recorded at 8 hours, 1 day, 3 days, 7 days and 28^{th} days. Their result shows that geopolymeric binder, irrespective of slag and metakaolin, showed better performance as a repair material than Portland cement. The ITZ produced by slag-based repair material is comparatively better than other repair materials. The addition of slag not only produces a better adhesion but significantly improves the compressive strength.

The use of industrial waste in the synthesis of geopolymer has made it a very appealing material, which motivated many researchers to investigate on the mechanical properties and its durability. Moreover, the rapid gain in strength and improved bonding properties indicate that geopolymer has a significant potential for its employment in structural application. If such material can be used as an alternative repair material for any type of structural members, then it can indirectly lead to huge saving of time and money in repairing and demolition work.

1.5.7 Transverse opening in RC beam

In modern building construction, transverse openings in RC beams are sometimes provided to facilitate the passing of utility ducts and pipes. These ducts are necessary in order to accommodate essential services like water supply, sewage, air-conditioning, electricity, telephone, and computer network. These ducts and pipes are usually placed underneath the soffit of the beam and, for aesthetic reasons, are covered by a suspended ceiling which creates dead space. An alternative way is to pass these ducts through a transverse opening in the floor beam, as shown in Fig. 1.7. Passing utility services through these openings in the floor beam

Figure 1.7: Transverse Opening in beams, Jabbar et al. (2016) and Ozkılıç et al. (2022)

leads to a significant reduction in the headroom. For small building the saving may not be significant compared to the overall cost but for multi-storied building, any saving in the storey height multiplied by the number of stories can represent a substantial saving in the total height, length of air conditioning and electrical ducts, and the overall weight of the structure. This encourages the designer to reduce the height of the structure by providing a web opening in the beam, which leads to a more economical design. But including transverse openings in the web of a reinforced concrete beam leads to sudden changes in the dimensions of the cross-section of the beam, which transforms the simple behaviour of the beam into more complex behaviour. Mansur and Tan (1999) reported that if a transverse opening is created in an existing beam, then the beam will exhibit early cracks, which get wider with time. In such cases the load carrying capacity of the beam reduces by approximately 29 % from that of a solid beam with no opening.

However, the degree of change in the behaviour of the beam due to the presence of an opening depends on several factors such as shape and size of the opening, position of the opening, reinforcement and type of loading. From the literature, it can be understood that the

size of the opening is the most important parameter that affects the beam behaviour. Several authors have classified the opening size as small and Large. According to Mansur (1984), an opening is small when it is circular, square or almost square, and hence no clear distinction could be made by the author. Whereas Somes and Corley (1974) defined that a circular opening may be considered as large if its diameter is greater than 0.25 times the depth of the web. The author also mentioned that the opening could be categorized as small or large depending on the structural response of the beam. If the opening is small enough to maintain the beam type behaviour or if the usual beam theory can be applied, then the opening may be called a small opening, and if the beam type behaviour ceases to exist, thereby changing the beam type behaviour in to frame type behaviour, then the opening may be classified as Large opening.

Meanwhile, Allam (2005) defined that a rectangular or circular opening may be considered as small if the opening depth or diameter is less than or equal to 40 % of the overall depth of the beam; otherwise, it is considered as a large opening. Beams with small openings have a negligible influence on the behaviour of the beam, and hence such beams can be designed with the conventional theory used in the case of a solid beam. But a large opening alters the overall structural behaviour and load path patterns of the beam, and hence special consideration shall be adopted in the designing of such beams. Nasser et al. (1967) reported that a large opening in concrete beams makes the beam behave like a frame. However, they discovered that if such beams are adequately strengthened with reinforcement, then they can retain their original strength. Their study reveals that the distribution of shear stresses in the beam depends on the relative cross-sectional area of the top chord and bottom chord. This is in contrast to the results of other studies that reported that the shear stress distribution depends on the relative stiffness of the chord.

Ali and Saeed (2022) explained the effect of opening in the RC beam during their experimental investigation and numerical analysis. They reported that the presence of an opening disturbs the distribution of strain. The usual strut and tie model of the beam is interrupted. This leads to a change in the load path. Because of the geometrical change, the compressive capacity of the strut in the beam is reduced as compared to its counterpart in solid beams. The absorbed energy needed to shear the chords of an opening is less than the energy dissipated to develop a complete diagonal crack throughout the entire depth of a solid beam. The presence of an opening in the shear zone makes the beam weakest in resisting shear stress

due to its reduced cross-sectional area. However, the effect is minimal if the load path is not interrupted.

It is obvious that transverse openings through beams are a source of potential weakness. Therefore, in the case of a preplanned opening, the sizes and locations of openings are known to the designer, and adequate strength and serviceability can be ensured by internally strengthening the opening area with an additional reinforcement scheme. But this not always happens; sometimes, the contractor needs to drill an opening for the sake of simplifying the arrangement of pipes or if a concrete core needs to be extracted from a beam in case of structural assessment or health monitoring purposes. In such cases, external strengthening is the only option to regain the original strength. Thus in an RC beam, either a pre-planned or a post-planned opening, adequate measures must be taken to enhance the strength of such members.

The effect of concrete strength and sizes of opening in the deep beam has been studied by Yang et al. (2006). They reported that, like a deep beam without an opening, the strength of the concrete in the presence of a small opening steadily improved the performance of the beam. But in the case of a large opening, significant degradation in the deformation capacity of the beam after the peak load is observed. Aykac et al. (2013) have studied the flexural behaviour of RC beam with multiple openings of different shapes (circular, rectangular and square) and strengthening with different reinforcement schemes. The authors reported that the presence of diagonal reinforcement was effective in preventing the shear failure of the beam, preventing the formation of plastic hinges and restraining the beam from behaving like a vierendeel truss. However, the performance depends on the amount of steel as the beam with minimum reinforcement having a square opening showed the worst performance.

Salama et al. (2018) presented an experimental study on a flanged beam with an opening, subjected to pure torsion, where the influence of various geometrical parameters (such as flange width, thickness and height of opening) are studied under torsion. The author reported that an increase in the flange width or thickness increases the torsional capacity and angle of rotation at different levels. The author has also proposed an analytical model based on the softened truss model for predicting the torsional behaviour of the beam. Their study shows that the torque vs rotation angle curve obtained from the experimental data and the analytical model are in good agreement with each other.

1.5.8 Retrofitting and Strengthening of RC structures

The effect of shear opening on the behaviour and strength of RC beam has been studied by Mansur (1998), who also proposed guideless for reinforcement to strengthen shear opening. Two types of failure patterns are identified in the case of beam with opening, namely beam type failure and frame type failure. The beam type failure is similar to that in a solid beam, except that the diagonal cracks passes through the centre of the opening. While in frame type failure, independent diagonal cracks exist in both the chord, and each member behaved independently, similar to a frame structure.

Strengthening of the web-opened beam using steel fiber reinforced concrete (SFRC) and steel plates was carried out by Suresh and Prabhavathy (2014). Several RC beams with web opening in the shear zone are strengthened by employing different strengthening schemes. Their study reveals that the presence of duct openings in the shear zone reduces the load carrying capacity by 55 to 70 %, and deflection reduces from 20 % to 55 %. However, by application of SFRC in the web opening, it can increase the load carrying capacity by up to 30 %, along with improvement in ductility. In addition to these, there was reduction in cracks, especially at the corners of the openings. While the beams, which are further enhanced by introducing steel plates in the opening, lead to significantly higher load carrying capacity, enhanced stiffness and improved strain hardening behaviour of the beams. In addition to this, the beam exhibited a better distribution of stress around the opening, which leads to lesser formation of cracks and delay in crack propagation around the opening.

Hassan et al. (2020) investigated a new strengthening technique to strengthen RC beam with an opening in the shear zone by using strain hardening cementitious composite (SHCC). These SHCC plates are initially developed in the laboratory and then pre-installed in the shear span of the beam. The strengthened beam with SHCC plates considerably improved the ultimate shear strength, energy absorption capacity and the post-peak stage of the load-deformation curve. However, the change in the opening length has a significant impact on the ultimate strength and failure pattern of the beam.

In another study by Lee and park (2015), steel tubes were installed in the opening as a strengthening material in the mid-span opening. An additive called Garnet, which increases the strength and brittleness of mortar, is used along with different fibers (steel, Nylon, Polypropylene) to enhance the ductile behaviour of opening with circular steel tubes. Their strengthening scheme results in an increase in the strength of the beam and crack controlling

effect. The test results are compared with predicted shear strength using ACI and AIJ methods, where the AIJ method showed the most satisfactory results.

Pimanmas (2010) carried out strengthening of RC beam with web opening using pre-fabricated internal reinforcement scheme and installation of FRP rods in different orientation, as shown in Fig. 1.8 (a) and (b). Their test results showed that full strength is recovered only when the FRP rods are placed diagonally alongside the opening throughout the entire beam depth. While the strengthening with pre-fabricated internal steel (Fig. 1.8. b) also exhibited a strong potential in retaining the full structural performance of the beam beam.

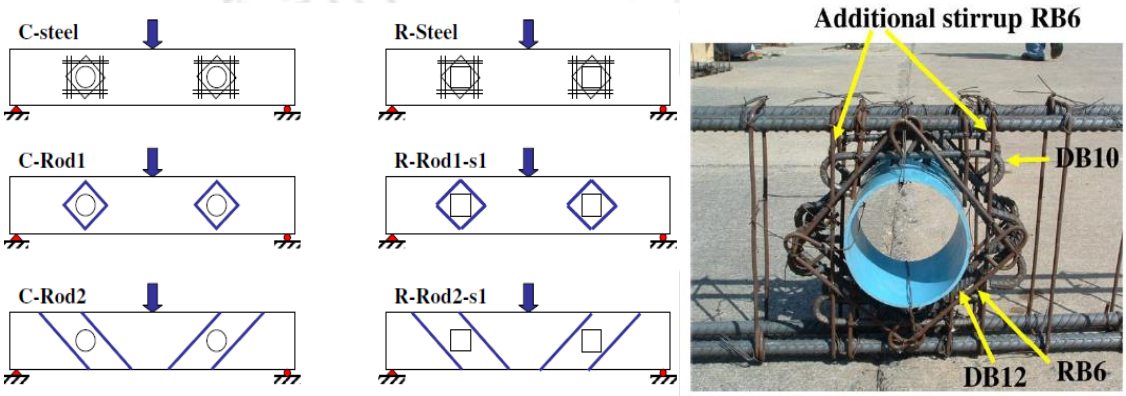

(a)With FRP Rods (b) Pre fabrication of Internal steel

Figure 1.8: Different strengthening Schemes, Pimanmas (2010)

Carbon fiber reinforced polymer (CFRP) material is also found effective in strengthening web opened beam as studied by El-Maaddawya and El-Ariss (2012). Web opened beam with opening in short shear span, reduced the load carrying capacity by 72 %. Such beams are strengthened by CFRP materials; and are found effective in enhancing the strength and stiffness like that of a solid beam with opening. However, it is observed that when the inclination of the load path in the shear span is greater than 11^0, strength technique with CFRP wrapping exhibits the complete restoration of the web opened beam. Investigation of RC beam with shear opening adjacent to the support was experimentally studied by Elansary et al. (2022). The web opened beam were strengthening using CFRP material; and are tested and attempt has been made to estimate the behaviour of the strengthened beam. The authors reported that introduction of opening leads to a reduction in deflection at the failure point and exhibits 43 % loss in the shear capacity. The strengthened beam attained a maximum load of 90 % to 95 % of that of a solid beam with no opening. Their mathematical model developed to predict the load deflection

behaviour are in good agreement to the experiment result. A similar study was carried out by Chin et al. (2016), where strengthening of large opening in flexural zone has been studied using externally bonded CFRP laminates and the results are validated by Finite element approach, ATINA. Two types of opening are considered large rectangular opening and rounded rectangular opening and various strengthening configuration were investigated based on the crack pattern of the beam and the most effective configuration of CFRP was recommended, which is shown in Fig. 1.9.

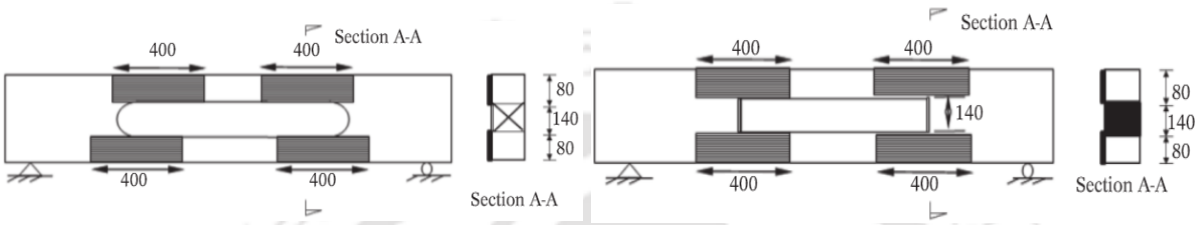

Figure 1.9: Strengthening scheme with CFRP Laminates (Chin at el., 2016).

They reported that large opening in the mid-span reduces the load carrying capacity up to 50 % however both the FEM analysis and the experimental program showed that 80 to 90 % of the lost capacity could be restored with the selected strengthening configuration. They also reported that openings with lengths 30–40 % of the effective span are not advisable unless the upper and lower chords are properly designed. Again the study showed that the rounded rectangular opening has proved to provide higher capacity and better distribution of stress concentration for a similar load, hence such shapes are preferable. In another study by Diggikar et al. (2013), the efficiency of glass fiber reinforced polymer (GFRP) and CFRP are studied and compared. They concluded that the strengthening with CFRP around and inside the opening is more efficient and is considered as best strengthening scheme than GRFP.

RC T-beam with web opening strengthened by FRP was studied by Nie et al. (2018) with an objective of enhancing the failure mode of existing structure, where the concept of strong column-weak beam was violated. The author proposed a novel seismic retrofit method based on the flexural weakening-shear strengthening (FWSS). This was achieved by creating an opening in the web of T-section beam, with a motive of reducing flexural capacity and simultaneously strengthen the beam with FRP material. The author reported that this method can transform the shear failure of the beam in to a ductile failure. All unstrengthened beam in such cases failed by sudden shear failure. While the beams with opening followed by local

shear strengthening although exhibits a reduced flexural capacity, but failed under mixed flexural and shear failure followed by crushing of concrete.

Ahmed et al. (2015) experimental investigated the effectiveness of CFRP over steel plates in repairing RC beam with web opening. Their work includes the repairing of damaged specimen with web opening with different thickness of CFRP and steel plates. The repair materials that were externally bonded around the opening is shown in Fig. 1.10.

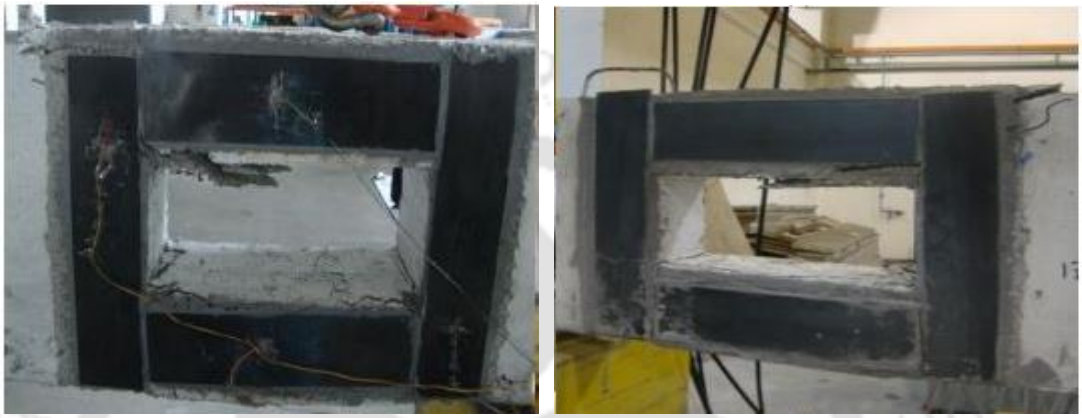

Figure 1.10: Externally bonded a) CFRP plates and b) Steel plates (Ahmed et al., 2015)

They reported that the effect of thickness of the steel plate has little effect on the maximum load carrying capacity. The effective distribution of stresses at the interface between the repair material and the substrate was more significant in CFRP than the steel plate. The beam repaired with the steel plate, exhibited debonding of steel plate, before reaching the ultimate load. However, in case of beams repaired by CFRP no such debonding was exhibited, the tested beams exhibited better load capacity of the beams.

Damages in concrete in the structural members are inevitable and there exist several other techniques of retrofitting and strengthening materials that are implemented in the last two decades. Retrofitting of cracked beam with different reinforcement scheme, using polymer modified mortar has been investigated by Ahmad et al. (2012). The efficiency of the repaired beam is evaluated on just after the third day of curing. Both the reinforcement scheme (with and without shear reinforcement) showed a substantial improvement in the load carrying capacity however stiffness degradation is found common in the beam without shear reinforcement.

Another material Ferrocement has lately acquired popularity as a cost-effective reinforcing technology, owing to its ability to offer better toughness, cracking resistance, confinement and the ease of application in difficult structures. Ferrocement is a type of thin composite material made of cement mortar reinforced with uniformly distributed and continuous layer of wire meshes. The provision of fine wire-mesh beneath repair material is not a new practice, especially in higher seismic zones where repairing of structures is frequently needed. The application of ferrocement as a repair material was first introduced by Romualdi (1987), for the rehabilitation of water retaining structures, relining of tunnels and sewer lines and for structural rehabilitation like retaining wall, unreinforced masonry walls etc.

Andrews and Sharma (1988) studied the repairing of RC beam by employing ferrocement layer attached with the surface of the beam and compared the result by the conventional method of repairing with concrete and mortar. The beam repaired by ferrocement exhibits higher cracking moment and deflection capacity then those repaired by conventional technique and also exhibits a ductile behaviour similar to original beam. These improvements are however lesser in the specimens where the monolithic action between the ferrocement layer and the beam have been lost during the test. The use of wire mesh with cement mortar has been already proved to be very effective composite materials for the seismic strengthening of masonry wall (Sergio et al. 2006). Its distinct features, such as high strength to weight ratio, high stiffness to weight ratio, fatigue resistance and durability makes it a good jacketing material (Soman and Mohan, 2018). Furthermore, all these properties are achieved within a thickness less than 40 mm, which can easily be cast into any shape to fit the contour of the elements being repaired.

Ong et al. (1992) strengthened eight rectangular beams with pre-fabricated ferrocement laminates which are attached to the surface of the beam using two types of anchorage system. These includes application of power driven nail which are installed at different spacing of 100 mm, 150 mm and 200 mm. While in another case anchorage bolt at a recommended spacing of 118 mm are installed in the concrete substrate and the effect of epoxy resin as an adhesive are also studied. It was revealed that composite action between the ferrocement laminates and the concrete substrate were sustained in the beams where the ferrocement laminates are attached via power driven nails at a spacing of 100 mm than that attached using epoxy resin adhesive. The author concluded that better composite action in ferrocement enhances the deflection and load capacities of the strengthened beams.

In another study, Paramasivam et al. (1998) reviewed the method of repair and rehabilitation of RC beam using ferrocement technique. The author has brought to light several interesting features of applying ferrocement composite on the surface of structural element. They reported that the main purpose of the fine mesh in ferrocement was simply for crack control and was not relied upon to contribute to the structural strength of the member. Addition of ferrocement laminates in beam can help in delaying the appearance of crack, prevents the cracks from widening, increase the flexural stiffness and load capacities of the strengthened beams. Furthermore, their study reported that a well roughened surface and closely spaced shear connector provides a better monolithic action at the interface of the substrate and the ferrocement laminates. However, it is dependent on the strengthening ratio required and the volume fraction of reinforcement used in the ferrocement laminate. Rehabilitation of damaged haunched beam, initially failed in shear, using Ferrocement laminates composed of light wire mesh and cement grouting, was studied by Tena-Colunga et al. (2020). The restored beam exhibits enhanced elastic stiffness and improved shear capacity. The welded wire mesh worked effectively in the restoration process and participated in improving the deformation capacity to the repaired beams.

The restoration of RC beam using epoxy injection and steel plates and ferrocement is studied by Basunbul et al. (1990). The author reported that the epoxy injection is found useful in restoring the structural integrity and ductility of the beam. However, better performance is obtained by the combination of epoxy resin and the ferrocement. The repaired beams showed higher cracking load, better rigidity and enhanced ultimate strength than the original beam. While the beam repaired by only ferrocement showed a decrease in the ductility with the increase in the damage level. Although epoxy resin has yielded several promising result but such material could not fill in to very fine cracks which leads to a further degradation when exposed to aggressive environmental condition.

Reinforced concrete jacketing is one of the traditional and cost effective technique for strengthening of structural members. The notion of reinforced concrete jacketing is mainly adopted, when it is intended to increase the structural capacity by enlarging the structural member cross-section. The process of RC jacketing in an old structure includes roughening of existing concrete structures and placing new RC layer. While special attention is needed in the bonding between the jacketing layer and the old concrete. Efficiency of reinforced concrete jacketing in rehabilitation of damaged RC beams was studied by Altun (2004). Concrete

jacketing was used to strengthen under reinforced RC beams that had reached the fully plastic stage, as shown in Fig. 1.11. The investigation took into account the cross-sectional aspect ratio, jacket thickness, and degree of reinforcement. Theoretically estimated values were compared to empirically collected data to validate the results. The findings of load deflection showed that jacketed RC beams behaved similarly to original RC beams. The quantity of reinforcement and the cross-sectional aspect ratio variations affected the RC beams' ductility. It was observed that predicted values were lower than those attained experimentally.

Figure 1.11: Jacketing methodology used in damaged RC beams (Altun, 2004).

Such method is very useful for strengthening purpose and success of these method depends on the adhesion between the newly cast jacketing layer and the old concrete. However, the method is cumbersome as it requires dowel bars or shear connectors which need to be installed by drilling in the core of concrete. Moreover, to have a better bonding several other adhesive agents are also required.

Ultrahigh performance fiber reinforced concrete (UHPFRC) is another material which is utilised by several researchers and attained a great achievement in strengthening of RC structures. UHPFRC is made up of Portland cement, very fine aggregate, micro silica with a large quantity of short steel fibers, which was firstly developed by Richard and Cheyrezy (1995). Such materials possess high compressive strength and modulus of elasticity and have high strength to weight ratio. Due to their compact matrix's and high density these material possess superior durability characteristics. All these characteristics made UHPFRC a very appealing material to be used in strengthening purposes.

Al Osta et al. (2017) investigated the effectiveness of UHPFRC for strengthening of RC beams. The strengthening work was carrying out with two different method i) by casting a layer

of UHPFRC around the beam with the help of mould ii) by bonding pre-fabricated UHPFRC with the beam using epoxy. The Jacketing layer in each strengthening scheme was applied in the beam in three different configurations i.e. applying the UHPFRC at the bottom, two longitudinal sides and a three side jacketing. Their study revealed that cast in-situ Jacketing technique performed better than the pre-fabricated UHPFRC strengthened due to its better monolithic action during the testing, which is attributed to better bond due to the sand blasting. The strengthened beam exhibits enhanced stiffness, improvement in crack load and delayed crack propagation.

In another study by said et al. (2022) UHPFRC was used as a strengthening material to improve the shear strength of RC beams. Several parameters are considered in their study such as thickness of the UHPFRC layer, effect of jacketing sides, quantity of steel fibers, distribution length of UHPFRC layers. Moreover, the study also reported the effect of in-situ case of UHPFRC layer and pre-fabricated anchoring system. Their study revealed that full casting of UHPFRC exhibits better performance than those of prefabricated laminates. The strengthening scheme exhibits enhanced ductility in the beam by 3.37 times and capable of improving the stiffness and shear capacity of the beam by 2.75 and 0.54 times.

Recently, novel techniques using Fibre reinforced concrete composites layers or jackets have also shown many promising results in retrofitting of structural elements. Jacketing with FRCC for retrofitting and strengthening purposes has been investigated in several studies (Ruano et al. 2014). Application of Fiber reinforced cement concrete (FRCC) as a jacketing material has several advantages such as it prevents brittle failure of the member, prevents shrinkage cracks, improves the post cracking behaviour and increases the durability. Above all it eradicates the limitation of thin jacketing layer which is not possible in case of steel reinforced jacketing where 60 to 70 mm of jacketing layer is needed to accommodate the reinforcement and the concrete cover (Martinola et al. 2010). All these features make FRC a very attractive material for jacketing RC structures. The effectiveness of FRCC also depends upon the bond between the fiber and the concrete matrix and between FRC matrix and the concrete substrate.

1.6 Critical comment on existing Literature

Previous works in literature reveals that opening in the web of the beams leads to high concentration of stresses in the opening area which leads to early cracking of beam, excessive deflection and also reduces

the ductility of the beam leading to sudden collapse of the beam. Such opening makes the beam weak, which may lead to early collapse under service load. Literature presents a large volume of work carried out with the conventional strengthening technique like CRFP composites and steel plates. However, such method is not always feasible due to their high cost and debonding issue. So far, several cementitious materials have been implemented for the repairing and the jacking of RC structures. These gave immense results after attainment the target strength of the jacketing layer. However, their composite action depends on the bond between the old RC structure and the new material which often fails leading to formation of cold joint. On the other hand, Geopolymer concrete possess extensively higher bond strength with any conventional OPC based concrete, which makes geopolymer as an exceptional low-cost repairing material. Such material, being able to offer very early strength has made it an attractive building material to be used in the field of retrofitting and rehabilitation.

1.7 Scope of the Present Study

Due to the rise in carbon footprint in the atmosphere and huge consumption of natural resources, researchers are paying a continuous effort to develop novel binding materials like geopolymer from industrial waste. It is evident from the literature that geopolymer has a strong potential to replace the current OPC binder and that it has the power to revolutionise the building sector. A review of the literature indicates that extensive research into geopolymer as a concrete binder has been conducted in order to improve the fresh and hardened characteristics, as well as the durability of the materials.

However, Geopolymer, being able to offer very early strength has made it an attractive building material. In addition to this, the superior bond strength between geopolymer with the PC-based concrete makes it the most suitable material for its employment in the retrofitting of damaged structural members. In addition to this, the early strength development of geopolymer can allow early removal of formwork, which can ultimately speed up the construction process, thereby saving time and expenditure.

The application of geopolymeric material as a repair material for damaged structures is relatively new. Numerous repair materials are commercially available such as polymer modified mortar, epoxy resin, fiber reinforced polymer etc. however, application of such materials is a costly affair as it needs time and skilled workmanship and is not always feasible when the structural member demands an emergency repairing. Furthermore, it is seen that strengthening by RC jacketing or fiber reinforced concrete jacketing of structural members is

mostly done with Portland cement-based concrete, which needs a longer time for its curing and also possesses a bonding issue with the original member.

Literature reveals that web opened beams in some special cases are unavoidable. Such opening makes the beam weak, which may lead to early collapse under service load. So far several techniques have been implemented to strengthen the web opened RC beam. But the repairing and strengthening of damaged web opened beams using geopolymeric material has not been addressed yet and needs to be investigated to extend its application in the construction industry.

1.8 Objective of the Present Work

The following are the objectives of the present study:

1) To develop ultrafine blast furnace slag (UBFS) and Fly Ash (FA) based Geopolymer mortar (GM) using silicate based alkali activator as a repairing mortar and assess their properties in the fresh and hardened state by conducting laboratory experiments.
2) To develop UBFS based Fiber reinforced geopolymer concrete (FRGC) mix using hooked end steel fiber as a Jacketing agent and investigate their workability and mechanical properties by performing laboratory experiments.
3) Repairing of damaged web opened RC beam using UBFS based GM, Portland cement mortar (PCM) and welded steel wire mesh and to investigate the behaviour under static monotonic-load.
4) Strengthening of damaged web opened RC beam using UBFS based FRGC and FRCC Jacket and study the behaviour of the jacketed beam subjected to static monotonic-load.

1.9 Organization of Thesis

The thesis has been organised in seven major chapters. In addition to this abstract, appendix and references are also included. A brief content in the chapters are given below

Chapter 1: This gives an introduction to Geopolymer and its significance as a sustainable binder. The chapter also introduces the effect of transverse opening in the RC beam. The

detailed literature review and scope of the present work have been included. Thereafter, the objectives of the work have been listed.

Chapter 2: This chapter contains the various engineering properties of the raw materials that have been used in the present work, along with the various laboratory test method involved.

Chapter 3: This chapter is dedicated to the development of alkali-activated GM, which includes the various tests performed to assess the fresh and the hardened state properties of the GM. The chapter also includes the microstructural study of the GM.

Chapter 4: This chapter first presents the development of the GPC followed by the development of the FRGC mixes. The chapter describes the details test methodology and the properties of the GPC and the FRGC mixes, followed by the microstructural characteristics.

Chapter 5: This chapter includes the preliminary investigation of the behaviour of web opened beam in comparison to a solid beam. This chapter also contains the repairing technique implemented in damaged web opened beams using GM and PCM. It also presents the experimental result of the repaired beams with opening tested under static monotonic load.

Chapter 6: This chapter describes the methodology undertaken to strengthen web-opened RC beams using FRGC and FRCC material. It also presents the experimental result of the strengthened web opened beam tested under static monotonic load.

Chapter 7: This chapter summarizes the work carried out in the present thesis and the major conclusions that could be arrived from the study. Suggestions for future work are also given in this chapter.

1.10 Closure

This chapter introduces Geopolymer technology and the various works carried out in the development and improvement of the properties such as fresh and hardened properties, durability, bond strength, fiber reinforced geopolymer and its properties as a repairing agent. This chapter also contains a thorough literatures review of web opened reinforced concrete beam and its various short coming. This chapter also discusses the different retrofitting and strengthening materials that have been used in the repair and rehabilitation of RC damaged and undamaged structural members. Finally, following a thorough examination of the literature, the scope and objectives of the current study were decided, which are also mentioned in this chapter.

Chapter 2

Material Characterization

2.1 Introduction

This chapter includes the properties of all the materials that has been used to develop the repairing materials and the jacketing material, which includes geopolymer mortar (GM), Fiber reinforced geopolymer concrete (FRGC), Portland cement mortar (PCM) and the Fiber reinforced cement concrete (FRCC). This chapter also presents the material that has been used to prepare the beam specimen, repairing work and the strengthening work. The mix proportion of concrete as per the desired strength, used in the preparation of specimen, are obtained by proper mix design. The details of the mix proportion are also presented in this chapter.

In the present study, reinforced concrete (RC) beam specimen were prepared to facilitate the work, intended to assess the efficiency of geopolymeric material in repairing and strengthening of damaged RC structure. The method of design of RC beam with web opening is also included in this chapter.

2.2 Materials

2.2.1 Portland Cement

In the present work Ordinary Portland Cement (OPC 43), as per IS 8112 (1989) has been used. The OPC cement has been procured from Dalmia, India and are tested in the laboratory to determine the standard consistency, setting time, specific gravity and compressive strength. All

the tests are conducted as per the provisions mentioned in the relevant Indian Standard code of practice. The test result of the laboratory experiment carried out on the OPC are presented in Table 2.1. The properties of the OPC are found within the range mentioned in the Indian Standard code of practice.

Table 2.1: Properties of Ordinary Portland Cement (OPC)

Tests Conducted	Indian Standard code of Practice	Test results
Standard Consistency	IS 4031 (Part 4) 1988	27%
Initial Setting time	IS 4031 (Part 5) 1988	90 min
Final Setting time	IS 4031 (Part 5) 1988	310 min
Specific gravity	IS 4031 (Part 11) 1988	3.11
Compressive strength (3^{rd} day)	IS 4031 (Part 6) 1988 IS 8112 :2013	24.89 MPa
Compressive strength (7^{th} day)		34.54 MPa
Compressive strength (28^{th} day)		44.07 MPa

2.2.2 Ultra-fine Blast Furnace Slag

Ultra fine blast furnace slag (UBFS) available indigenously has been used as the main binder in the preparation of geopolymer. UBFS is supplied by Counto Microfine Products, Goa India. The colour of the UBFSS was whitish grey. The morphology was captured by Field emission scanning electron microscope (FESEM) in Sigma 300, IIT Guwahati, India. The physical appearance and the microstructural image of the UBFS can be seen in the Fig. 2.1. The specific gravity of UBFS was determined in the laboratory using le chatelier's flask as per provisions

a) Physical appearance b) FESEM image

Figure 2.1: Ultra-fine blast furnace slag

given in IS 4031-Part 11 1988. The specific surface area of UBFS was evaluated in specific surface area analyser (Autosorb-IQ MP, IIT Guwahati). The chemical composition of UBFS was determined by X-Ray Fluorescence Spectrometer (XRF) is provided by the supplier. The chemical composition and the physical properties of UBFS is presented in Table 2.2.

Table 2.2: Properties of Ultrafine blast furnace slag

	Oxides (% Mass)	UBFS
Chemical Composition	Silicon dioxide (SiO_2)	33.61
	Aluminum dioxide (Al_2O_3)	22.5
	Calcium Oxide (CaO)	34
	Ferric Oxide (Fe_2O_3)	1.31
	Potassium Oxide (K_2O)	-
	Magnesium Oxide (MgO)	6.8
	Titanium Oxide (TiO_2)	0.64
	Sulphur Tri Oxide (SO_3)	0.15
	Manganese Oxide (MnO)	0.17
Physical Properties	Specific surface area (cm^2/g)	30100
	Specific gravity	2.9

2.2.3 Fly ash

Class-F Fly Ash (FA), as per the specification of ASTM C618 (2019), is procured from the nearby cement factory TOPCEM (Guwahati) whose main source is the coal-based power station of NTPC in Bhagalpur, Bihar, India. The FA materials are dark grey in colour. The physical appearance and the FESEM image of the FA can be seen in the Fig. 2.2.

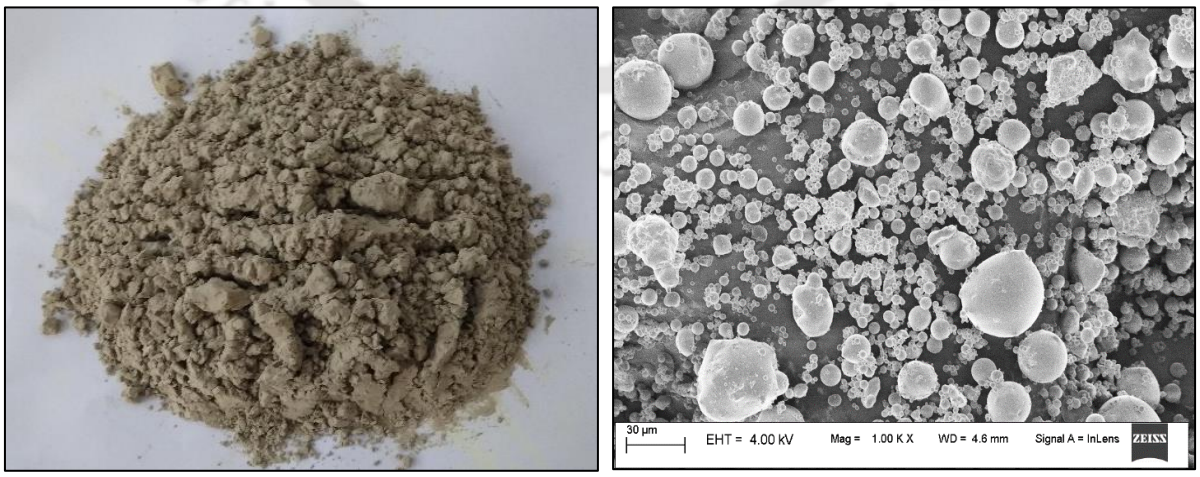

a) Physical appearance b) FESEM image

Figure 2.2: Fly Ash

The chemical composition of FA is determined with the help of XRF (Rigaku Corporation, Japan) at IIT Kanpur. The FESEM image shows that FA particle are spherical in shape (Fig. 2.2. b), whereas the UBFS are angular (Fig. 2.1. b). This spherical nature of FA helps in the mobilization of the particle and filling the micro void spaces created by the angular particle of UBFS, which is the main motive for incorporating FA with the UBFS binder. The fineness of the FA particle is determined be testing sample of FA particles in BET analyser (Autosorb-IQ MP) at IIT Guwahati. The specific gravity of the FA is determined similar to that of UBFS as per IS 4031-Part 11 1988. The chemical composition and the physical properties of FA is presented in Table 2.3.

Table 2.3: Properties of Fly Ash

	Oxides (% Mass)	FA
Chemical Composition	Silicon dioxide (SiO_2)	59.67
	Aluminum dioxide (Al_2O_3)	27.52
	Calcium Oxide (CaO)	2.05
	Ferric Oxide (Fe_2O_3)	5.41
	Potassium Oxide (K_2O)	0.73
	Magnesium Oxide (MgO)	0.79
	Titanium Oxide (TiO_2)	2.36
	Sulphur Tri Oxide (SO_3)	-
	Manganese Oxide (MnO)	0.07
Physical Properties	Specific surface area (cm^2/g)	6290
	Specific gravity	2.23

2.2.4. Alkali activators

To activate the geopolymerization process consisting of UBFS and FA, sodium hydroxide (NaOH) and sodium silicate (Na_2SiO_3) has been opted. The reason of choosing NaOH is that such Sodium based alkali solution gives better mechanical properties (John et al. 2021) than the Potassium based activator and lime based activator. Such activator also possesses greater capacity to liberate silicate ions and aluminate monomers in the solution (Duxon et al. 2007), which leads to better geopolymeric products. While, Altan and Erdogan (2012) reported that combination of Na_2SiO_3 and NaOH as activators leads to 22 % higher strength than geopolymer activated with Na_2SiO_3 and potassium hydroxide (KOH). Moreover, due to issues related to short and long term development of strength and cost effectiveness, Na_2SiO_3 and NaOH are

considered as the most suitable alkali activators for geopolymerization process (Hardjito et al. 2004, Phoo-ngernkham et al. 2015).

In the present study, the GM that that are developed for the repairing work are activated by both NaOH and a combined solution of NaOH and Na_2SiO_3. The NaOH solution is designated as SH while the combined solution of NaOH and Na_2SiO_3 is designated by SHSS solution. Moreover, the SHSS solution being highly viscous is restricted only in the preparation of the GM. Therefore, SH is the only alkali solution employed for the preparation of the geopolymer concrete (GPC) and the Fiber reinforced geopolymer concrete (FRGC).

Commercially available Na_2SiO_3 solution and NaOH pallets Sodium hydroxide pellets are used for the preparation of SH solution and the SHSS solution. The NaOH pallets of 98% purity (Rankem) are purchased from the local vendor and the Na_2SiO_3 solution is supplied by Lova Chemicals Pvt. Ltd, India, which are shown in Fig. 2.3.

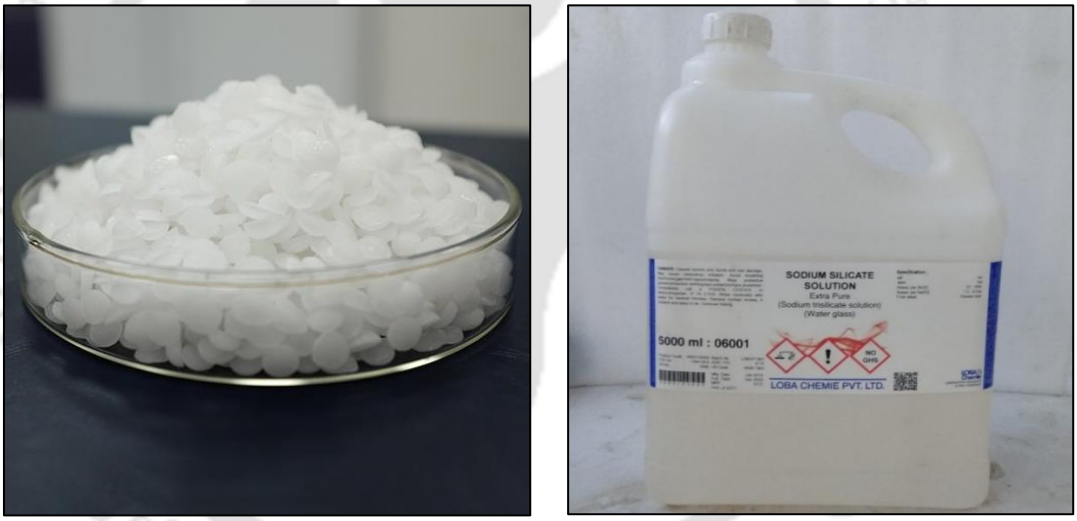

a) Sodium hydroxide pallets b) Sodium silicate solution

Figure 2.3: Alklai activator

The Na_2SiO_3 solution consist of (25% - 28%) SiO_2 and (7.5% - 8.5%) Na_2O and comes in the liquid form which can be directly used in the geopolymer mix but the SH solution is prepared in the laboratory by mixing SH pallets in to distilled water. The SH solution of the required molar concentration used in the GM has been prepared according to previous work reported by Laskar and Talukdar (2017). For example, an 8M solution of SH is prepared by dissolving 320 grams of solid SH pallets in 1 litre of distilled water. In order to obtain superior reactional products with the SHSS solution, the SS and SH solutions are blended one day before the time of mixing, as recommended in previous literature (Elyamany et al. 2018).

2.2.5 Aggregate

The fine aggregate that is used in the present work are the Alluvial river sand procured from a local vendor. These fine aggregate are stored in the laboratory and various tests are conducted to determine its physical properties. The specific gravity of the sand was found to be 2.60 and water absorption equal to 1.7 %, when tested as per the provisions mentioned in IS 2386 Part-3 1963 (1997). The sieve analysis of the fine aggregate is done as per IS 2386 Part I 1963 (1997). The fine aggregate was found to be conforming to zone III with fineness modulus (FM) of 2.24 as per IS 383 1970 (2002). The result of the sieve analysis is presented in Table 2.4.

Table 2.4: Sieve analysis of Fine Aggregate

IS seive size	Weight retained (g)	Percentage weight retained (%)	Cummulative weight retained (%)	Percentage fine (%)	Remarks
4.75 mm	0.0	0.0	0.0	100.0	Zone III as per Table-4 IS 383-1970 FM=2.24
2.36 mm	4.7	0.5	0.5	99.5	
1.18 mm	60.7	6.1	6.5	93.5	
600 μ	245.3	24.6	31.1	68.9	
300 μ	570.0	57.1	88.2	11.8	
150 μ	102.0	10.2	98.5	1.5	
Pan	15.3	1.5	100	0	

Table 2.5: Sieve analysis of Coarse Aggregate

IS seive size	Weight retained (g)	Percentage weight retained (%)	Cummulative weight retained (%)	Percentage fine (%)	Remarks
25 mm	0	0	0	100	20 mm as per IS 383-1970 FM-2.86
20 mm	264.4	13.2	13.2	86.8	
16 mm	351.7	17.6	30.8	69.2	
12.5 mm	580.4	29.0	59.8	40.2	
10 mm	437.7	21.9	81.7	18.3	
4.75 mm	365.7	18.3	100.0	0.0	
pan	0	0	100	0	

Further, well graded angular coarse aggregates of size 20 mm have been used in the preparation of ordinary concrete for casting the beam specimen. While the GPC concrete and FRGC are prepared with coarse aggregate of maximum size 10 mm. The test result specifies that the specific gravity of coarse aggregate is 2.66 and the water absorption of coarse aggregate is

0.7 % as per the provisions of IS 2386 (Part 3) 1963. The result of the sieve analysis of the coarse aggregate is shown in Table 2.5.

2.2.6 Admixture

The geopolymer paste activated by SHSS solution exhibited a very fast setting and poor workability. Thus to improve the setting time, sodium tetraborate (Borax or Boratre), has been used as a retarder to control the setting time in the geopolymer paste and the GM.

To improve the workability of the GPC and the FRGC, a super plasticizer (SP) named Conplast SP430 G8 having specific gravity 1.18 is added in all the mixes. Conplast SP430 is a chloride free, super-plasticising admixture based on selected sulphonated naphthalene polymers. Conplast SP430 disperses the fine particles in the concrete mix, enabling the water content of the concrete to perform more effectively. While Auromix 300 SP, which is a polycarboxylic ether polymer based SP with long lateral chains, has been used in the preparation of FRCC concrete. Auramix 300 combines the properties of water reduction and workability retention.

2.2.7 Steel reinforcement rebar

Steel reinforcement bars of different sizes of grade Fe 500 SD (TATA Tiskon) as per IS 432 Part-1 1982 (1992), possessing yield stress of around 500 MPa are used as longitudinal bar and stirrups for the preparation of RC beams. These bars are tested in the universal testing machine (UTM) as per provisions of IS 1608 2005 (2008). All the rebars possess superior ductile behaviour. The material properties of the various steel reinforcement obtained from the tensile test are presented in Table 2.6.

Table 2.6: Tensile properties of Steel rebar

Diameter (mm)	Yield stress (N/mm^2)	Tensile strength (N/mm^2)	Young's Modulus	Elongation (%)
8	566	676.39		18.67
10	505	626.69	2×10^5	16.67
16	507.35	678.34		18.00

2.2.8 Welded Wire-mesh

Wire mesh has been used in the repairing process which is applied locally in the damaged specimen as shown in the Fig. 2.4. The wire mesh is made up of mild steel (MS) and is procured from local vendor, as per availability in the market. To assess the property of the wire mesh,

Figure 2.4: Mild steel welded wire mesh

coupon specimens of length 254 mm are taken out from the wire mesh are tested in an UTM of 250 kN capacity. The tensile test is conducted as per the provisions given in ASTM A 370 92 (2021). The properties of the tested wire mesh are presented in Table 2.7.

Table 2.7: Properties of MS wire mesh

Properties	Values
Mesh size (mm)	45 × 32.9
Wire Diameter (mm)	1.5
Tensile strength (N/mm^2)	552.25
Yield stress (N/mm^2)	268.15
Elongation (%)	1.55
Density (kg/m^3)	7850

2.2.9 Drop bolt anchor

The drop bolt anchor of diameter 8 mm and length 45 mm has been used to clamp the wire mesh to the surface of the beam. Fig. 2.5. shows the drop bold anchor used in the present work.

Figure 2.5: Drop bolt anchor

2.2.10 Hooked end steel fiber

The FRGC materials and the FRCC material that has been used for the jacketing of repaired beam are developed by utilizing steel fiber. In several literatures it is report that steel fiber significantly improves the tensile strength, flexural strength, toughness and ductility of the concrete. However, the hooked end steel fiber is the most effective in improving the compressive strength and flexural behaviour of the matrix than strain or crimped shaped fiber

Figure 2.6: Hooked end steel fiber

(Rashad et al. 2020). Hence hooked end steel fiber, of aspect ratio 66.67, has been chosen for the preparation of FRGC and FRCC material, as shown in Fig. 2.6. The fibers have been acquired from Fiber Zone India. The properties of the hooked end steel fiber as provided by the supplier is given in Table 2.8.

Table 2.8: Properties of hooked end steel fiber

Steel fiber	Diameter (D) (mm)	Length (L) (mm)	Aspect ratio (L/D)	Ultimate Tensile strength (kN/mm^2)
Hooked end	0.75	50	66.67	1181

2.3 Mix Design

In order to improve the precision of the experimental work, mix design calculation is done to determine the mix proportions to achieve the desired strength of concrete. The mix design was carried out in accordance with the guidelines of the Indian Standard code of practice IS 10262 (2009). The detail of the mix design is presented in Appendix B.

The properties of raw materials required in the mix design calculation were evaluated by conducting laboratory tests as explained in previous section 2.2. The mix design for the concrete mix used in the preparation of the beam specimen was done for a target strength of 20 MPa using OPC 43, which is designated as CM1. Before preparing the fiber based concrete (FRGC and FRCC), suitable mix proportion of GPC mix is determined. The mix proportion of the GPC is calculated with the help of IS 10262 (2009) and the previous published literature Reddy et al. (2018) by adopting several water to solid (w/s) ratio ranging from 0.37 to 0.52. The details of the mix design calculation for a trial mix of GPC is given Appendix A (A3). As soon as the mix proportion of the GPC mix is determined, mix design for PC based controlled mix (CM2), that has been used against the GPC for comparison, is calculated by adopting w/c ratio equivalent to w/s ratio obtained in GPC. To prepare the FRGC and FRCC mix for Jacketing purpose, suitable volume of fiber is incorporated in the GPC mix and the controlled mix CM2 to develop the jacketing material. Table 2.9. shows the mix proportion of the controlled mix CM1 used for the preparation of beam, whose characteristic compressive strength was 28.44 MPa.

Table 2.9: Mix proportion of PCC mix

Mix	Cement (kg/m^3)	Fine Aggregate (kg/m^3)	Coarse Aggregate (kg/m^3)	w/c ratio	Compressive strength, f_{ck} (MPa)
CM1	358	661	1152	0.55	28.44

2.4 Design of Reinforced Concrete beam

In the present study the opening in the RCC beam has been simulated as a post planned opening and hence no special reinforcement has been provided around the opening. The beam specimens are rather designed as a solid beam and opening is provided at different location during the casting of specimens. The reinforced concrete beams were designed as per Indian Standard Code of Practice (IS 456 2000). In the present work the beams were designed as doubly reinforced beam possessing flexural load carrying capacity of 145 kN. The crosssectional was 180 mm × 270 mm and length was 2000 mm. The span of the beams while testing was 1800 mm. Appendix B presents the procedure of the design of an RCC beam. The load carrying capacities of the beam evaluated by theoretical and experimental methods are presented in Table 2.10.

Table 2.10: Load carrying capacity of Solid beam

Theorotical load carrying capacity (kN)	Experimental load carrying capacity (kN)
145.56	174.56

2.5 Closure

A detailed description about the properties of all materials essential for casting, repairing and strengthening of reinforced concrete beams is presented in this chapter. Mix designs were carried out for deciding the mix proportion of concrete for casting of the reinforced concrete beams. The various methods for testing of the materials are mentioned in this chapter. Design of reinforced concrete beams were carried out for deciding the beam size, which is reported in this chapter.

भारतीय प्रौद्योगिकी संस्थान गुवाहाटी
Indian Institute of Technology Guwahati

Chapter 3

Development of silicate activated UBFS based Geopolymer Mortar as Repair material

3.1 Introduction

The deterioration of Portland cement based concrete is inevitable, which requires repair or replacement with time. Various repair materials, which are commercially available like cementitious mortars, polymer-modified cementitious mortars, resinous mortars, etc. have been utilized to rectify the problem. However, sustainable repair materials with reduced carbon footprint have been in huge demand by the construction industry. Over the last few decades' alkali activated geopolymer mortars (GM) prepared from industrial waste materials are emerging as prominent sustainable repair materials due to their several environmental benefits and cost effective features.

Numerous literature has been published on the development of alkali activated mortar with different base material (John et al., 2021). The effect of ultrafine binder has been investigated by Teng et al. (2013), who reported that increased fineness of the binding material accelerates the pozzolanic reactions, thereby enhances the early strength. Moreover, the ultrafine material also contributes as a filler leading to better packing, reduces porosity and also improves the interfacial transition zone (ITZ), which enhances the strength and homogeneity of the concrete (Sengul and Tasdemir 2009). In addition to this it also accelerates the dissociation of Al^{3+} and Si^{4+} ions from the source material and helps in early formation of geopolymeric products leading to fast hardening and improved early strength of geopolymer (Li et al., 2021).

Previous literature reported that Slag/FA based geopolymer undergo remarkable performance at a high temperature (Chithambaram et al. 2019) and more resistant to sulphate and acidic media (Ren et al., 2020). Because of its high calcium concentration, slag features good chloride resistance (Babae and Castel 2018) and shrinkage characteristics (Humad et al., 2019). The key characteristics of this calcium-based geopolymer (slag) are that it sets quickly, gains strength early, and exhibits excellent bonding at the interface (Huseien et al., 2017, Lee et al., 2016). These advantages facilitate the future use of such materials in emergency repairing of bridges, roadways and runway as such cases needs immediate attention to make it serviceable for public convenience. Moreover, calcium-rich geopolymer produces more C-S-H gel, which provides a better adhesion property in the interfacial transition zone (Wang et al., 2021; Hu et al., 2008). Even though slag-based geopolymer is effective as a repair material, its employment in this sector is limited because of its rapid setting and hardening when activated by silicate-based alkali solution (Lee et al., 2016; Saha and Rajasekaran, 2017).

To a certain extent, the setting time can be controlled by adjusting the binder and dosage of the alkali activator. However, such control is limited considering the mechanical strength and longevity of geopolymer (Lee at al., 2016; Laskar and Talukdar, 2016). To eradicate this problem, various superplasticizers (SP) like Naphthalene-based superplasticizer (SP) or Polycarboxylate ether-based SP has been extensively used in the past several years (Nematollahi and Sanjayan, 2014; Criado et al., 2009). But such SP simultaneously causes a strength reduction in geopolymer. Another admixture, sodium tetraborate, which is well documented as a retarder for cementitious material, is also helpful in retarding the setting time in alkali-activated cement (Nicholson et al., 2005).

The ultrafine calcium rich geopolymeric binder suffers from various drawbacks because of its unusual fast setting and loss in workability which restricts its application in many situations. This chapter reports the works performed in the thesis to overcome those limitations by developing enhanced GM mix using mineral additive (Borate). The materials used, methodology for the mortar development and results of the laboratory investigations performed for this purpose are reported in this chapter. The factors considered to determine the optimal mix proportion of GM are FA content, the molar concentration of SH, alkali to binder ratio (a/b) and mass ratio of silicate solution (Mass ratio- Ratio between Sodium silicate (SS) to Sodium Hydroxide (SH) i.e. SS/SH). Besides this, the setting time and workability of the geopolymer mortar are also altered by adding several dosages of retarder. The fresh properties and the hardened properties of several mixes are evaluated by conducting tests like setting time,

workability, compressive strength and flexural strength. Apart from this, the microstructure of geopolymer is investigated by conducting FESEM.

3.2 Experimental Investigation

The main criteria of repair material are the early strength properties and workability of mix. The silicate activated GM possesses poor setting and workability issues. In order to determine an idle mix proportion of GM several adjustments in the ingredient are investigated along with the inclusion of retarder. Different laboratory tests are conducted to ascertain the fresh and hardened properties of GM. The tests included setting time test of the mixes, workability test, compressive strength test and flexural strength. Each mortar mix was tested at 1, 3, 7 and 28 days to access the strength gain behaviour at both early and later ages.

3.2.1 Material

3.2.1.1 Geopolymer mortar

The main binding materials used in the preparation of GM are Ultrafine blast furnace slag (UBFS) and Fly Ash (FA). UBFS has been employed as the primary base material, while FA and borate is incorporated as a mineral admixture in the GM. The properties of the UBFS, FA and borate are furnished in the sub-sections 2.2.2, 2.2.3, 2.2.6 of Chapter 2. In order to study the effect of the mineral admixture and activator solution, in improving the properties of geopolymer, the fineness of the individual binder is kept same throughout the study. The spherical nature of FA helps in the mobilization of the particle and filling the micro void spaces created by the angular particle of UBFS, which is the main motive for incorporating FA with the UBFS binder. The geopolymer synthesis is carried out by using both sodium hydroxide (SH) and a combined solution of sodium hydroxide and sodium silicate (SHSS) solution. The SH solution is prepared by mixing commercially available SH pallets in distilled water one day before mixing of geopolymer. To obtain a better consistency in mixes and to obtain better reaction products, the SHSS solution is prepared 24 hours before the preparation of the geopolymer. Borate, which is usually used as an anti-setting additive in a cementitious binder, is adopted here to deaccelerate the setting property of geopolymer. Sub-section 2.2.4 of Chapter 2 presents the details of the SS and the SH used in the preparation of GM. Local river sand has been used as fine aggregate whose details are given in sub-section, 2.2.5 of Chapter 2.

3.2.1.2 Portland cement mortar

Ordinary Portland cement (OPC 43) 43 was utilized for preparing the Portland cement mortar (PCM). The details of the properties of OPC are presented in sub-section 2.2.1 of Chapter 2. The fine aggregates used in the preparation of PCM was same as used in preparation of GM. Portable water available in the laboratory was used for preparation of PCM mix.

3.2.2 Mix Proportion

The mixes of GM with various adjustments in the ingredients are made to obtain a satisfactory property. The mix proportion of GM has been designed based on the provisions given in IS 1727 – 1967 (2004) and ASTM C311/C311M (2018). In order to determine an idle mix proportion, the effect of the various parameters influencing the properties of GM have been studied and all these mixes are categorised into four different groups. The effect of these various parameters are ascertained by the setting time, workability, compressive strength and flexural strength of the mixes.

Group I: To investigate the effect of different FA content (20 %, 30 %, 40 % and 50 %) by partially replacing UBFS in GM.

Group II: To study the properties of GM activated by SH with varying molar concentrations (8M, 10M, 12M and 14M)

Group III: To study the properties of GM activated with the various mass ratio of SHSS solution (SS/SH=1.0, 1.5, 2.0 and 2.5) with different a/b ratio (0.6 and 0.65) and molar concentration of SH (8M, 10M and 12M)

Group IV: To study the effect of retarder dosage (2 %, 4 %, 6 % and 8 % by mass of binder) in GM.

The various mixes of GM that has been investigated in the present work is presented in Table 3.1. Group-I mixes are primarily examined to identify the amount of FA content necessary to make a workable mix in addition to a satisfactory compressive strength. To achieve this, different quantities of FA, such as 20 %, 30 %, 40 %, and 50 % (by mass per cent), are simultaneously introduced in the GM mix by partially replacing the UBFS content. The maximum addition of FA is limited to 50 %, as an excess quantity of FA in geopolymer demands elevated curing for its geopolymerization process (Kong and Sanjayan 2008, Sengul and Tasdemir 2009), and a minimum of 20 % of FA addition is necessary to bring a notable

change in the mix. For better comparison, the other ingredient constituting the mix is kept constant. These mixes are designated as GM1, GM2, GM3 and GM4.

Table 3.1: Mixes with different parameters of GM

	Mixes	UBFS (%)	FA (%)	a/b	Molarity	SS/SH	Borate (%)
Gr I	GM1	80	20	0.6	10	1.5	-
	GM2	70	30				
	GM3	60	40				
	GM4	50	50				
Gr II	GM5	70	30	0.6	8M	-	-
	GM6	70	30	0.6	10M	-	-
	GM7	70	30	0.6	12M	-	-
	GM8	70	30	0.6	14M	-	-
Gr III	GM9- GM10	70	30	0.6 - 0.65	8M	1	
	GM11-GM12	70	30	0.6 - 0.65	8M	1.5	-
	GM13-GM14	70	30	0.6 – 0.65	8M	2	-
	GM15-GM16	70	30	0.6 - 0.65	8M	2.5	-
	GM17-GM18	70	30	0.6 - 0.65	10M	1.5	-
	GM19– GM20	70	30	0.6 – 0.65	10M	2	-
	GM21-GM22	70	30	0.6 - 0.65	12M	1.5	-
	GM23-GM24	70	30	0.6- 0.65	12M	2	-
Gr IV	GM17_2R	70	30	0.6	10M	1.5	2
	GM17_4R	70	30	0.6	10M	1.5	4
	GM17_6R	70	30	0.6	10M	1.5	6
	GM17_8R	70	30	0.6	10M	1.5	8

Previous literatures report that Slag/FA based geopolymer requires 50 % to 55 % of alkali content to produce a better strength (Madhav at el., 2018). But the quantity of alkali content is dependent on the amount of amorphous content present in the material and the physical characteristics of the particle (John et al., 2021). This factor creates a variation in the demand for alkali solutions in different source materials towards obtaining a standard consistency. From the initial trials, it is observed that UBFS having a large surface area which results in a very dry and stiff mix at an alkali content below 60 %. On the other hand, in SHSS solution the solid content is more, which make the solution denser and hence the upper limit of alkali content is fixed to 65 %.

In Group II, the effect of SH as the sole activator is investigated on the properties of GM. The proportion of UBFS and FA in all the other groups are fixed to 70 % and 30 %. Keeping the binder proportion (UBFS/FA) and the alkali content as constant, the mixes are

activated with SH solution of different molarity (8M, 10M, 12M and 14M), which are designated as GM5, GM6, GM7 and GM8.

The use of SHSS solution as an alkali activator is intended to improve the characteristics of GM since multi-compound alkali solutions may exhibit superior characteristics at low concentrations than SH with high molarity (Lee and Lee, 2016; Farnandez and palomo, 2005). Therefore, the Group III mixes (GM9–GM24) are primarily designed to evaluate the effects of silicate solution, which is accomplished by replacing the alkali activator of Group II with SHSS solution.

SS is one of the most expensive components used in the production of geopolymer. In addition to this, excess silicate concentration affects compaction and degrades workability and strength (Chithambaram et al., 2019). Thus, to acquire an optimum silicate content, the investigation was carried out by considering several mass ratios (SS/SH-1.0, 1.5, 2.0 and 2.5) of SHSS solution. Furthermore, the various SS/SH ratio are also investigated considering different alkali content (60% and 65%), i.e. a/b of 0.6 and 0.65. Besides this, their combined effect is also investigated with a varying molarity of SH (8M – 12M) in the SHSS solution.

The mixes in Group IV are prepared to determine the optimum dosage of retarder. At this stage, the most suitable mix proportion is selected from Group III and is modified by adding various dosages of borate. To investigate the retarding capacity of borate in GM mix, the mix GM17 is chosen for further investigation. This mix is modified by adding different borate content (2%, 4%, 6% and 8%) and are further renamed as GM17_2R to GM17_8R.

In order to study the efficiency of GM, Portland cement based mortar (PCM) mix is also prepared. Table 3.2 presents the mix proportion of PCM. The mix proportion was prepared, as per the recommendations given in IS 1727 1967 (2004), for testing of cementitious mortar. For comparison, the water/cement (w/c) ratios of PCM mix has been kept equal to the water/solid (w/s) ratios of the GM mixes.

Table 3.2: Mix proportion of PCM

Mix	Cement (kg)	Fine Aggregate (kg)	water to cement (w/c) ratio
PCM	100	300	0.4

3.2.3 Specimen Preparation and Curing

The SH solution of the required molar concentration used in the GM has been prepared according to previous literature (Elyamany et al., 2018). The process of preparing the alkali activator (SH and SHSS) is described in sub-section 2.2.4 of Chapter 2. The mineral admixture i.e. Borate, which is in powder form, is pre added directly in to the SHSS solution 24 hours prior to the mixing of geopolymer. This pre added SHSS solution is then thoroughly stirred

a) Addition of ingredients b) Dry Mixing

c) Addition of alkali activator d) Freshly prepared GM mix

Figure 3.1: Preparation of GM mix

using glass rod unless all of the solid particles completely dissolve in the SHSS solution and is kept in a cool place maintaining a temperature of 20 ± 2^0 C. The dry amounts of FA and UBFS are calculated as shown in Table 3.1, and the amount of fine aggregate is taken as three times the total binder (IS 4031: Part 6 2006). In order to prepare the GM based specimens, the following steps are followed in all the mixes:

I. Initially, the dry components of GM (FA, UBFS and Fine aggregate) are mixed by hand for 2 to 3 minutes to get a satisfactory dry mix as shown in Fig. 3.1. (a)-(b).

II. To this dry mix, the alkali solution is added, see Fig. 3.1 (c), and mixed thoroughly for 3 minutes, or until a homogeneous mix is achieved, see Fig. 3.1 (d).

III. Once the freshly prepared GM mix is ready, the workability test is conducted immediately with the help of flow table.

IV. Upon completion of the workability test, the GM mix is immediately filled in the respectively pre oiled moulds for preparing specimens.

To fill the mould, the mortar mixes are placed in two successive layers in the cube mould and the prism mould. However, to ensure proper compaction each layer is vibrated for 2 minutes

a) Casting of prismatic specimen

b) Cast cube specimen

c) Curing of cube specimen

Figure 3.2: Preparation of mortar specimen

in a portable vibrator. The cast moulds were then kept undisturbed for 24 hours in a safe place as shown in Fig. 3.2 (b), till the time of demoulding. After completion of 24 hours cast specimen are demoulded are then immersed in water tank for curing at an ambient temperature ($22^0 \pm 2^0$C), as shown in Fig. 3.2. (c).

3.2.4 Experiments

The setting time of the geopolymer paste is determined by performing setting time test using Vicat apparatus in accordance with IS 1727-1967 (2004), equivalent to ASTM C311/C311M-13 (2018). The geopolymer paste used in the study has been prepared separately for each mix by adding the alkaline solution to the dry binder mix. The mixing of paste is continued for 4 to 5 minutes till a light grey homogenous paste is achieved. The paste is then poured into the Vicat mould and initial and final setting time are determined, as shown in Fig. 3.3.

Figure 3.3: Setting time test using Vicat apparatus

To measure the flow property of the geopolymer mortar, a flow table test is performed immediately after the freshly produced GM mix is ready, as specified in ASTM C1437 (2020) and ASTM C230M (2021). A flow table apparatus is shown in the Fig. 3.4. The flow characteristics of the freshly prepared mix are represented by the Flow Index (FI).

$$FI = \frac{FD - ID}{ID} \times 100 \qquad (3.1)$$

where, FI= Flow index (%); FD = Final diameter after jolting; ID= Initial Diameter

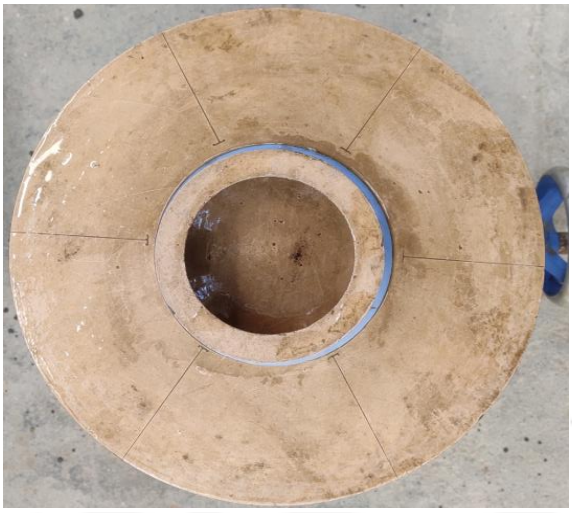

Figure 3.4: Flow table Test apparatus

The compressive strength of GM is evaluated using a 50×50×50 mm cube as per ASTM C109/C109M (2021), while the flexural strength is examined using prisms of size 40×40×160 mm as per specification of ASTM C348-14 (2014). The cube specimen is tested in a compressive testing machine at a loading rate of 0.9 kN/sec, and the prisms are tested in a universal testing machine using the centre point loading method at a loading rate of 2.64 kN/sec, as shown in Fig. 3.5.

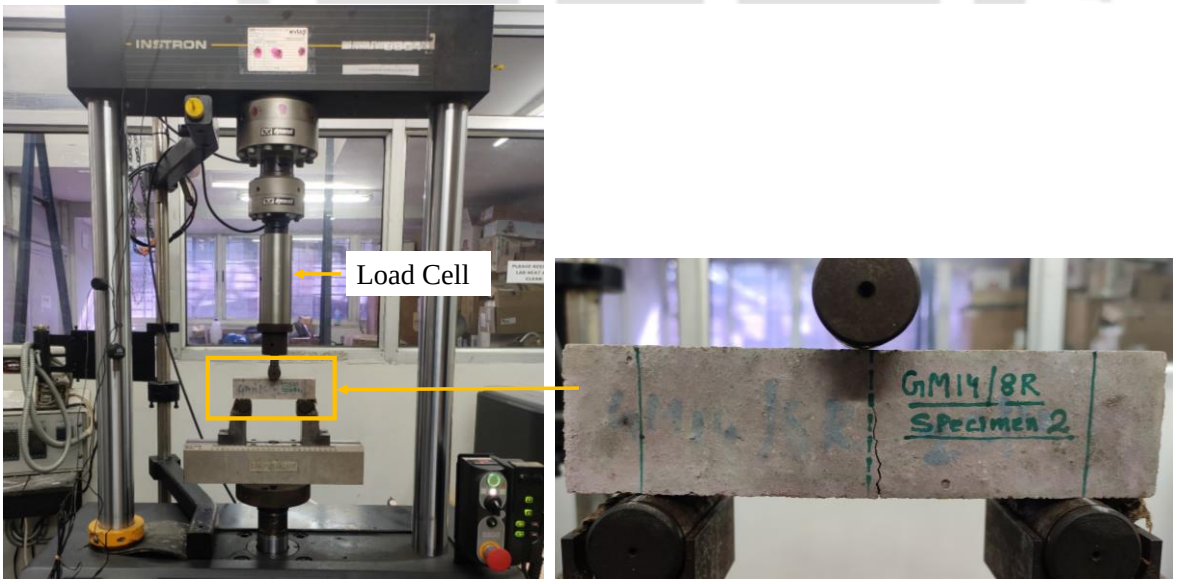

a) Test setup b) Failed Specimen

Figure 3.5: Flexural Test of GM prism

The flexural strength (S_r) of the prism is calculated as

$$S_r = 0.0028P \tag{3.2}$$

where, P= Total maximum load withstand by the specimen.

In order to investigate the microstructure of GM, samples are collected from the tested specimen at various ages. Powdered samples are prepared by crushing and sieving with 75 microns IS sieve. The powered sample is completely dried by keeping it in an oven at 105^0C for 24 hours to avoid any moisture content. The morphology and the texture of microstructure are then viewed under FESEM.

3.3 Experimental Observation

The ability of mortar has been investigated by several laboratory experiment conducted on the fresh and hardened state of the GM and PCM.

3.3.1 Geopolymer mortar

In view of selecting an idle mix of GM for its application as a repairing material, effect of several parameters influencing the properties of GM has been studied in detail.

3.3.1.1 Effects of FA content in UBFS based Geopolymer mortar

Setting time and workability

Preliminary tests (Gr I mix) are carried out predominantly to acquire the desired quantity of FA, which can improve the fresh property of UBFS based GM. The effect of different FA content on the fresh state of mortar has been determined by test results obtained from setting time and flow table test, presented in Fig 3.6. It is observed that the addition of FA by 20 % in the mix GM1 produces a very viscous mix with lesser fluidity and exhibited the lowest FI of only 14 %. With successive increment in the FA content by 10 % in the mixes GM2, GM3 and GM4, fluidity of the mixes eventually increases, resulting in an increase in the value of FI by 38 %, 42 % and 66 %, respectively.

This rapid rise in fluidity in the mixes with increased quantity of FA is caused by the increase in the fraction of spherical FA particles in the total binder. With increase in FA quantity, the spherical nature of FA facilitates better mobility in the alkali environment (Chithambaram et al., 2019), thereby increases the spread of the mix. Furthermore, the

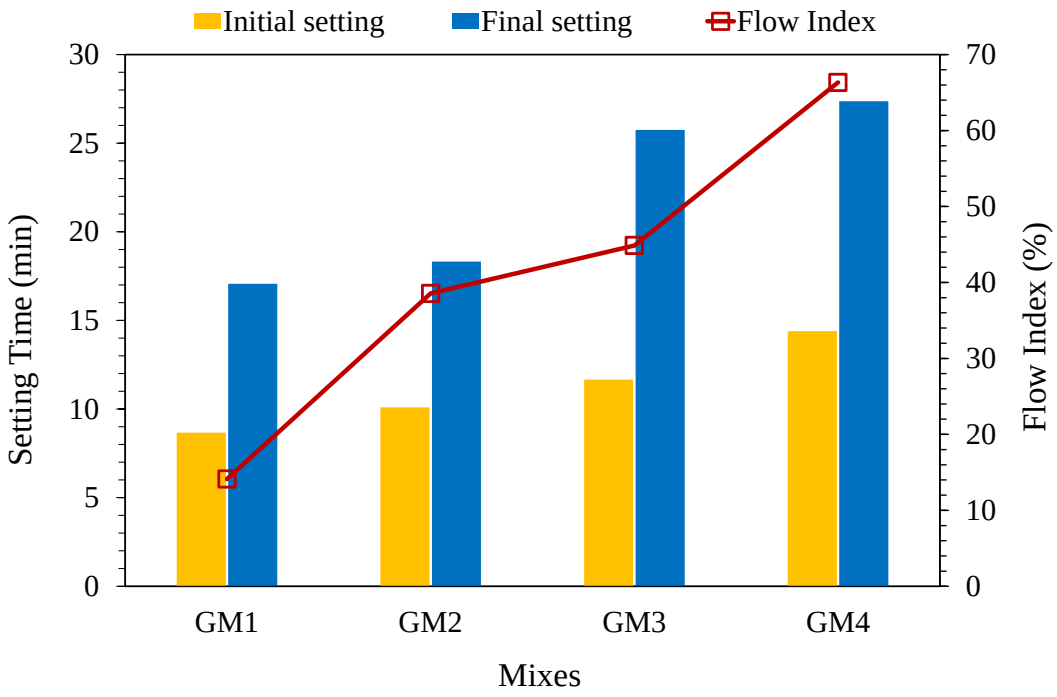

Figure 3.6: Effect FA content on Setting time and Workability of GM

spherical shape of FA reduces the total surface area of the binder, allowing more availability of fluid particles, which helps in improving the flow characteristics of the mortar mix. The geopolymer paste sets relatively quicker due to the high calcium content of UBFS and its fineness (Babaee and Castel 2018). The mix GM1 with only 20 % FA exhibited the shortest initial and final setting time of 8.67 and 17.07 minutes, respectively. This fastest setting of the mix GM1 is due to the calcium concentration and high surface area of the UBFS particle, which together enhanced the geopolymeric reaction. However, it is observed that as more FA quantity is added in the later mixes; the setting time gradually increases. This is attributed to two main reason. Firstly, with substitution of UBFS by the Class-F FA, the calcium concentration in the total binder becomes low, this slows down the formation of C-S-H gel (Rattanasak et al., 2011). Secondly it is well documented in literature (Li et al., 2021) that fineness of the binder significantly influences the dissociation of Al^{3+} and Si^{4+} ions from the AS material, which then takes part in geopolymerization. With inclusion of more FA, which is comparatively coarser, the fineness of the overall binder reduces causing a retardation in the geopolymerization process thereby improves the fast setting of geopolymer.

Furthermore, it can be observed that the influence of FA in enhancing the setting is more apparent in mixtures (GM3 and GM4) which comprises of more than 30 % FA content. In the mix containing 40 % FA (i.e. GM3), the initial and final setting times increased to 11.67 min and 25.75 min, respectively. This indicates that a sufficient quantity of UBFS (above 30%)

has to be replaced by FA for a better setting property. Further increase in the FA content exhibits a comparable increase in the setting time but largely improves the workability of the mix, as seen in mix GM4.

Mechanical properties

The compressive strength of all mixtures has been measured at different ages (1, 3, 7, and 28 days) and is computed by taking the average compressive strength of three mortar cubes. The influence of FA content on compressive strength can be readily seen in the results shown in Fig. 3.7. The mix GM1, which contains a maximum quantity of UBFS (80 %), exhibits a faster rate of strength development at the early stage which eventually slows down with time. The strength development on the 1st day, 3rd day and the 7th day of the mix GM1 is approximately 79 %, 93 % and 97 % of the ultimate strength (28th day). With the incorporation of additional FA in later mixes, this pattern ultimately subsides. The early strength gain behaviour is more prevalent in mix GM1 and GM2, which includes 80 % and 70 % of UBFS, respectively. This early gain in compressive strength is attributed to the role of calcium in the early formation of C-S-H gel, as witnessed in UBFS-dominated mixes. while, the formation of N-A-S-H gel in these mixes (GM1 and GM2) are less due to a lesser quantity of FA. Early development of C-S-H gel give rise to better microstructure and thereby enhances the strength (John. et al., 2021).

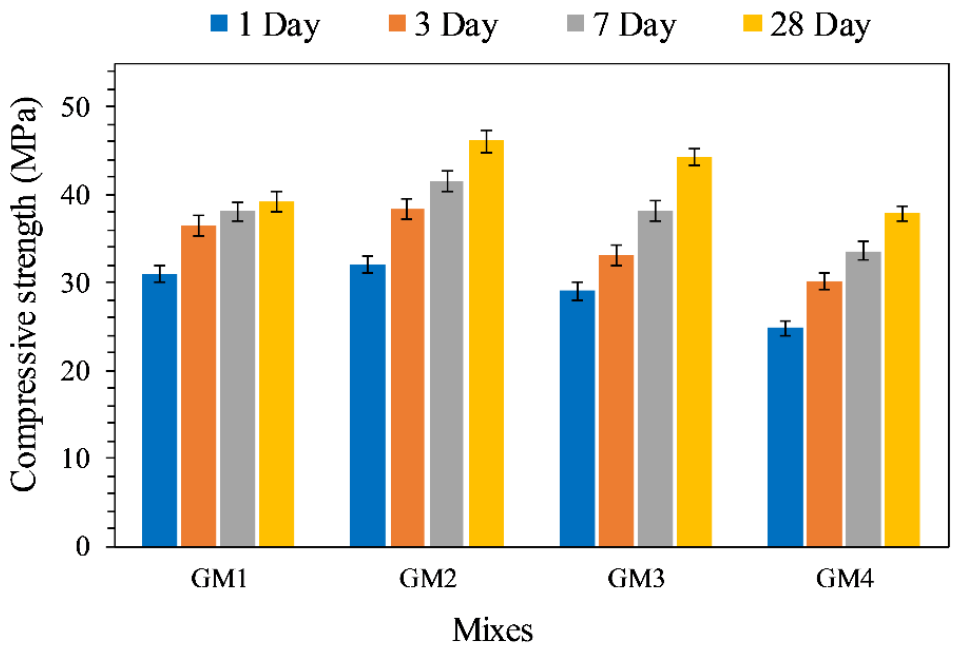

Figure 3.7: Effect of FA content on Compressive strength of GM

The inclusion of FA in various quantity played a major role in the ultimate strength of GM. As previously stated, the large quantity of UBFS (80 %) makes the mix highly viscous, resulting in entrapped air voids in mixes. These minute air voids make the mix porous resulting in loss of strength, as shown by mix GM1 (39.20 MPa). Moreover, it is also reported in the literature that high slag content in geopolymer produces shrinkage cracks in the microstructure, which results in reducing the ultimate strength (Jang and Lee 2014). When the FA content is increased to 30 %, the maximum compressive strength of 46.13 MPa is obtained, which is attributable to the better formation of reaction products and yield better strength. But when the FA content surpasses 30 %, it introduced a negative impact on the compressive strength. The mix GM3 and GM4, which includes a FA content of 40 % and 50 % of the total binder, exhibited a reduced compressive strength of 44.28 MPa and 37.87 MPa on the 28th day (see Fig. 3.7). This indicates that an optimum quantity of FA (30 %) and UBFS (70 %) is required to obtain the best mechanical properties in GM.

From the above discussion, it is seen that FA used as a mineral admixture played an essential role in improving the characteristics of the UBFS binder. The spherical nature of the FA particle which retains during alkali activation helps in dispersing the particle, and the smaller FA particle also act as a filler (Yang et al., 2018) in between the voids of UBFS particle. But the mechanical strength development is mainly governed by rate of formation of the reaction products, which gets reduced upon increasing the FA content. This is because as the FA quantity increases, the reaction products synthesized upon activation of UBFS is also reduced while the development of N-A-S-H produced by FA increases. But as the curing is done at an ambient temperature, the formation of N-A-S-H gel is not as fast as the C-S-H gel. Because of this, lesser compressive strength is gained by the mixes (GM3 and GM4) containing higher FA content. Similar results were also reported by Berna et al. (2013) who reported that the N-A-S-H gel generated by FA is more porous and includes a strong alkaline pore solution which is susceptible to carbonation. Whereas C-A-S-H gel contains lesser pores than N-A-S-H gel, thereby reduces the risk of carbonation and contributes to the improvement of the ultimate strength.

3.3.1.2 Effect of Sodium Hydroxide solution

Setting time and workability

Fig. 3.8. depicts the influence of molar concentration of SH solution on setting time and workability of the mixes in Group II. Test results indicate that the UBFS/FA-based geopolymer

activated by SH alone exhibits relatively better setting time and workability rather than its mechanical property.

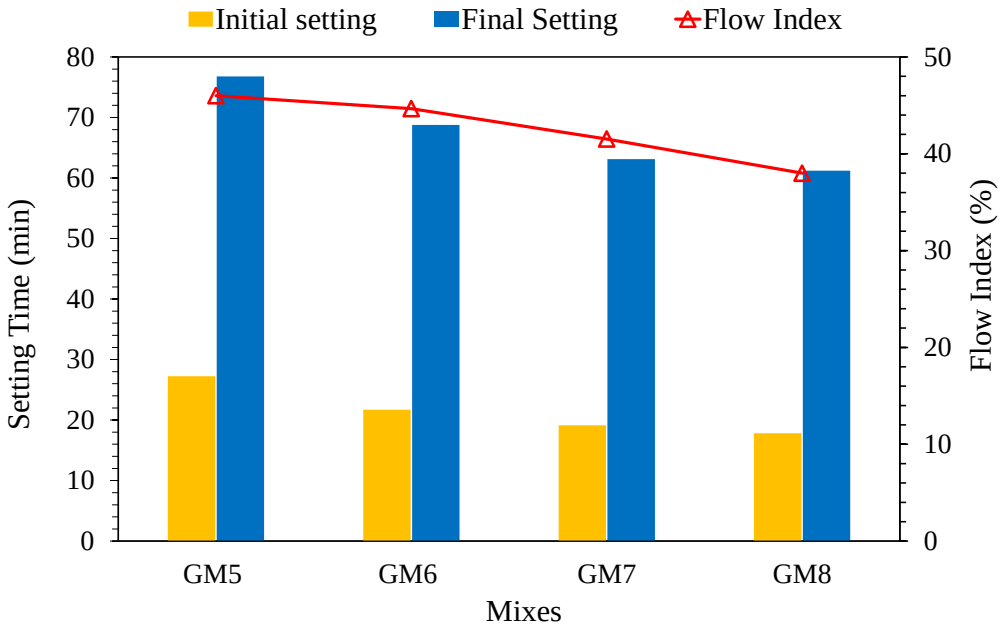

Figure 3.8: Effect of SH on Setting Time and Workability of GM

The geopolymer paste (GM5) prepared with 8M SH exhibits an initial and final setting time of 27.25 min and 76.78 min. This setting time reduces with further increment in the concentration of SH. When the molarity of SH is increased to 14M as shown in mix GM8, the initial and final setting time drops down to 17.82 min and 61.20 min. The same aspect is also noticed in the workability of mixes. Nonetheless, it is significant to highlight that SH as an alkali activator shows better results in fresh properties compared to the mix activated by SHSS solution in Group I. Literature reports that aluminosilicate precursors can dissociate better in an alkali solution consisting of SH (John et al., 2021; Singh et al., 2015). With the increase in the concentration of SH, more Na^+ and OH^- ions get available for leaching of Al^{3+} and Si^{4+} ions from FA and UBFS, which takes part in geopolymerization (Elyamany et al., 2018). This ultimately expedites the reaction process in the pastes and results in the early setting of the geopolymer.

On the other hand, SH being a less dense solution improves the consistency of the mortar and results in better workability compared to mixes activated by the SHSS solution. The mix GM5 activated with 8M SH exhibits a FI of 46 %. But with the increase in the molar concentration in SH solution, the FI of the mixes decreases progressively. From the test result, it can be determined that FI decreases by 3 % for every 2M increase in the concentration of

SH. This is due to the fact that as the molar concentration in the mix increases, so does the overall solid content, resulting in a loss of fluidity. This reduction in fluidity causes difficulty in particle mobilization and, as a result, affects the FI of mortar.

Mechanical Properties

The mechanical characteristics of GM activated by SH solution are not as impressive as those of fresh properties. Fig. 3.9 shows that the development of compressive strength of GM at various ages activated by SH of various molar concentrations. While the effect of SH on the development of flexural strength is reported in Table 3.3.

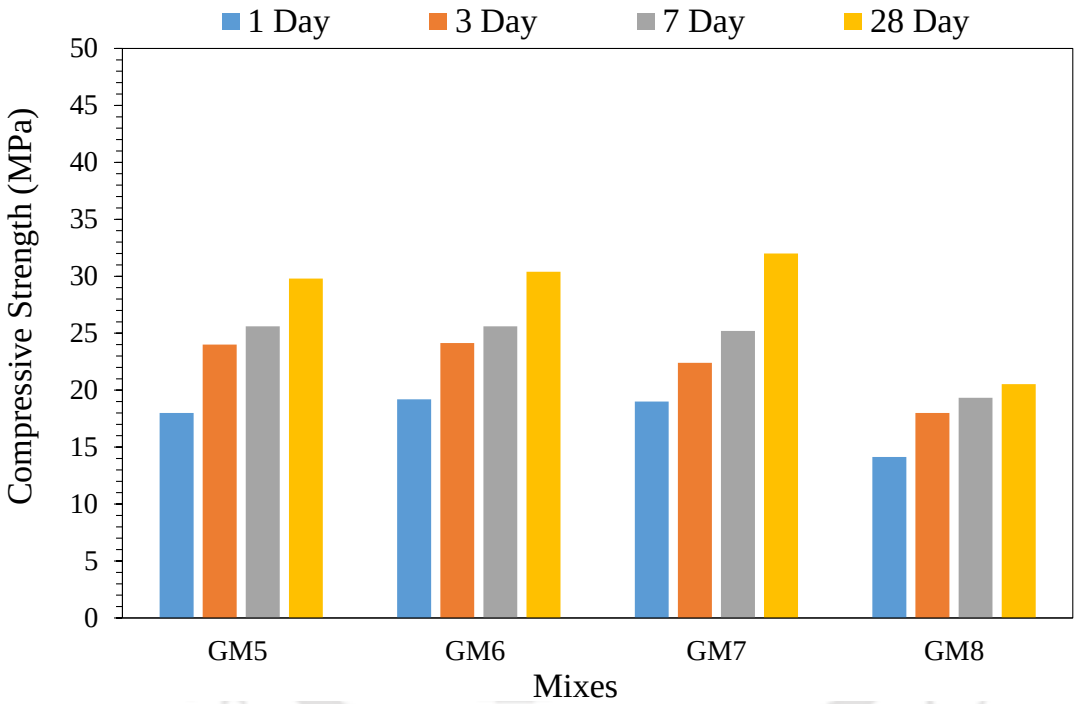

Figure 3.9: Effect of SH on Compressive strength of GM

The mechanical strength of GM is mainly provided by the development of reaction products after geopolymerization. While, the formation of the geopolymeric products depends on the dissociation of oxides present in the source material and is strongly affected by the pH value or the alkalinity of the activator, as reported in the previous work (Fernandez et al., 2005). The Mix GM5 activated with an 8M alkali solution has an ultimate compressive strength of 29.80 MPa. With an increase in the concentration of SH to 10M (GM6), compressive strength steadily increases to 30.40 MPa, which indicates the participation of SH concentration towards significant development in the compressive strength of GM. However, it can be observed that

variation in the molar concentration of SH, has no remarkable improvement in the flexural strength of GM (see Table 3.3).

Table 3.3: Flexural strength of GM mix activated by SH (Group II)

Mixes	Flexural strength, S_r (MPa)	
	7^{th} day	28^{th} day
GM5	3.83	5.13
GM6	4.20	5.41
GM7	4.99	5.69
GM8	4.21	4.88

The mix GM7 activated by 12M SH solution achieves the highest compressive strength of 32.0 MPa and flexural strength of 5.69 MPa. But as the molar concentration is further increased to 14M in the mix GM8, both compressive strength and flexural strength drops down to 20.53 MPa and 4.88 MPa. This declination of strength is attributed to the fact that in 14M of SH solution, the alkali solution becomes highly concentrated due to mixing of large content of solid SH pallets. Since the alkali content is kept fixed to 0.6b in all the mixes of Group II, the total solid content in the mix activated by 14M SH becomes very high. This loss in fluidity makes the mix very stiff and viscous and creates entrapped air bubble during compaction and finishing (Wang et al., 2015), which makes the specimens porous and ultimately reduces the strength. Moreover, it is also observed that the mix GM8 containing 14M SH exhibits excessive efflorescence at the surface of all the specimens within 24 hours of the cast. This ultimately causes a strength reduction in the mix when activated by SH concentration of 14M.

3.3.1.3 Effect of combined alkali activator solution

Setting time and workability

Fig. 3.10 represents the effect of mass ratio of SHSS solution, with an a/b ratio of 0.6, on the setting time and workability of GM. The plot is categorized into three sections indicating mixes examined under varying molar concentrations of SH (8M, 10M and 12M). In addition to this, the same mixes are also investigated by considering an a/b ratio of 0.65, which is represented by Fig. 3.11.

The test results reveal that the addition of SS with the SH solution produces a substantially faster setting in all geopolymer pastes of Group III. This quick setting has already been reported in the literature, where a rapid setting is observed in the calcium-rich binder

(Slag) when activated by silicate (Lee et al., 2016; Saha and Rajasekaran, 2017). However, in the present study, due to the use of ultrafine nature of UBFS, it has further enhanced the setting property, resulting in a faster setting time than those reported in the previous works of literatures.

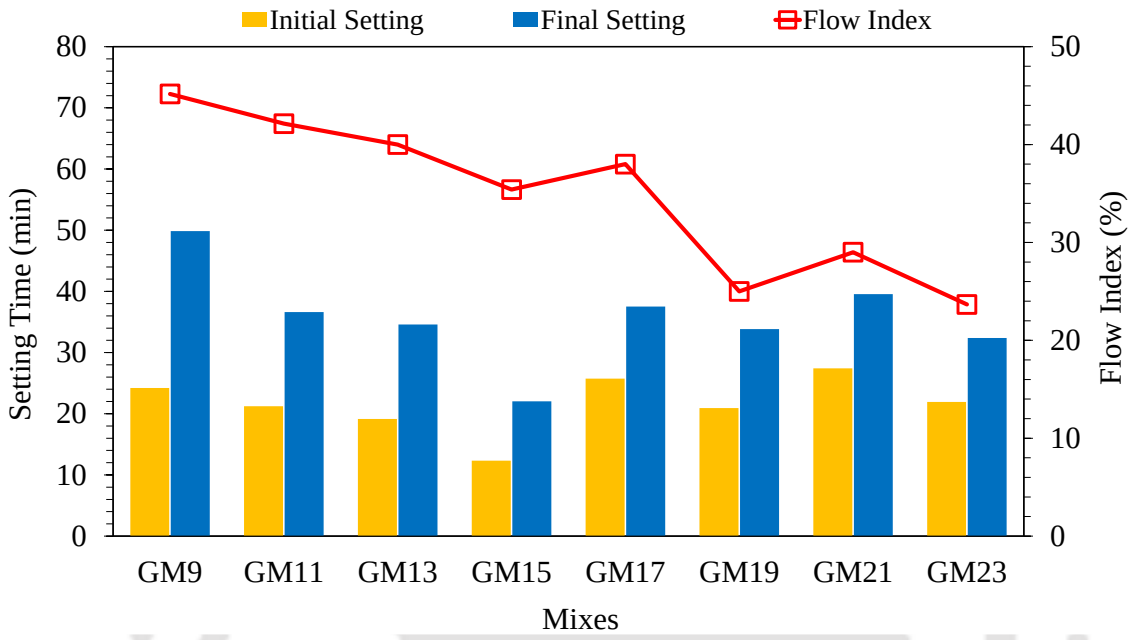

Figure 3.10: Effect of SHSS in the Setting Time and Flow index of mixes with a/b-0.6

As already discussed in the previous section 3.3.1.2, the setting time of mixes, activated with only SH, reduces with the rise in molar concentration. But this phenomenon is completely reversed in the case of mixes (in Group III) activated by SHSS solution. Up on activated by SHSS solution of 8M, initial and final setting time of GM11 is found out as 21.23 min and 36.63 min. As the molar concentration is increased to 10M in SHSS, the initial and final setting time of mix (GM17) slightly increased to 25.73 min and 37.53 min. The setting time is further delayed as the concentration of SHSS increased to 12M, as shown in Fig. 3.10. Similar results are also reported by Rattanasak et al. (2011). This is attributed to the fact that UBFS has a large quantity of CaO (34.0 %). At a lower concentration (8M) of SHSS solution, the free Ca^{2+} ions readily combine with silicate to form C-S-H gel. The structure of these C-S-H gel are open and pervious in nature which allows greater movement of alkali/water through the gel. These open and porous structure of C-H-S gel provides more reaction sites which aid in further development of gel, thereby reducing the setting time.

On the other hand, as the molar concentration in the SHSS solution increases it significantly affects the dissociation of AS material. The molar concentration of the SHSS

solution, increases the Na^+ and OH^- in the solution which enhances the leeching of Al^{3+} and Si^{4+} ions and hinders the dissociation of Ca^{2+} ions in the solution. The dissociation of AS precursor in alkaline environment is a geopolymeric reaction and is comparatively slower than the dissociation of Ca^{2+} ions which is a hydration reaction of calcium ions (Elyamany et al., 2018; Mallikarjuna Rao and Gunneswara Rao, 2015). At higher molar concentration the hydration reaction is hindered by the geopolymeric reaction, which is comparatively slower and as a result of which the setting time of the mixes with higher molarity in SHSS solution also increases.

The SHSS solution operates as both viscous and watery due to the addition of a highly dense SS solution. Mixing this highly viscous SHSS solution with the ultra-fine binder (UBFS) causes a significant loss in workability compared to mixes activated by only SH solution. The FI of the mix GM11 activated by 8M SHSS solution, which is equivalent to GM5 (activated by SH), reduces to 42.14 %. With increases in molar concentration to 10M and 12M, the FI further decreases to 38 % and 29 %. This drastic drop in fluidity is attributed to the increase in the dense nature of SHSS solution due to the addition of a highly concentrated SH solution with the SS solution.

On the other hand, changing the a/b ratio to 0.65 (see Fig. 3.11), results in a considerable change in the fresh characteristics and strength of the geopolymer. When the alkali content is increased in the mix GM12 (a/b=0.65), which is comparable to GM11 but only differs in the a/b ratio (0.6), demonstrated a modest rise in the initial and final setting time of 23.20 min and 37.2 min, respectively. But at the same time exhibits a remarkable improvement in the flow, pertaining to more alkali solution. The FI obtained for GM12 is 61.33 %, is approximately 45 % greater than the FI of the GM11. This enhancement in the setting and fluidity can be attributed to the fact that as the alkali content in the mix increases, the consistency of mixes also improves. This increases the dispersion capacity of the particles, which delays the formation of the bond between the geopolymeric products, thereby delays the setting time and contributes in improving the flow of GM. At a higher molar concentration of SHSS solution (i.e. 10M and 12M), a similar trend is observed in between the mixes with an a/b ratio of 0.6 and 0.65, as compared from the Fig. 3.10 and Fig. 3.11.

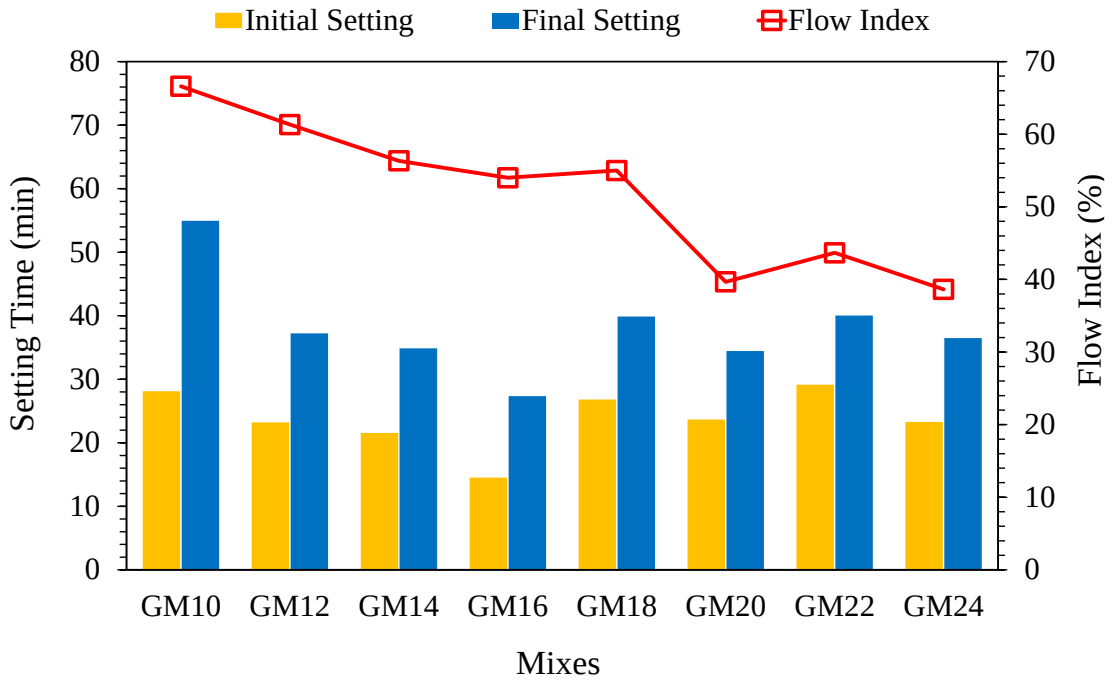

Figure 3.11: Effect of SHSS in the Setting Time and Flow index of mixes with a/b-0.65

From test results, it is observed that setting time and workability of a particular mix reduces with more inclusion of SS in the SHSS solution. The mix GM9 activated by a SS/SH ratio of 1 exhibited an initial and final setting time of 24.20 min and 49.85 min, respectively. While, the FI of the particular mix (GM9) is obtained as 45.17 %. With the increase in the SS/SH to 1.5 (Mix GM11), the initial and final setting time reduces to 21.23 min and 36.36 min, and the FI reduces to 42.14 %. Further reduction in the setting time and FI is observed with further increase in the SS/SH ratio to 2 and 2.5. This implies that the presence of excess silicate in the SHSS solution, has a negative effect on the characteristics of GM. This is because, in the case of a high SS/SH ratio, the SiO_2 concentration in the SHSS solution also increases, which accelerates the setting time of the pastes caused by the fast geopolymerization. Moreover, the viscous nature of the SS solution presents a barrier in the dispersion of particles, causing the geopolymer to lose its fluidity. As already observed that in the case of SHSS solution, the setting property improves with a higher molar concentration. However, no such improvement is noticed in the case of workability. The trend of reduction in the FI becomes more destructive in highly concentrated SHSS solutions, provided the alkali solution content increases.

Mechanical Properties

The application of SHSS solutions in the GM results in a significant improvement in mechanical strength. Fig. 3.12 and Fig. 3.13 depicts the compressive strength of GM activated

by SHSS solution with a/b ratio equal to 0.6 and 0.65. Whereas the flexural strength on the 7th day and 28th day of the mixes activate by SHSS solution are incorporated in Table 3.4. From the test results (shown in Fig. 3.12 and Fig. 3.13), it can be determined that GM activated by SHSS solution exhibits a compressive strength of approximately 32 % more than the mix activated by SH alone. This is because, during the geopolymerization process of mixes activated by SHSS solution, more Si^{4+} ions are available in the SHSS solution, which takes part in geopolymerization. This increases the formation of reaction products and gives rise to enhanced mechanical strength (Mallikarjuna Rao and Gunneswara Rao, 2015). The effect of SHSS solution in the development of compressive strength in the 1st day, 3rd day and 7th day of the mixes (irrespective of molar concentration) is approximately 64 %, 86 %, and 91 % of the ultimate strength (28th day). Whereas, in the case of flexure, 70 % - 80 % of the ultimate flexural strength is achieved on the 7th day.

Table 3.4: Flexural strength of GM mix activated by SHSS (Group III)

Mixes	Flexural strength, S_r (MPa)		Mixes	Flexural strength, S_r (MPa)	
	7th day	28th day		7th day	28th day
GM9	4.05	5.25	GM17	4.95	6.81
GM10	3.95	4.70	GM18	4.57	5.60
GM11	4.67	5.46	GM19	4.76	6.16
GM12	4.11	4.57	GM20	5.27	5.69
GM13	4.29	4.90	GM21	6.25	6.81
GM14	4.48	5.23	GM22	5.04	6.07
GM15	4.21	4.60	GM23	5.79	6.63
GM16	3.89	4.20	GM24	5.46	6.16

From the test result, shown in Fig. 3.12 and Fig. 3.13, it is evident that high compressive strength can be achieved by utilizing an optimal SS/SH ratio and alkali content. However, the mass ratio of the SHSS solution has no significant effect on the flexural strength of GM. At a minimum silicate content (SS/SH =1), as adopted for the mix GM9, compressive strength of 37.73 MPa is achieved on the 28th day. When the SS/SH ratio is increased to 1.5 (GM11), the compressive strength of the mix increases to 43.73 MPa. As the ratio of SS/SH reaches 2 (GM13), a comparable compressive strength of 43.07 MPa is achieved, which is nearly equal to the compressive strength of GM11. Meanwhile, for different SS/SH ratios, the flexural strength of the mix GM9, GM11 and GM13 are obtained as 5.25 MPa, 5.46 MPa and 4.90

MPa, respectively. As the SS/SH ratio reaches 2.5 (GM15), a negative effect in both compressive and flexural strength can be noticed.

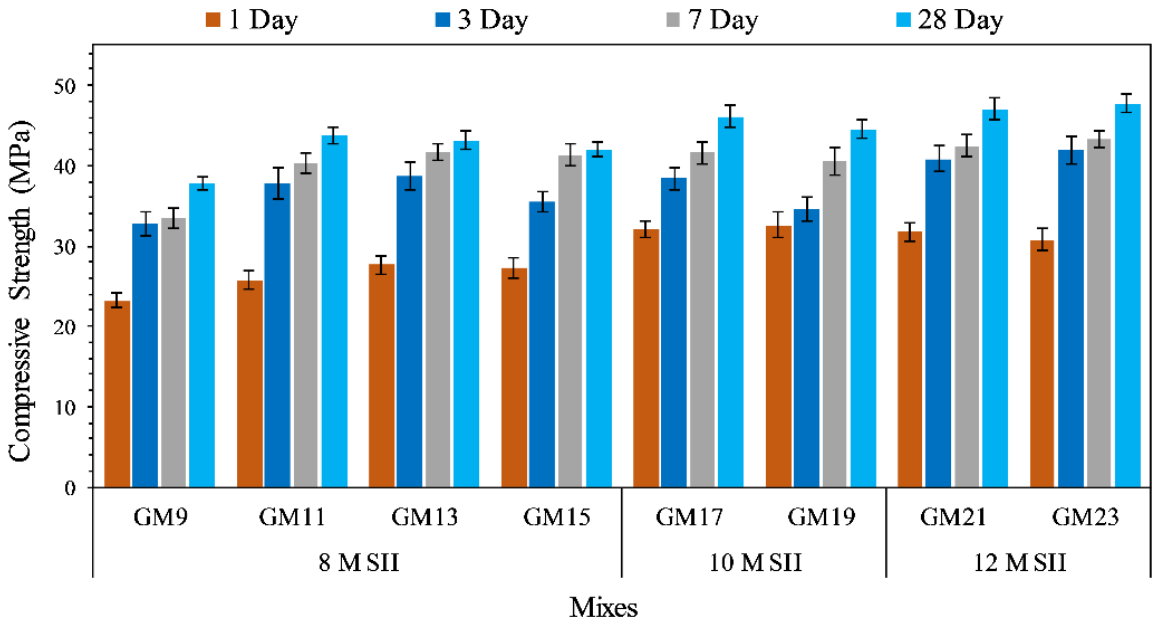

Figure 3.12: Effect of SHSS solution in the compressive strength of GM with a/b-0.6

This degradation at a higher mass ratio of silicate is attributed to excess silicate content affecting the structure of geopolymer (John et al., 2021; Chi and Huang, 2013). The optimum mass ratio for geopolymer depends on the SiO_2 content of the source material, which dissociates in an alkali media to liberate Silicate ions. A higher value of SS/SH ratio may lead to excess availability of silicate ions in the solution, which ultimately affects the geopolymer structure, resulting in to reduced compressive strength. From this, it is clear that the mass ratio in SHSS solution must have a balance with the SiO_2 content of the source material to produce better geopolymerization products.

Furthermore, when these mixes are activated by a higher a/b ratio (0.65), a slight reduction in the compressive strength and flexural strength is observed, as exhibited by the mix GM10, GM12 and GM14 (see Fig. 3.13 and Table 3.4.). For example, the mix GM11, containing 60 % alkali content, exhibited a compressive strength of 43.73 MPa and flexural strength of 5.46 MPa. When the mix is further modified (GM12) with a higher alkali content (65 %), the compressive and flexural strengths fall to 42.93 MPa and 4.57 MPa, respectively. But, at higher alkali content, a significant improvement in the fluidity of the mix is observed as the FI increased from 42.14 % to 61.33 %. The decrease in strength properties is caused by

the increase in water content in SHSS solution, which inhibits the geopolymerization reaction. A similar trend is also followed by other mixes, which differ in the mass ratio. Although the modification in the a/b ratio from 0.6 to 0.65 results in a minor change in the strength qualities, it results in a significant increase in the fluidity of the GM.

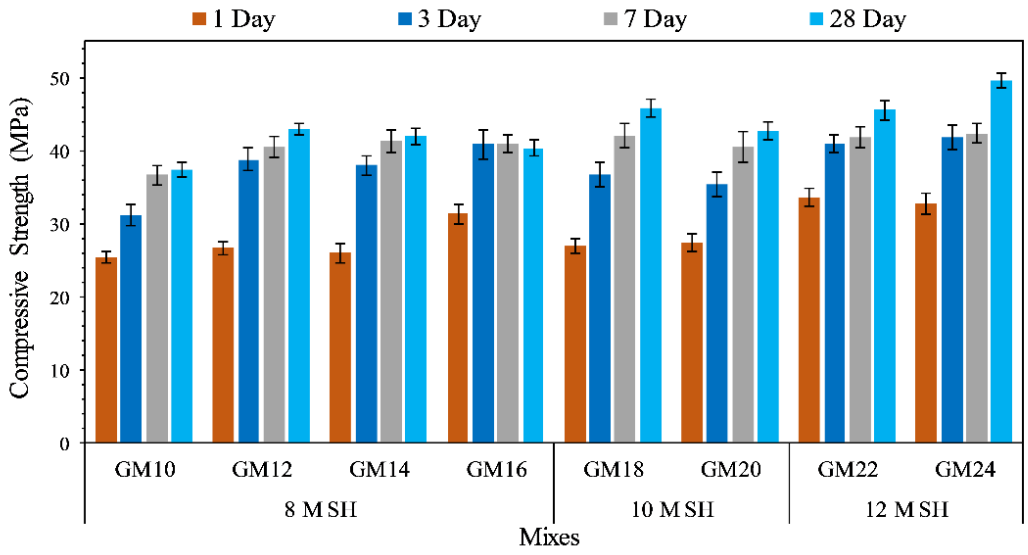

Figure 3.13: Effect of SHSS solution in the compressive strength of GM with a/b-0.65

The effect of higher molar concentration in SHSS solution is studied by restricting the SS/SH ratio within a range of 1.5 and 2. When the molar concentration in the SHSS solution is increased to 10M, more improvement in the compressive strength and flexural strength is observed. The mix GM17 activated by 10M SHSS solution and mass ratio of 1.5 exhibits compressive and flexural strength of 46.13 MPa and 6.53 MPa, respectively. But with a change in the SS/SH equal to 2, as shown by mix GM19, a reduction in the compressive strength (44.53 MPa) is observed. As the molar concentration in SHSS solution reaches 12M, maximum compressive strength of 49.60 MPa is achieved but with an a/b ratio of 0.65. whereas the mix (GM21) with an a/b ratio of 0.6 shows a lesser compressive strength of 47.0 MPa. This is due to the fact that at 12 M, the SHSS solution becomes very viscous and containing a huge amount of solid. The water content in the 12M SHSS solution, corresponding to an a/b ratio of 0.6, is not sufficient to provide a standard consistency in the mix. Due to this reason, there exists a difficulty in obtaining a homogeneous mix and proper compaction, which ultimately affected the compressive of GM.

Further it is also observed that the effect of concentration of the SHSS solution also has an influence in the matrix of the GM cubes as shown in the Fig. 3.14. The mix GM11 with 8M,

exhibits a light greenish colour as seen in the Fig. 3.14 (a). Whereas mixes with 10M, have a homogeneous dark greenish colour, which also indicated better geopolymerization as shown in Fig. 3.14 (b) and (c). While, the mixes activated by 12M are comparatively light in colour and white efflorescence products are also identified in the core of the cubes prepared by GM22 and GM23.

a) GM11 b) GM17 c) GM18

d) GM22 e) GM23

Figure 3.14: Crushed cube specimen of GM

The above discussion clearly reveals that the mechanical strength of GM mixes is considerably improved by activating with SHSS solution rather than SH alone. However, better compressive strength is achieved by considering the mass ratio with a range of 1.5 to 2. The application of both a/b ratios is wise enough in developing strength. However, a highly concentrated SHSS solution demands a minimum alkali content (65 %) in the mortar mix to develop a satisfactory strength. Due to the presence of high CaO in UBFS, it does not require any special curing regime and can be cured at ambient temperature. Slag is highly reactive in an alkaline environment and exhibits a fast setting property. Moreover, due to the ultrafine nature of the

slag it is capable of gaining high strength at an early age. This will facilitate the use of such binder in several engineering works like roads and RCC building repairing work, where early gain in the strength of mortar/concrete is essential.

3.3.1.4 Relation between compressive strength and flexural strength

It is clear that the flexural strength of the geopolymer gradually increases along with the increase in compressive strength. In addition to this, it is observed that better mechanical properties are observed with the SS/SH ratio within a range of 1.5 and 2. In order to predict the strength properties of each type of GM mix (subjected to different SS/SH ratios) in a varying alkali concentration, linear relationships have been established between the compressive strength and the flexural strength with the aid of regression analysis.

Fig. 3.15. shows the plot between the compressive strength and flexural strength of the two types of mixes (Group III). The type of mixes that are considered in each plot are the mixes which consist of different SS/SH ratios (1.5 and 2), where each type constitutes the mixes

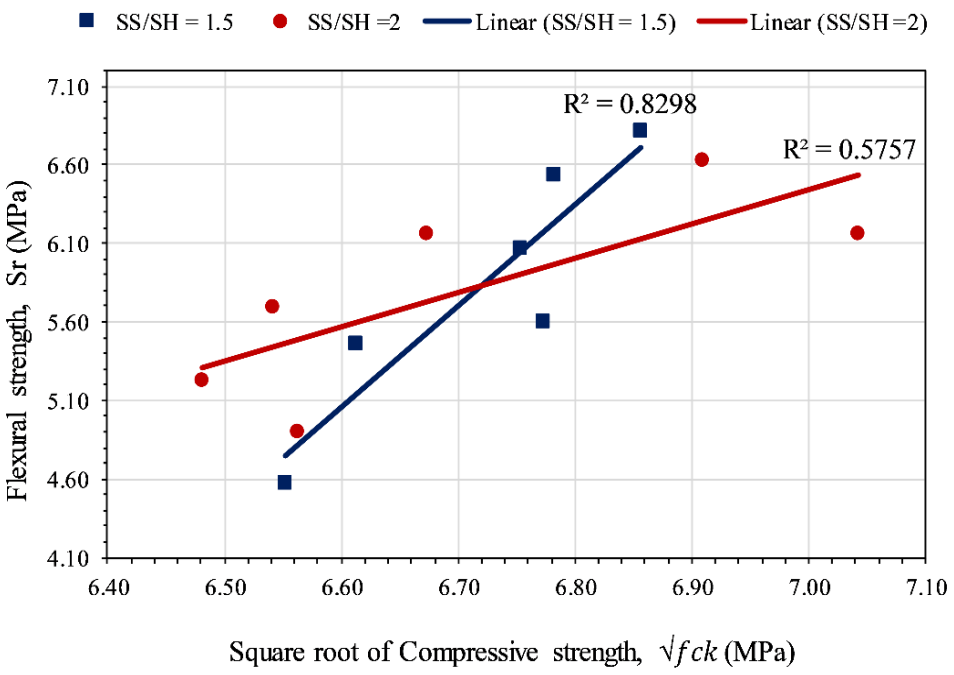

Figure 3.15: Relationship between Flexural strength and Compressive strength of GM

having both a/b ratio of 0.6 and 0.65. The strength values are taken corresponding to all concentrations of SHSS solution. The trend line for both types of mixes in each plot exhibits a linear relationship between the compressive strength and the flexural strength. The coefficient of determination (R^2) obtained in the regression analysis for each type of mixes (SS/SH=1.5

and SS/SH=2) can be seen from Fig. 3.15. It can be observed that the mixes with SS/SH ratio equals to 1.5, exhibits a better relationship between the compressive strength and the flexural strength (R^2 = 0.829). However, no consistent linear relationship could be established for mixes activated by a mass ratio of 2, due to its inconsistent coefficient of determination (R^2 = 0.575). This is attributed to inconsistent variation in the strength properties of GM specially at higher molarity (12M) and hence no regression model could be developed between the mixes with SS/SH ratio of 2. In addition to this the SHSS solution with mass ratio equal to 2 makes the mix very stiff, which ultimately influences the compressive strength. This causes a significant difference in compressive strength between the mix corresponding to separate a/b ratio of 0.6 and 0.65. The relationship established between the compressive strength and the flexural strength at 28th day in GM is given as,

$$S_r = 0.87\sqrt{f_{ck}} \tag{3.3}$$

3.3.1.5 Effect of Retarder in the properties of Geopolymer mortar

Effect of Retarder in Setting time and workability

The setting property and the workability of mixes (Group IV) altered by various dosages of borate (retarder) are determined and presented in Fig. 3.16 and Fig. 3.17. The test result shows that the inclusion of 2 % borate (GM17_2R) elongates the initial setting by 89 % and the final setting by 77.51 %. Successive addition of borate shows a linear increase in the initial and final setting time and keeps increasing up to a borate dosage of 8%. However, the test results show that a minimum borate dosage is necessary to bring an effective improvement in the setting property of geopolymer.

In the present case, the addition of 4% borate dosage causes a significant improvement in the mix GM17_R4, which exhibit an initial and final setting time of 61.25 min and 83 min. Such improvement in the setting property of geopolymer is completely acceptable so far as the engineering works are concerned. The borate dosage beyond 4 % cause further enhancement in the setting time, and the effect is more pronounced in the final setting time, as shown in Fig. 3.16. As the borate content reaches 8 %, the mix GM17_R8 showed the highest initial and final setting of 98.2 min and 187 min. A similar trend is also reported by Oderji et al. (2019) while evaluating the setting time of geopolymer paste. The retarding effect of borate is already seen in the cementitious binder, where borate inhibits the nucleation reaction of calcium hydroxide (Bensted et al., 1991) by forming a layer calcium-based borate gel around the cement grains which

deaccelerated the hydration process in OPC (Zhang et al., 2019). While, in the case of geopolymer, the retardation mechanism is considerably different.

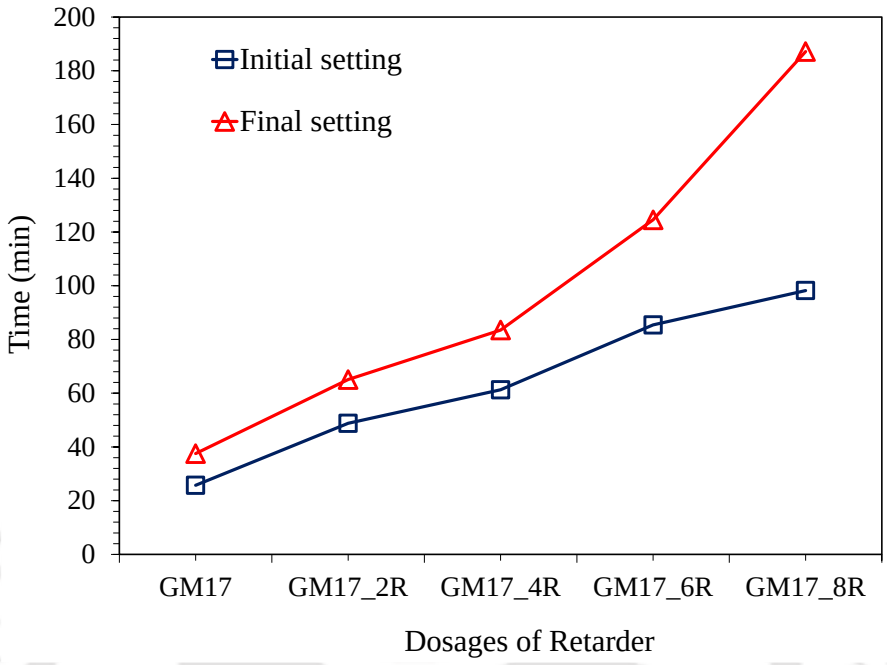

Figure 3.16: Effect of retarder on the setting time of Geopolymer paste

In the mix GM 17 where no borate is added, the silicate ions present in the solution reacts with aluminate present in the solution and undergo polymerization forming Si-O-Al-O bond. But when borate is pre added in the SHSS solution, as mentioned in section 3.2.3, a part of it readily reacts with the silicate group forming B-O-Si bond in the alkali solution. In B-O-Si bond, boron possesses a four coordinated bond which is having a weak bond energy. When this solution is mixed with the binder, the aluminate $[AlO_4]^-$ ions that is released in the solution by AS material breaks the B-O-Si bond and then links with it by forming B-O-Al-O-Si bond, which is a more stable structure of boron having three coordinated bond (Teng et al., 2013). This transformation is due to the reason that in B-O-Si bond, boron is having a tetrahedral geometry which is unstable and possess weak bonding energy and have a tendency to break and rearrange in to trigonal planner coordination which is more stable with higher bonding energy (Li et al., 2021). This change in the boron silicate network from B-O-Si to B-O-Al-O-Si causes a delay in the formation of the Si-O-AL bond. This is the reason that the addition of borate retards the formation of geopolymer product, and that is why the setting and hardening times of geopolymer paste were elongated.

The fluid retaining capacity of mixes subjected to the addition of borate is studied by conducting a flow table test at every 5 min interval by taking the final reading at 30 min. Fig. 3.17 shows change in flow characteristics of GM with time upon addition of different dosages of borate. The effect of borate in improving the spread of the freshly prepared GM can be identified from the Fig. 3.18.

From the Fig. 3.17., it can be observed that the mix without any retarder (GM17) drastically loses its fluidity within 20 min, whereas the flowability in the mix GM17_2R (2 % borate) lasts for a longer time. The addition of 2% of borate increases the instantaneous value FI from 38 % to 57 %. With the increase in borate content to 4 % and 6 %, FI of the mixes enhances to 63 % and 66 %, and simultaneously the rate of loss in the fluidity of these mixes also improves. The mix GM17_4R and GM17_6R retain a better fluidity, as seen in Fig. 3.18. (c) – (d), which continued even more than 30 min (see Fig. 3.17.). This improvement may be attributed to a delay in the formation of geopolymerization, which ultimately prolongs the hardening of mortar.

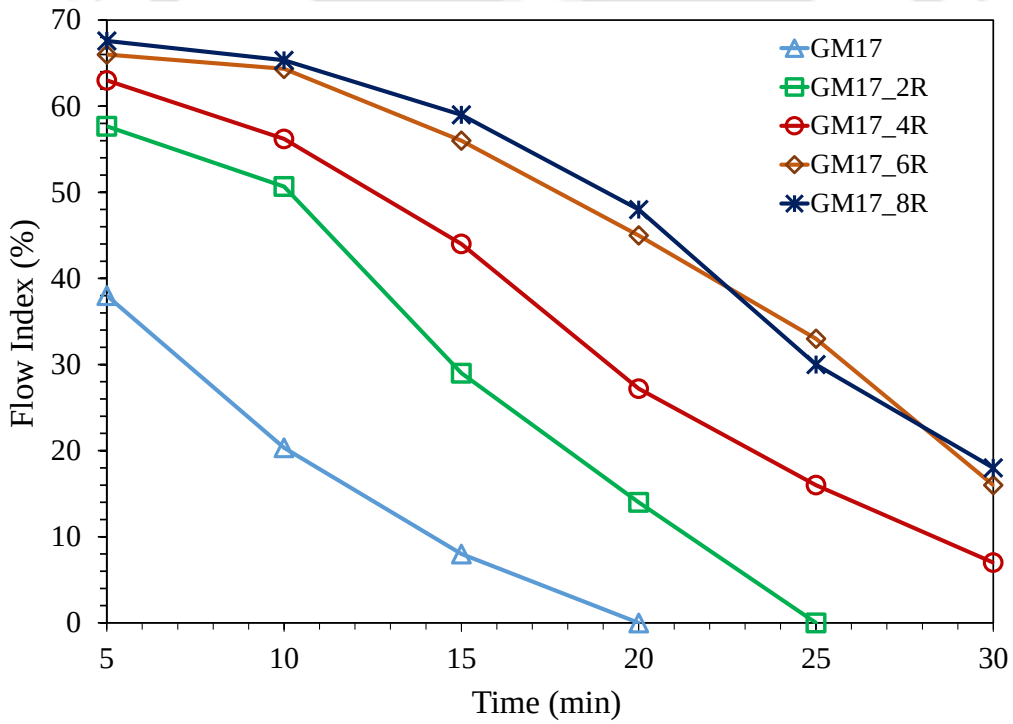

Figure 3.17: Effect of retarder on Workability of GM

In addition to retarding capacity, borate also possesses a water-retaining nature, which ultimately contributes to better flowability (FI) of the mixes (Zhang et al., 2019; Wang et al., 2020). Meanwhile, further addition of borate exhibits almost a comparable FI similar to

GM17_6R, but at the same time it also affects the strength property of the mortar. From test results it can be seen that borate has strong ability of retarding the setting time of GM and also increase the fluidity of the mix. Hence to the properties and action of all mixes in the Group IV, Borate can be placed in the Type B retarding admixture as per ASTM C494 (2019).

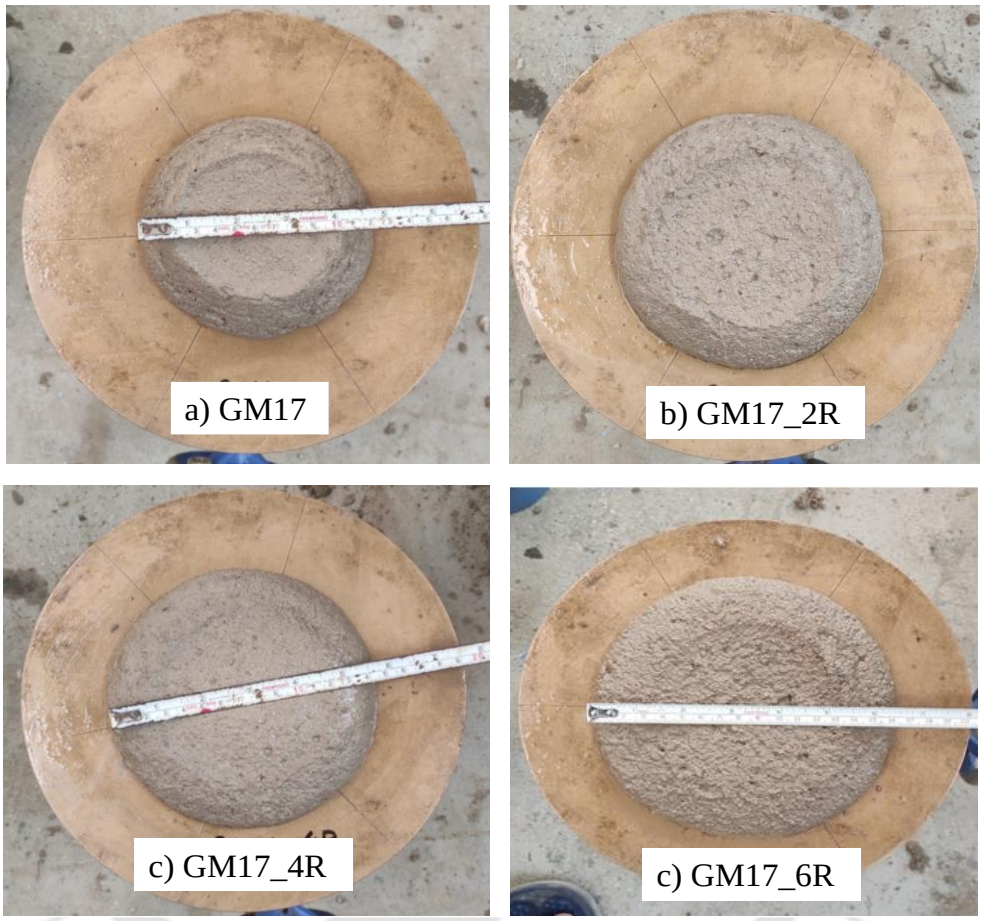

Figure 3.18: Effect of Borate in the spread of GM

Effect of Retarder in Mechanical properties

Compressive strength and flexural strength of geopolymer mortar with different dosages of retarder are shown in Fig. 3.19. Although borate is mainly employed as an additive to improve the setting property of geopolymer, it also improves the fluidity of the mix and brings a significant improvement in the mechanical properties of GM.

When 2 % borate is added to the SHSS solution, a significant improvement in the compressive strength is observed. The mix GM17_2R achieves a compressive strength of 50.93 MPa, which is much higher than the compressive strength (46 MPa) of the original mix (GM17) containing no borate. Whereas flexural strength at 2 % borate dosage shows no remarkable

improvement. As the borate percentage reaches 4 %, in mix GM17_4R, a slight reduction in the compressive strength (48 MPa) is noticed, although higher than the mix (GM17) with no

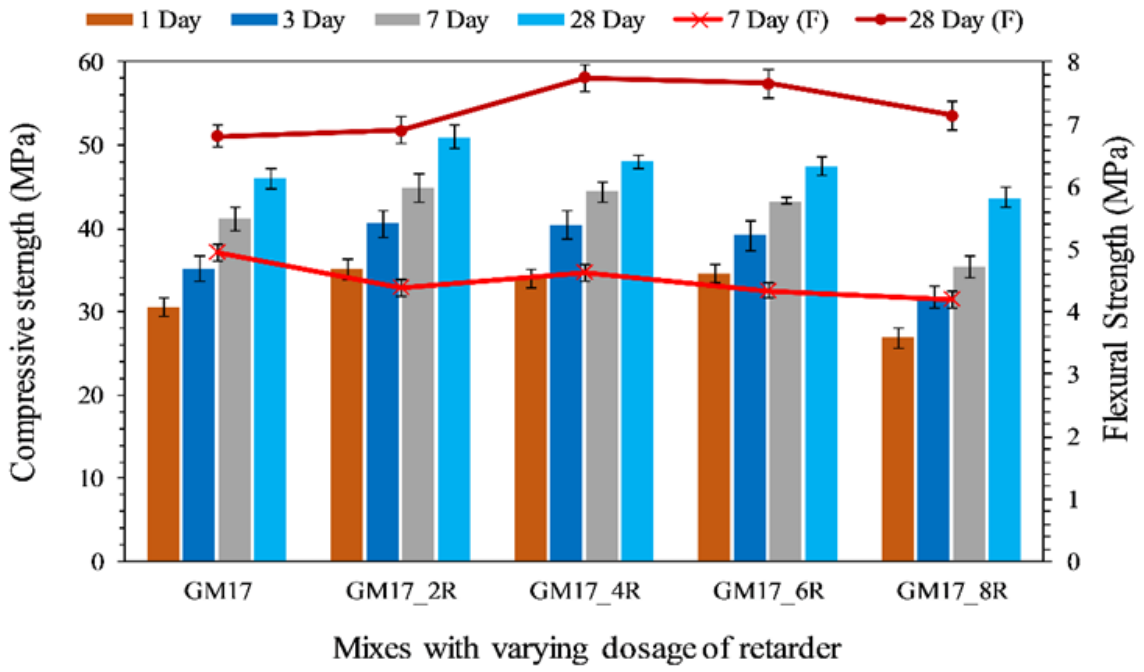

Figure 3.19: Effect of retarder on the Compressive strength and Flexural strength of GM

retarder. At the same time, the particular blend exhibit significant improvement in the flexural strength of 7.75 MPa. This improvement in the strength properties is attributed to the dense microstructure obtained after the inclusion of borate. As the borate dosage is further increased to 6 %, a slight decline in compressive strength (47.43 MPa) occurs, while the flexural strength (7.65 MPa) remains nearly the same. Further increase in the borate to 8% caused a sudden drop in the compressive strength (43.73 MPa) and slightly lesser flexural strength (7.14 MPa).

This sudden drop may be due to excessive addition of borate which also makes the solution denser and ultimately hampers the strength of GM. Although the highest compressive strength is achieved for borate content of 2 %, but better flexural strength and flow retaining capacity (more than 30 min) of mixes is observed higher in the mixes with 4 % (GM17_4R) and 6% (GM17_6R) of borate dosages. This dissimilarity in the trend of mechanical properties may be attributed to the fact that, Slag bases geopolymer is prone to shrinkage cracks (Singh et al., 2015) and it well documented in the literature that borate is a good water retainer that enables the mix in reducing the shrinkage cracks (Oderji et al., 2019).

Moreover, from Fig. 3.20 (a), in the succeeding subsection 3.4, it can be clearly observed that at the 7th day, shrinkage cracks are observed in the mix GM17 whereas no such cracks developed in the matrix of GM17_4R (Fig. 3.20. b). Therefore, it can be believed that 2 % of borate addition may not be sufficient to control the shrinkage cracks in the mix GM17_2R which resulted in to a lesser flexural strength in GM17_2R. On the other hand, Fig. 3.17 clearly shows that the effect of borate in retraining the workability turns effective when the addition of borate is more than 2 %. Hence addition of borate by 4 %, aids in controlling the shrinkage cracks and resulted in to better flexural strength in the mix GM17_4R.

Both the mix GM17_4R and GM17_6R exhibits almost a comparable strength property, which is significantly higher than the mix containing no borate content. Therefore, in the present study, the optimum retarder dosage is taken as 4 %, however higher dosage up to 6% can leads to a higher flow retaining capacity with a slight decline in the strength. Although the determining the borate dosage within a range of 4 % to 6 % can be opted based on the purpose for which the mix will be utilized.

3.3.2 Portland cement mortar

The compressive strength of PCM, which was prepared as per Table 3.2, were obtained at various ages and are presented in Table 3.5. The 1st day strength of PCM is approximately 20 % of the 28th day compressive strength. While, the compressive strength obtained on 3rd day and 7th day strength is nearly 47 % and 69.70 % respectively. This demonstrates that OPC-based cement mortar (PCM) with the same w/c ratio as that of w/s of GM ratio has lesser strength. Furthermore, the degree of strength development in PCM is substantially slower than in GM.

Table 3.5: Compressive strength of PCM

Mix	Compressive strength (MPa)			
	1 Day	3 Day	7 Day	28 Day
PCM	7.06	16.25	23.80	34.15

3.4 FESEM analysis

In order to study the changes in the microstructure of the GM upon addition of borate, the FESEM images of the mix GM14_4R is studied and also compared with GM17 containing no borate, which is shown in Fig. 3.20. The main reason of choosing mix GM17_4R is due to its

outstanding performance in terms of strength and workability, which also represent the mixes constituting Group IV. For better comparison, small samples of mixes are observed under the electron microscope after attaining the 7th day and 28th day of geopolymerization.

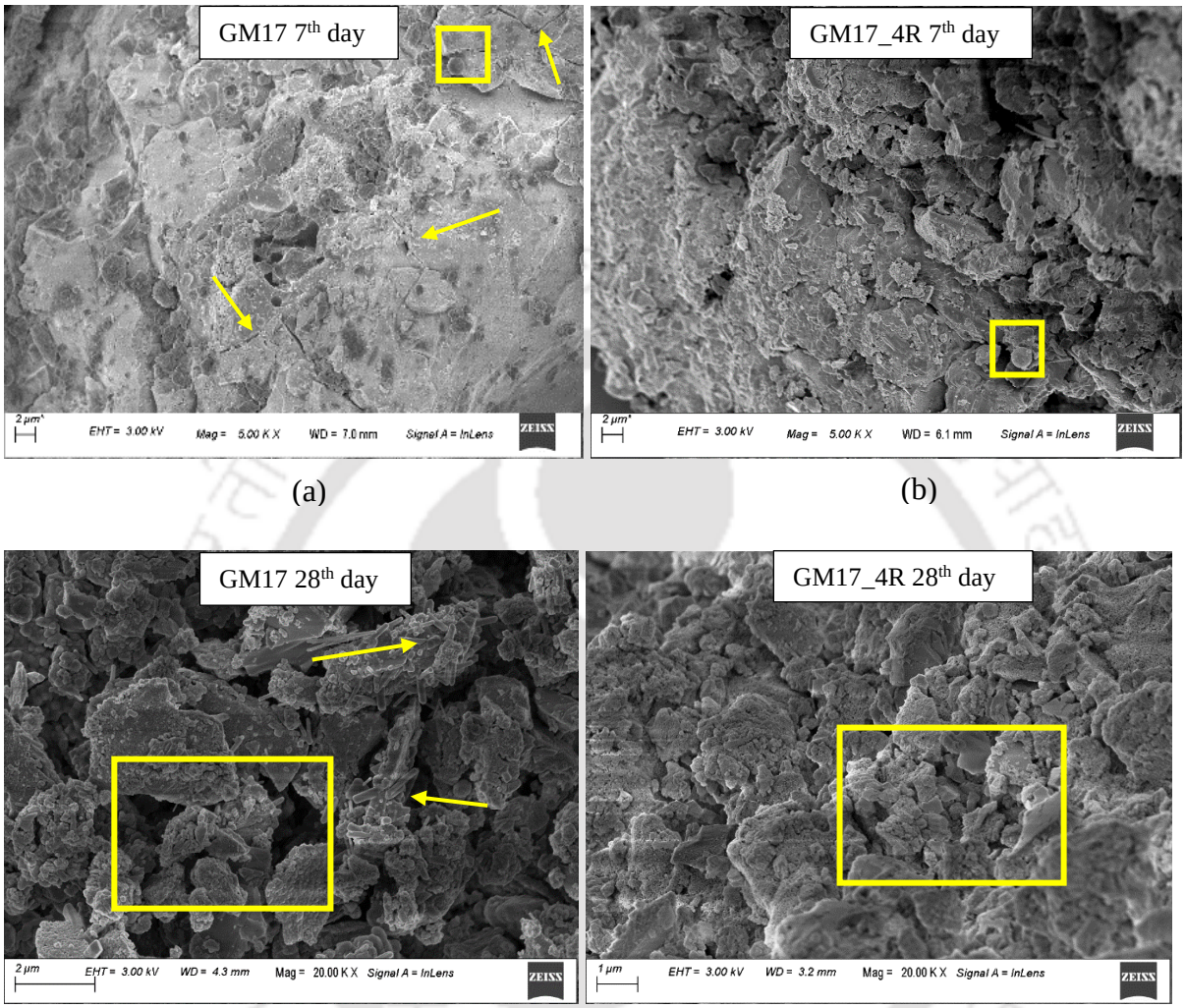

Figure 3.20: FESEM images of the geopolymer mixes on 7th and 28th day

From Fig. 3.20. (a) and (b), which represent the 7th day microstructure of the mixes, it can be apparently seen that both microstructures show traces of unreacted FA particles. In contrast, no unreacted slag particles can be identified in either of the matrices for specified region of study. This implies that UBFS has a higher reactivity in SHSS solution, resulting in superior geopolymerization products at an earlier age. The mix GM17 (7th day) clearly reveals the presence of fracture in the matrix, which may be attributed to early shrinkage in the matrix. In contrast, no such cracks could be detected in the mix containing borate.

UBFS based geopolymer is prone to shrinkage (Singh et al., 2015), but it is reported in the literature that borate is a good water retainer that enables the mix in reducing the shrinkage cracks (Racherla, 2002). This may be the reason that no shrinkage cracks are observed in the mix Fig. 3.20 (c) and (d), which shows the microstructure of the same mixes subjected to complete geopolymerization. At the same level of magnification (20KX), both the mix appears to produce a homogeneous reaction product (mainly C-S-H phase), but the microstructure of the mix without borate appears to be loose and less dense. In comparison, the microstructure containing 4 % borate (Fig. 3.20. (d)), seems to be more densely packed. Apparently this difference in the microstructural image can be attributed to the structural change of the geopolymeric gel due to the addition of Borate as explained under the head: *Effect of Retarder in Setting time and workability* in subsection 3.3.1.5**.** Thus inclusion of borate yields a better microstructure, resulting in high mechanical strength in the mix GM17_4R. In addition to this, the microstructure of GM 17 exhibits the presence of a needle-like structure (see Fig. 3.20 (c)) in the matrix, which is significantly less in the mix containing borate. Such needle-like structures are weak in compression, which may cause a reduction in the mechanical strength of geopolymer GM17_4R (7^{th} day) pertaining to the addition of borate.

3.5 Statistical analysis of Test results

Statistical analysis is conducted to determine the error in the measurement which are evaluated by calculating the standard deviation (σ) and coefficient of variation (ρ) from the data obtained in the tests. Table 3.6. presents the σ and ρ of compressive strength obtained at 7^{th} day and 28^{th} days. Where Table 3.7. presents the σ and ρ of flexural test data obtained on 7^{th} day and 28^{th} day. Both σ and ρ aids in the understanding of quality control maintained during the experimental works and also indicate the accuracy and reproducibility of the test procedure. The compressive strength data of the specimen shows that the σ are in the range of 0.46 MPa to 2.01 MPa whereas the ρ are in the range of 1.07 to 4.05 %. While in case of flexural strength the σ are in the range of 0.11 MPa to 0.26 MPa and the ρ are in the range of 2.51 to 4.11 %. The low σ and ρ values indicate a close distribution of the data around the mean value, reflecting a high degree of precision and dependability of the studies performed (Swamy and Chandrasekhar 2014, Montgomery and Runger 2010).

Table 3.6: Statistical data of compressive strength of GM

Mixes	σ (MPa)	ρ	σ (MPa)	ρ	Mixes	σ (MPa)	ρ	σ (MPa)	ρ
	7th Day		28th Day			7th Day		28th Day	
GM1	1.03	2.69	1.20	3.06	GM15	1.40	3.40	1.01	2.37
GM2	1.21	2.89	1.22	2.65	GM16	1.22	2.99	1.06	2.62
GM3	1.20	3.12	1.01	2.27	GM17	1.39	3.33	1.29	2.79
GM4	1.06	3.15	0.83	2.20	GM18	1.67	3.95	1.30	2.84
GM5	0.80	3.13	0.72	2.42	GM19	1.40	4.05	1.14	2.55
GM6	0.80	3.13	1.14	3.73	GM20	2.01	1.20	1.20	2.80
GM7	0.72	2.86	0.95	2.94	GM21	1.60	3.77	1.40	2.98
GM8	0.64	3.31	0.61	2.98	GM22	1.40	3.36	1.31	2.88
GM9	1.21	3.60	0.83	2.21	GM23	1.01	2.32	1.22	2.56
GM10	1.40	3.83	1.10	2.67	GM24	1.31	3.09	1.06	2.13
GM11	1.33	3.31	0.92	2.11	GM17_2R	1.74	3.89	1.40	2.76
GM12	1.47	3.64	0.83	1.94	GM17_4R	1.20	2.70	0.80	1.67
GM13	1.06	2.54	1.14	2.64	GM17_6R	0.46	1.07	1.06	2.26
GM14	1.62	3.87	1.06	2.52	GM17_8R	1.33	3.77	1.22	2.79

Table 3.7: Statistical data of flexural strength of GM

Mixes	σ (MPa)	ρ	σ (MPa)	ρ	Mixes	σ (MPa)	ρ	σ (MPa)	ρ
	7th Day		28th Day			7th Day		28th Day	
GM5	0.14	3.73	0.15	3.00	GM17	0.13	2.55	0.17	2.51
GM6	0.16	3.71	0.17	3.16	GM18	0.14	3.14	0.18	3.12
GM7	0.15	3.09	0.19	3.27	GM19	0.15	3.20	0.20	3.28
GM8	0.17	4.10	0.16	3.26	GM20	0.16	3.05	0.20	3.49
GM9	0.14	3.48	0.15	2.93	GM21	0.26	4.11	0.21	3.14
GM10	0.13	3.18	0.14	2.98	GM22	0.15	3.04	0.23	3.84
GM11	0.14	3.02	0.18	3.20	GM23	0.18	3.15	0.23	3.42
GM12	0.11	2.76	0.14	3.14	GM24	0.17	3.17	0.22	3.61
GM13	0.13	3.10	0.16	3.18	GM17_2R	0.14	3.21	0.21	3.10
GM14	0.13	2.86	0.17	3.23	GM17_4R	0.14	3.03	0.21	2.76
GM15	0.13	3.14	0.15	3.20	GM17_6R	0.13	2.96	0.23	3.03
GM16	0.128	3.3	0.141	3.35	GM17_8R	0.13	3.09	0.23	3.17

3.6 Closure

This chapter consists of the experimental results of the laboratory tests conducted in the development of Ultrafine blast furnace slag-based (UBFS) based geopolymer mortar (GM). Total 28 numbers GM are tested, considering several important factors affecting the fresh and hardened properties of the mortar. The high volume of UBFS in GM, activated by both SHSS solution and SH solution, have been investigated by their fresh and hardened properties in various concentration of the alkali activator. The silicate-based solution significantly enhances

the mechanical properties of the GM as compared to the SH bases alkali activator. Desirable properties are obtained by various modifications in the mass ratio of SHSS solution. But the intrinsic adhesive character of silicates-based geopolymer caused difficulty in regulating the setting and hardening time of binders. The addition of Borate dosage in the SHSS predominantly prolonged the setting property of geopolymer and also improved the flowability of the mortar mixes by transforming the conventional O-Al-O-Si bond in geopolymer to B-O-Al-O-Si bond. The FESEM images show that borate addition results in a more densely packed microstructure, which improves both compressive and flexural strength. On the other hand, the PCM mix that was prepared with the same water content as that contained by the GM mix exhibits a much inferior strength property than the GM. The experimental findings obtained during the development of GM possess the desirable quality that is sought in a repair material.

भारतीय प्रौद्योगिकी संस्थान गुवाहाटी
Indian Institute of Technology Guwahati

Chapter 4

Development and Testing of Geopolymer concrete and Fiber reinforced geopolymer concrete

4.1 Introduction

Over the last few decades, extensive research has been carried out in developing energy-efficient and sustainable building materials. Conventionally, concrete is the most common building material, and its use is increasing daily. Nowadays, the development of alternatives binder has become the newest area of research. Geopolymer is considered to be one such building material due to its several environment-friendly benefits and its efficiency in replacing the traditional binder.

Several researchers (Assi et al., 2020) have intended to develop geopolymer concrete (GPC) from various alumino-silicate (AS) materials like Metakaolin, Rice husk or industrial waste like Flyash, Slag etc. However, Flyash is the most widely used base material due to its easy availability and intrinsic features in providing strength and workability (Mohd. M.A et al., 2011). On the other hand, slag is material rich in calcium and is amorphous in nature. Due to these features, slag accelerates the polymerization reaction causing problem in its setting time and workability (Wang et al., 2020). To overcome this problem, FA is occasionally blended with slag, which can bring down the fast reaction process and improves the fresh quality of the geopolymer (IsLlam et al., 2014; Deb et al., 2014).

Over the past two decades, numerous research articles have been published on the effect of source materials and chemical activators affecting the properties of geopolymer. Nadoushan

and Ramezanianpour (2016) investigated the effect of alkali solution in slag-based geopolymer paste. They reported that the mixture of Potassium hydroxide (KOH) and sodium silicate (SS) solution is superior to the mixture of sodium hydroxide (SH) and SS solution in terms of strength and workability. In comparison, Thunuguntla and Rao (2018) reported that a slag-based GPC activated by a moderate concentration of SH (8M) could lead to significant strength and better inhibit the acid attack. The properties of GPC are also dependent on the proper mix proportion of ingredients. Reddy et al. (2018) recommended a method of mix proportionating by integrating the physical properties of the raw materials used in geopolymer. In normal mix design, 70 % to 80 % of the concrete volume is occupied by coarse aggregate and fine aggregate, which affects the strength, stiffness and durability of the concrete.

Development in early strength is always a desirable characteristic in any repair material. Slag is one such binder with a high rate of development in strength. In addition to this, it also possesses superior bond strength and abrasion resistance than one made with metakaolin (Hu. et al., 2008). These intrinsic features of geopolymer has also led researchers to test the efficiency GPC in strengthening of damaged structural members and serviceability of the strengthened beams in aggressive environment (Guades et al., 2021).

This chapter presents the works undertaken in the thesis to develop the Ultrafine blast furnace slag (UBFS) based Fiber reinforced geopolymer concrete (FRGC), to be used as a concrete jacketing agent. In view of developing FRGC, GPC concrete is initially prepared by considering several critical parameters which affect the fresh and hardened properties of geopolymer. In order to study the effect of steel fiber, suitable GPC mixes are modified by various dosages of steel fiber to produce FRGC composite. The efficiency of the FRGC mixes are investigated by conducting workability and strength test. The various parameters that have been considered to develop an ideal mix of GPC are the alkali content, concentration of SH and variation in the volume of fine aggregate to total aggregate (*s/a*) ratio. Whereas the FRGC mixes are studied by variation in *s/a* ratio and volume fraction (V_f) of steel fiber. The fresh and the hardened property of the mixes are investigated by various laboratory experiments, whereas the microstructure of the geopolymer matrix is studied by FESEM.

4.2 Experimental Investigation

The UBFS based GPC and FRGC mixes are investigated following Indian standard codes and ASTM codes. The various test that have been conducted to develop the GPC and FRGC

composite are slump test, vee bee consistometer test, compressive strength test, split tensile test, flexural test and slant shear test.

4.2.1 Materials

4.2.1.1 Geopolymer concrete and Fiber reinforced geopolymer concrete

The primary binding material employed in the present study is UBFS and low calcium 'Class F' Fly Ash (FA), which is used as a mineral admixture by partially substituting the UBFS in the mix proportion. The details of the binder have been presented in the subsection 2.2.2 and subsection 2.2.3 of Chapter 2. The alkali solution used as an activator in the synthesis of geopolymer is SH solution. The SH solution, of required molar concentration, is prepared by mixing commercially available SH pallets in tap water 24 hours prior to the time of mixing geopolymer. The detail of the alkali activator is presented in subsection 2.2.4. of Chapter 2. Locally available river sand well graded coarse aggregate of two different size 10 mm and 16 mm respectively are used for the preparation of GPC and the substrate specimen. The physical property of the aggregate has been presented in the subsection 2.2.5. of Chapter 2. Generally, slag based GPC concrete possesses a sticky characteristic due to the angular shape of the slag particle. Thus to meet the desired slump, a sulphonated naphthalene based super plasticizer (Conplast SP430) is also added to enhance the properties of freshly mixed GPC. Hooked end steel fiber is used for preparing the FRGC mixes. The properties of the steel fiber and the superplasticizer can be found in subsection 2.2.10. and 2.2.6. of Chapter 2.

4.2.1.2 Portland cement concrete and Fiber reinforced cement concrete

Portland cement concrete (PCC) was prepared using OPC 43 grade cement. Subsection 2.2.1. of Chapter 2 presents the details of the properties of the OPC. The fine aggregate and coarse aggregate used in the preparation of Fiber reinforced cement concrete (FRCC) is used same as that in FRGC. The detail of super plasticizer used in the FRCC composite is given in subsection 2.2.6. of Chapter 2. The fine aggregate and coarse aggregates used in the preparation of PCC were same as used in preparation of GPC. Steel fiber that has been used in the FRCC composite are same as that used in FRGC composite.

4.2.2 Mix Proportion

The main requirement of any jacketing material is its workability, rate of gain in strength and good bonding with the old substrate material. Previous literatures have witnessed many favourable benefits of geopolymer however, the application of such material is limited due its

varying material property and standard guidelines. In the present work, several mixes of GPC are designed to ascertain their workability, strength development and the adhesion property. Suitable mix proportion of GPC are further modified with fiber to produce FRGC mix. Apart from this PCC and FRCC mixes were also prepared as a controlled mix to compare with the geopolymer mixes.

In order to develop the GPC and FRGC, UBFS is employed as the main binding material, but due to the high content of calcium oxide, application of such material leads to poor workability and fast setting. To improve the fresh property, 30 % of FA is also added by partial substitution of UBFS, which helps in controlling the fast setting and workability as well. The UBFS based GPC is designed by incorporating all the physical properties of the materials with the aid of IS 10262 (2009) and the previous works of literature (Reddy et al., 2018). T The detail mix calculation of steps of the PCC mix and GPC trail mix (MG1) is presented in the section A.1, A.2 and A.3 in the Appendix A.

4.2.2.1 Mix proportion of Geopolymer concrete

Total 15 number of mix design are prepared to study the fresh and hardened properties of GPC and the mix proportion are given in Table 4.1. Several parameters that has been studied in the development of GPC are:

I. Effect of different alkali content viz. 291.20 kg/m^3, 276.64 kg/m^3 and 262.08 kg/m^3 in the mix of GPC
II. Effect of varying molar concentration of the alkali activator ranging from 4M to 12M in the mixes of GPC
III. Effect of *s/a* ratio in the properties of GPC mixes.

The alkali solution to the total binder (a/b) affects the strength of the geopolymer in the same way as the w/c ratio does. The previous researcher achieved a considerable mix proportion of slag-based GPC by incorporating an alkali content ranging between 35 % and 45 % (Deb et al., 2012; Nath and Sarkar, 2017). However, the use of a high volume of UBFS demands a higher quantity of alkali content to obtain satisfactory properties. Thus several trial mixes have been initially conducted and based on the test results, the a/b ratio for all mixes is set at 0.67.

Depending on the parameters selected for the investigation of GPC, the mixes are divided into four groups. The major purpose of Group I mixes is to figure out how much alkali solution is needed to attain the appropriate consistency and strength attributes. Then after

determining the optimal quantity of alkali solution in Group I, the rest of the mixes in Groups II, III and IV are prepared using the same amount of alkali. Based on the results published in the past literature (Laskar and Talukdar, 2017), the first trials of Group I were conducted with an alkali concentration of 10M. In this group (Group I), three different trials of alkali content (291.20, 276.64 and 262.08 kg/m3) are employed; and constant water to solid (w/s) ratio of 0.40 is maintained in all these mixes. The mixes are denoted as MG1, MG2 and MG3; and are calculated by adopting a *s/a* of 0.33.

Table 4.1: Mix proportion of GPC

	Mixes	UBFS	FA	Fine Aggregate	Coarse Aggregate	Alkali content	Molarity	s/a	Water	SP
		(kg/m^3)	(kg/m^3)	(kg/m^3)	(kg/m^3)	(kg/m^3)	(M)		(kg/m^3)	(%)
Gr I	MG1	304.28	130.39	551.67	1095.60	291.20	10	0.33	17.04	1.5
	MG2	289.02	123.86	568.29	1128.60	276.64	10	0.33	17.56	-
	MG3	273.81	117.35	584.90	1161.61	262.08	10	0.33	18.07	-
Gr II	MG4	289.02	123.86	568.29	1128.60	276.64	4	0.33	17.56	1.5
	MG5	289.02	123.86	568.29	1128.60	276.64	6	0.33	17.56	-
	MG6	289.02	123.86	568.29	1128.60	276.64	8	0.33	17.56	-
	MG7	289.02	123.86	568.29	1128.60	276.64	12	0.33	17.56	-
Gr III	MG8	289.02	123.86	702.00	991.80	276.64	4	0.41	18.87	1.5
	MG9	289.02	123.86	702.00	991.80	276.64	6	0.41	18.87	-
	MG10	289.02	123.86	702.00	991.80	276.64	8	0.41	18.87	-
	MG11	289.02	123.86	702.00	991.80	276.64	10	0.41	18.87	-
Gr IV	MG12	289.02	123.86	835.72	855.00	276.64	4	0.49	20.19	1.5
	MG13	289.02	123.86	835.72	855.00	276.64	6	0.49	20.19	-
	MG14	289.02	123.86	835.72	855.00	276.64	8	0.49	20.19	-
	MG15	289.02	123.86	835.72	855.00	276.64	10	0.49	20.19	-

Note: Gr-Group

After determining an optimum quantity of alkali content, the mix MG2 is further modified by various molar concentrations of SH ranging from 4M to 12M, as shown by the mixes of Group II. In any concrete, a major portion is occupied by aggregates (60% ~ 80%), which has an effect on workability and the strength properties and also on the cost per unit volume (Sagoe et al., 2001). Hence the mixes in the Group III and Group IV are further studied by varying *s/a* ratios and also investigated with different level of molar concentrations. Therefore, the mixes in the Group III and Group IV, which includes the mix M8 to M11 and MG12 to MG15, are prepared by *s/a* ratios equivalent to 0.41 and 0.49, and also varying in molar concentration in between 4M to 10M. Workability is a major problem in GPC, especially in the application of a high

volume of UBFS binder. Hence SP of the required quantity is added while mixing GPC, and in order to have a better comparative study, the dosage of SP is kept constant (1.5 % by weight of binder) for all the mixes.

4.2.2.2 Mix proportion of Fiber reinforced geopolymer concrete

The investigation on FRGC composite are done by preparing several mixes and are studied by evaluating the workability and strength properties of the mixes. Suitable mixes identified from Table 4.1. are further modified by incorporating various volume fraction (V_f) of steel fiber. Based on the properties of the GPC mixes, three mixes containing different volume of *s/a* are adopted and are altered by addition of fiber. The details of the mixes are provided in Table 4.2. The mix MG6, is initially modified by adopting different (V_f) of fibers ranging from 0.5 % to 2 %, as shown by the mixes MG6_0.5 to MG6_2. However, to optimise the fiber content, the mixes MG9 is modified by restricting the (V_f) within 1 % to 1.5 %, as shown by the mix MG9_1 to MG9_1.5. While in the last set of mixes with *s/a* ratio 0.49, similar quantity of fibers is added to modify the mix MG13. The mixes MG13_1, MG13_1.3 and MG13_1.5 represents FRGC mixes containing 1 %, 1.3 % and 1.5 % (V_f) of steel fiber.

Table 4.2: Mix proportion of FRGC.

Mixes	UBFS	FA	Fine Aggregate	Coarse Aggregate	V_f	Alkali content	Molarity	s/a	w/s ratio	Water	SP
	(kg/m^3)	(kg/m^3)	(kg/m^3)	(kg/m^3)	(%)	(kg/m^3)	(M)			(kg/m^3)	(%)
MG6_.5	289.02	123.86	568.29	1128.6	0.5	276.64	8	0.33	0.43	17.56	1.5
MG6_1	289.02	123.86	568.29	1128.6	1	276.64	8	0.33	0.43	17.56	1.5
MG6_1.5	289.02	123.86	568.29	1128.6	1.5	276.64	8	0.33	0.43	17.56	1.5
MG6_2	289.02	123.86	568.29	1128.6	2	276.64	8	0.33	0.43	17.56	1.5
MG9_1	289.02	123.86	702	991.8	1	276.64	6	0.41	0.47	18.87	1.5
MG9_1.3	289.02	123.86	702	991.8	1.3	276.64	6	0.41	0.47	18.87	1.5
MG9_1.5	289.02	123.86	702	991.8	1.5	276.64	6	0.41	0.47	18.87	1.5
MG13_1	289.02	123.86	835.72	855	1	276.64	6	0.49	0.47	20.19	1.5
MG13_1.3	289.02	123.86	835.72	855	1.3	276.64	6	0.49	0.47	20.19	1.5
MG13_1.5	289.02	123.86	835.72	855	1.5	276.64	6	0.49	0.47	20.19	1.5

4.2.2.3 Mix proportion of controlled mix using Ordinary Portland cement

All Controlled mixes are prepared using OPC 43 grade. Table 4.3. presents the various PCC mixes used for preparation of beam specimen and other PCC and FRCC mix used for comparison with that of the same type of geopolymer mixes. Moreover, the substrate part which was required to conduct the slant shear test, has been cast using the same PCC based

concrete mix (CM1) used for casting beam specimen. However, in this mix the maximum size of coarse aggregate in the concrete for substrate preparation was restricted to 16 mm. The compressive strength of the PCC mix used in substrate part exhibits a 28th day compressive strength of 30.13 MPa.

Whereas, the controlled mix CM2, has been prepared to compare the strength properties of GPC mixes with the conventional PCC based concrete. In order to have a better comparison in between the PCC and GPC mix, the water/cement (w/c) of the mix CM2 is taken equivalent to the water/solid (w/s) ratios of the mix GPC, which was mainly chosen for preparing the jacketing mixes (FRGC). The mix design of CM1 and CM2 is furnished in the section A.1 and A.2 of Appendix A.

Table 4.3. Mix proportion of the controlled mixes with OPC

Mix	Cement	Fine aggregate (kg/m^3)	Coarse aggregate (kg/m^3)	water to cement (w/c)	Steel fiber (% V_f)	SP (%)
CM1	358	661	1152	0.55	-	-
CM2	450	860	826	0.47	-	0.15
CM3	450	860	826	0.47	1.3	0.15

4.2.3 Specimen preparation

4.2.3.1 Preparation of specimen for Concrete mixes

The alkali solution of required molar concentration which is used in the preparation of GPC are prepared following the previous literatures. The details of the preparation of alkali activator is given in subsection 2.2.4 of Chapter 2. The following are the steps that has been involved during the preparation of the GPC mixes

I. To prepare the dry mix, required quantity of UBFS, FA, Fine aggregate and Coarse aggregate are initially mixed together in a mechanical pan mixture for 2 min.
II. The dry mixing is then followed by the addition of alkali solution and further mixed for 4 to 5 min, until a homogeneous dough like mixture is obtained.
III. During this process of mixing in step II, required dosage of SP are added directly in to the mixture of GPC in three successive intervals, which has been done to ensure proper distribution of the SP in developing a fresh GPC mix.

As soon as the freshly prepared GPC mix is ready, as shown in Fig. 4.1, the slump cone is immediately filled with the GPC mix in four layers while each layer is tamped uniformly with

a tamping rod. The slump cone is then raised slowly and vertically and the slump values of all the mixes are measured and recorded.

Figure 4.1: Freshly prepared GPC mix

a) Cube specimen

b) Cylindrical specimen

Figure 4.2: Demoulded specimen cast with GPC

As soon as the workability tests are conducted, the freshly prepared GPC mixes are immediately placed in the mould, which are oiled in advance, to prepare the specimen for compressive strength test and flexural strength test. The GPC material is placed in the mould in three successive layers and for better compaction each layer is vibrated properly using a portable vibrator table. The cast specimens are then finished properly using trowel and are kept

undisturbed for 24 hours. After 24 hours, all the specimens are demoulded and are kept in water for curing, maintaining a temperature of $20^0 \pm 2^0$ C. The demoulded specimen prepared with GPC is shown in the Fig. 4.2.

In the slant shear test specimens, the GPC constituted half of the volume. The other half, i.e. the substrate is prepared using PCC concrete (CM1), whose detail is mentioned in section 4.2.2.3. The PCC substrates were prepared with the help of dummy specimens which were cast, cured for 28 days and hand finished to give the perfect shape with a slant angle of 30°, as shown in Fig. 4.3. (a). The volume of each dummy specimen was half of that of cylindrical mould of size 75 mm diameter and 150 mm height, as per the provisions given in ASTM C882/C882M-13a. (2005). Prior to the casting of the PCC substrate for slant shear test, the dummy specimens were placed into the cylindrical moulds, and the bonding surface is covered with polyvinyl sheet, which acted as a debonding media between the PCC substrates and dummy specimens. The fresh concrete (CM1) is then prepared and placed into the moulds such that it occupies the other half of volume of the mould and kept for 24 hours at temperature of 20 ± 2 ºC. The specimens were later demoulded and cured till 28 days from date of casting

a) PCC substrate b) Curing of PCC substrate part

Figure 4.3: Preparation of substrate part of Slant shear specimen

by submerging inside water tank, maintaining the water temperature at 20 ± 2 ºC. After 28 days, the PCC substrates have been taken out from water tank, and further curing has been done in the open air up to 12 months from the date of casting, as shown in Fig. 4.3. (b).

After completion of dry curing, the substrate specimens are cleaned using wire brush to peel off the dust layer. In order to cast the specimen for slant shear test, the cleaned PCC

substrate part is initially placed inside the cylindrical mould occupying half of the volume of cylinder and tightened properly. As soon as the mould for slant shear specimen is ready, the GPC mix is prepared and slump test for individual mix is conducted. On completion of the slump test, the other half of the cylindrical mould is filled with the GPC mixes, as shown in Fig. 4.4. (a). For proper compaction, all specimens are cast in three successive layer and each layer is vibrated for 2 minutes using a portable mechanical vibrator. The cast specimens are then finished properly using trowel and are kept undisturbed for 24 hours. After 24 hours, all the specimens are demoulded and are kept in water for curing, maintaining a temperature of $20^0 \pm 2^0$ C.

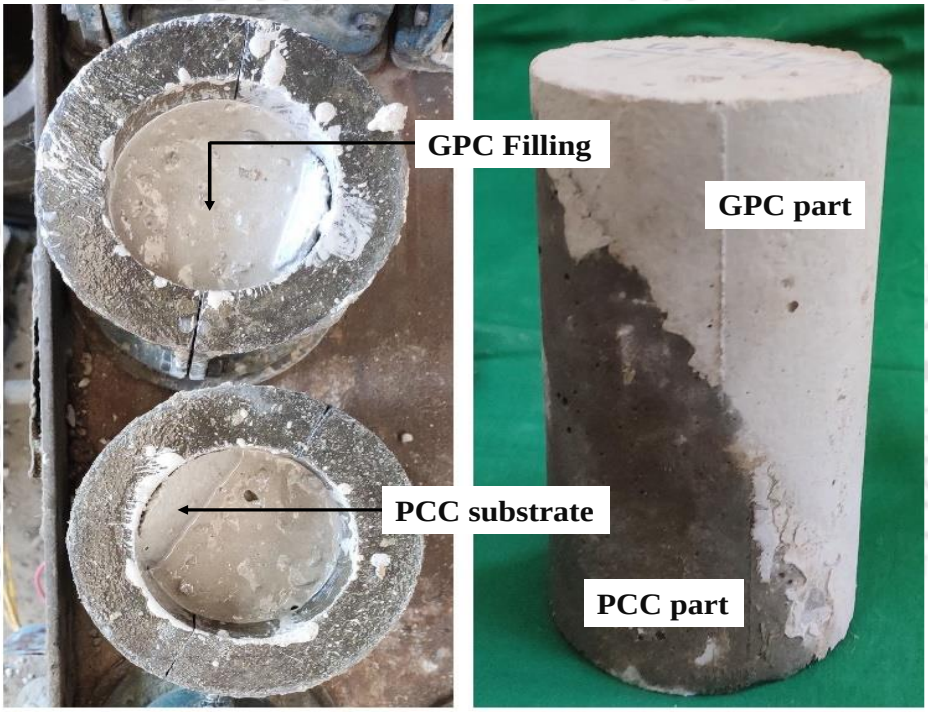

a) Casting of slant shear specimen

b) Cast slant shear specimen

Figure 4.4: Preparation of Slant shear specimen

4.2.3.2 Preparation of specimen for Fiber reinforced concrete mixes

To prepare the FRGC mixes, the dry mixing of the constituent materials is initially mixed in a mechanical pan mixture in the same process as described in the previous section 4.2.3.1. After the dry mixing, fibers are added directly and mixing is continued for 3 minutes. To avoid any balling action and to obtain a homogeneous distribution of steel fiber, the fibers are added incrementally during the mixing process. As soon as a homogenous dry mix is achieved, the alkali solution is added and continued mixing. To this mix, chemical admixture (SP) is then

added and mixing is continued for 4 to 5 minutes till a homogeneous FRGC mix is prepared. The consistency of a freshly prepared FRGC mix is the controlling parameter for its application is any specific engineering works. Hence the present work intends to parameterize the effect of steel fiber on the fresh property of FRGC by conducting workability test followed by casting of specimen for strength test. With the inclusion of steel fiber, FRGC reach to a very stiff consistency hence the workability of the FRGC mixes are evaluated by both slump test and the vee bee consistometer test.

As soon as the workability tests are conducted, the freshly prepared FRGC mixes are immediately placed in the pre oiled mould to prepare the specimen for compressive strength test and flexural strength test. The FRGC material is placed in the mould in three successive layers and for better compaction each layer is vibrated properly using a portable vibrator table. The details of the specimen preparation can be seen from the Fig. 4.5. The cast specimens are then finished properly using trowel and are kept undisturbed for 24 hours. After 24 hours, all

a) Freshly prepared FRGC mix

b) Vee-bee consistometer Test

c) Cast cube and prism with FRGC

Figure 4.5: Casting and preparation of FRGC specimen

the specimens are demoulded and are kept in water for curing, maintaining a temperature of $20^0 \pm 2^0$ C.

4.2.4 Experimental program

4.2.4.1 Geopolymer concrete

The workability of the freshly prepared GPC and the FRGC mixes is determined immediately by standard slump test in accordance to IS 1199-1959 (2004). The compressive strength of GPC is evaluated using a cube mould of size 150×150 mm as per the provision mentioned in IS 516-1959 (2004). To ascertain the rate of gain in strength of the various GPC mixes, the compressive strength tests are conducted at 3, 7, 28 and 56 days. Compressive strength of concrete is an indicator of all the other mechanical properties of concrete hence the split tensile strength of GPC mixes is determined only for the 28th day. Cylindrical mould of size 150×300 mm is used to determine the split tensile strength and are tested as per IS 5816-1999 (2004). For slant shear test, cylindrical mould of size 75×150 mm is used to conduct the slant shear test as per the provision given in ASTM C882 C882/882M-13a (2005). The split tensile strength (f_{ct}) and the bond strength (B_{sc}) of GPC mix are evaluated by the following equations.

$$\text{Split tensile strength, } f_{ct} = \frac{2P}{\pi l d} \tag{4.1}$$

$$\text{Bond strength, } B_{sc} = \frac{F_c}{A_c} \tag{4.2}$$

where, P is the maximum load applied to the specimen, l is the length of the specimen, d is the cross-sectional dimension of the specimen, F_c is the load carried by the specimen at failure, A_c is the area of the bonded surface.

4.2.4.2 Fiber reinforced geopolymer concrete

The workability of the freshly prepared FRGC mixes is conducted immediately after the mix is prepared, in to two different ways. The slump value of the individual mixes is conducted by Slump test in accordance to IS 1199-1959 (2004) and Vee-bee consistometer test as per IS 10510 (1983). The strength parameters of each mixes of FRGC is obtained at the 28th day of curing. To determine the compressive strength of FRGC, cube mould of size 150×150 mm is used; while prismatic specimen of size 150×150×700 is used for flexural strength test of FRGC,

as per the provision mentioned in IS 516-1959 (2004). The flexural strength of FRGC material are calculated by

$$\text{Flexural strength, } f_b = \frac{Pl}{bd^2} \tag{4.3}$$

where P is the maximum load, l is the length of the span, b is the width of the specimen and d is the depth of the specimen.

The specimens at various ages are determined by testing the specimen day in a Universal testing machine (UTM) and the strength properties are determined by taking the average of three test result.

4.3 Experimental Observations

4.3.1 Result and discussion of Geopolymer Concrete

4.3.1.1 Workability

Slag based geopolymer possesses a very sticky characteristic which has a tendency to flocculate in a strong alkali medium. Nevertheless, the use of naphthalene based SP dramatically enhances the flow property in all the GPC mixes. As soon as the dosage of SP (1.5%) is added to the GPC mixes, the fluid content trapped inside the flocs gets released and becomes available to provide fluidity in the mix. The slump test of all the mixes are conducted immediately as soon as the freshly prepared GPC mix is ready. Fig. 4.6 shows the various types of slump achieved during the test and the effect of various parameters on the slump value is presented in Fig. 4.7.

The effect of alkali content on the slump of GPC mixes, with a constant w/s ratio (0.4) and molarity (10M), can be observed from the mixes corresponding to Group I. The mix MG1 with an alkali content of 291.20 Kg/m^3 exhibited a slump value of 210 mm; this value rapidly falls as soon as the amount of alkali content is reduced in the mix MG2 and MG3. This degradation in the workability is due to the reduction of alkali solution in the later mixes, resulting in a lower slump value of 175 mm and 55 mm as achieved by the mix MG2 and MG3. The workability and strength qualities of Group I mixes are mainly evaluated to determine the optimum alkali level. Thus based on the test results of mixes of Group I, the optimum value of alkali content is fixed to 276.64 kg/m^3 and further investigation is carried out to study the effect of alkali concentration and *s/a* ratio.

a) Collapsed slump

b) Partially collapsed slump

c) True slump

d) Dry slump

Figure 4.6: Types of slump

The mixes in group II, which are prepared with a *s/a* ratio of 0.33, exhibit the maximum fluidity as compared to other groups. However, variation in the concentration from 4M to 12M, affects the slump of the mixes. The measured value of slump for the mix MG4 and MG5, activated by 4M and 6M, was found as 280 mm and 250 mm (see Fig.4.7). But these mixes exhibited a collapsed slump during the test. A typical collapsed slump exhibited by such mix can be seen in the Fig. 4.6. (a). This is attributed to the fact that at low alkali concentration, the w/s ratio becomes significantly high (as understood from Table. 4.1); this causes an increment in the water content resulting in high fluidity in the mix. Apart from this, such mixes activated with 4M and 6M of SH also showed segregation and bleeding in their fresh state. Apparently, this is due to the SP dosages at a low alkali concentration. However, this defect seems to be vanished at high molarity and/or with an increase in the *s/a* ratio.

With the increase in molarity to 8M, the mix MG6 showed a partially collapsed slump of 190 mm. A typical partially collapsed slump exhibited by MG6 is shown in Fig. 4.6. (b). With further increase in molar concentration (10M), the consistency of the mix is drastically affected. The mix becomes sticky, and the viciousness of the mixes were increased, which created difficulty in obtaining a homogeneous mix. This is the most common phenomenon in

slag based geopolymer, as reported in the past works of literature (John et al., 2021). This is because at high molar concentrations, the leeching of Al^{3+} and Si^{4+} ions rapidly increase, which

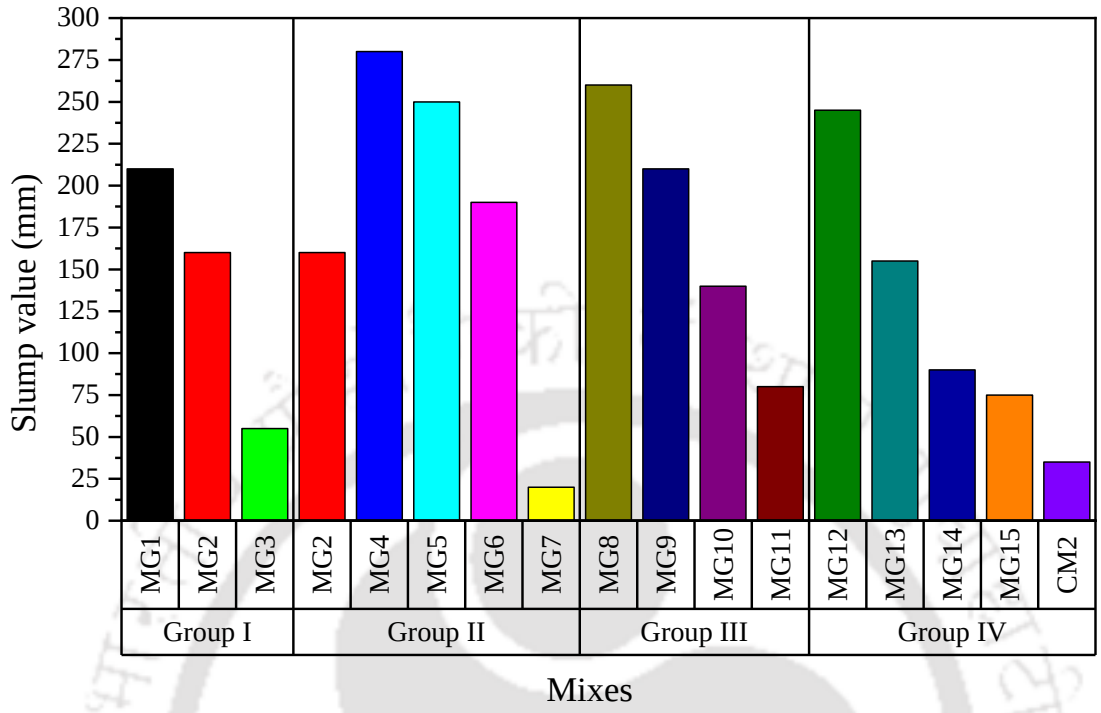

Figure 4.7: Slump value of GPC mixes

leads to fast geopolymerization causing instant setting. This also leads to a low workability in the mixes. With a further increase in molarity to 12M, the mix MG7 becomes very stiff and cohesive. During the slump test, the mix retained the shape of the slump cone with no sign of movement and exhibited a dry slump, as shown in Fig. 4.6. (d). This is due to the fact that at high molar concentration, the solid content in the mixes is increased. The high fluid demand due to the ultrafine nature of the UBFS material and the fast reaction of the Ca^{2+} with the alkali medium makes the mix very cohesive. Due to such cohesiveness, there occurs a problem in particle mobility, increases the difficulty in mixing of concrete and ultimately reduces the workability of the mix (Fang et al., 2018).

The change in the volume of sand has a significant effect on the slump value of mixes. In Group III, the mix MG8 to MG11 are prepared with a constant *s/a* ratio of 0.41 but with a varying concentration of alkali activator (See Table 4.1). Due to increased fine aggregate in these mixes, the water demand for such mixes also increased. It is also observed that the mortar paste of these mixes becomes much denser in comparison to the mixes of Group I and II. However, it is worth noticing that no segregation can be identified in the mixes even with a low alkali concentration of 4M and 6M. Rather, the mix MG8 with 4M SH exhibits a partial

collapse slump of 260 mm. With the increase in molar concentration to 6M, 8M and 10M, the fluidity of the mixes decreases and eventually, the workability changes from a collapse slump to a true slump, as shown by Fig. 4.6. (c). Moreover, the slump value obtained for the mix MG9, MG10 and MG11 is also reduced to 210 mm, 140 mm and 80 mm, respectively. However, it is noticed that the concentration of alkali still has an effect similar to the previous mixes. A similar pattern in the slump value is also observed when the value of *s/a* is further increased to 0.49, as exhibited by the mixes of Group III, as seen in Fig. 4.7.

On the other hand, the PCC mix CM2 is prepared with an *s/a* ratio of 0.49; hence this mix is also included along with the mixes of Group IV of GPC mixes, as shown in Fig. 4.7. The workability of the PCC mix, CM2, containing the same w/c ratio as that of w/s ratio of the GPC mix, exhibited lower slump value of 45 mm. From the above discussion, it can be summarised that the fresh properties of the GPC are significantly better than the PCC mix even prepared with the same w/s ratio. The workability of GPC is mainly governed by the SP, concentration of alkali activator and w/s ratio in the mix. However, the variation of volume in the sand has a considerable effect on the slump. The slump value of the GPC concrete decreases almost linearly with the rise in molar concentration and *s/a* ratio.

4.3.1.2 Compressive strength

Effect of variation in the alkali content

The quantity of liquid in any GPC mix is a key factor in the variation of workability and the long-term mechanical properties. The effect of three different amounts of alkali content on the compressive strength of the mixes of Group I is shown in Fig. 4.8. As observed in the preceding section, a high alkali concentration of 291.20 kg/m^3 greatly enhances the workability of the GPC mix (MG1), but it has a detrimental influence on the strength qualities. But as the alkali content is steadily lowered, the compressive strength improves from 41.93 MPa (MG1) to 48.07 MPa (MG3) at the loss of workability. This trend is quite similar to the effect of the w/c ratio in ordinary concrete. This is because, as the alkali content is reduced, the water content in the solution also reduces, which facilitates in production of better geopolymeric products, resulting in improvement in the strength. A similar effect is also reported in the works of previous literature (Deb et al., 2014). But it is noteworthy to mention that GPC mixes are cohesive, and minimum fluid quantity is required to obtain the desired consistency in the mix for handling and proper compaction.

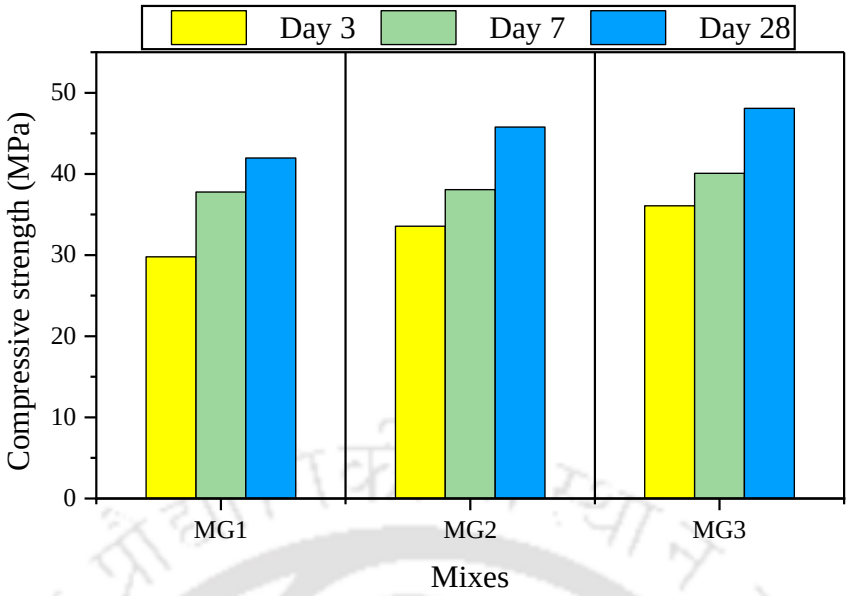

Figure 4.8: Effect of alkali content in compressive strength of GPC mixes

Further lowering the alkali content, as in the mix MG3, results in a further improvement in compressive strength but results in a significant reduction in slump value, which is already seen in the Fig. 4.7. in the previous subsection 4.3.1.1. This shows that the mix MG3 possessing high compressive strength is suitable only for foundation and cannot be used for RCC due to its poor workability. Thus based on the fresh and the hardened properties of the mixes in Group I, it can be seen that the mix MG2 shows a considerable workability (slump 175 mm) with a compressive strength of 45.78 MPa. Hence for the rest of the mixes, the total alkali content is fixed at 276.64 Kg/m^3.

Effect of variation in the molar concentration of alkali activator

As soon as the quantity of alkali activator is determined from the mixes of Group I, the effect of the various molar concentration of SH (4M - 12M) is further investigated for different proportions of fine aggregate volume. Fig. 4.9., Fig. 4.10. and Fig. 4.11 show the compressive strength development of GPC mixes with different *s/a* ratios, as per the Table. 4.1, presented under the previous subsection 4.2.2.1.

To study the strength-gain behaviour the compressive strength of all the GPC mixes are determined up to 56th day. From the test result, it can be observed that slag-based GPC develops high strength at a very early age (3rd day) and eventually slows down with age. The early compressive strength achieved by each mix on the 3rd day and 7th day is approximately 72 % and 83 % of the compressive strength on its 28th day. However, it is worth noting that strength

gain continues even after the 28th day. But the rate of strength development is reduced at a later age, and hence 6 % - 7 % of strength increment can be noticed at the age of 56 days.

This trend is in line with the results reported by previous researchers (Nath and Sarkar, 2014). The rapid strength gain of the GPC mixes can be attributed to the presence of high calcium oxide in the UBFS binder. When a large amount of UBFS is utilized, the precursor is capable of releasing more ca^{2+} ions into the alkali environment, resulting in the development of more C-A-S-H gel rather than the N-A-S-H gel generated by FA (Al-Majidi et al., 2016). Due to the highly reactive nature of UBFS, the production of C-A-S-H gel is quicker, resulting in a faster rate of strength gain (John et al., 2021). Furthermore, the UBFS's fineness allows for additional surface area to participate in the pozzolanic process, which ultimately accelerates the strength of GPC (Teng et al., 2013).

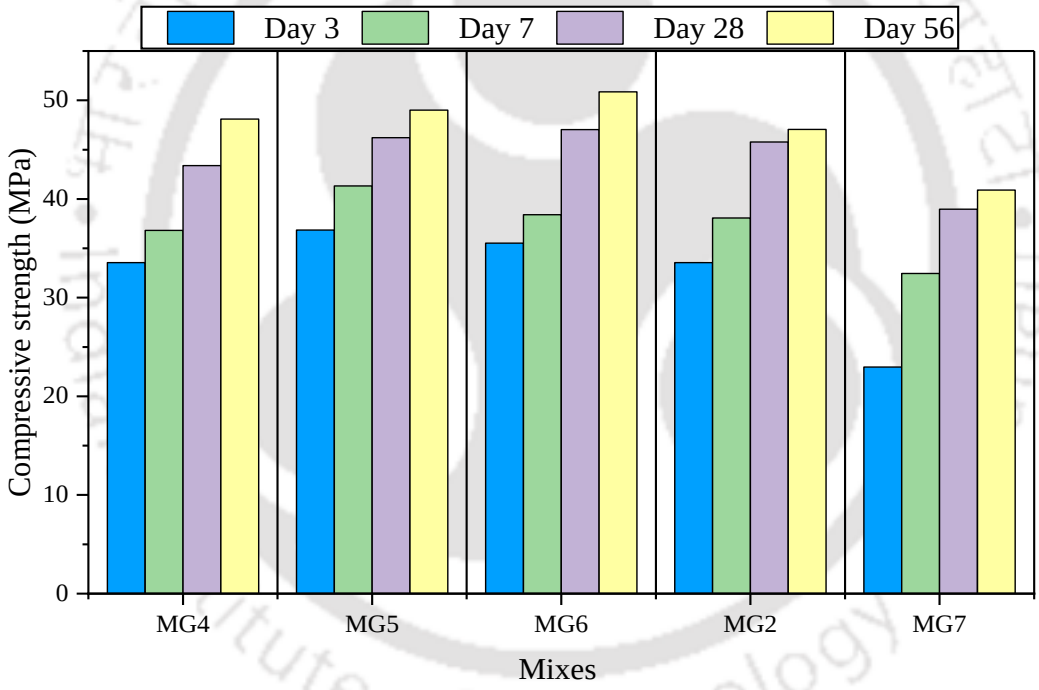

Figure 4.9: Effect of molar concentration on compressive strength with *s/a* = 0.33 in GPC

As seen in the preceding section, alkali concentration strictly controls the rheological property of the GPC, but it also has a significant effect on the strength properties of geopolymer. Fig. 4.9. shows that the mixes of Group II, where it can be seen that at a very low alkali concentration (4M), i.e. the mix MG4 attains an ultimate strength (28th day's compressive strength) of 43.38 MPa. When this molar concentration is increased to 6M, i.e. in the mix MG5, a compressive strength of 46.22 MPa on the 28th day and 49.0 MPa on the 56th day is achieved.

However, this increasing trend in the compressive strength is found to be limited up to MG6, activated by 8M, which exhibits a maximum compressive strength of 47.04 MPa and 49.39 MPa on the 28th day and 56th day, respectively. The reason of getting maximum compressive strength with rise in molarity is due to the high molar concentration which is responsible for better reaction products. This is also supported by the slump property as explained in the previous section 4.3.1.1, where the mixes with low molarity showed defects like collapsed slump, bleeding and segregation which eventually improved with the increase in the molarity to 8M.

Furthermore, it is seen that a further increase in the concentration beyond 8M degrades the compressive strength of GPC. This reduction in the strength can be attributed to two prime factors: (i) High alkali causes workability issues, thus making the mix porous in nature; and (ii) at higher alkalinity, the geopolymeric gels cannot form an integral matrix and cracks and pores are formed in the microstructure, this is also reflected in the microstructure image (FESEM), which is shown in Fig. 4.21. (h) and (i) of the succeeding subsection 4.4.

The effect of molar concentration in Group III and Group IV, prepared with a higher volume of sand, is nearly similar to that obtained in Group II. From Fig. 4.10., it can be seen that the mix MG8, activated by 4M, exhibits compressive strength of 44.94 MPa (28th day). Further increase in molarity leads to further improvement and the highest compressive strength

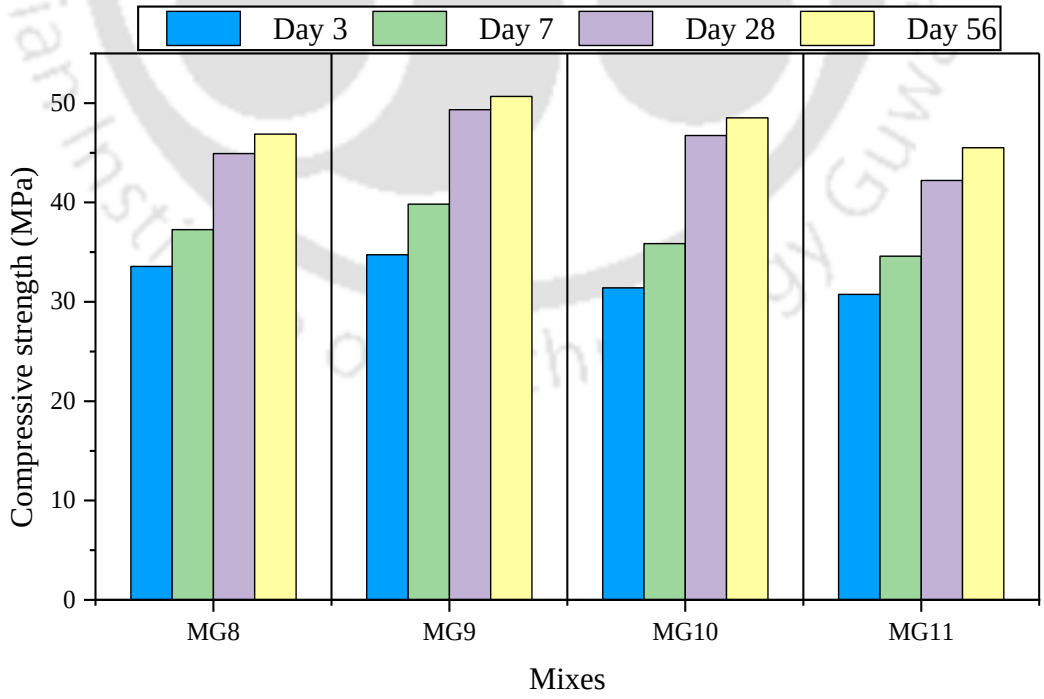

Figure 4.10: Effect of molar concentration on compressive strength with *s/a* = 0.41 in GPC

of 49.33 MPa and 50.67 MPa on the 28th and 56th day, is exhibited by the mix MG9 activated with 6M SH. But when activated by 8M and 10M, the compressive strengths begin to decline, and attains a considerably lower compressive strength of 46.73 MPa and 42.20 MPa on the 28th day.

However, it is worth noticing that in previous Group II mixes, maximum compressive strength is achieved when activated by 8M, whereas in Group III where the volume of sand is increased, the maximum compressive strength is achieved by mix with 6M. This is attributed to the fact that group II mixes with a lower volume of sand (*s/a* – 0.33), which showed significant bleeding and segregation when activated by low alkali in the range of 4M to 6M. This bleeding leads to excess free water on the surface of the concrete mix, which ultimately leaves pores on the surface and underside of the coarse aggregate, causing a reduction in the strength (Coo et al., 2015) of GPC. However, when the molarity is increased to 8M, the bleeding of the mix is totally eliminated, resulting in an improvement of compressive strength at the 8M.

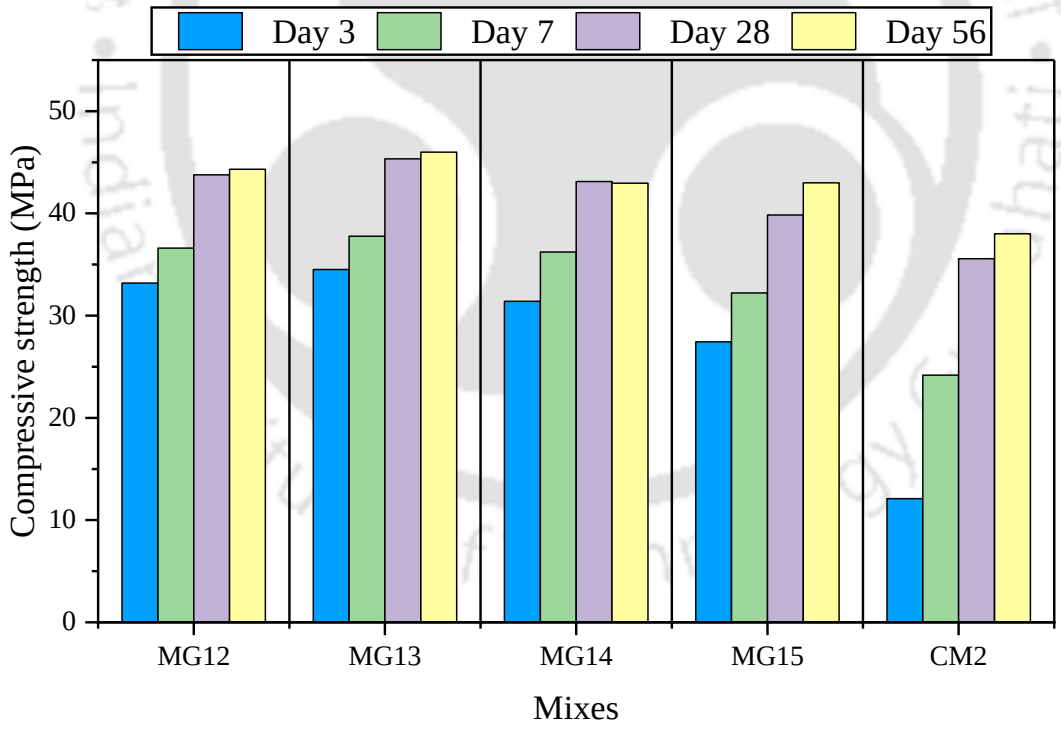

Figure 4.11: Effect of molar concentration on compressive strength with *s/a* = 0.49 in GPC

Whereas, in the case of Group III and Group IV, due to an increase in the volume of the *s/a* ratio, the mixes exhibited a rich geopolymer mortar paste, and better compressive strength was achieved at a low molar concentration (6M), as seen from the Fig. 4.10. and Fig.

4.11. This is due to the fact that as more volume of sand is included, the bleeding and segregation are totally eliminated, which were earlier noticed in the mixes of Group II with low alkali concentration. This ultimately leads to improvement of the microstructure and shrinkage cracks in the geopolymeric gel, resulting in better mechanical properties in the hardened state. The better compressive strength obtained at low alkali concentrations like 6M is contradictory to several authors (Laskar and Talukdar 2017, Verma and Dev 2021) who reported better mechanical properties at higher alkali concentrations. But, there are instances in literature where a similar trend in the results is obtained (He et al., 2013; Gorhan and Kurklu, 2014). The most likely reason behind these contrasting features can be attributed due to two reasons. At high molar concentration, excessive OH- ions are available in the alkali solution, which causes early precipitation of the geopolymeric gel, thereby preventing it from taking part in the reaction process (Somna et al., 2011). Apart from this, higher molar concentration also disrupts the leaching of Al^{3+} and Si^{4+} ions to take part in the polycondensation reaction process. Moreover, it is well observed that, in UBFS-based GPC, the specimens are susceptible to efflorescence at a high molar concentration, which leads to a loss in compressive strength. Therefore, from the above discussion, it can be understood that the selection of an optimum concentration of alkali is very important while developing an ideal GPC mix with satisfactory strength and workability.

Effect of variation in the volume of fine aggregate

The impact of the *s/a* ratio on the compressive strength of the GPC mix can be clearly identified from the Fig. 4.9 to Fig. 4.11. It is noted that as the *s/a* ratio is raised from 0.33 to 0.41, the compressive strength of the GPC mix increases moderately. This is because, with the increase in the fine aggregate content, the mixes appear to be more rich as observed in the fresh state. This facilitates to a homogeneous distribution of the aggregate in the GPC mix while casting and ultimately contributes to the mechanical properties in the hardened state in the mixes of Group III. The improvement in the mechanical properties can also be attributed to the fact that as the *s/a* ratio is increased to 0.41 better packing density is achieved in the mixes of Group III. Moreover, increasing the finer aggregate in Group III also helped in reducing the volume of voids and makes the concrete denser in comparison to the mixes of Group II.

The denser mixes show reduction in the volume of voids or pores which ultimately contributes to the mechanical properties of the mixes of Group III. This is also supported by the observation marked by Mohammed and Rahman (2016), in their work related to the effect

of different volumes of aggregate. Moreover, an increase in the fine aggregate volume also reduces the internal micro-cracks and porosity, as pointed out by Neville (1995). In addition to this, it was also noticed that that adjustment in the aggregate volume significantly improved the slump property and prevents the tendency of bleeding and segregation, especially at low alkali.

However, as per IS 10262 (2009), a slightly higher content of fine aggregate (*s/a* = 0.49) is suggested to prepare concrete with smaller size of aggregate. But in GPC when the fine aggregate content is further increased to 0.49 in the mixes of Group IV, the mixes showed a declining trend in the strength parameters. This is due to an excess of fine aggregate in the mix, which increases the volume of geopolymer mortar paste, making the mix brittle in its hardened form and reduces compressive strength. The compressive strength achieved in the mixes of Group IV are comparatively lesser than the mixes of the other groups. As a consequence of the test findings, it is clear that for a given volume of fine and coarse aggregate, the GPC mix offers satisfactory workability and delivers the best characteristics to the concrete.

Meanwhile, the strength development of the PCC mix, CM2, can be observed in the previous Fig. 4.11. The mix exhibited a compressive strength of 12.09 MPa, 24.18 MPa and 35.56 MPa on the 3^{rd}, 7^{th} and 28^{th} day. Even though the w/s ratio of the PCC mix is kept equivalent to that of w/c ratio of the GPC mix, the compressive strength attained by the mix CM2 is much lower than the GPC. Moreover, unlike GPC mixes, the early strength of the PCC mix is not remarkable as GPC.

4.3.1.3 Split tensile strength

The split tensile test of the cylinder is used to determine the indirect tensile strength of the GPC mixtures. Fig. 4.12. illustrates the split tensile strength of the GPC mixes at the age of 28 days. The tensile strength of GPC is mainly dependent on the bond between the geopolymeric paste and the coarse aggregate in the Interfacial Transition Zone (ITZ) (Ryu et al., 2013). From the test result, it can be observed that the tensile strength of all the GPC mixes are almost in line with the compressive strength of the mix. Like compressive strength, the tensile property of the GPC mixes also varies with the change in the molar concentration of SH.

In mixes of Group II, which contains lower fine aggregate (*s/a* = 0.33), the mix MG4 developed a tensile strength of 2.71 MPa. With the increase in molar concentration, the tensile strength of GPC gradually improves and achieves maximum strength of 3.27 MPa for mix MG6, activated by 8M SH. Beyond 8M, the concentration of SH has a negative effect; hence,

the tensile strength declines to 2.88 MPa and 2.51 MPa, as shown by the mixes MG2 and MG7. A similar trend is also found in the compressive strength noticed in the previous section, which supports the behaviour of the tensile strength.

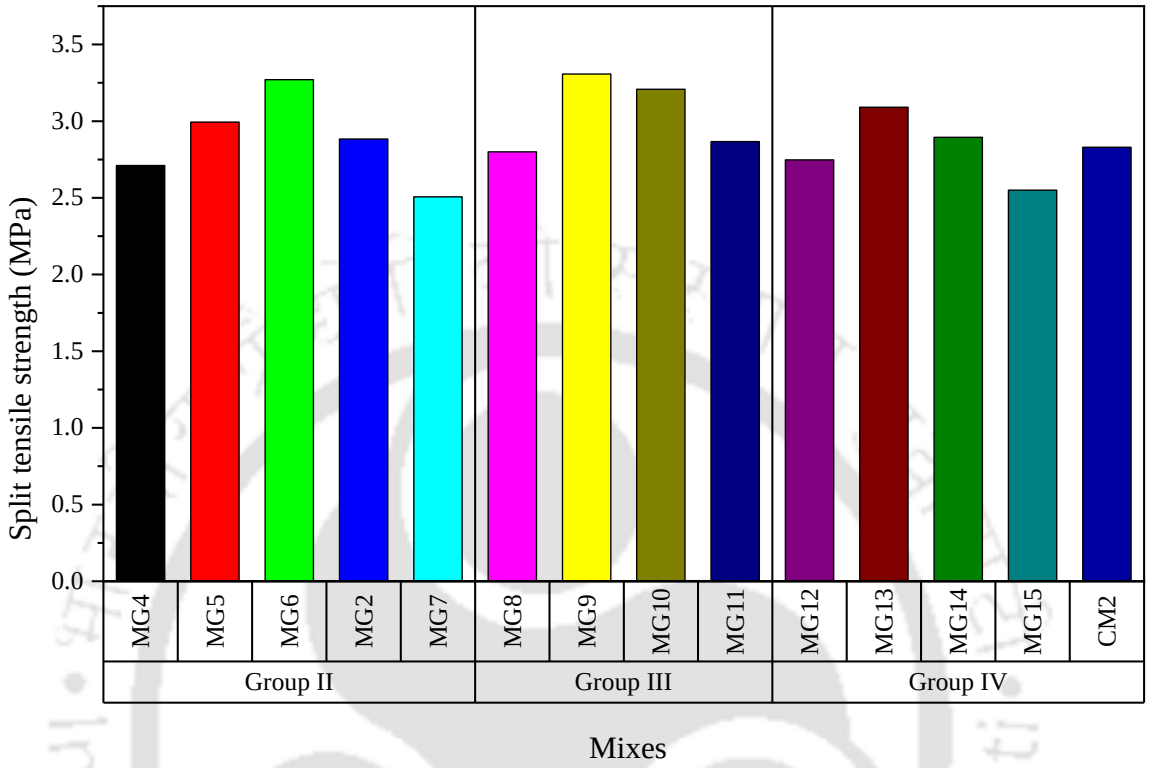

Figure 4.12: Split tensile strength of GPC mixes

The change in volume of the fine aggregate does not show any significant difference in the tensile property in the tensile strength. However, slightly better tensile properties are obtained for the mixes of Group III prepared by a *s/a* ratio of 0.41. At a *s/a* ratio of 0.41, the mix MG9 and MG10 of Group III, activated by 6M and 8M, exhibited a slight improvement in the strength value to 3.31 MPa and 3.21 MPa, as shown in Fig. 4.12. This improvement in the tensile properties exhibits the similar trend obtained in the compressive strength test. This may be attributed to an increase in the volume of sand, which improves the voids and porosity in the GPC mixes.

But with a further increase in the volume of fine aggregate (*s/a* = 0.49) i.e. in Group IV the effect of molar concentration was found to be similar, but a considerably larger degradation in tensile strength is seen as compared to the mixes of Group II and Group III. This is due to the fact that as the sand volume is increased in the mixes of Group IV, geopolymer mortar paste in the mixes becomes sufficiently thicker. The increased thickness of the geopolymer paste

surrounding each aggregate increases the possibility of cracks in the geopolymer matrix (Chu 2019). Moreover, using a higher volume of sand makes the ITZ relatively weaker (Teng et al., 2013), thereby increases the brittleness of the specimens. Thus it is clear that the role of the molar concentration and s/a ratio in developing the tensile strength is significant in GPC mixes. The better tensile strength within 6M to 8M resembles a dense geopolymer paste in the ITZ, which improves the homogeneity and ultimately improves the tensile property of the GPC mixes.

On the other hand, the tensile property of the PCC based mix, CM2, exhibits almost a comparable tensile strength of 2.83 MPa like GPC, which is comparatively better than some of the mixes of GPC with high molar concentration. From the above discussion it is clear that an ideal mix of UBFS based GPC mixes develops an enhanced tensile strength than the conventional concrete. The role of molar concentration of the alkali solution in developing the strength property is significant in GPC mixes. The better tensile strength within 6M to 8M, resembles a dense geopolymer paste in the ITZ which improves the homogeneity and ultimately improves the tensile property of the GPC mixes (Teng et al., 2013).

4.3.1.4. Bond strength

The shear bond strength between GPC and PCC substrate, which is evaluated on the 3rd day and 28th day, which is illustrated in Fig. 4.13. All GPC mixes exhibit an exceptionally good bond strength. The bond strength result of GPC tends to follow a similar pattern to that of the

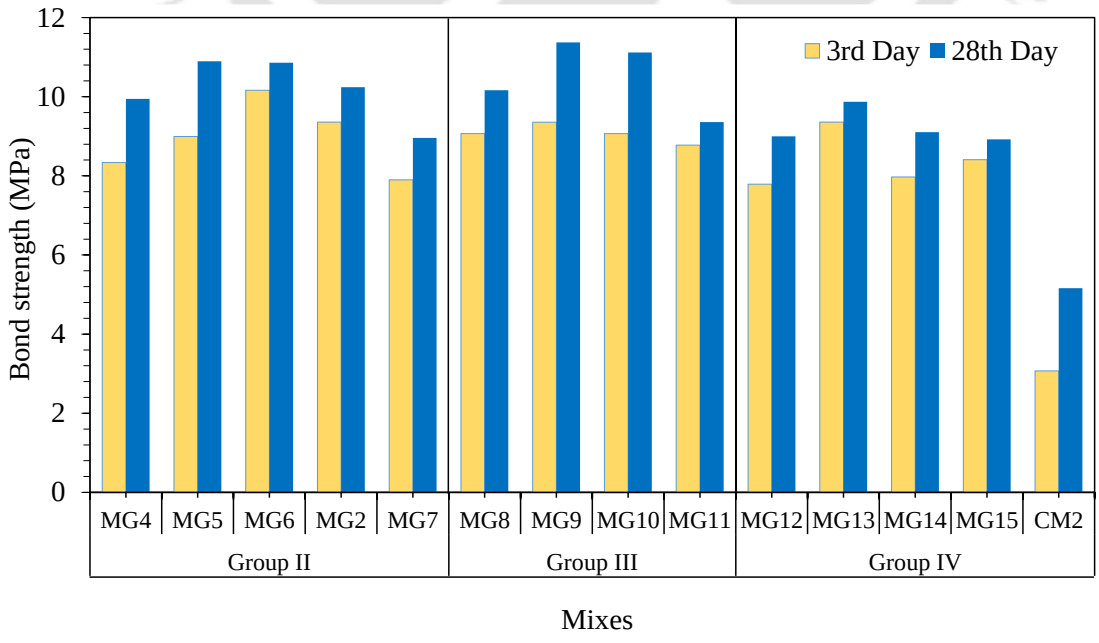

Figure 4.13: Bond strength property of GPC mixes at the 3rd and 28th day

compressive strength as discussed in the previous subsection 4.3.1.2. It is observed that on the third day of curing, the average bond strength of GPC is roughly 89 % of the bond strength on the 28th day. From the test result, it is seen that the bond strength is heavily influenced by the molar concentration of SH, as shown in Fig. 4.13. The volume of aggregate, on the other hand, has a relative influence on bond strength, similar to the tensile properties. Although the volume of fine aggregate in the mixes of Groups II and III differs, there is no discernible change in bond property. However, as demonstrated by the result, when a larger amount of fine aggregate (*s/a* - 0.49) is introduced into the mix, it results in a considerable decrease in bond strength. It is also noticed during the slant shear test that the failure pattern of slant shear specimen is significantly affected by the bond strength between the GPC and the PCC substrate. Three types of failure patterns have been identified in the slant shear specimen, as shown in Fig. 4.14. (a)-(c). and Fig. 4.15.

a) Type - A

b) Type - B c) Type - C

Figure 4.14: Different modes of failure in slant shear specimens of GPC

The three types of failure obtained in the slant shear specimens are

Type A- Failed by sudden splitting purely at the interface.

Type B- Partial splitting at the interface and crushing of GPC and PCC matrix.

Type C- Axial splitting cracks across the interface similar to normal cylinder.

Type-A failure is commonly found in the mixes with low bond strength and especially in the mixes activated by low alkali concentration. The mixes MG4, MG8 and MG12, which are activated by 4M, exhibit a relatively low bond strength of 9.95 MPa, 10.17 MPa and 9.0 MPa. The main reason if low bond strength is due to the slow polymerization process (Musaddiq Laskar and Talukdar, 2017; John et al., 2018) owing to the low molarity of SH, resulting in inferior geopolymeric products with poor internal structural strength. All these specimens followed a similar Type-A failure mode, as shown in Fig. 4.14. (a). Such failure indicates that adhesion at the interface between the GPC and PCC part is comparatively weaker than the adhesion property within the GPC and PCC matrix. This leads to a clear bond failure in the specimen, resulting in low bond strength.

However, this behaviour tends to change when the mixes are activated with a higher concentration of SH solution. Fig. 4.13., shows that bond strength values with 6M and 8M are comparatively higher than the bond strength achieved in any other molar concentration. The mixes MG5, MG9 and MG13, activated by 6M molar concentration of SH, exhibited a bond strength of 10.9 MPa, 11.37 MPa and 9.87 MPa, while the same mixes, when activated by 8M, exhibited a bond strength of 10.86 MPa, 11.12 MPa and 9.10 MPa respectively. This indicates that the high bond strength at a moderate alkali concentration exhibits superior adhesion in the interface. Furthermore, this improved bond strength is found maximum at 6M, which is almost in line with the other mechanical properties of GPC mixes. This is because as molar concentration increases, the pH value in the mix also increases, which accelerates the dissociation of oxides present in the binder, leading to better formation of geopolymeric gel resulting in a dense internal structure (Fernandez and Palomo 2005). The improvement in the geopolymeric gel results in a denser matrix at the interface between the GPC and PCC, which resists the separation at the interface. The failure mode Type-C also supports this statement that took place in most of the specimens which exhibited high bond strength. Fig. 4.14. (c) shows the typical failure pattern of the mixes, which is referred to as Type-C failure mode. Such failure initiates by axial splitting cracks, which propagate in the GPC and PCC matrix

rather than at the interface and, finally, tend to burst like a normal cylinder. This typical failure pattern indicated the superior bond strength at the interface, which turned the failure pattern of the slant shear specimen like that of a normal cylinder.

On the other hand, the use of a high molar concentration has a detrimental influence on bond strength. As the concentration of SH is increased to 10M and 12M, the bond strength monotonously decreases, as exhibited by the mixes MG2, MG7, MG11 and MG15. This can be attributed to the fact that, as the molar concentration rises, so does the amount of OH^- ion in the solution. This affects the polycondensation reaction, subjected to early precipitation of C-A-S-H gel (Part et al., 2015), leading to poor formation of reaction products and a weaker matrix at the interface. In addition to this, at a high concentration of 12M, the overall amount of solid components also increases, which degrades the consistency of the mix. This leads to poor compaction, resulting in degradation of strength in the GPC. Due to this lower strength of GPC, the failure surface at the interface of GPC and PCC also tends to propagate within the GPC and the PCC matrix. All such specimen mostly exhibits a Type-B failure mode, shown in Fig. 4.14. (b).

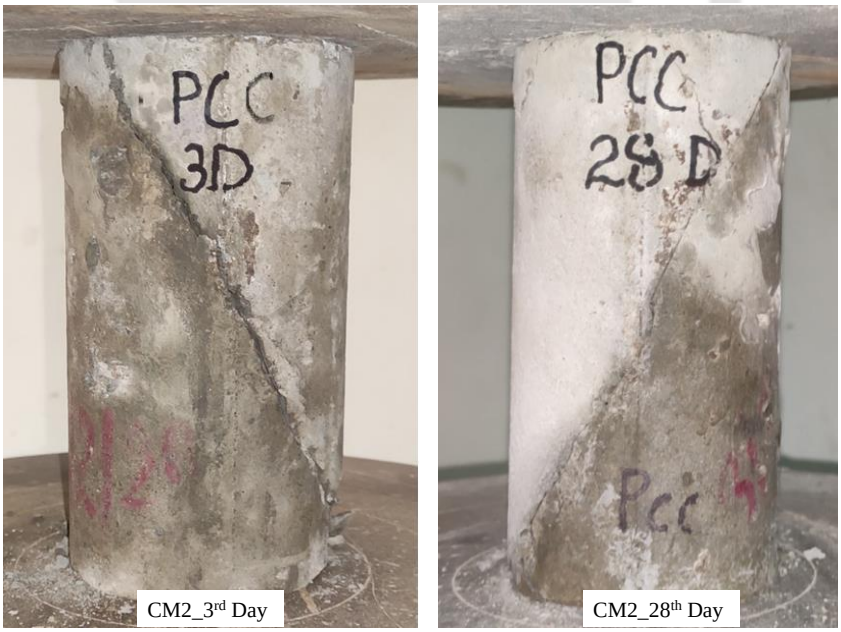

Figure 4.15: Mode of failure in slant shear specimens of PCC

On the other hand, the bond strength obtained between the PCC to PCC are much lower compared to GPC. The 3rd day and 28th day bond strength of the mix CM2 with the substrate part is obtained as 3.07 MPa and 5.16 MPa. Due to this poor bond strength between the two PCC part, the specimen failed by splitting at the interphase as shown in the Fig. 4.15.

4.3.2 Result and discussion of Fiber reinforced geopolymer concrete

Based on the results obtained from the GPC mixes, three mix proportion are selected to study the effect of steel fiber. The FRGC mixes are prepared using various V_f of steel fiber and the workability and the strength properties of the mixes are studied.

4.3.2.1 Workability

The result obtained from the slump test and Vee-bee test conducted on the fresh FRGC and FRCC mixes are presented in Fig. 4.16. The test result shows that addition of steel fiber leads to tremendous losses in the workability of the mixes. With addition of steel fibers an exponential decay in the slump value is observed. When 0.5 % V_f of steel fiber is added in the mix MG6_0.5, a significant lower slump value (120 mm) is obtained, which was earlier obtained as 190 mm for the mix MG6 with no fiber. Successive increment in the V_f of steel fiber shows a rapid drop in the slump value. However, it is observed that FRGC mixes retains a sufficient workability till the V_f of the steel fiber is increased to 1 %. Beyond 1.5 % of V_f, the mix (MG6_1.5), becomes very stiff in nature and slump value drops to 20 mm. With further increment of steel fiber to 2 % (mix MG6_2%) almost a zero slump is achieved.

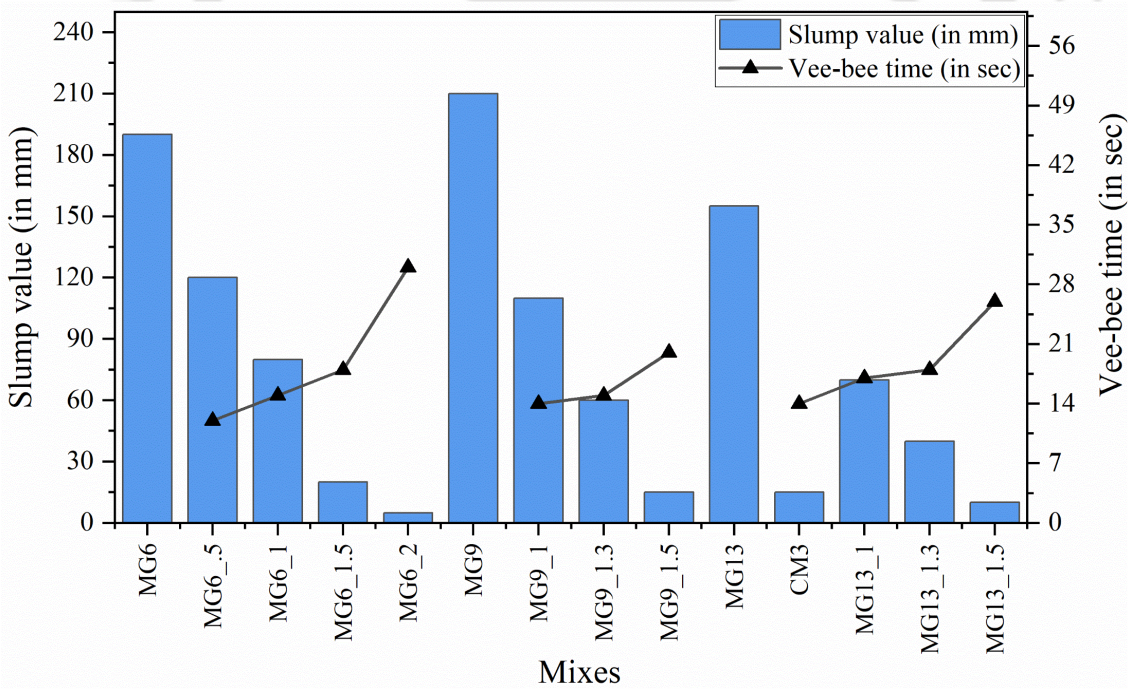

Figure 4.16: Workability of FRGC mixes

However, it can be seen from Fig. 4.16. that as the slump value tends to become zero, there is an exponential rise in the Vee-bee time. This indicates a poor workability, which can be

attributed to the loss of fluidity due to the increased surface area in the mix associated with the increase in fiber content (Yu et al., 2014). Thereby making the mix very dry and stiff resulting in high Vee-bee time. Moreover, the increased fiber content promotes the balling action of the steel fiber, which also restricts the flowabilty of the FRGC mixes (Farhan et al., 2018), resulting in to a loss in the workability.

This declining trend of workability, with variation V_f of steel fiber, is found to be similar in the other mixes, but are additionally affected by the increment of fine aggregate content. This can possible be understood by comparing all the FRGC mixes, which are modified from MG9 and MG13 by addition of steel fiber. These mixes (MG9_1 to MG9_1.5 and MG13_1 to MG13_1.5) are activated with same alkali concentration (6M), but they contain different volume of fine aggregate (*s/a* ratio 0.41 and 0.49). For example, the mix MG9_1%, which is similar to MG13_1% in terms of V_f of steel fiber and molar concentration, shows a slump value of 110 mm. But with increase in the fine aggregate (s/a = 0.49), the slump value of the mix MG13_1 reduces to 70 mm. Similar result is also found from the other mixes, with same fiber content but different *s/a* ratio. This is attributed to the fact that as the solid content in the mix proportion increases, the FRGC mix gets dehydrated which ultimately affects the workability of the mix.

It is also possible to observe from Fig. 4.16. that the mixes with fiber content up to 1.3 %, shows no significant variation in the vee-bee test results. This is because all these mixes still have a considerable slump value of more than 20 mm, even after the addition of steel fiber. The FRGC concrete settles down instantly as soon as the vibration starts. The vee-bee time of all such mixes (with V_f less than 1.5%) ranges in between 12 to 18 sec. However, an exponential increase in the vee-bee time can be noticed for the mixes with V_f beyond 1.3 %.

Based on the properties of the FRGC mixes, the FRCC mix is also prepared by addition of 1.3 % V_f of steel fiber. The test result shows that; inclusion of steel fiber reduces the workability of CM3 to 20 mm. But interestingly, it can be noticed that vee-bee time is comparative lesser (15 sec) than FRGC, due to relatively low cohesion in FRCC unlike FRGC.

4.3.2.2 Mechanical Properties

The compressive strength and flexural strength of the FRGC mixes with different V_f of steel fiber are determined on the 28th day of curing. Upon completion of 28th day of curing, the specimens are taken out of the curing tank and are kept in open air for drying. After proper

drying of the specimen, compressive strength test and flexural strength test are carried out in UTM as shown in Fig. 4.17. (a) – (c). The compressive strength and the flexural strength are determined by taking the average strength of three test results.

a) Cube without fiber

b) Cube with fiber

c) Test setup for Flexural test

Figure 4.17: Testing of FRGC specimens

Fig. 4.18. represents the effect of steel fiber on the compressive strength and flexural strength of FRGC mix, with an *s/a* ratio of 0.33 activated by 8M of SH. The test result shows that the mechanical properties of the GPC material are largely enhanced by the incorporation of steel fiber. It is observed initially, that the mix MG6 with no fiber exhibits a compressive strength and flexural strength of 47.04 MPa and 6.90 MPa, respectively. With addition of steel fiber by 0.5 % and 1 % V_f, the compressive strength gradually improved to 52.30 MPa and 55.11 MPa, respectively, which is approximately 11 % and 17 % higher than the mixes containing no fiber.

At the same time, the flexural strength of the aforementioned mixes, increased significantly to 8.36 MPa and 9.07 MPa, respectively, which is 21 % and 31 % higher than the mix with no steel fiber. Further increase in the V_f of steel fiber causes a slight degradation in

the compressive strength (54.07 MPa) but flexural behaviour still steadily improved and exhibited a maximum flexural strength of 10.36 MPa at 1.5 % V_f of steel fiber.

This mismatch between the flexural strength and compressive strength is also pointed out by Song and Hwang (2004) while investigating high-strength fiber composite. However, V_f of steel fiber beyond 2 % drastically degrades both the strength property of the FRGC. The improvement in compressive strength due to fiber addition is due to the fact that addition of steel fiber provides a confinement effect in the concrete (Das et al., 2018) which resist the crack induced during loading. This phenomenon improves the stiffness of the concrete resulting in increased compressive strength. On the other hand, at a high dosage of fiber (2 % V_f), the balling action of fiber comes in to play, as noticed in the mix MG6_2%. The mixes become dry, with low workability which leads to improper compaction. This causes porosity in the matrix, which ultimately effects the mechanical strength of FRGC (Faran et al., 2018). From above discussion, it could be concluded that the addition of steel fiber largely improves the mechanical property of the GPC. However, an excess quantity of steel fiber degrades the mechanical characteristics of the FRGC. Hence the rest of the mixes are investigated by adopting V_f of fiber within a range of 1 % to 1.5 %.

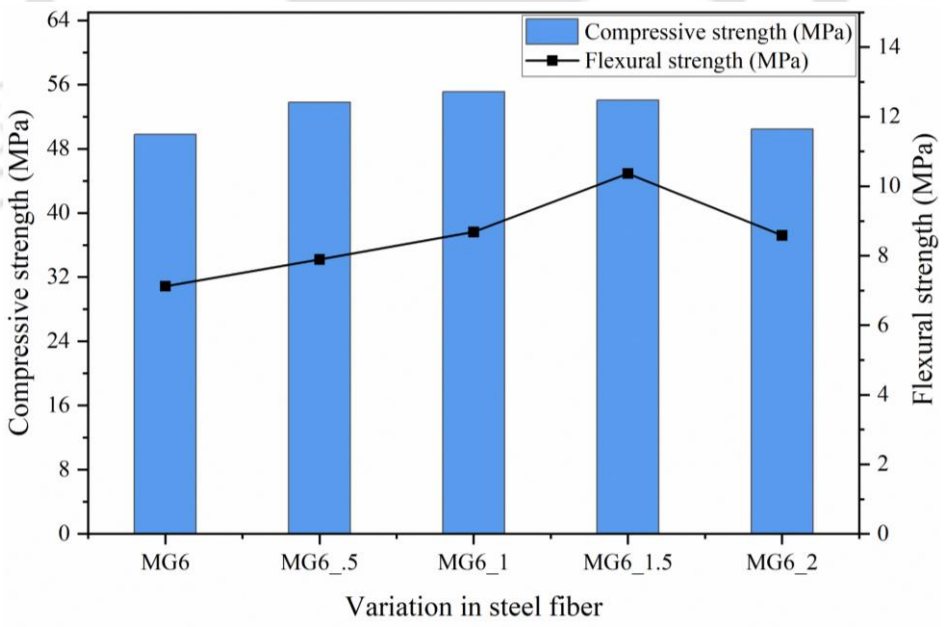

Figure 4.18: Compressive strength and flexural strength for *s/a* = 0.33 and 8M solution in FRGC mixes

Fig. 4.19. and Fig. 4.20., depicts the effect of steel fiber in the mixes subjected to increased volume of fine aggregate and activated by a common molar concentration of 6M. The test data

clearly shows that the effect of steel fiber in the later mixes with higher fine aggregate content are almost in line with the previous mixes prepared with lower content of fine aggregate content. The mix MG9 with no fiber exhibits a compressive strength and flexural strength of 49.33 MPa and 7.12 MPa. Inclusion of fiber content by 1 % improves the compressive strength and the flexural strength by 5 % and 28 %. Further increase in the fiber content to 1.3 % V_f (MG9_1.3%), improves the compressive strength and flexural strength to 12 % and 59 %. This shows that the addition of 1.3 % of steel fiber shows the maximum improvement in the flexural strength than all the other mixes. It is seen that the addition of steel fiber enhances the mechanical strength by delaying the initiation and propagation of micro cracks. However, when these quantity of the steel fiber increases to 1.3 % (V_f), it leads to a reduction in the average spaces between the steel fiber, and a more effective crack bridging action (Liu et al. 2020) takes place which leads to improve the flexural strength of the FRGC mix.

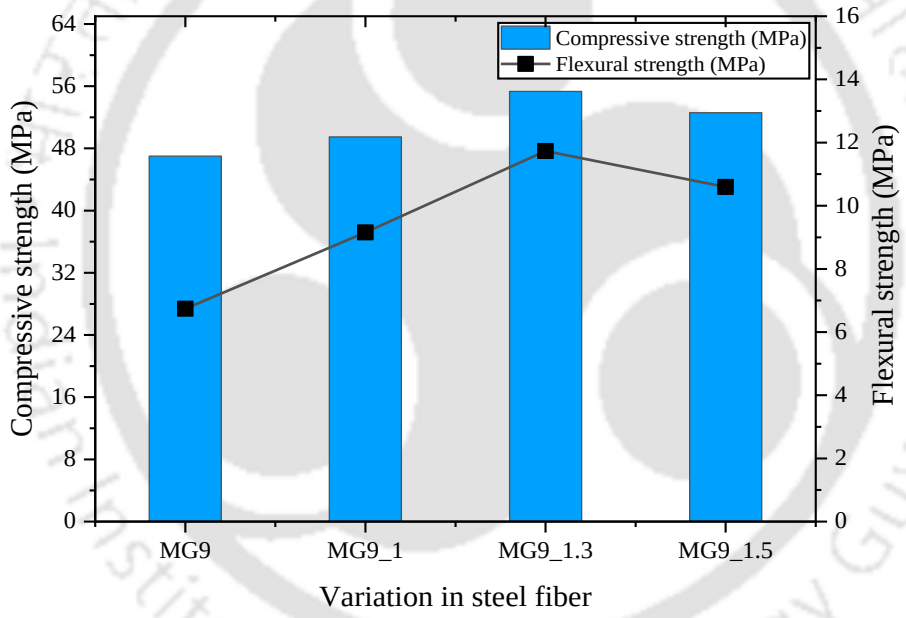

Figure 4.19: Compressive strength and flexural strength for *s/a* =0.41 and 6M solution in FRGC mixes

But at 1.5 % V_f, a decline in the compressive strength is observed. This shows that maximum compressive strength is attained at a V_f of 1.3 % in the mixes prepared by *an s/a* ratio of 0.41. This contradicts the result of the previous mix (MG6_1), prepared with *an s/a* ratio of 0.33, where maximum compressive strength is obtained for a V_f of 1 %. This could be attributed to the fact that as the amount of *s/a* ratio is increased from 0.33 to 0.41, in the mix MG9_1.3. The amount of fine aggregate increases in the MG9_1.3 mix, which contributes to forming a dense

FRGC mix. This also leads to a better distribution of fiber, which improves the fiber matrix bonding, thereby improving the mechanical property of the mix.

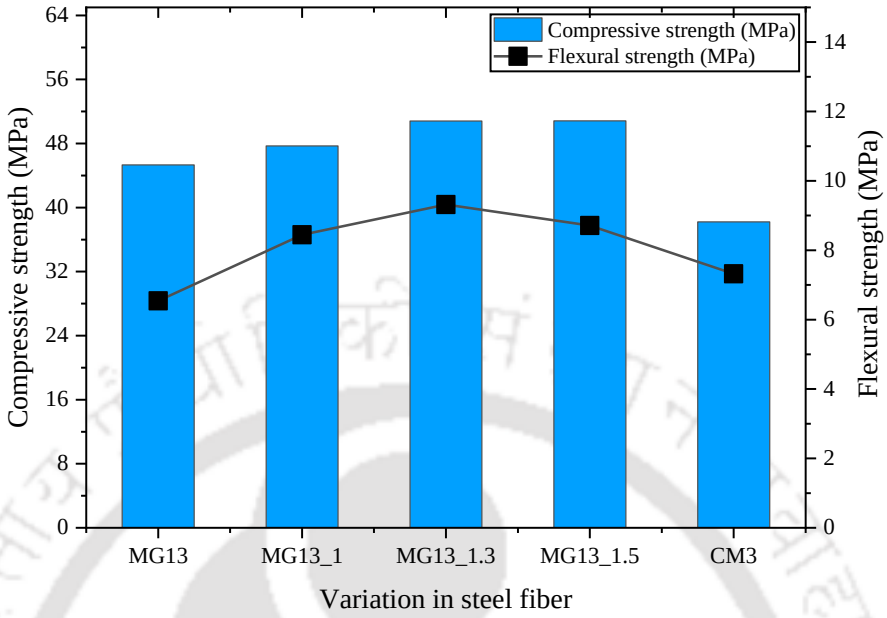

Figure 4.20: Compressive strength and flexural strength for *s/a* = 0.49 and 6M solution in FRGC mixes

The effect of steel fiber in the FRGC mixes (MG13_1 % to MG13_1.5 %) containing fine aggregate volume of 0.49, follows the similar patterns as exhibited by the previous mixes. But their strengths are much lower as compared to previous mixes. The mix MG9_1.3 %, exhibits the maximum compressive strength and flexural strength of 55.33 MPa and 11.38 MPa. In contrast, the mix MG13_1.3 (similar to MG9_1.3, which contain lesser fine aggregate), exhibits a compressive strength and flexural strength of 50.81 MPa and 9.31 MPa. This shows that both compressive strength and flexural strength in the later FRGC reduces by 8 % and 18 % mixes respectively. Apparently, the degradation in the aforementioned mix, is due to the increased volume of fine aggregate which makes the mix brittle in nature and results in to decrease in the strength properties.

From the above discussion, it is revealed that 1.3 % (V_f) of steel fiber exhibits a better performance and hence for better comparison the PCC mix CM2 is also modified by adding 1.3 % of V_f of steel fiber (which is referred as CM3), for a better comparative study. From Fig. 4.20. it can be seen that the FRCC mix, CM3, up on addition of steel fiber exhibits a compressive strength of 38.22 MPa and flexural strength of 7.32 MPa. Which is approximately 7 % and 32 % higher than the mix CM2 with no fiber. This shows that the combination of steel

fiber with GPC is much more effective than PCC. This is because in the FGRC with 1.3 % steel fiber (MG9_1.3%), the maximum compressive strength enhanced by 12 % and flexural strength enhanced by 59 %, which is much higher than that showed by FRCC.

4.4 Microstructure

Fig 4.21 illustrates the FESEM images of mixes, which represent the mixes constituting the same molarity, taken at a magnification of 5 kX and 20 kX. The microstructure of the UBFS based GPC matrix showed a homogeneous formation of C-A-S-H gel in all the mixes. The unreacted particles of binder which are often found in FA based geopolymer (Part et al., 2015) are negligible in the UBFS based GPC mixes even after curing at ambient temperature. However, relative differences were identified and attempted to relate them with the mechanical properties of the GPC mixes. The microstructure of MG4, activated by a molar concentration of 4M, shows the presence of partially reacted FA particles, which shows the traces of geopolymeric gel partially covering the surface of the FA particle, as shown in Fig 4.21 (a).

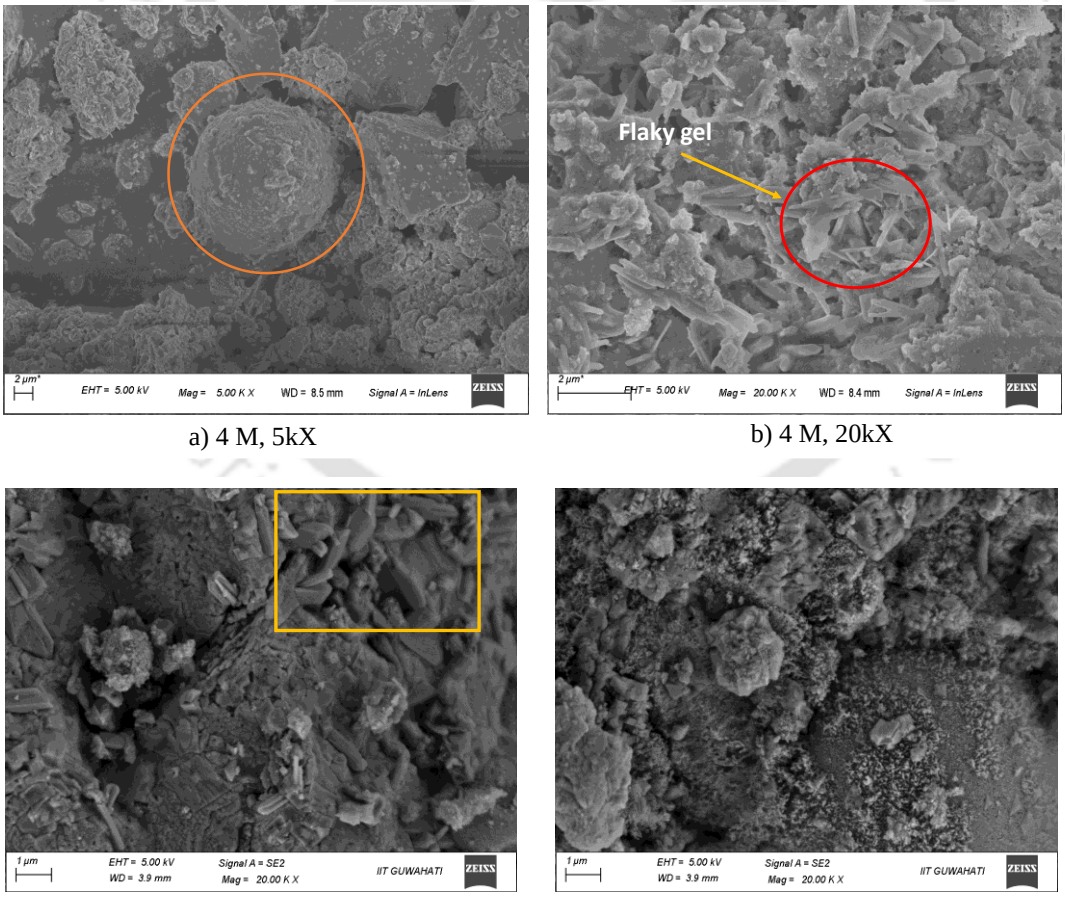

a) 4 M, 5kX

b) 4 M, 20kX

c) 6M, 5kX

d) 6M, 20kX

Figure 4.21: FESEM image of GPC mixes

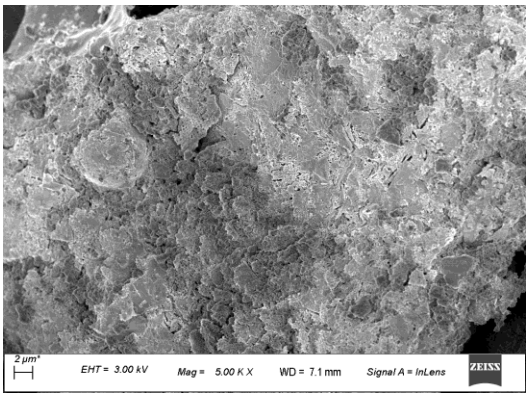

e) 8M, 5kX

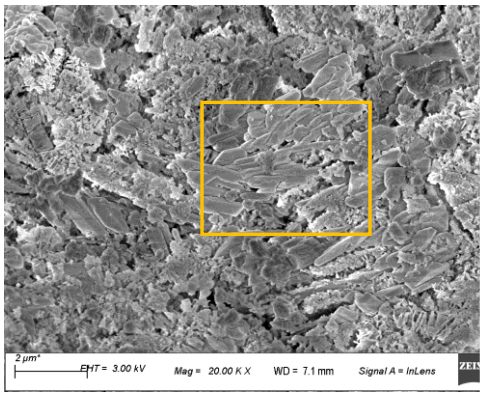

f) 8M, 20kX

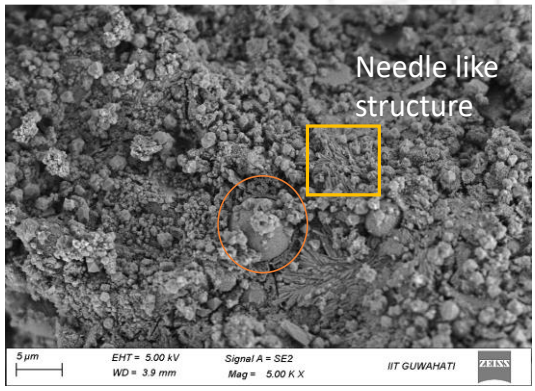

g) 10M, 5kX

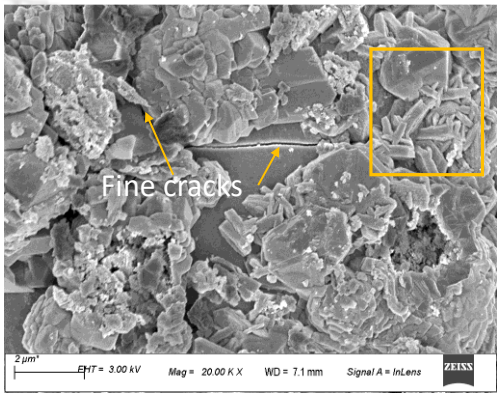

h) 10M, 20kX

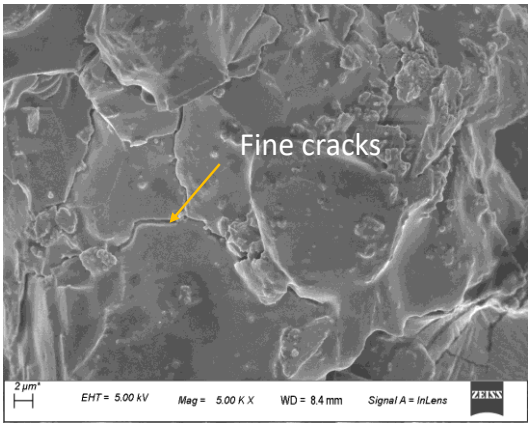

i) 12 M, 5kX

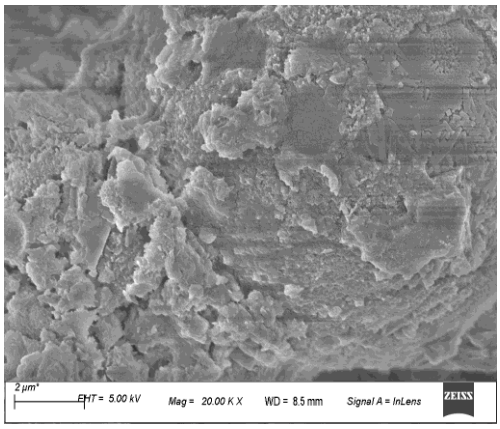

j) 12 M, 20kX

Figure 4.21: FESEM image of GPC mixes

This can be attributed to the fact that lower concentration of SH, affects the leeching of Al^{3+} and Si^{4+} to participate in the geopolymerization. This finding is in line with work reported by previous researchers (Mohammed et al., 2016). But unlike other GPC matrix it could not form a dense three dimensional network like structure. In fact, the microstructure appears relatively loose and porous, as seen from Fig 4.21 (b), showing numerous flaky geopolymeric gel.

Meanwhile, the microstructure of the mixes (Fig 4.21. (c)-(f)) between 6M and 8M, appears to be relatively more homogenous and contains no unreacted microspheres of FA in

the area under supervision. This supports the better mechanical properties of the mixes activated by 6M and 8M. The distinct needle like structure appearing in the Fig 4.21 (c), (f) and (h) shows semi crystalline nature of specimen and implies proper adoption of alkali activator solution (Neville 1995) contributing to the strength of the GPC mixes.

The microstructure of the mixes, activated by 10M and 12M, as seen in Fig 4.21 (g)-(j), appears to be similar. However, distinct cracks can be observed in the matrix of the later mixes. Due to very high alkalinity, the geopolymeric gels cannot form an integral matrix and cracks and pores are formed. Moreover, in a highly alkaline medium, the pH level increases and the geopolymeric gel precipitates at an early stage (Somna et al., 2011), which leads to less development of the geopolymeric product, as seen in Fig. 4.21 (j), causing a reduction in the strength.

4.5 Statistical analysis

The statistical analysis of compressive strength data was carried out for all the GPC mixes to find out mean (μ), standard deviation (σ) and coefficient of variation (ρ). The strength result of

Table 4.4: Statistical data of the strength parameters of GPC and PCC

Mix	Compressive strength, f_{ck}			Split tensile strength, f_{ct}			Bond strength, B_{sc}		
	μ (MPa)	σ (MPa)	ρ	μ (MPa)	σ (MPa)	ρ	μ (MPa)	σ (MPa)	ρ
MG4	43.37	0.72	0.017	2.71	0.202	0.075	9.95	0.621	0.062
MG5	46.22	1.18	0.025	2.99	0.026	0.009	10.9	1.706	0.157
MG6	47.04	1.94	0.041	3.27	0.101	0.031	10.86	0.31	0.029
MG7	38.96	1.03	0.026	2.51	0.003	0.001	8.96	0.233	0.026
MG8	44.92	1.63	0.036	2.8	0.236	0.084	10.17	0.465	0.046
MG9	49.33	1.6	0.032	3.31	0.161	0.049	11.37	0.31	0.027
MG10	46.73	1.3	0.028	3.21	0.069	0.021	11.12	0.465	0.042
MG11	42.2	0.85	0.02	2.87	0.12	0.042	9.36	0.155	0.017
MG12	43.78	1.11	0.025	2.79	0.08	0.029	8.7	0.155	0.018
MG13	45.33	1.78	0.039	3.09	0.184	0.06	9.87	0.31	0.031
MG14	43.11	1.6	0.037	2.9	0.192	0.066	9.1	0.543	0.06
MG15	39.85	0.68	0.017	2.55	0.08	0.031	8.92	0.931	0.104
MG2	47.04	1.7	0.036	2.88	0.027	0.009	10.24	0.776	0.076
CM2	35.56	1.18	0.033	2.83	0.16	0.057	5.16	0.931	0.181
MG3	48.07	1.9	0.04						
MG1	41.93	1.51	0.036						

Table 4.5: Statistical data of FRGC and FRCC

Mix	Compressive strength, f_{ck}			Flexural strength, f_b		
	μ (MPa)	σ (MPa)	ρ	μ (MPa)	σ (MPa)	ρ
MG6_.5	52.3	1.12	0.021	8.36	1.01	0.12
MG6_1	55.11	0.89	0.016	9.07	0.67	0.074
MG6_1.5	54.07	1.8	0.033	10.36	1.11	0.107
MG6_2	50.44	1.11	0.022	8.59	0.48	0.056
MG9_1	51.7	1.12	0.022	9.16	0.58	0.063
MG9_1.3	55.33	1.53	0.028	11.38	1.01	0.088
MG9_1.5	52.59	1.36	0.026	10.59	0.8	0.076
MG13_1	47.7	1.43	0.03	8.45	0.66	0.078
MG13_1.3	50.81	1.8	0.035	9.32	0.57	0.061
MG13_1.5	50.83	1.44	0.028	8.71	1.26	0.144
CM2_1.3%	38.22	1.18	0.031	7.32	0.38	0.052

both GPC and PCC are analysed and given in Table 4.4 and the strength result of the FRGC and FRCC mixes are given in Table 4.5. From Table 4.4, it can be seen that standard deviation (σ) of the test data of GPC are in the range of 0.026 MPa to 1.94 MPa while coefficient of variation (ρ) are in the range of 0.00 to 0.181. While that in FRGC mixes, σ ranges between 0.48 to 1.8 MPa and ρ of the mixes ranges between 0.016 to 0.144. The low σ and ρ values indicate a close distribution of the data around the mean value, reflecting a high degree of precision and dependability of the studies performed (Montgomery and Runger 2010).

4.6 Correlation between the mechanical properties

After all the experimental investigation, the mechanical properties of the various mixes are plotted and an attempt has been made to establish a relationship between each other. The correlation equation between compressive strength, splitting strength and flexural strength is suggested based on the findings of destructive experiment tests of various mixtures.

4.6.1 Relationship between Tensile strength, Bond strength and Compressive strength in GPC

From test result it can be observed that both split tensile strength and bond strength has a linear relationship with the compressive strength. In order to predict the strength properties of GPC linear relationships have been established between the compressive strength with the split tensile strength and bond strength. Fig. 4.22. shows the relation between the split tensile and

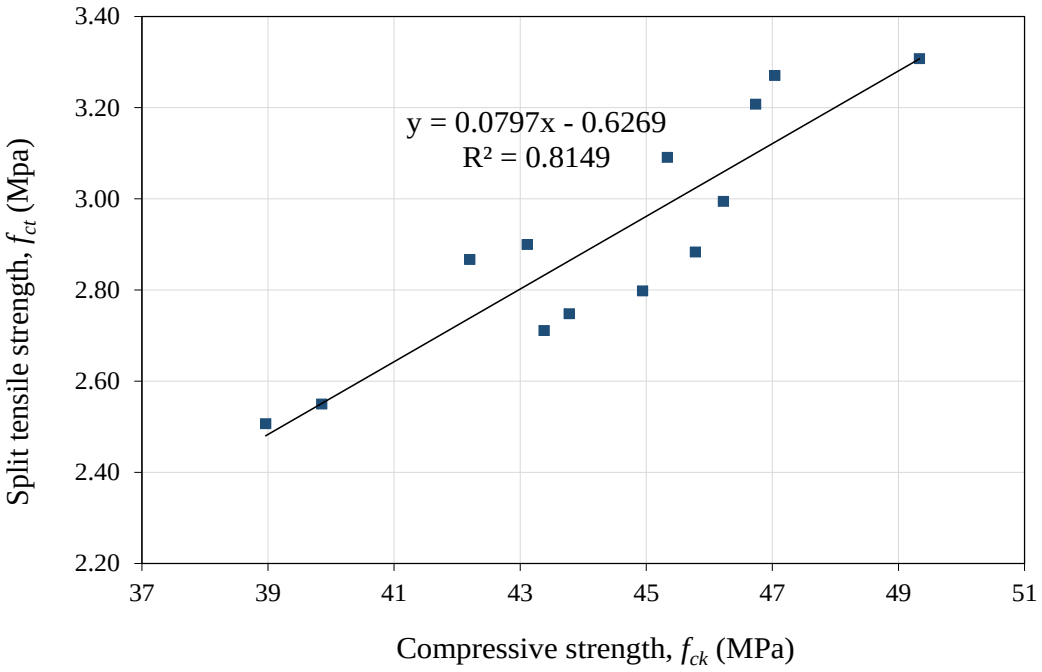

Figure 4.22: Relationship between split tensile and compressive strength of GPC

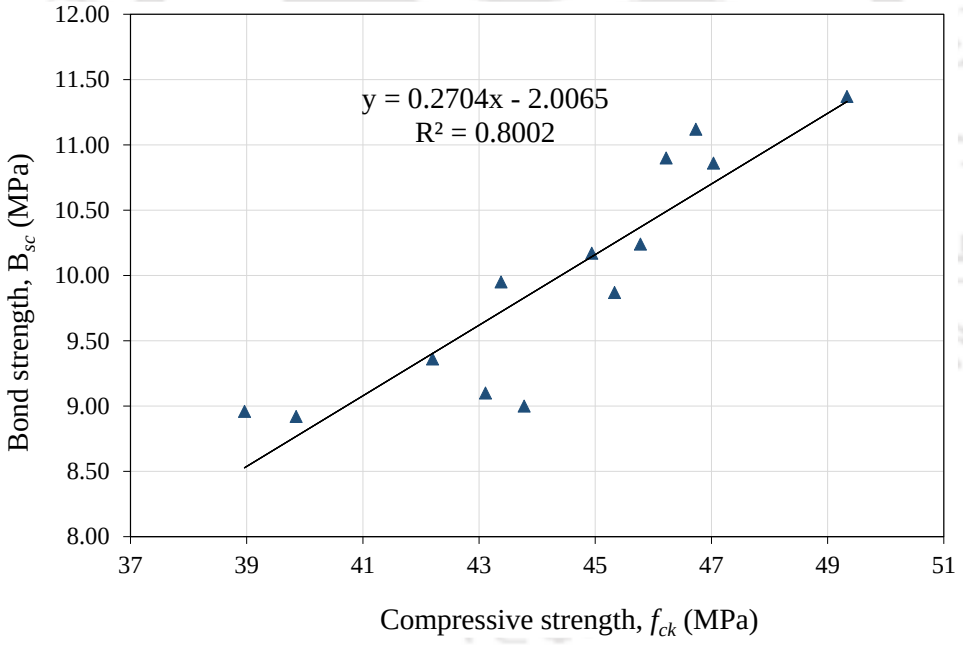

Figure 4.23: Relationship between bond strength and compressive strength of GPC

the compressive strength. Whereas, Fig 4.23 shows the relation between bond strength and the compressive strength. The trend line for both types of mixes in each plot exhibits a linear relationship between the compressive strength and split tensile strength. The coefficient of determination (R^2) obtained in the regression analysis for each type of mixes are consistent and hence linear relationship could be developed between the strength parameters. The regression

models obtained to estimate the split tensile strength and the bond strength of the GPC mixes are the form, as given in equation below-

$$\text{Split tensile strength},\ f_{ct} = 0.079 f_{ck} - 0.63 \quad (4.4)$$

$$\text{Bond strength},\ B_{sc} = 0.27 f_{ck} - 2.0 \quad (4.5)$$

4.6.2 Relationship between Flexural strength and Compressive strength of FRGC

Fig. 4.24 shows the relationship between the flexural strength and compressive strength of the FRGC mixes. From the plot, it can be observed that flexural strength of the FRGC mixes increases linearly with the increase in the compressive strength. The trend line between the two parameters shows linear relationship between flexural strength and the compressive strength. The coefficient of determination (R^2) obtained in the regression analysis is not so consistent. Apparently, this is due to the mismatch between the compressive strength and flexural strength in the FRGC mixes modified from MG6. The mixes MG6 which is investigated by various V_f of fiber showed remarkable improvement in the flexural property up to 1.5 % V_f of fiber, But the compressive strength could be improved only up to a fiber addition of 1 %. However, a linear equation is developed to understand the relation between the two parameters, which is shown in the Fig. 4.24.

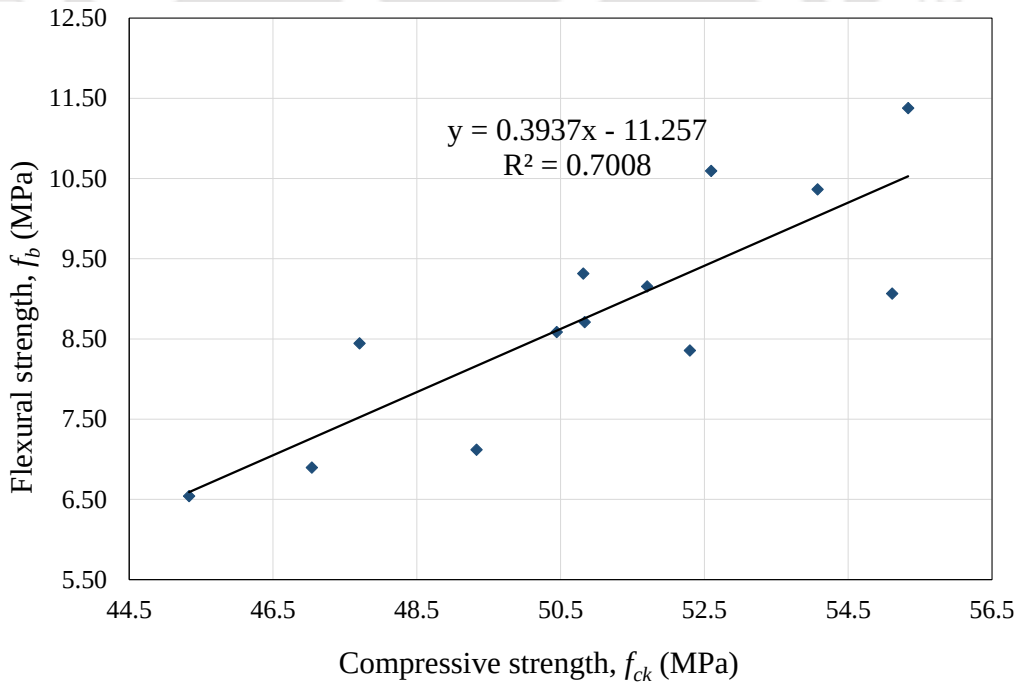

Figure 4.24: Relationship between bond strength and compressive strength of FRGC

4.7 Closure

This chapter presented the test results of laboratory experiments performed on GPC and the FRGC mixes to evaluate the workability, compressive strength and bond strength of the various GPC and FRGC mixes. The mix proportion of GPC, using high volume UBFS and activated by single alkali solution showed enhanced flow characteristics which further promotes the strength characteristics of FRGC mixes. The utilization of calcium rich binder (UBFS) in GPC exhibits a high rate of gain in strength at an early age. The early compressive strength achieved by each mix on the 3rd day and 7th day is approximately 72 % and 83 % of the compressive strength on the 28th day. Moreover, the bond strength of the GPC with PCC surface is found to be satisfactory at both early and later ages. The different *s/a* ratio that has been considered during the mix design of the GPC mixes, shows a significant effect on the workability and strength properties of GPC. The study reveals that a moderate value of *s/a* 0.41 leads to a better workability and strength properties.

The inclusion of hooked end steel fiber significantly improved that mechanical properties of the FRGC composite. Increase in the volume of fine aggregate up to 42 % (i.e. *s/a* – 0.41), produces a homogeneous and a denser FRGC mix. This in turn contributed to the mechanical properties of the FRGC mix. The optimum value of steel fiber achieved in the present study is 1.3 % V_f. Moreover, PCC and FRCC based controlled mix (CM2 and CM3) are prepared with same w/c ratio as that of w/s ratio of GPC, with the conventional OPC cement. The FRGC mixes developed in the present study possesses sufficient workability as compared to FRCC mix.

Chapter 5

Repairing of Web opened RC beam using Geopolymer mortar

5.1 Introduction

Concrete cracking in reinforced concrete (RC) members occurred due to various factors such as excess loading on the structures, earthquakes, accidental impacts, including man-made impacts, corrosion in reinforcement and so on. Concrete cracks are also caused by shrinkage, thermal strains, chemical reactions, weathering, and ageing. If such fractures in structural members go unnoticed, they will likely widen and spread away from the surface of the members into the inner area. Furthermore, such fractures allow water and toxic ions to enter the concrete, resulting in physio-chemical reactions within the crack. This results in further deterioration, and ultimately the structural member loses its strength. Fig. 6.1 depicts some of the damages to RC structural members produced by various factors. The existence of cracks in concrete affects the deflection of the structure and also the load-bearing capability of the structure. Such a member performs terribly when they are subjected to cyclic load or under dynamic loading like seismic forces, increasing the structures' vulnerability. Dismantling and replacing these damaged parts becomes a challenging task and also a very costly affair. In such circumstances, repair and rehabilitation become the ideal alternative not only to utilise them for their intended service life but also to ensure the safety and serviceability of the connected components.

a) Failure of beam due to over loading

b) Cracks in column

c) Cracks in slab due to thermal stress

d) Cracks in beam due to corrosion in steel

Figure 5.1: Deterioration of concrete in the structural member

In recent years, the repairing of RC structures has been one of the most crucial and emerging fields of research in the construction industry. There are numerous retrofitting materials that have been implemented in the last two decades, as seen in previous works of literature (Hassan et al., 2018, Nie et al., 2018, Ahmed et al., 2012). Some of the repairing and strengthening materials found in the previous literature are: epoxy resin, carbon nanotubes, OPC grouting, OPC mortar, Shrinkage compensating mortar, Free flow micro concrete, Fiber reinforced polymer (FRP), Steel plates jacketing, Reinforced concrete jacketing etc. Amongst the most widely used repairing and strengthening, materials are epoxy resin and the wrapping of Carbon Fiber Reinforced Polymer (CFRP). Although such repairing or strengthening schemes have yielded many positive results at the same time, they also possess their own shortcomings. Moreover, repairing works with such materials is expensive. So the need of low-cost repairing material for the purpose of immediate repairing of RC structures is an essential need for society.

Recently one such cementitious binder called Geopolymer has attained a great achievement for its use in structural application. Some unique features of Geopolymer as a repair material, mentioned by Huseien et al. (2017), are high compressive strength, corrosion

resistance, water resistant, high temperature resistant and above all the bond strength between the substrate material (i.e. concrete) and the repair material (geopolymer) is very strong.

Previous literature reveals that the presence of an opening in the web of beam leads to a disturbance in the normal flow of stresses. Accumulation of this stress around the opening leads to early and wide cracks, which makes the beam weak and fails at an early stage. These deteriorations can be avoided to some extent by the application of extra reinforcement around the opening if the opening is pre-planned. Because in the case of pre-planned opening, the sizes and locations of openings are known to the designer, and adequate strength and serviceability can be ensured by internally strengthening the opening area using additional reinforcement. But in the case of post-planned opening, such members can be rehabilitated by repairing, and external strengthening since demolition and reconstruction of these damaged members are often not feasible as they involve extensive consumption of resources such as cost, time, labour and materials.

The application of geopolymer as concrete repairing and strengthening material for RC structures is relatively new, and its application in the rehabilitation of a damaged web opened beam must be explored. Based on this, the work presented in this chapter aims to develop and implement a new retrofitting technique to repair web opened beams by the application of geopolymer mortar and welded wire mesh.

The work carried out in this chapter is mainly divided in to two parts as follows:

1. Experimental investigation of the RCC beam with web opening at different locations.
2. Repairing of the damaged RCC beam with web opening.

For the purpose of the study of the effect of web opening in the RCC Beam, several RCC beam with opening in the flexure and in the shear zone are initially tested. In order to understand the effect of opening in beam, a solid beam with no opening is also prepared as a reference specimen. In the present study, it has been established that geopolymeric material possesses early strength gain property even at ambient temperature (Chapter 3). Moreover, the superior bond strength of geopolymer with the old concrete substrate, established in Chapter 4, is also a contributing factor which makes it suitable to use geopolymer as a repair material for RCC members. Moreover, in order to study the efficiency of geopolymer mortar (GM) as a repairing material, the performance of GM repaired beam is compared with that of specimens repaired by Portland cement mortar (PCM).

5.2 Experimental Program

5.2.1 Test Matrix

In the current investigation, a rectangular opening has been selected, considered the most critical shape (Mansur and Kiang, 1999) due to its sharp edges creating trouble in the flow of stress. The investigation of the effect of the opening is carried out by considering two critical opening locations this is in the flexure zone and in the shear zone. Both the openings are located symmetrically in the flexure zone and in the shear zone. However, the opening in the shear zone is considered to be the most critical one as it interrupts the natural load path, that is, the line connecting the loading point and the support system. In order to investigate the effect of web opening and the repairing work, nine numbers of RC specimens are cast. These beam specimens are categorised in to three types based on the presence of opening, which are as follows:

a) RC solid beam (SB)

b) RC beam with an opening in the flexural zone (BMS) and

c) RC beam with an opening in shear zone (BSS).

Out of the nine beams, one solid beam with no opening, referred to as "SB", is prepared as the reference beam for the sake of comparison. While in the remaining eight beams, four beams have opening in the flexure zone, which are referred to as "BMS". While four other beams with opening in the shear zone are referred to as “BSS". The length of all the beams are kept same as 2000 mm, with a clear span length of 1800 mm and the cross-section of the beam is adopted as 180×270 mm. The depth of the opening is kept as 33% of the total depth of the beam and the length of the opening is adopted as 300 mm. The size of the opening is kept constant for all the beam specimens. In the present work, the opening is simulated as a post-planned opening; hence, no additional reinforcement is provided around the opening. Therefore, all the beams are reinforced with the same amount of reinforced steel, where the reinforcement in the opening zone has been given in the form of U-shape to simulate the opening as a post planned. The details of the reinforcement are given in Fig. 5.2.

All the beam specimens are tested experimentally under four-point loading scheme, and the results are compared. The specimens that have been tested are loaded with static monotonic load until failure and hence are considered fully damaged specimens. The SB that has been

tested is mainly employed as the reference specimen for the comparative study of web opened beams. While the other specimen of BMS and BSS types that were fully damaged during the

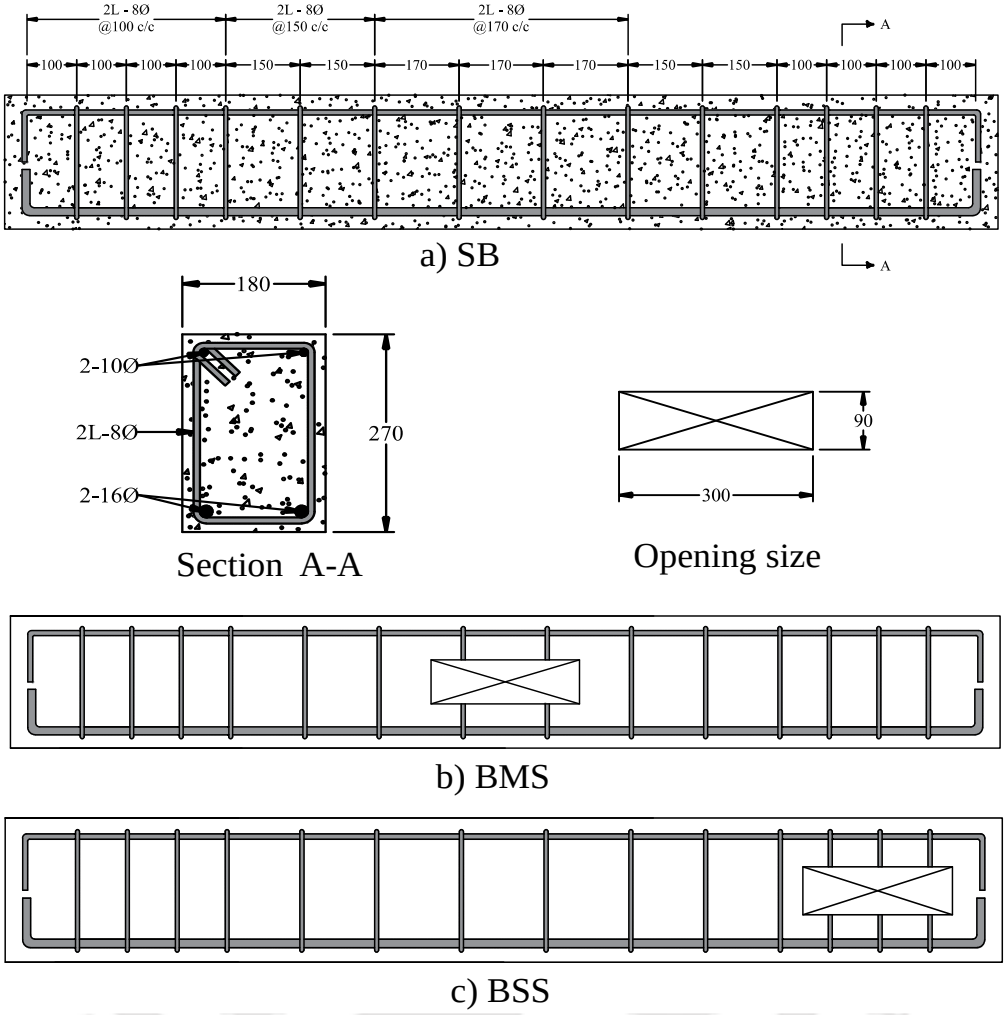

Figure 5.2: Reinforcement detailing of Beam specimen (All dimensions are in mm)

test and are further used to carry out the repairing work. The repair is carried out using both GM and PCM as the repairing material. The characteristics of the tested beam and their designation are summarised in Table 5.1. Total of 8 beams are repaired, out of which four specimens (S2, S7, S4 and S8) with different locations of opening have been repaired using GM. While the other four (S1, S6, S3 and S5) have been repaired using PCM. Moreover, in order to study the effectiveness of the repair material at an early age, the repaired beams are tested on the 3rd day as well as on the 28th day. From the test result of the beam specimen, the following aspects have been thoroughly studied:

1. Yield load and corresponding Deflection of beam.
2. Peak load and deflection at the ultimate load.

3. Ductility ratio (DR).
4. Strength enhancement ratio (SER).
5. Load at 1st crack.
6. Cracking pattern of the tested beam.

Where ductility ratio (DR) is defined as the ratio between the displacement at the ultimate load to the displacement at the yield load of the tested beam (Rakhshanimehr et al., 2014). While Strength enhancement ratio (SER) is defined as the ratio between the ultimate load of the repaired beam to that of the controlled beam.

Table 5.1: Experimental test matrix for Repairing work

Types	Designation of undamaged Beam	Opening Location	Repairing scheme	Designation of Repaired Beam	Tested on
Solid Beam "SB"	S0	No Opening	*Reference beam*		
Beam with opening in mid span "BMS"	S1	Flexure Zone	PCM	R1_PC	28 Days
	S2	Flexure Zone	GM	R2_GM	28 Days
	S6	Flexure Zone	PCM	R6_PC	3 Days
	S7	Flexure Zone	GM	R7_GM	3 Days
Beam with opening in shear span "BSS"	S3	Shear Zone	PCM	R3_PC	28 Days
	S4	Shear Zone	GM	R4_GM	28 Days
	S5	Shear Zone	PCM	R5_PC	3 Days
	S8	Shear Zone	GM	R8_GM	3 Days

Furthermore, before carrying out the new repairing technique on the original specimen, the efficiency of the repairing technique is evaluated by repairing and testing of prototype specimen. In view of this small prismatic RC beam of size 150×150×700 mm are initially damaged by applying load. These damaged specimens are then repaired and are tested on the 7th day of repairing.

5.2.2 Materials

The raw materials that has been utilized during the process of casting of beam specimen and thereafter their repairing are described elaborately in this section under the following heads.

5.2.2.1 Geopolymer paste

The geopolymer paste (GP) adopted in the process of repairing is mainly utilized to serve two purposes. Firstly, in order to have a proper bonding between the mortar and the old concrete, GP is used as a bonding agent in the interface between the repairing site and the geopolymer

layer. Secondly, it is noticed that finer cracks are developed in the damaged beam, which may not be possible to be filled by the GM due to its granular nature. These fine cracks were filled using GP.

The GP has been prepared using the same UBFS and FA binder. Moreover, a mixture of sodium hydroxide and sodium silicate (SHSS) has been used as the alkali activator in the GP. The properties of UBFS and FA have been discussed in section 2.2. of Chapter 2. In addition to this 2 % of Borate is also included to control the setting of the GP. The detail of the alkali activator and the retarder is also given in subsection 2.2 of Chapter 2. In order to establish a GP of good consistency, different quantities of alkaline solution were adopted to prepare GP unless a desirable consistency in the GP is achieved. Table 5.2 presents the mix proportion of the GP prepared. Total three numbers of mixes of GP have been prepared to check the consistency as well as the strength. To evaluate the strength properties of GP, cube specimens are cast with the GP, as shown in Fig 5.3. (a). Six number of cube have been cast using a 50×50 mm cube mould, and the compressive strength of different mixes of GP are evaluated on the 3rd and 28th day in the Compression Testing Machine (CTM).

Table 5.2: Mixes of Geopolymer Paste

Mix	Alkali to Binder	SH	SHSS solution	Binder (%)		Borate
	(a/b)	(M)	SS/SH	Flyash	UBFS	(%)
GP1	0.55	10	1.5	30	70	2
GP2	0.60	10	1.5	30	70	2
GP3	0.65	10	1.5	30	70	2

a) Cube casting with GP b) Cube testing of GP

Figure 5.3: Compressive strength test of GP

The fluidity of the GP primarily depends on the quantity of alkali activator added to the GP. When an a/b ratio of 0.55 is adopted for the mix GP1, a sticky paste is produced, which created problem in handling due to its low workability. But the fluidity of the GP tends to increase with the increase in the a/b ratio. Table 5.3. shows the compressive strength of GP mix on the 3rd day and 28th day. From the test results, it is found that the strength of GP is directly related to the a/b ratio of the mixes. The paste having a/b ratio of 0.55 resulted in the lowest workability, but due to the low water content, high compressive strength of 49.07 MPa was achieved. The compressive strength further drops as the alkali content is increased, but the fluidity of the paste significantly improves. The lowest compressive strength (34 MPa) was found in the GP having a/b ratio of 0.65. The low strength is attributed to the fact that the mix GP3 containing the maximum alkali content showed segregation of GP constituents. Therefore, based on the fluidity and the strength of the mixes, GP2 has been decided to be used as the repairing paste.

Table 5.3: Properties of Geopolymer paste

Mix	Alkali to Binder	Compressive strength (MPa)	
	(a/b)	3rd Day	28th Day
GP1	0.55	41.22	49.07
GP2	0.60	37.84	44.00
GP3	0.65	27.85	34.93

5.2.2.2 Portland cement paste

In the repairing work, Portland cement paste (CP) was used to fill up the fine cracks, where the PCM mortal filling is not possible. Ordinary Portland cement (OPC) was used for preparing the paste. The properties of OPC are discussed in sub-section 2.2.1 of Chapter 2. Table 5.4. shows the water/cement (w/c) of the CP tested for use as a repairing agent.

Table 5.4: Properties of cement paste

Mix	Water to cement	Compressive strength (MPa)	
	(w/c)	3rd Day	28th Day
CP	0.4	25.91	45.83

The mix proportion was selected such that the w/c ratio of CP matches with the total water/solid (w/s) ratio of GP. Laboratory tests were performed to evaluate hardened properties of the CP. The tests were performed as per guidelines of IS 1727 (1967). Similar to the tests conducted for GP, compressive strength test is conducted at 3rd and 28th days on the CP to observe early

and later age strength development behaviour. The test result shows that CP exhibits almost a comparable strength of 45.83 MPa like that of GP2, on the 28th day. However, the 3rd day strength is not so significant compared to the compressive strength achieved by GP2.

5.2.2.3 Geopolymer Mortar

The GM that has been used as a repair material is prepared by using UBFS and FA. Both sodium hydroxide and sodium silicate are used to prepare the alkali activator (SHSS) solution, which is used in the preparation of the GM mix. Chemical admixture, Borate is used to enhance the retarding effect in the GM. Local river sand conforming to Zone III (IS:383-1970 2002) has been adopted as the fine aggregate. The details of the raw materials used in the preparation of GM are furnished in section 2.2. of Chapter 2. The mix design of GM is initially established by considering several parameters. The properties of the various mix proportion prepared for the development of GM mix as repairing materials is given in Chapter 3. Based on the fresh and hardened properties suitable mix (GM17_2R) is chosen for carrying out the repairing work. The detail of the mix proportion GM17_2R used in the repairing work is given in Table. 5.5.

Table 5.5: Mix proportion of GM used in Repairing

Mix	Total Binder		Fine Aggregate	alklai/binder	Molarity	SS/SH	Borate
	UBFS (kg)	FA (kg)	(kg)	(a/b)	(M)		(%)
GM17_2R	70	30	300	0.6	10	1.5	2

The compressive strength test was conducted on 50 mm cubes of GM in CTM, and results of the 3rd and 28th days were obtained. A workability test was performed using a flow table when the mortar was in the fresh state. Vicat apparatus was used for conducting the setting time test. The tests were conducted as per IS 1727-1967 (1996). The setting time was also found to be sufficient for placing the mortar into the cracks. The strengths attained at both early and later

Table 5.6: Test results of GM used in Repairing (GM17_2R)

Test	Values
Initial setting time	48.80 min
Final setting time	65.07 min
Workabilty (FI)	57.67%
Compressive strength (3rd Day)	40.53 MPa
Compressive strength (28th Day)	50.93 MPa

ages were also comparatively high. The fresh and hardened state properties of the GM mix GM17_2R are presented in Table 5.6.

5.2.2.4 Portland cement mortar

Portland cement mortar (PCM) is used as the alternative repairing material to study the efficiency of GM. Hence damaged specimen of similar types is also repaired using the conventional PCM in the same as done by GM. The PCM is prepared using ordinary Portland cement as described in section 3.2.2 of Chapter 3. Fine aggregate that has been used for the preparation of GM is also used for the preparation of PCM. In order to prepare the PCM, the quantity of sand is taken as three times of the cement. While the water to cement (w/c) ratio is taken as 0.4, which is similar to total water to solid (w/c) ratio of the GM17_2R. The fresh and hardened state properties of PCM are given in Table 5.7.

Table 5.7: Properties of PCM

Test	Values
Initial setting time	135 min
Final setting time	256 min
Workabilty (FI)	19.67%
Compressive strength (3rd Day)	16.25 MPa
Compressive strength (28th Day)	34.15 MPa

5.2.2.5 Portland cement concrete

To cast the beam specimen PCC mix, CM1 has been initially prepared using ordinary Portland cement. The details of raw materials used in the preparation of PCC have been described in subsection 2.2 of Chapter 2. The mix proportion of the concrete mix, CM1 is furnished in Table 2.9 under sub-section 2.3 of Chapter 2. Compressive strength test was performed on 150 mm cubes of PCC in CTM, and the results of the 3rd and 28th days are evaluated. For determining

Table 5.8: Properties of mix CM1

Test	Result
Slump Value	70 mm
Compressive strength (3 Day)	15.07 MPa
Compressive strength (28 Day)	28.44 MPa
Split Tensile strength (3 Day)	1.16 MPa
Split Tensile strength (28 Day)	2.01 MPa

the tensile strength, cylindrical mould of 150 mm diameter and 300 mm height were cast, which were tested in the Universal testing machine (UTM). The workability properties of the mixes were evaluated using slump cone. The fresh and hardened properties of the mix CM1 is given in the Table. 5.8.

5.2.2.6 Reinforcement

The different reinforcements that has been used in the preparation of RC beams were 2 numbers of 16 mm diameter tor steel bars and 2 numbers of 10 mm diameter bar, which are the main reinforcement of the beam. On the other hand, 2-legged 8 mm diameter tor steel bars were used as the shear reinforcement. The details of the steel reinforcement have been provided in the sub-section 2.2.7 of Chapter 2.

5.2.2.7 Welded wire mesh and Drop bolt anchor

The repair work is carried out on the damaged beam is further strengthened by a three side wrapping of welded wire mesh, which has been attached to the surface of beam using drop bolt anchor. The detailed specification of the welded wire mesh and the drop bolt anchor is furnished in sub-section 2.2.8 of Chapter 2.

5.2.3 Preparation of Controlled beam

Total nine numbers of RC beams were cast for the work presented in this Chapter. All beams in the undamaged state are considered controlled beams. The opening in the web of the RCC beam has been simulated as post planned opening hence the design of the web open beam has been kept identical in all cases. As a result, these beams are designed as doubly reinforced concrete members in accordance with IS 456 2000. The beam's theoretical ultimate load bearing capability is calculated to be 149.42 kN. The detail calculation of the RC beams specimen and the reinforcement detailing are presented in Appendix B. The design is done to limit the beam's load bearing capability and to produce the situation of failure due to bending, i.e., flexural failure. The RC beams were 180 mm × 270 mm in size, and 2 m in length. The reinforcement details are shown in Fig 5.2. The main reinforcement consists of two longitudinal bars consisting of 16 mm diameter at the bottom and two numbers of 10 mm diameter bar at the top. Moreover, stirrups of two-legged with 8 mm diameter bar have been used as the shear reinforcement. The stirrups are provided at a center to center spacing of 100 mm at a distance of 500 mm from both the and remaining middle portion of 1000 mm length was provided with stirrups at a spacing of 150 mm and 170 mm centre to centre.

In order to prepare the RCC specimen, form work has been prepared initially, as per the dimensions of the specimen. Since the opening in the RCC beam are simulated as a post planned opening, the form work of the specimen is provided with a pre-installed wooden box exactly in the size of opening (300×90 mm), in order to restrict the entry of concrete in to the opening location. Fig. 5.4. shows the various steps involved during the casting of the beam specimen. The casting of the RC beams was carried out as per guidelines laid in IS 516 1959 (2006). The concrete used in the mix is prepared with Portland cement (OPC 43 grade) as discussed in the preceding sub-section 5.2.2. As soon as the freshly prepared concrete mix is made ready, it is immediately placed inside the formwork in three layers. During the casting process, an electrically operated needle vibrator is used for proper compaction of concrete, as shown in Fig. 5.4. (c). As soon as the task of placing the conrete into the formworks is over,

a) Pre installed box in the form work

b) Form work ready for casting

c) Casting of beam

Figure 5.4: Preparation of Beam specimen

Figure 5.5: Curing of specimen

the cast specimens are left undisturbed for 24 hours. On the next day, the formwork of the cast beam was removed and kept for curing. The curing is done in the laboratory at an ambient temperature of 20 ± 20 C for 28 days by wrapping them with wet gunny bags, as shown in Fig. 5.5. The beam specimens are cured for up to 28th day with water. As the curing with water is over, the gunny bags are removed, and the beam specimen are kept in the open air for another 28 days. As the time of testing approached, a fine layer of whitewash was applied over the surface of the beams for the ease of identifying and marking the cracks during testing.

5.2.4 Experimental setup and Instrument

The testing of both the controlled specimen and the repaired specimen are executed as per the test setup shown in Fig. 5.6. All beams are tested under simply supported condition with an effective span of 1800 mm. The tests were conducted by applying four-point loading. The beams were subjected to static flexural load using MTS actuator, having a load capacity of 1000 kN and stroke length of 500 mm. Displacement based monotonic loading has been vertically applied at the rate of 0.01 mm/s. All the specimens are loaded till the ultimate load is achieved and loading is continued till the load drops to 85% of the ultimate load. The midspan displacement was recorded using a linear variable differential transformer (LVDT) of 300 mm capacity, which is attached in the soffit of the beam with the help of an acrylic sheet.

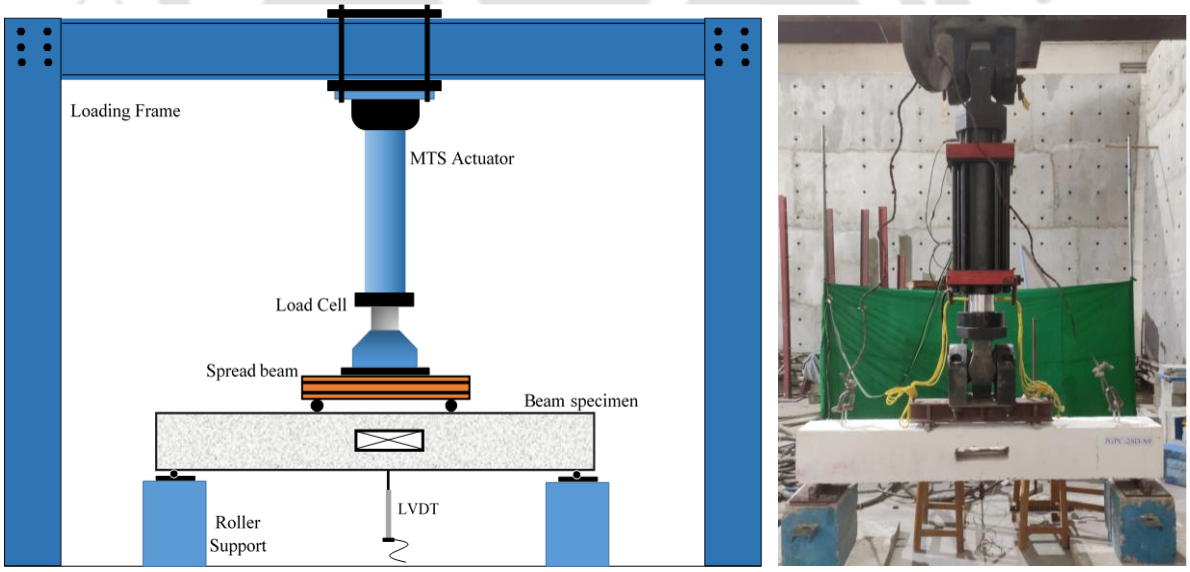

Figure 5.6: Test setup of Four-point bending for repairing work

5.2.5 Method of beam preparation for Repairing work

From the present study, it is observed that cracks that develop in the web-opened beam (BMS and BSS) are comparatively wider than the SB, especially in the area of the high moment and

shear zone. These cracks are repaired locally using GP and GM. However, on close observation, it was noticed that such cracks are also accompanied by their branch cracks, which are relatively finer. Apart from this, there also exist closely spaced fine cracks around the opening. Repairing or removing these damaged parts is not economically feasible in all situations.

Meanwhile, it has been revealed from the past works of literature that ferrocement laminates are very effective in resisting crack widening (Andrews and Sharma 1988), which also leads to an improvement in the durability of the structure (Soman and Mohan, 2018). On the other hand, GM, due to its high bond strength with old concrete and steel (Ueng et al. 2012), can act more effectively than the conventional cement mortar used in ferrocement laminates.

Therefore, in the present repairing scheme, the major cracks (i.e. 1 to 3 mm width) are repaired locally using GP and GM. While the opening area, subject to high moment (flexural zone) and shear stress (shear zone), is additionally strengthened by the wrapping of wire mesh, covering the three sides of the beam. Moreover, the present work of repairing the damaged beam is intended to do without any sectional enlargement. Thus in view of this, a groove of 13 mm is created in order to accommodate the anchored wire mesh and the repair material. The repairing of the damaged beams that has been carried out includes the following steps.

1. The tested beams that have been subjected to ultimate load developed a residual deformation after testing. Thus before carrying out the repairing work, these deformed beams are straightened by applying load unless the original shape is regained.

2. As soon as the tested beams are brought back to their original shape, the concrete fragments that are loosely attached to the beam surface are removed, and the cracks in the surface of the beam are identified and marked.

3. The cracks are then enlarged up to an average depth of 50 mm and width of 40 mm, which is done for the easy and effective application of repairing material (paste and mortar) as shown in Fig. 5.7. (b). To facilitate the works of crack widening, hammer and chisel are mainly used along with other necessary tools, as shown in Fig. 5.7 (f). The broken concrete particles in the cracks were removed carefully with the help of a brush such that no free particles remained attached to the surface of the cracks.

a) Tools for Repairing

b) Widened cracks

c) Cutting of concrete with grinder

d) Surface preparation (Bottom chord)

e) Surface preparation around opening

f) Chipping of concrete using chisel

g) Prepared surface

h) Application of paste

i) Filled cracks with mortar

j) Repaired beam before wrapping wire mesh

Figure 5.7: Surface preparation and initial repairing

4. In order to strengthen the opening area locally, a groove of 13 mm depth is initially created along the three sides of the beam around the opening location. The main purpose of creating this groove is to accommodate the wire-mesh and the mortar layer without any change in the cross-section. Since the strengthening with wire-mesh is done only around the opening, length of the groove is taken as 600 mm, which is similar to the length of the shear zone and flexure zone. To ease this work, an angle grinder is used to cut the concrete up to a depth of 13 mm as shown in the Fig. 5.7 (c)-(e).
5. The concrete layer is carefully removed with the help of hammer and chisel, such that no further crack occurs and a groove of length 600 mm and 13 mm depth can be obtained. This process is followed for all the three sides of the flexural span or shear span. Fig. 5.7. (e) – (g) shows the preparation of groove for fixing wire mesh.
6. The beams are then subjected to air blow with the help of air blower to remove the dust and minute free particles and to prepare the surface for further treatment.
7. This method of crack cleaning and surface preparation is similar to that used by the field engineers and technical persons while repairing concrete structures with epoxy resin, cement grout, etc.
8. As soon as the surface preparation of the damaged beam is completed, the repairing paste (GP or CP) is first applied to fill the cracks with the help of brush, as shown in Fig. 5.7 (h). Due to high flowability of the paste, it can penetrate inside the fine cracks which are not wide enough to allow entry of mortar.
9. After applying repairing paste, the larger cracks are then filled up by the repairing mortar (GM or PCM). The repairing mortar was placed inside the cracks with the help of trowel. During the process the repair material are compacted with the tamping bar for better placement and removal of voids within.
10. The mortar was continued to be filled inside the cracks till it fills the cracks up to the level of groove and then finished, as shown in Fig. 5.7. (i). On completion of the crack filling process, the repaired beams were kept un disturbed at an ambient temperature for 24 hours.
11. On the next day, pieces of wire mesh are cut to wrap the three surface of the opening area, including the bottom of the top chord. Thus two pieces of wire-mesh are cut separately. One piece of wire mesh is initially used to wrap the top chord of the beam. Later on another piece of wire mesh is wrapped in the entire area, covering the three surface of the opening as shown in Fig. 5.8. (b)-(c).

a) Installing of drop bolt anchor

b) Fitting of wire mesh

c) Three side wrapping of wire mesh

d) Application of GP for bonding

e) Application of PCM over wire mesh

f) Finishing of GM over wire mesh

g) Repaired beam with opening in shear Zone

h) Repaired beam with opening in Flexural zone

i) Curing of repaired beam

Figure 5.8: Wrapping of wire mesh and final repairing

12. The cut piece of wire mesh is placed in direct contact with the beam faces and are fastened using industrial anchors (drop bolt anchor) installed with a power actuated tool. During the process of fitting the wire mesh a uniform spacing of 80 mm to 100 mm is maintained throughout the repairing work, as shown in Fig. 5.8. (a).
13. As soon as the fixing of wire mesh is completed, GP is applied in the area wrapped by the wire mesh, as shown in Fig. 5.8. (d). The repairing material is then applied immediately all over the wire mesh up to the level of original dimension of the beam. The repair materials are applied using masonry tools and are finished properly as shown in Fig. 5.8. (f)-(g).
14. As soon as the finishing work is completed, the specimen is kept an ambient temperature. After 24 hours the repaired beams are kept for curing with wet rags till the day of testing, as shown in Fig. 5.8. (i).

5.2.6 Preliminary investigation of Repairing technique

In order to evaluate the efficacy of the new repairing methodology, the repairing technique is initially applied in some prototype specimen. This preliminary repairing work is conducted with a motive of studying the effect of wire mesh in repairing damaged beam with geopolymer. Thus in view of this four number of RC prism of size 150×150×700 mm, which are considered as controlled specimen (CS), have been prepared and are named as CS1, CS2, CS3 and CS4. All these specimens are prepared with two bottom bar and two top bar of 8 mm diameter. Nominal shear reinforcement with 8 mm bar are provided at a spacing of 300 mm center to center. The detail of the beam is given in the Fig. 5.9.

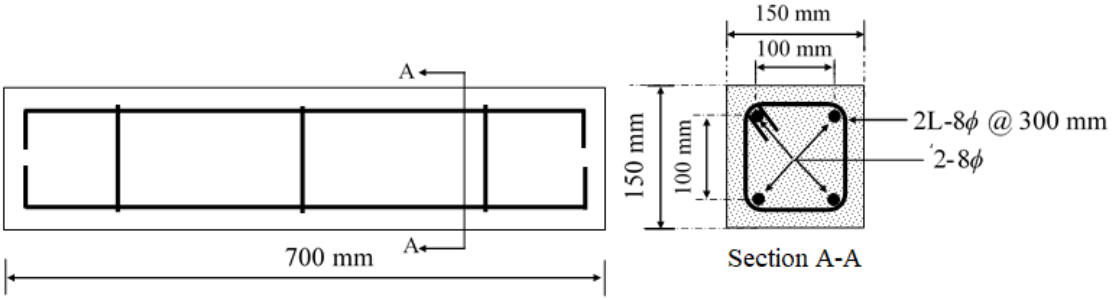

Figure 5.9: Detailing of the Prismatic beam

These specimens are cast using a PCC mix (CM1) of compressive strength 28.44 MPa. The details of the concrete mix CM1 is discussed in the preceding sub-section 5.2.2.5. After casting, these specimens are initially cured for 28 days in water followed by 56 days in the open air. After completion of 56 days the specimens are subjected to four-point loading in Universal

testing machine (UTM) and are loaded up to its ultimate load. The damaged specimens after testing are categorized in to two groups. First group consist of two number of damaged specimen which are repaired alternatively with PCM mortar and GM. These specimens are repaired only with GM and the PCM and after repairing the specimens are renamed to R_CS1 and R_CS2. While the second group consist of other two damaged specimens which are repaired and as well as strengthened using welded wire mesh alternatively with PCM and GM material. These specimens are further renamed to J_CS3 and J_CS4.

The repairing of the damaged beam has been done using the same procedure as mentioned in preceding sub-section 5.2.5. However, in this case the entire beam is wrapped with the wire mesh. The wire mesh is wrapped in the three faces of beam leaving the compression side. The detail of the repairing technique using wire mesh can be understood from the Fig. 5.10. The repairing work of crack filling of all the specimen are conducted on the same day, while the additional repairing work of wrapping of steel wire mesh on the specimen (J_CS3 and J_CS4) is carried out on the next day. All these specimens after repairing are cured with wet rags for 7 days and then tested again.

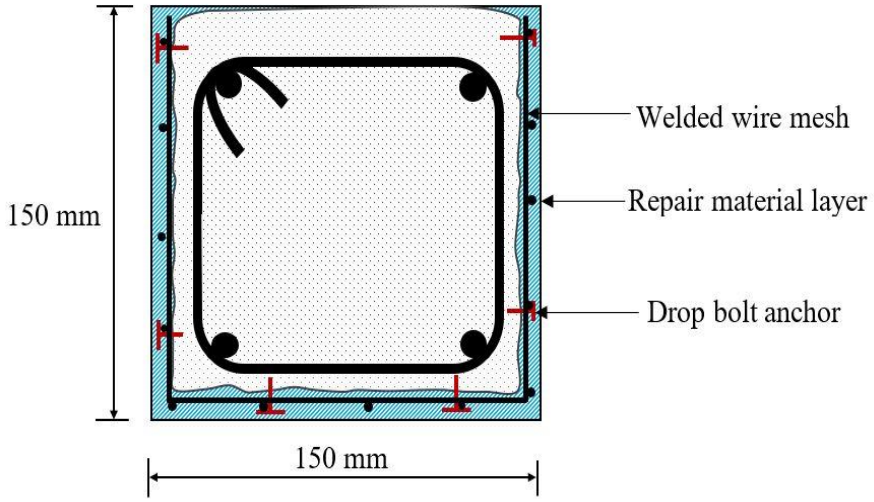

Figure 5.10: Detail of repairing using wire mesh

5.3 Experimental Observations

5.3.1 Test result of the repaired prismatic beam

All retrofitted specimens are tested immediately after the 7th day of curing and are tested again in the UTM. Table 5.9. shows the load carrying capacity of the controlled specimen and the repaired specimen. It can be seen that R_CS2, which is repaired only by GM, withstand a

maximum load of 100.60 kN, which is 82.45 % of the load attained by controlled specimen CS_2. In comparison, R_CS1 repaired by PCM, withstand an ultimate load of 48.70 kN, which is 34.78 % of the controlled specimen, CS2. The better strength enhancement by R_CS2 is attributed to the high compressive strength of GM at 7 days and their better bonding, which played a significant role in the strength enhancement of the repaired beam.

The wrapping of wire mesh technique investigated in the present study is found to be very effective in enhancing the strength of a damaged structure without increasing the cross-sectional area. The ultimate load attained by J_CS4 is 144.70 kN, which is 11 % higher than the original load attained by the controlled specimen CS4. Whereas specimen J_CS3, repaired by PCM, attained an ultimate load of 88.8 kN, which is 66.27 % of the load attained by the controlled specimen. Such specimen failed by early cracking of the repaired area and debonding of the wire mesh, caused by anchorage failure. On close observation, it was noticed that during loading, the anchor got pulled out. This is attributed to the poor bonding of the PCM with the anchor and the poor compressive strength of PCM on the 7th day. However, that in beam J_CS4 repaired by GM significantly improved the strength of the damaged beam. The better performance of J_CS4 is due to the strong bond and high strength gain property of GM.

Table 5.9: Test result repaired prismatic beam

Specimen	Repairing Scheme	Ultimate Load before repairing (kN)	Ultimate Load after repairing (kN)	Strength Enhancement Ratio (SER)
R_CS1	PCM	140	48.7	0.35
R_CS2	GM	122	100.6	0.82
J_CS3	PCM and WM	134	88.8	0.66
J_CS4	GM and WM	130.9	144.7	1.11

Note: WM-Wire mesh

The repairing technique followed by strengthening using wire mesh used in the later specimen (J_CS3 and J_CS4) improved the strength by 1.6 times (average) better than that of the specimen (R_CS1 and R_CS2) repaired only by filling of crack with mortar. Thus, this outstanding performance of the repairing technique using wire mesh has encouraged for its application in damaged web opened beam for its successful restoration and rehabilitation.

5.3.2 Behaviour of Reinforced concrete beam with Web opening

The test result of the different types of beam varying in the location of opening are presented in Table 5.10. Both SB and the beam BMS exhibits almost a similar flexural behaviour. However, the presence of opening in the shear transformed the flexural failure to a sudden shear failure.

The typical crack pattern of all the beams (SB, BMS and BSS) tested under flexure are shown in Fig. 5.11. (a)-(c). The behaviour of SB is found to be linear elastic until the appearance of the 1st flexural crack at a load of 40.89 kN in the pure flexural zone. With increase in load more cracks (vertical and sub vertical) developed uniformly in the mid-span, subjected to constant bending moment. The first diagonal tension crack (crack no. 4) appears in the shear zone at higher load 64.34 kN. Simultaneously, more cracks appear in the shear zone and flexural cracks start propagating towards the neutral axis. As soon as the load tends to reach its peak, the concrete directly under the loading head starts local crushing.

Table 5.10: Test result of controlled beam with opening

Specimen	Yield load (kN)	Deflection at Yield load (mm)	Peak load (kN)	Deflection at ultimate load (mm)	Load at 1st Crack	DR	Failure mode
SB	139	10.88	174.56	50.87	40.89	4.68	Flexural Failure
BMS	138	10.79	169.62	32.98	30.70	3.06	Flexural Failure
BSS	61.5	5.50	79.99	9.32	16.86	1.69	Shear Failure

Where as in case of BMS, the 1st crack appeared exactly at the mid-span but at a load of 30.07 kN. The appearance of crack, at this early level of loading, indicates higher tensile stress (Mansur 1999) in the bottom chord. With increase in the loading more flexural cracks (crack number 2, 3, 4 and 5) appears as shown by Fig. 5.11. (b). The 1st shear crack in BMS appeared at a loading of 55.40 kN. With increase in load more shear cracks appear and at this moment the flexural cracks at the bottom chord significantly widens as compared to those in SB. The shear cracks that appear at the later stage follows the similar pattern like that in SB and tends to propagate towards the loading. However, it was noticed that as the load tends to reach its peak the top chord starts crushing much rapidly than that seen in SB. This early crushing ultimately affected the failure pattern and deformation capacity of the beam. The early crushing of top chord can be attributed to geometrical change at the mid-span, due to which the compressive capacity of the strut developed at this stage is reduced (Ali and Saeed, 2022).

However, the beam exhibits a flexure behaviour, similar to SB i.e., by yielding of steel followed by crushing of concrete under the load.

On the other hand, the crack pattern in the BSS specimen significantly differs from that observed in the case of SB and BMS, which can be differentiated from Fig. 5.11 (c). Unlike BMS, the 1st crack appears in the shear zone, rather than the flexural zone, at a loading of 16.86 kN, which propagates from the corner of the opening (crack number 1). Since the presence of an opening in the shear directly interrupts the load path between the loading and the support. This leads to an accumulation of stress around the opening, which leads to the early appearance of cracks in the shear zone. With the increase in loading, more shear cracks (crack no 2, 3) appears around the vicinity of the opening and another shear crack (crack no 4) emerges from the other corner of the opening. As the loading is increased to 40.12 kN, the 1st flexural cracks (crack number 6) appeared. Out of all the cracks, crack number 5, as shown in Fig. 5.11. (c), propagating diagonally through the top chord, is found to be the most critical crack. With a further increase in the loading, the crack no. 5 widens and finally splits, which leads to a sudden shear failure of the beam. This sudden shear failure can be attributed to the loss in shear capacity of BSS, owing to the presence of an opening which reduced the sectional area of the shear span.

a) Crack pattern in SB

b) Crack pattern in BMS

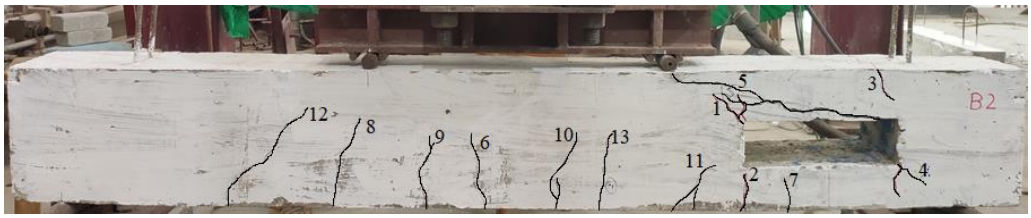

c) Crack pattern in BSS

Figure 5.11: Crack pattern in different types of beam a) SB b) BMS c) BSS

The load-deformation response of different types of beam with and without opening is presented in Fig. 5.12. Both the beam BMS and SB show a similar elastic stiffness up to the loading of 100 kN, beyond which degradation in the stiffness occurs in the BMS. While larger stiffness degradation is noticed in the beam BSS after a load of 25 kN. This stiffness degradation is due to the early cracks in the beam BMS and BSS, which gets much wider with the increase in load as compared to those in SB.

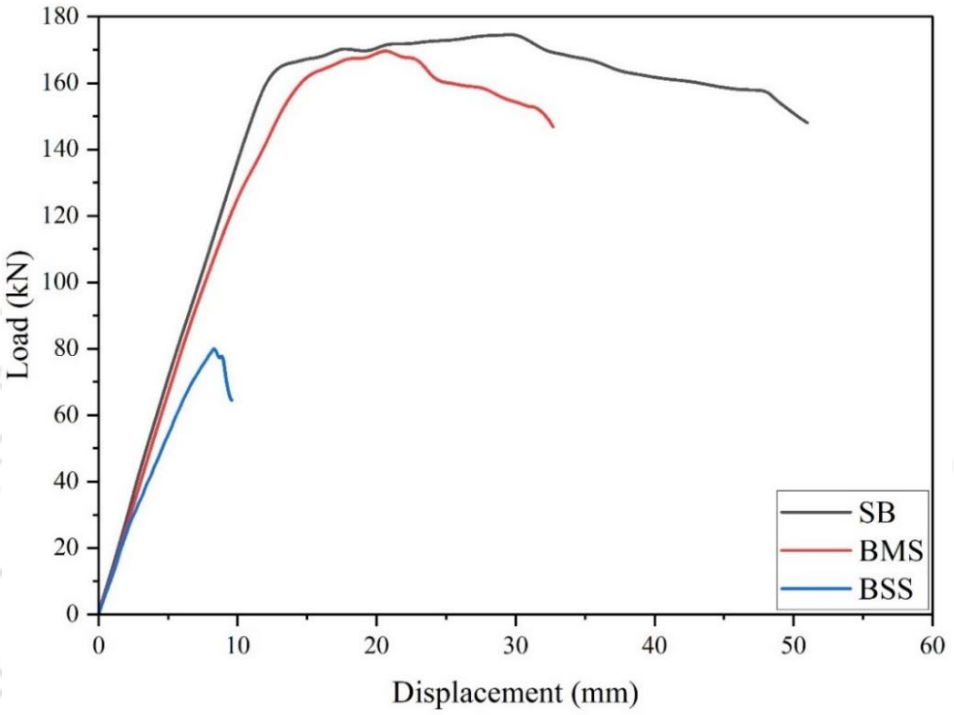

Figure 5.12: Load Displacement curve of tested beam with and without opening

The peak load attained by the beam BMS is 169.62 kN, which is approximately 97 % of the load attained by SB (174.56 kN). While the specimen BSS could attain only 46 % of the peak load attained by SB. This shows that the presence of an opening in the mid-span does not have any significant effect on the load carrying capacity of the beam. Another reason that supports the aforementioned statement is that the location of the opening is far below the theoretical neutral axis depth (43.02 mm, Appendix B) and hence does not interrupt the compressive stress block developed in the compression zone. However, the effect of opening in the mid-span is clear from the stiffness and post-peak response of the beam. The maximum displacement attained by SB at the peak load was 30 mm. But in BMS and BSS, the displacement corresponding to their peak load was 20.62 mm and 8.32 mm, respectively. The SB exhibits a ductility ratio (DR) of 4.68, while a substantial reduction in the DR (3.06) is noticed in the beam BMS, which is further reduced to 1.69 (DR) in the case of BSS. This drastic reduction in the DR in the BSS is due to the sudden drop in the load-deformation curve caused by shear

failure. The loss in the ductility of BMS and BSS can be attributed to the presence of an opening in the mid-span and shear span, which leads to premature failure of the top chord subjected to high compressive stress and shear stress, respectively.

5.3.3 Experimental observations of repaired beam with web opening

The damaged beams that are repaired using different repairing material are designated by the letter 'R' instead of 'S' opted for the controlled specimen. For example, the controlled specimen S1 after repairing by PCM is renamed as R1_PC. The testing of the repaired specimen is conducted in the same way as done for the controlled specimen as mentioned in section.

5.3.3.1 Behaviour of repaired beam with web opening in the Flexure zone

The behaviour of the repaired beam is found nearly similar to that of the controlled beam. The crack pattern of the controlled beams and the repaired beam tested on the 3rd day and 28th day are marked during the loading and the corresponding load for each individual cracks are also recorded. The results obtained from static flexural load test on the RC beams with opening in the flexure zone are presented in Table 5.11.

3rd Day testing

The cracks pattern of the controlled beam and the repaired beams with PCM and GM, which are tested on the 3rd day, are shown in Fig. 5.13. In the beam R6_PC repaired by PCM, the 1st crack appeared at a loading of 19.89 kN, which is much lower than the 1st crack load in the controlled beam (S6), which appeared at 30.18 kN. The appearance of the first crack at a very early stage is attributed to the low tensile strength of the PCM mortar on the 3rd day. With an increase in load, more flexural cracks appear, followed by shear cracks. On close observation, it is observed that shear cracks occur approximately in the same location as that in the controlled beam, and the crack took place in the filled-up repair material. At the same time, the flexural cracks in the repaired beam appear to be more distributed and larger in number compared to the controlled beam. This phenomenon is due to the effect of wire mesh in the flexural zone, which restricts the widening of cracks, and this leads to a distribution of cracks.

As the load in R6_PC increases beyond 110 kN, the repair materials in the top chord start crushing and simultaneously, the layer of repair material also starts debonding laterally from the top chord, as shown in Fig. 5.13. (b). Due to this debonding, the repair material

eventually starts spalling out as the loading in the beam increases. As the load approaches the ultimate load, the entire concrete in the top chord crushes and a sudden failure of the repaired beam R6_PC is observed. This failure is due to the poor compressive strength of the repair material (PCM), which is supported by the compressive strength of PCM as discussed in the sub-section 3.3.2 of Chapter 3. Moreover, due to the weak bond strength of PCM with the PCC substrate, debonding of the repair material is seen at a very early stage.

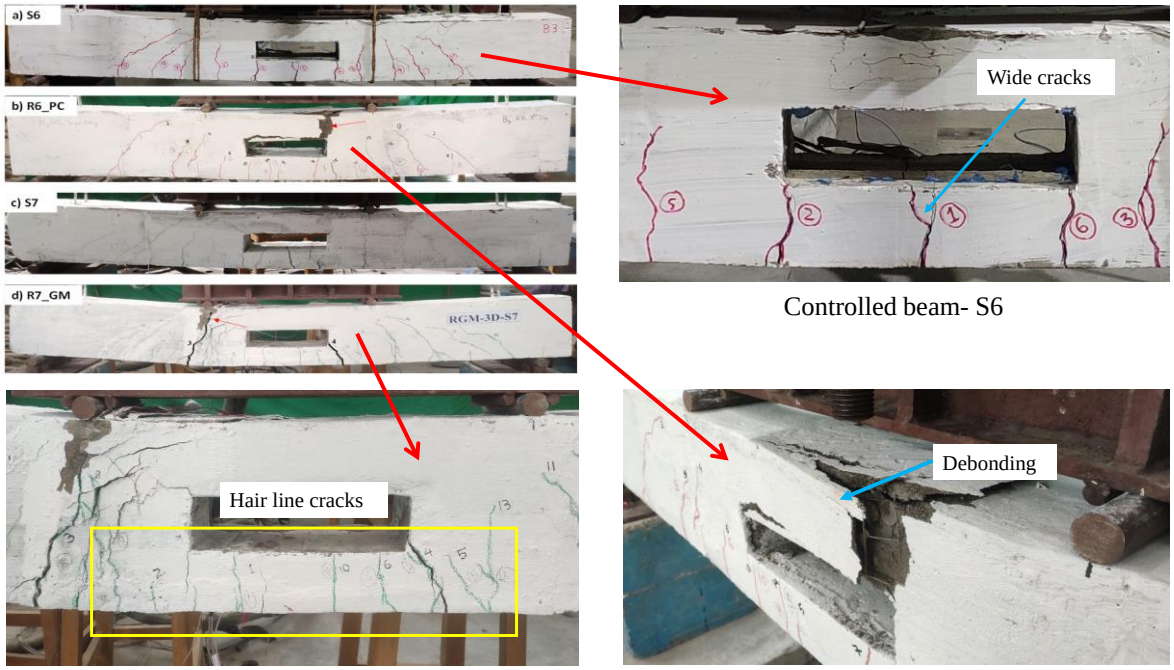

Figure 5.13: Crack pattern of controlled and repaired beam with mid-span opening (3rd Day)

In contrast, the specimen R7_GM, repaired by GM, the 1st crack appears in the mid-span at a loading of 32.32 kN, which is higher even than the controlled specimen (S7), where the 1st crack appeared at 27.74 kN. This delay in the appearance of 1st crack in R7_GM indicates enhanced tensile strength of GM, even on the 3rd day of testing. The effect of wire mesh is clearly understood as soon as the loading in the beam increases. Because it was seen that, as load increases in R7_GM, the widening of the cracks in the repaired beam is significantly restricted in the strengthened area (mid-span), this crack restricting feature leads to distributed fine cracks, as seen in Fig. 5.13. (d), as compared to the controlled specimen S7. Moreover, strengthening with wire mesh around the opening resulted in shifting of the crack's concentration to the concrete adjacent to both ends of the jacket. The beam exhibits no debonding or spalling of repair material, unlike that repaired by PCM. This is due to the better

strength gain propertied of GM as established in subsection 3.3.1 of Chapter 3. As the load increases and tends to reach the ultimate loading, the tension in the wire mesh increases and later yields and tears and simultaneously crack numbers 3 and 4 enlarges followed by crushing of the concrete in the top chord.

The load-deformation curve of the repaired beam and the controlled beam on 3rd day of testing is depicted in Fig. 5.14. The beam, R6_PC, withstands a maximum load of 134 kN, which is nearly 79 % of the load achieved by the controlled beam. On the other hand, the beam R7_GM, repaired by GM, exhibited a load carrying capacity of 177.48 kN, which is approximately 5 % higher than the controlled specimen. However, the load-deflection curve of both the repaired beam exhibits stiffness degradation. The load-deformation curve of R6_PC shows a sudden drop after attaining the peak load. This causes a reduction in the DR of R6_PC, which is 1.10, as given in Table. 5.11; and is significantly lower than that of the controlled beam, S6. This loss in ductility is due to the premature failure of the beam R6_PC.

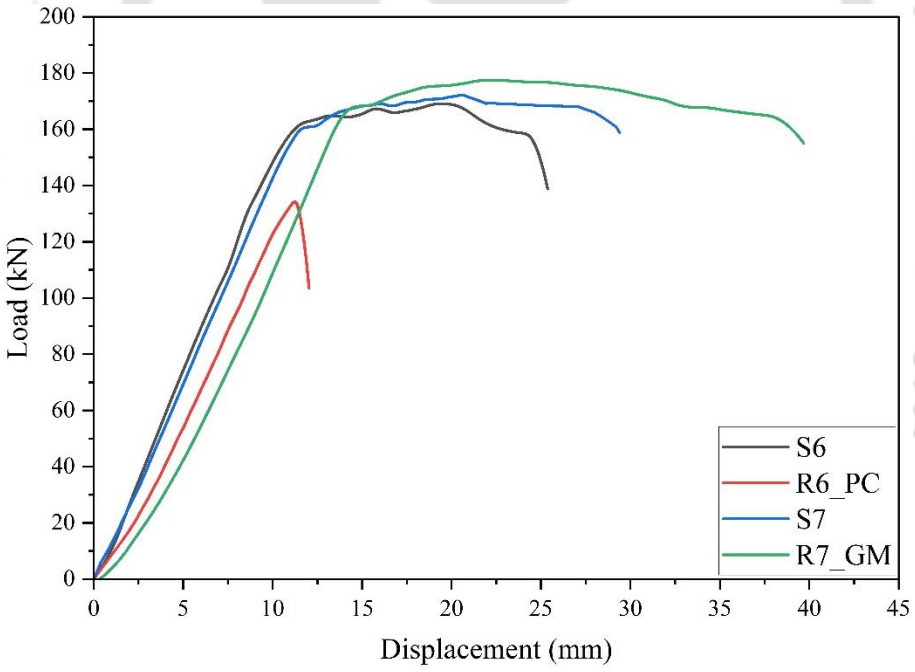

Figure 5.14: Load deflection curve of controlled and repaired beam with mid-span opening (3rd Day)

On close observation of the failed specimen (R6_PC) it has been observed that failure of this specimen caused by crushing in the top chord exactly at the same damaged area where the PCM mortar is filled for repairing. On the hand the beam repaired by GM exhibits enhanced deformation after the peak load. Improved deformation capacity of R7_GM can be attributed

to better compressive stress resisted by the top chord of the specimen, even tested on the 3rd day. This can be attributed to high early strength of GM and superior adherence with the concrete and wire mesh, which gave a better confinement to the top chord resulting to higher load and deformation capacity. As a result, the beam exhibited a DR of 2.99, which is even better than the DR of the controlled beam.

Table 5.11: Test result of controlled and repaired beam with mid-span opening

Specimen	Test Day	Reparing Agent	Yield Load (kN)	Deflection at Yield load (mm)	Peak load (kN)	MCC (kN.m)	Deflection at ultimate load (mm)	Load at 1st Crack (kN)	DR	SER
S6	56	_	145.00	10.21	169.09	50.73	25.18	30.81	2.47	_
S7	56	_	146.19	11.65	172.11	51.63	31.68	27.74	2.72	_
R6_PC	3	PCM	125.00	10.78	134.17	40.25	11.85	19.89	1.10	0.79
R7_GM	3	GM	168.25	13.58	177.48	53.24	40.6	32.32	2.99	1.03
S1	56	_	138.00	10.89	169.62	50.89	32.98	30.7	3.03	_
S2	56	_	132.00	11.00	162.03	48.61	32.17	29.9	2.92	_
R1_PC	28	PCM	145.00	11.23	179.08	53.72	37	35.01	3.29	1.06
R2_GM	28	GM	175.00	11.03	191.91	57.57	36.79	36.44	3.34	1.18

Note: MCC- Moment carrying capacity

28th Day testing

The crack propagation of the controlled specimen and the repaired beam tested on 28th day is presented in Fig. 5.15. The beam R1_PC, repaired by PCM, exhibits the 1st crack load of 35.01 kN, which is higher than that of the controlled specimen S1. The cracks, in the repaired beam are evenly distributed and finer in nature as compared to controlled beam S1. Usually the flexural cracks have a tendency to propagate vertically as the load is increased. But it is seen that due to the presence of opening in the mid span, the crack no 1, 4 and 6 at the vicinity of the opening, changed their direction with the increment of loading and propagates towards the corner of opening, as shown in Fig 5.15. (b). The concentration of cracks around the corners of the opening indicates high stresses, exceeding the flexural strength of the repair material. The 1st shear crack appeared at a load of 57.67 kN and with increase in loading more shear cracks appears which propagates in similar nature like that of the previous repaired beams.

As the loading reaches its peak, the top chord starts cracking, leading to spalling of repair mortar in R1_PC. While in the bottom chord, the widening of cracks is effectively resisted by the wire mesh and the shear crack (crack no 7) adjacent to the strengthened area starts widening. Even on the 28th day, the spalling and debonding of repair wire mesh were

observed. The high stresses in the compression side also lead to an anchorage failure of the wire mesh exactly in the repaired area, and eventually, the beam fails. This behaviour is also seen in the repaired beam tested on the 3rd day but occurred at an early stage of loading. However, due to 28 days of curing, the repaired beam with PCM exhibits a considerable performance, which was not achieved on the 3rd day.

The crack pattern in the repaired beam R2_GM tested on the 28th day is found to be nearly similar to R1_PC but exhibits better performance due to the enhanced properties of GM. In this specimen, the appearance of 1st crack in the flexural span took place at a much higher load (36.44 kN) than that of the controlled specimen (S2) and the specimen was repaired by PCM. The 1st shear cracks appeared in the beam when the loading reached 50 kN, which is relatively earlier than that repaired by PCM. Apparently, this is due to the better tensile property in the flexural zone being repaired by GM and wire mesh, as compared to the shear zone. As a result of which, shear cracks appeared at a much lower load instead of flexural cracks. With an increase in the loading, more cracks appeared in the flexural zone, and the cracks started propagating towards the compression side, while some cracks, crack no 1, 4, 14 and 15, tend

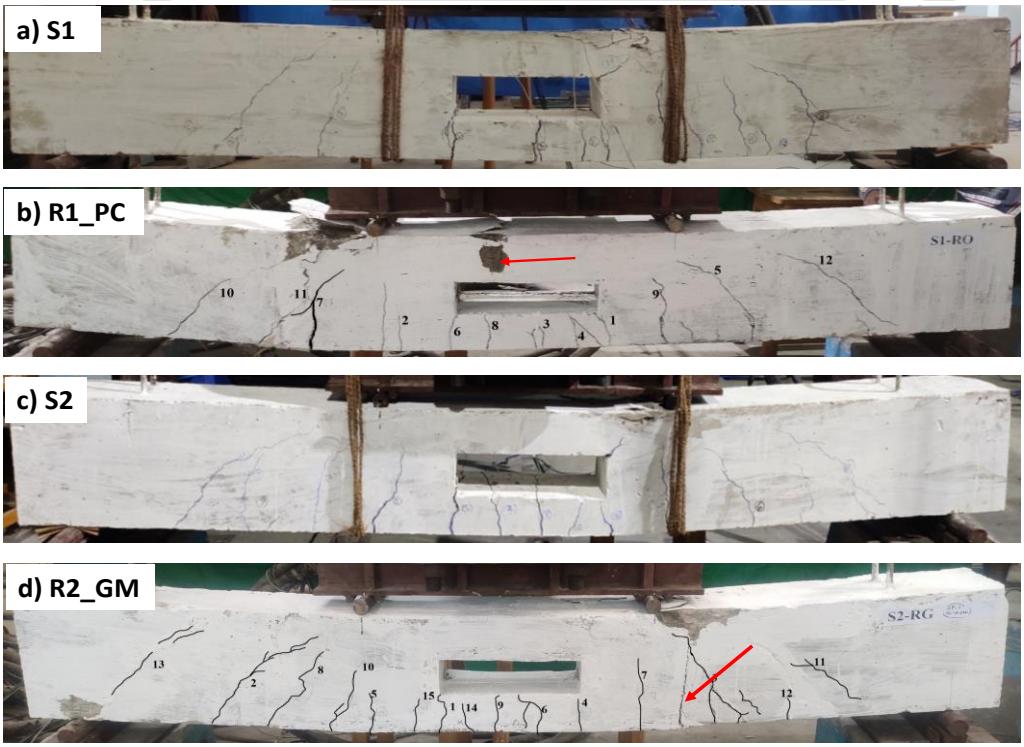

Figure 5.15: Crack pattern of controlled and repaired beam with mid-span opening (28th Day)

to propagate toward the corner of the opening, as shown in Fig. 5.15. (d), similar to the controlled specimen, shown in Fig. 5.15. (c).

The widening of cracks is a very common phenomenon in the beam specimen, but due to the strengthening with GM and wire mesh, the flexural cracks are significantly restricted from widening. This effect is almost similar in both the beam repaired by PCM or GM, as shown in Fig. 5.15 (b) and (d). This is attributed to the cracks resisting features of the wire mesh which controlled the widening of cracks. When the loading reaches the peak 191.91 kN, the cracks no 3 in R2_GM, which is located in the shear zone starts widening and simultaneously local crushing under the load in the top chord initiates.

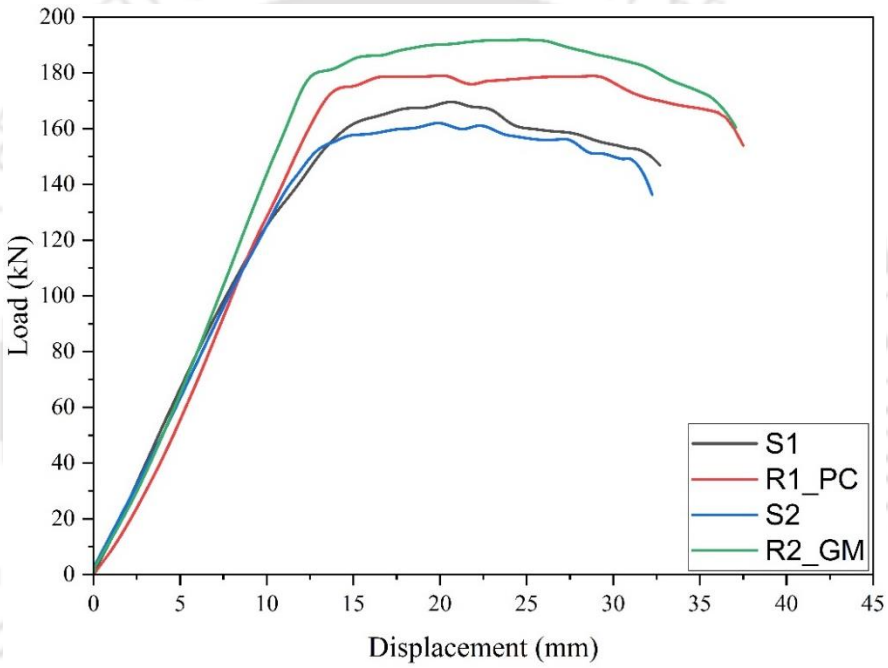

Figure 5.16: Load deflection curve of controlled and repaired beam with mid-span opening (28th Day)

The load-deformation plots of all the repaired beams and the controlled beam tested on the 28th day of testing are depicted in Fig. 5.16. The load-deflection curve of the repaired beam R1_PC shows a slight degradation in the elastic stiffness of the beam, which eventually improves with the increase in the load deflection. This improvement in the stiffness can be attributed to the fact that as the load increases, the beam starts deflecting and the tension in the wire mesh eventually increases, leading to better transfer of stresses to the wire-mesh laminates. While in the case of the beam repaired by GM (R2_GM), the material GM possess a better adhesion property, which provides a better monolithic action leading to better transfer of stress. As a

result of which, no stiffness reduction is seen in the load-deformation curve of R2_GM. The improvement in stiffness is also due to the effectiveness of the filled cracks with repair material and the participation of wire mesh in resisting the widening of the cracks.

The peak load attained by R1_PC is approximately 5.6 % higher than the original load, and the ductility of the beam improved to 3.29 (DR), which is 8.6 % higher than the DR of the controlled beam. While in the case of R2_GM, the beam exhibits a load carrying capacity of 18 % higher than the original beam. Apart from this beam exhibits significant deformation capacity up to the ultimate loading and hence showed an improved DR of 3.34, which is approximately 14 % higher than the DR of the controlled beam. The better performance in the load carrying capacity of the R2_GM is due to the high compressive strength of GM and its excellent bonding with the wire mesh and the PCC matrix. Apart from this, the wire mesh wrapped around the top chord and the entire GM layer as a whole provides better confinement to the top chord. This enables the beam R2_GM to exhibit better load carrying capacity than R1_PC. The beam repaired by GM, therefore, exhibits an enhanced SER of 1.18, which is much better than the SER (1.06) of the beam repaired by PCM (see Table 5.11.)

From the above discussion, it is seen that the beams repaired by newly developed GM and the technique of three-side wrapping of wire mesh have effectively restored the damaged beam and also improved the strength of the beam even at an early age of testing. While at a later age (28^{th} days), successful restoration of the beam is achieved by both GM and the PCM. The repairing carried out by GM exhibited an outstanding performance by showing a significant improvement in both strength, stiffness and ductility of the beam.

5.3.3.2 Behaviour of repaired beam with web opening in the shear zone

The behaviour of the repaired beam with opening in the shear zone is found similar to the controlled beam. The crack pattern of the controlled beams and the repaired beam tested on the 3^{rd} day and 28^{th} day are marked during the loading and the corresponding load for each individual cracks are also recorded during the test. The results obtained from static flexural load test on the repaired RC beams with opening in the shear zone are presented in Table 5.12.

3^{rd} Day testing

Fig. 5.17. shows the final crack pattern of the controlled beams and the repaired beam tested on the 3^{rd} day of repairing. The beam R5_PC repaired by PCM exhibits the 1^{st} shear crack at a loading of 15.72 kN, whereas the 1^{st} shear crack appeared in the controlled beam at 16.86 kN.

With the increase in the load beyond 20 kN, more shear cracks appeared. Crack no 1 and 2 initiate from the corner of the opening and propagate between the loading point and support, as shown in Fig. 5.17. (b). While the other cracks that appeared at higher load in the shear zone tend to propagate towards the corner of the opening. The pattern of these cracks were nearly similar to the controlled beam and were mostly concentrated near the corner of the opening.

With an increase in the loading in R5_PC, the flexural cracks, crack no 4, 6, 7, 9 and 12 in R5_PC, starts appearing in the flexural span at a load level of 35.67 kN to 60.84 kN. These flexural crack patterns in the repaired beam are approximately similar to that in the controlled specimen S5, shown in Fig. 5.17 (a). During this load increment, the most critical crack, crack no 1, widens along with several new branch cracks, as shown in Fig. 5.17. (b). The aforementioned crack is similar to crack no 5 in the controlled specimen, which rapidly widens with the application of load followed by shear failure of the top chord. As the load tend to reach its peak in the specimen R5_PC, the repairing layer from the top chord starts debonding and spalling of the repair material from the wire mesh is noticed.

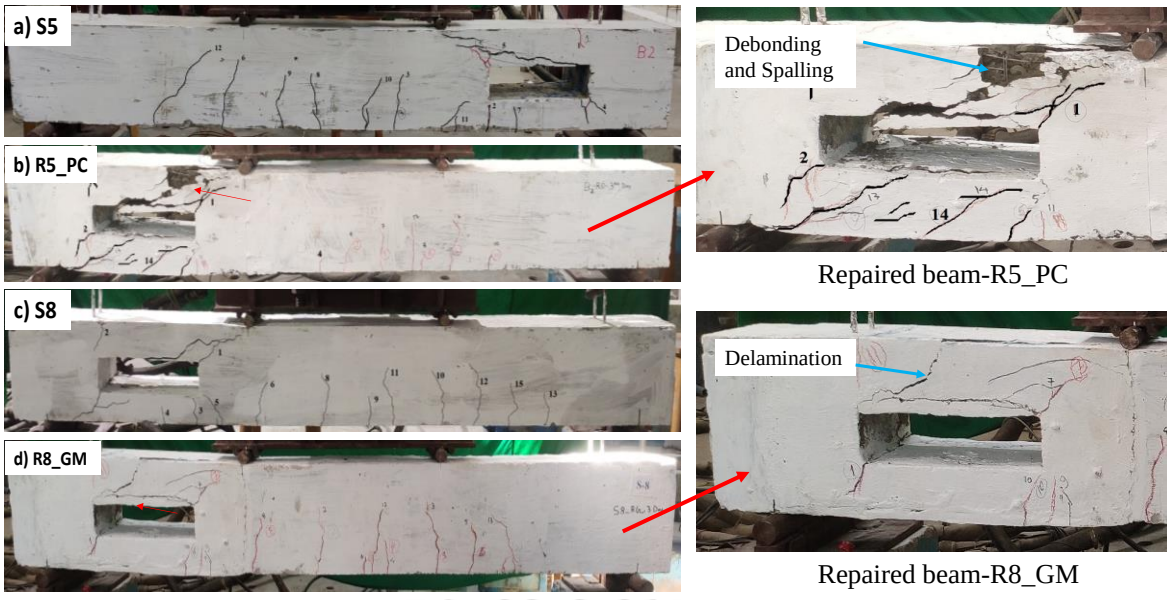

Figure 5.17: Crack pattern of controlled and repaired beam with shear opening (3rd Day)

On the other hand, the beam R8_GM, repaired by GM, exhibits 1st crack at a loading of 21.57 kN, whereas the 1st crack in the controlled beam S8 appeared at a loading of 16.98 kN. This delay in the occurrence of crack can be attributed to the better tensile properties and bond between GM with substrate and wire mesh. With increases in loading, more cracks become visible, but unlike the beam R5_PC, these crack does not appear in the shear zone rather starts appearing in the flexural zone. Usually, in the case of opening in the shear zone (i.e. BSS), the

beam initially starts cracking in the shear span, followed by flexural cracks when the load increases. But in the repaired beam R8_GM, which is also having opening in the shear zone, cracks no 2, 3, 4 and 5 appears in the flexural zone of the beam, shown in Fig. 5.17. (d). This dissimilarity in the location of the cracks can be attributed to the strengthening of the shear zone using wire mesh and GM, which provides a significant tensile strength to resist the occurrence of crack in the shear zone and hence the flexural cracks starts appearing earlier than the shear cracks.

When the load reaches 48 kN, shear cracks again start appearing in the vicinity of the opening corner. From Fig. 5.17. (d), it can be observed that the major cracks, crack no 1 and 7, initiates from the two corners of the opening and start proceeding towards the loading and the support. As the load tends to reach the peak, crack no 7, which is considered to be the major crack, tends to widen. However, in this specimen (R8_GM) no collapse or debonding of the repair material is seen like that of the beam repaired by PCM. The beam finally failed due to tearing of the wire mesh and splitting of the top chord.

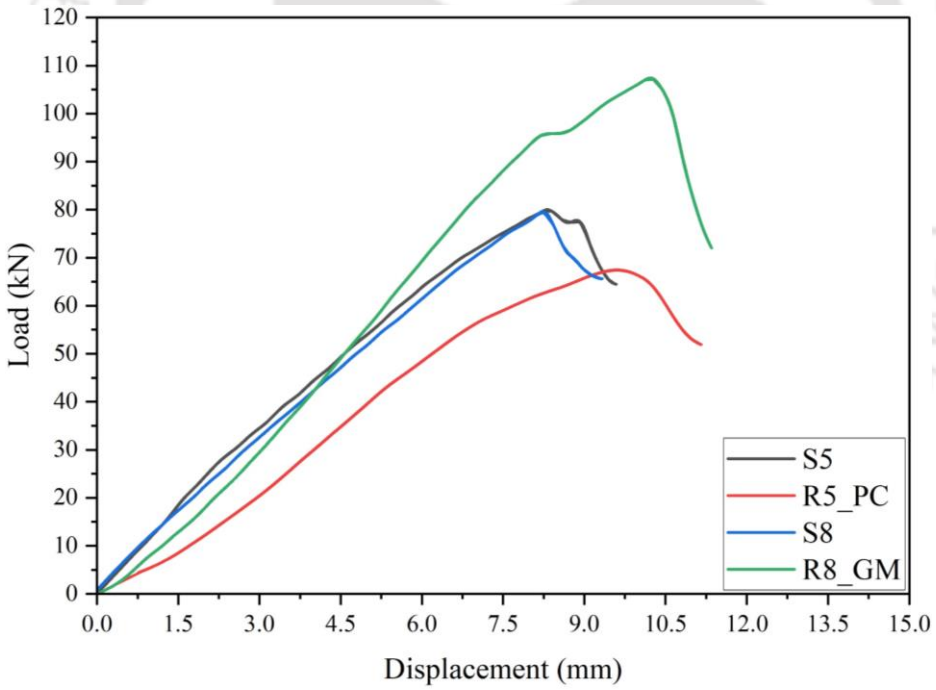

Figure 5.18: Load deflection curve of controlled and repaired beam with shear opening (3rd Day)

The load-deformation curve of the tested beam on the 3rd day is presented in Fig. 5.18. Unlike the beam with an opening in the flexural zone, the failure of the beam with opening in the shear is sudden. The beam R5_PC repaired by OPC sustained a maximum load of 67.42 kN on the

3rd day, which is 16 % lesser than the ultimate load of the controlled beam, S5. The beam also showed a larger stiffness degradation and exhibited a lesser DR ratio of 1.41 as compared to the controlled beam.

On the other hand, the beam R8_GM repaired by GM exhibits full restoration of strength even on the 3rd day. From the load-deformation curve, it can be seen that the repaired beam exhibits an initial stiffness degradation during loading, which eventually improves with the increment in load. This effect can be attributed to the fact that as the load increases, the tension in the wire mesh increases, which eventually resists the cracks and the deflection of the beam. The increase in the load also leads to the yielding of the wire mesh, and at a certain point of loading, the wire mesh starts tearing. Hence, it can be noticed from the plot of R8_GM that the load-deformation curve suddenly drops at a displacement of 8.5 mm, which is attributed to the tearing of wire mesh. But the beam continues to take more load until it reaches the peak at 107.40 kN, which is 35 % higher than the load sustained by the controlled beam S8. However, the beam exhibits a DR of 1.32, which is lesser than the controlled specimen.

Table 5.12: Test result of controlled and repaired beam with shear opening

Specimen	Test Day	Reparing Agent	Yield Load (kN)	Deflection at Yield load (mm)	Peak load (kN)	MCC (kN.m)	Deflection at ultimate load (mm)	Load at 1st Crack (kN)	DR	SER
S5	56	_	65.01	6.25	79.99	24.00	9.25	16.86	1.48	_
S8	56	_	62.12	6.28	79.57	23.87	9.15	16.98	1.46	_
R5_PC	3	PCM	58.06	7.56	67.42	20.23	10.68	15.72	1.41	0.84
R8_GM	3	GM	91.87	8.35	107.4	32.22	10.99	21.57	1.32	1.35
S3	56	_	65.18	7.35	85.1	25.53	12.5	17.9	1.70	_
S4	56	_	66.56	8.02	78.3	23.49	10.57	18.61	1.32	_
R3_PC	28	PCM	85.06	9.60	92.01	27.60	11.5	19.46	1.20	1.08
R4_GM	28	GM	102.55	12.00	110.49	33.15	14.6	22.12	1.22	1.41

28th Day testing

The final crack pattern of the controlled beams and the repaired beam tested on the 28th day is shown in Fig. 5.19. The beam R3_PC repaired by PCM exhibits the 1st shear crack at a loading of 19.46 kN, whereas the 1st shear crack appeared in the controlled beam at 17.90 kN. With the increase in load up to 44.35 kN, more number of shear cracks develops around the opening in the repaired area. Beyond that, flexural cracks also develop, which occurred in the same crack location of the controlled beam S3, as shown in Fig. 5.19. (a)-(b). With the increase in the loading, the shear cracks, crack no 1 and 5, widen, but no sign of debonding in the PCM layer

is observed. Whereas, in the case of the specimen (R5_PC) tested on the 3rd day, spalling and debonding of the repair material is observed at the same level of load.

On the other hand, in the case of the specimen R4_GM, repaired by GM, the 1st crack load appeared at a loading of 22.12 kN, while the 1st crack load of the controlled specimen S4 is found as 18.61 kN. With the increase in the load, a similar crack pattern around the opening can be seen in the repaired area as seen in the controlled beam, S4; and also in the repaired beam tested on the 3rd day. With a further increase in the loading up to 45.47 kN, flexural cracks are developed. At the same time, the shears crack 7, which is considered to be the most critical crack, tends to propagate toward the loading point. It is also noticed that the presence of wire mesh restricts the widening of the shear cracks and makes the specimen capable of sustaining more load. The failure of the beam took place by tearing the wire mesh and widening crack no 7.

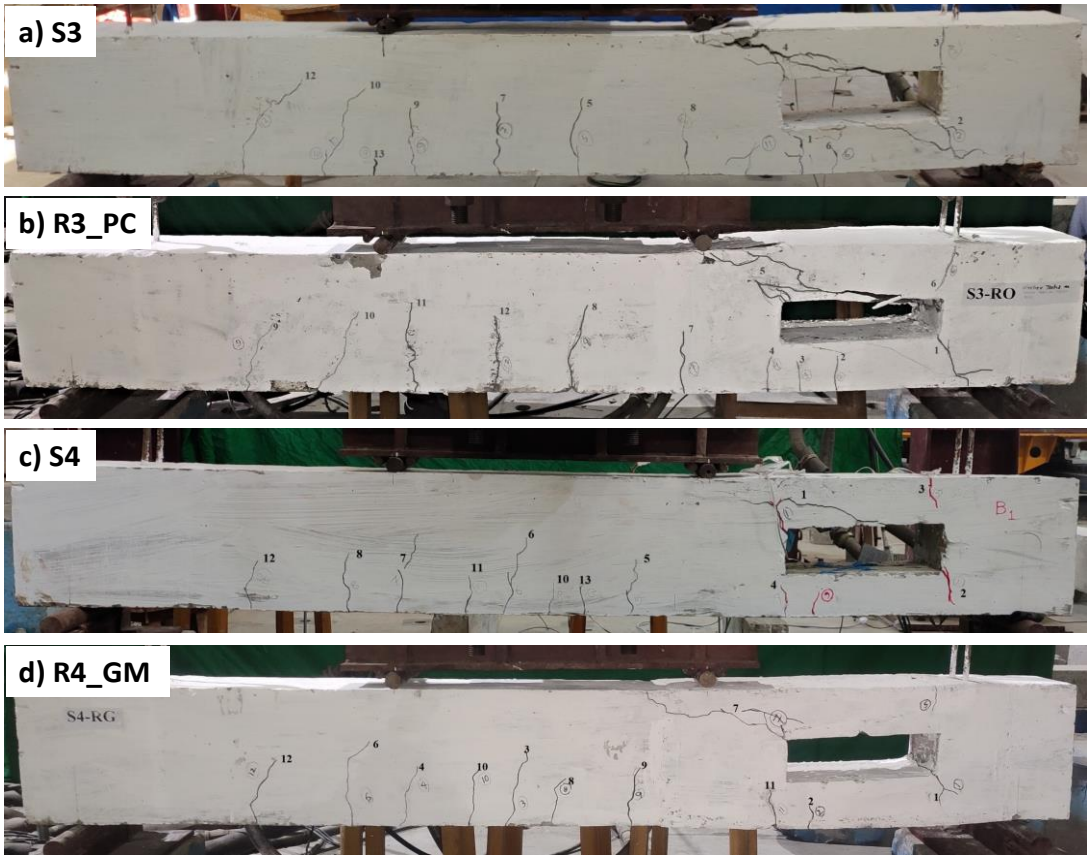

Figure 5.19: Crack pattern of controlled and repaired beam with shear opening (28th Day)

Fig. 5.20. shows the load-deflection curve of the controlled specimen and the repaired specimen tested on the 28th day. It can be observed that the beam R3_PC repaired by PCM

could sustain a higher load of 92.01 kN, which is approximately 9 % higher than the ultimate load carried by the S3. The beam exhibited lesser DR (1.20) than that of the controlled specimen S3, whose ductility ratio was 1.70. This shows that repaired beam showed no improvement in ductility of the beam even on the 28th day. The beam fails by splitting the shear crack in the top chord. On the other hand, the repaired beam R4_GM exhibits an ultimate load carrying capacity of 110.49 kN, whereas the ultimate load sustained by the controlled specimen S4 is 78.30 kN. This shows that the beam repaired by GM enhances the strength by 41 % more than the controlled specimen. The repaired beams exhibit a marginal degradation in the initial stiffness. However, as the crack widening is resisted by the presence of the wire mesh, the stiffness of the repaired beam eventually improved with the increase in the loading.

From Table. 5.11., it can be noticed that the repaired beam with GM exhibits a DR of 1.22, whereas the controlled beam possesses a higher DR of 1.32. This degradation of ductility in repaired beams with the shear opening is seen in all the repaired specimens. This may be attributed to the fact that the repairing with wire mesh enhances the rigidity of the beam by controlling the crack widening; this leads to a steep rise of the load-deformation curve up to the ultimate load. Beyond that, the specimen fails in shear by splitting the top chord, which is

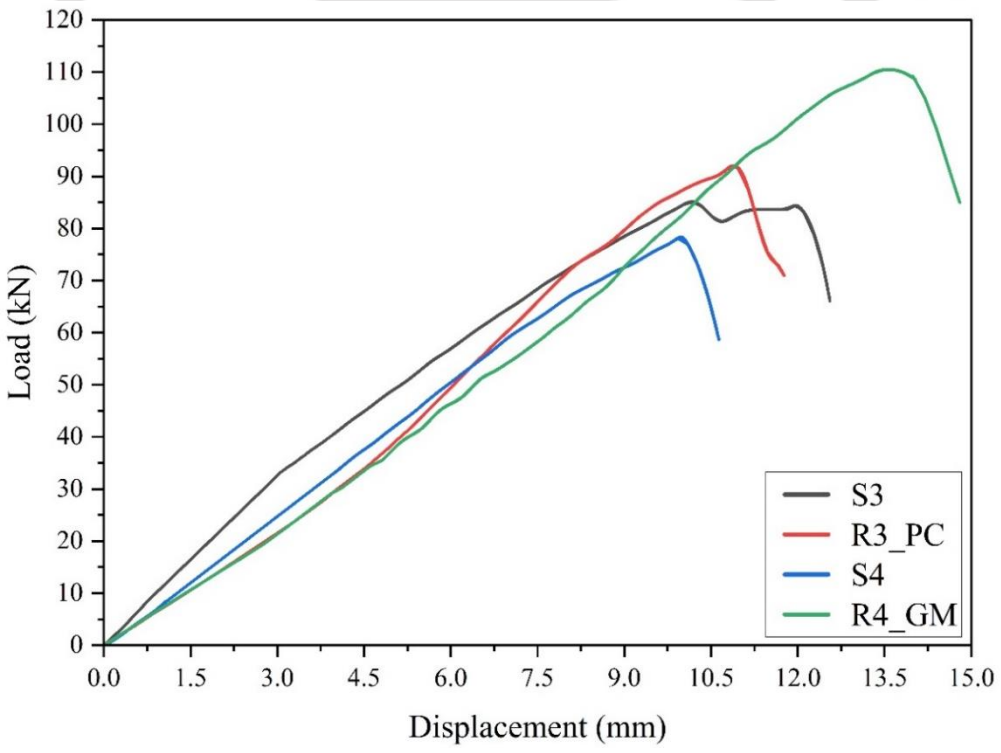

Figure 5.20: Load deflection curve of controlled and repaired beam with shear opening (28th Day)

a sudden failure. This causes a reduction in the ductility of the repaired beam with an opening in the shear zone. However, the failure of the repaired beam is found to be less sudden as compared to the controlled specimen.

From the above discussions, it can be understood that the repairing technique with wire mesh and the GM can be used successfully to repair the damaged beam with an opening. The repair material GM applied in the damaged beam shows no debonding or spalling during the application of load. The repaired beam is able to attain an appreciable flexural load even on the 3rd day of testing. Whereas all the specimens exhibit enhanced load carrying capacity on the 28th day, however, such method shows no significant effect in improving the ductility of the repaired beam. The present method can also resist the widening of cracks around the opening, which will ultimately enhance the durability of the repaired beam.

5.4 Closure

This chapter mainly deals with the repairing of the damaged web-opened RC beam by the application of a newly developed repairing technique with geopolymer mortar (GM). To explore the efficiency of the repairing technique, the repairing technique is initially applied to the prototype specimen. Based on the performance of the prototype specimen, the repairing strategy is further carried out on the full-scale specimens of RC beams with opening in the web. To evaluate the efficacy of GM, conventional Portland cement mortar (PCM) is also used as an alternate repair material.

The chapter also includes the experimental study on the behaviour of beams with an opening at different location. Thus eight numbers of RCC beams with web opening at a distinct location of the beam are cast. To study the effect of the opening, one solid beam of the same size and reinforcement is also cast, which is considered as a reference beam. All the beam specimens are tested with static monotonic load with a four-point loading scheme. It is noticed that the RC beam with opening developed early and wide cracks, which makes the beam weak and collapses at a lower load exhibiting poor ductility.

The damaged beams are then repaired using GM and PCM along with welded steel wire mesh and are retested again. The GM possess early strength achievement property, which makes it most advantageous to be used as a repairing agent and hence can be used to repair damaged RC structural members and put to re-use earlier. The results of the study reveal that the new repairing technique with GM has a strong potential for emergency repairing due to its capability of restoration of the original strength in three days.

All specimens repaired by GM showed better performance than those repaired by PCM. The damaged beams repaired by GM, which are tested on the 3rd day, exhibit full restoration with more than 100 % strength enhancement. The present technique of repairing is found very effective in the restoration of a beam with a mid-span opening. The repaired beam with a web opening in the mid-span exhibits an enhanced load carrying capacity and shows better ductility than that of a solid beam with no opening. While in the case of the beam with an opening in shear, the repaired beam GM exhibited only better load carrying than the controlled beam and also showed improvement in the failure pattern. Hence, it is recommended that repairing material and the repairing technique developed in the present chapter for retrofitting the RC structural member in a short period with GM is the effective way of restoring the structure to its functional use at the earliest period possible.

Chapter 6

Jacketing of Web opened RC beam using Fiber Reinforced Geopolymer Concrete

6.1 Introduction

Reinforced concrete (RC) structures often require repairing and/or strengthening to extend their service life as well as for their rehabilitation. This type of situation arises when there is a need for change in utilization of the existing structure, change in the design philosophy, ageing or deterioration of concrete due to environmental conditions, faults in construction or damage due to the seismic hazard (Obaidat et al. 2011). There are different techniques available for retrofitting and strengthening RC structural members. Global strengthening of structures includes the building of shear walls, installation of bracing, base isolation system, installation of dampers etc. While local strengthening in structural members involves ferrocement jacketing, reinforced concrete jacketing, external bonding of steel plates, fiber reinforced polymer (FRP) plates etc.

Among these, Reinforced concrete jacketing is the most traditional and cost-effective technique for strengthening structural members (Sheikh et al., 2017). Jacketing is a technique in which the section of the original member is enlarged to restore or increase its strength capacity. Besides this, it also increases the stiffness and ductility of the member. Jacketing can be done by adding a new concrete layer to the existing structural member. But the most important issue in jacketing is the adherence between the existing element and the jacketing layer. For successful retrofitting work, both the jacketing layer and the old member shall act as

a single unit like that in a monolithic composite structure. This can be achieved by maintaining proper bonding between the original member and the jacketing agent. The application of epoxy resin, dowel bars, shear connectors etc., are some of the common materials that are usually employed for better bonding between the structural member and the jacketing layer.

Recently, novel techniques using Fibre reinforced cement concrete (FRCC) layers or jackets have shown many promising results in retrofitting structural elements. Jacketing with FRCC for retrofitting and strengthening purposes has been investigated in several studies (Ruano et al., 2014). The application of FRCC as a jacketing material has several advantages, such as it prevents brittle failure of the member, prevents shrinkage cracks, improves the post cracking behaviour and increases the durability. Above all, it eradicates the limitation of thin jacketing layer, which is not possible in case of steel reinforced jacketing, where 60 to70 mm of jacketing layer is needed to accommodate the reinforcement and the concrete cover (Martinola et al., 2010). All these features make FRCC a very attractive material for jacketing RC structures. The effectiveness of FRCC also depends upon the bond between the fiber and the concrete matrix and between the FRCC matrix and the concrete substrate (Nanni 2012).

Over the last two decades, extensive research has been conducted on Fibre reinforced geopolymer concrete (FRGC). FRGC is a concrete similar to FRCC, which can be produced by the addition of fiber in geopolymer concrete (GPC). Recently, research on GPC has gained momentum due to its environmental friendliness, superior mechanical properties, durability and sustainability (Singh et al., 2015). Unlike ordinary concrete, GPC gains strength very early, even at ambient temperature and also possesses superior bond strength to steel and Portland cement concrete (PCC).

So far, considerable research has been carried out on the mechanical properties of FRGC; however, no study addresses the application of FRGC as a Jacketing material for the rehabilitation of damaged structural members. The application of FRGC for the restoration of a web opening beam is a novel technique, and its potential in the rehabilitation of a damaged web opened beam should be investigated. Thus in view of this, several RCC beam with an opening has been tested under a four-point load till failure. The damaged beams are then repaired and jacketed on the three sides with a layer of FRGC material. In order to evaluate the effectiveness of the FRGC, damaged specimens are also jacketed by FRCC material, and the jacketed specimens are tested at different ages of curing.

6.2 Experimental Program

The main objective of the experimental investigation is to evaluate the effectiveness of the newly developed FRGC material in Jacketing of damaged web opened beam. Thus in view of this RCC beam with opening at different location are prepared in the laboratory using PCC concrete. These beams are considered as controlled specimen and are tested under static monotonic load. The damaged beams are then repaired using mortar and are jacketed again with FRGC and FRCC materials.

6.2.1 Test Matrix

In order to investing the effect of FRGC in jacketing of web opened beam, two types of opening location have been adopted. Total eight number of RC beam with opening are prepared. Based on the location of the opening these beams are categorised as

a) RC beam with opening in the Flexural zone (BMS).
b) RC beam with opening in the shear zone (BSS).

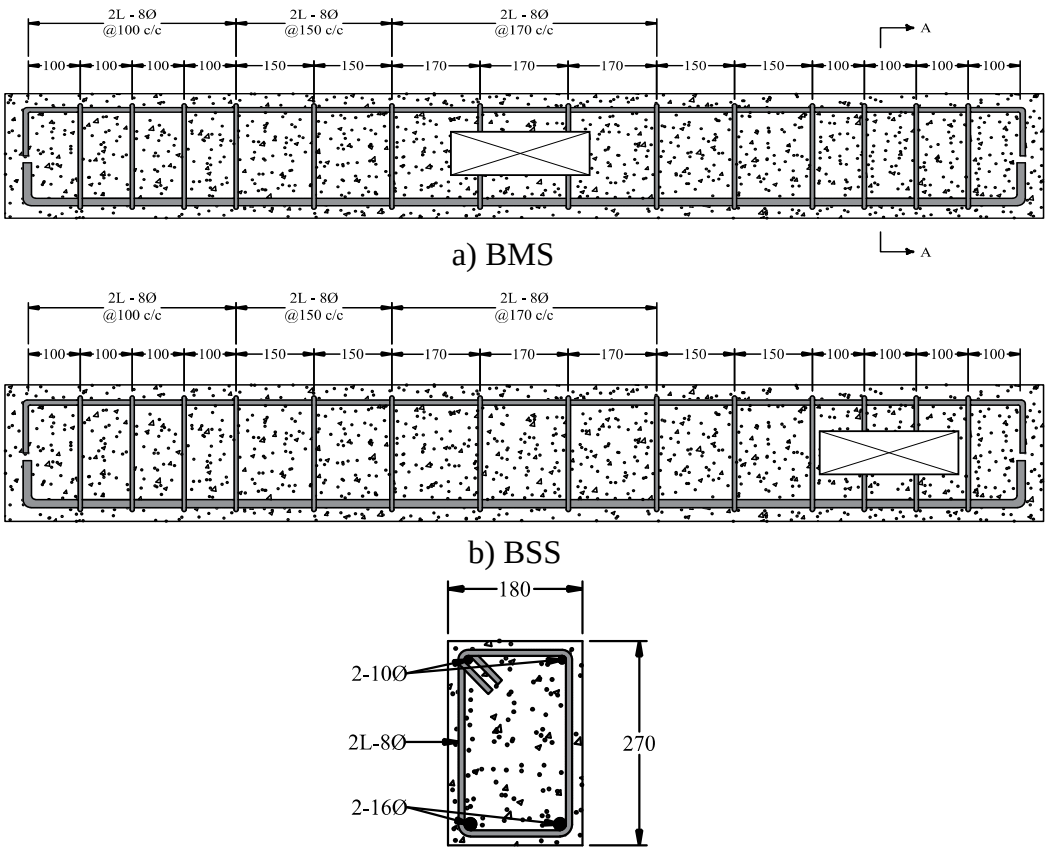

Figure 6.1: Detail of the Reinforced concrete specimen for Jacketing work

Out of the eight beam, four numbers of beams are prepared with an opening in the flexural zone. Whereas four other beams are prepared with opening in the shear zone. The position of the opening in similar to that adopted for the repairing work as described in subsection 5.2.1. of Chapter 5. The length of all the beams are kept same as 2000 mm, with a clear span length of 1800 mm and cross-section of beam is adopted as 180×270 mm. The depth of the web opening is kept as 33 % of the total depth of the beam and the length of the opening is adopted as 300 mm. The size of the opening is kept constant for all the beam specimen. All the beams are reinforced with the same amount of reinforced steel and the details of the reinforcement are given in the Fig. 6.1.

The controlled specimens are initially cast and prepared in the laboratory with PCC. These specimens are then tested under four-point loading scheme subjected to static monotonic load. During the test, the specimens are loaded till failure and hence these beams are considered as fully damaged beams. The detail of the tested specimen and the Jacketing scheme is given in Table 6.1.

Table 6.1: Experimental test matrix for Jacketing work

Types	Designation of Controlled Beam	Opening Location	Jacketing Material	Designation of Jacketed Beam	Tested on
Beam with opening in mid span "BMS"	S16	Flexure Zone	FRCC	JS16_FRC	3rd Day
	S12	Flexure Zone	FRGC	JS12_FRGC	3rd Day
	S14	Flexure Zone	FRCC	JS14_FRC	28th Day
	S9	Flexure Zone	FRGC	JS9_FRGC	28th Day
Beam with opening in shear span "BSS"	S15	Shear Zone	FRCC	JS15_FRC	3rd Day
	S13	Shear Zone	FRGC	JS13_FRGC	3rd Day
	S11	Shear Zone	FRCC	JS11_FRC	28th Day
	S10	Shear Zone	FRGC	JS10_FRGC	28th Day

The beam S16, S12, S14 and S9 are the controlled specimen with opening in the flexure zone. While the beams S15, S13, S11 and S10 are the beam with opening in the shear zone. These beams after testing are repaired and jacketed by different jacketing material (FRCC and FRGC). Moreover, to study the efficiency of the FRGC material as an emergency retrofitting material, the specimens are also tested on 3rd day and 28th day as per Table 6.1. From the test results of the beam specimens, the following aspects have been thoroughly studied:

1. Yield load and corresponding Deflection of beam.
2. Peak load and Deflection at the ultimate load.
3. Moment carrying capacity (MCC)

4. Ductility ratio (DR).
5. Strength enhancement ratio (SER).
6. Load at 1st crack.
7. Cracking pattern of the tested beam.

The FRGC material that has been utilised in the damaged beam for jacketing is specially developed with ultrafine slag-based binder, as described in Chapter 4. Before conducting the Jacketing of the damaged web opened beam, the efficiency of the Jacketing material is evaluated by repairing and jacketing of a prototype specimen. In view of this small prismatic RC beam of size 150×150×700 mm are initially damaged by applying load in a universal testing machine (UTM). These damaged specimens are then repaired by mortar followed by Jacketing with FRGC and FRCC. The strengthened specimens are then tested on the 7th day of curing.

6.2.2 Materials

The materials used for preparation of beam specimen till the jacketing of the damaged specimen are discussed elaborately in the following sub-sections:

6.2.2.1 Geopolymer Paste

The geopolymer paste (GP) adopted in the process of strengthening is mainly utilised to serve two purposes. Firstly, it is used to fill the fine cracks where granular mortar cannot penetrate. Secondly, the GP pastes have been employed here as a bonding agent between the concrete substrate and the Jacketing layer.

The GP that has been utilised consists of the same binder, i.e. ultra-fine blast furnace slag (UBFS) and Fly ash (FA). The alkali activator consists of a mixture of sodium hydroxide and sodium silicate (SHSS) solution. The properties of UBFS and the FA have been discussed in section 2.2. of Chapter 2. In addition to this, 2 % of Borate is included to control the setting of the GP. The detail of the alkali activator and the retarder is given in section 2.2 of Chapter 2. In view of developing a consistent GP, several mix proportions (GP1, GP2 and GP3) are initially tested. Out of which, GP2, with an alkali to binder ratio (a/b) of 0.6 and compressive strength of 44 MPa (on 28th Day), has been chosen. The detail of the mix proportion of the various GP and the strength properties of the GP (GP2) obtained on the 3rd day and 28th day is given in Table.5.3. under subsection 5.2.2.1. of Chapter 5.

6.2.2.2 Portland Cement paste

Ordinary Portland cement (OPC) was used for preparing the cement paste (CP) utilised in strengthening. The properties of OPC are discussed in sub-section, 2.2.1 of Chapter 2. The mix proportion was selected such that the w/c ratio of CP matches with the total water/solid (w/s) ratio of GP. The mix CP attains a compressive strength of 45.83 MPa at the 28th day. The details of testing of the CP and the strength properties are given in Table. 5.4. under the subsection 5.2.2.2. of Chapter 5.

6.2.2.3 Geopolymer Mortar

Geopolymer mortar (GM) has been used as a repair material for filling up the larger cracks developed in beam specimens during loading. This mortar is prepared by using UBFS and FA. The alkali activator used in the mix consists of a combined mixture of sodium hydroxide and sodium silicate named SHSS solution. To avoid a fast setting, Borate is also incorporated into the mortar mix. Local river sand has been used as the fine aggregate. The details of the raw materials used in the preparation of GM are furnished in subsection 3.2.1 of Chapter 3. To develop the GM, several mix designs are prepared, and the fresh and the hardened properties are evaluated. The properties of the various mix proportion of GM mix is furnished in subsection 3.3.1 of Chapter 3. Based on the desirable properties of repair material, the mix GM17_2R, with compressive strength of 50.93 MPa on the 28th day, has been chosen. The detail of the mix proportion of GM17_2R and the various properties in the fresh state and in the hardened state is given in the Table. 5.6. under subsection 5.2.2.3. of Chapter 5.

6.2.2.4 Portland Cement Mortar

Portland cement mortar (PCM) is also used as an alternative mortar to fill the cracks. The PCM is prepared using ordinary Portland cement as described in section 3.2.2 of Chapter 3. Similar to GM, local river sand of Zone III has been utilised as the Fine aggregate. To prepare the PCM, the quantity of sand is taken as three times the cement. The water to cement (w/c) ratio is taken as 0.4, which is similar to the total water to solid (w/c) ratio of the GM17_2R. The compressive strength of the PCM mix is 34.15 MPa on the 28th day. The fresh and hardened state properties of PCM are also given in Table. 5.7. under subsection 5.2.2.4 of Chapter 5.

6.2.2.5 Portland Cement Concrete

All the beam specimens are cast with PCC mix. This mix is initially prepared with OPC 43 Cement and is named CM1. The properties of the raw materials used in the preparation of CM1

have been described in the sub-section 2.2.1 of Chapter 2. The mix proportion of the concrete mix, CM1, is furnished in Table 4.3 under subsection 4.2.2.3 of Chapter 4. To evaluate the properties of the mix CM1, tests like slump test, compressive strength test and split tensile strength are conducted. The compressive strength achieved by the mix PCM on the 28^{th} day is 28.44 MPa. The details of the test procedure to evaluate the fresh and hardened properties of the mix CM1 is given in the Table. 5.8. under subsection 5.2.2.5 of Chapter 5.

6.2.2.6 Fiber Reinforced Geopolymer Concrete

The fiber reinforced geopolymer concrete (FRGC) has been prepared by adopting Ultrafine ground granulated blast furnace slag (UBFS) as the main binding material. At the same time, Fly ash (FA) and superplasticizer (SP) are incorporated to enhance the fresh properties of the FRGC material. The details of UBFS, FA and SP are presented in sub-section 2.2 of Chapter 2. Moreover, to ease the pouring of FRGC material into the thin jacketing section, the maximum size of the coarse aggregate has been restricted to 10 mm. Local river sand conforming to Zone III has been used as the fine aggregate. Hooked end steel fiber of size 50 mm in length and diameter 0.75 mm of tensile strength 1400 MPa, has been used in the development of FRGC. The details of the fiber are also furnished in the sub-section 2.2.10 of Chapter 2.

In order to develop the FRGC for jacketing, several Geopolymer concrete (GPC) mixes are initially developed. These mixes are prepared by considering several parameters that affect the workability and the strength properties of GPC. The details of the various mix proportion of GPC that has been investigated are given in Table 4.1. under the sub-section 4.2.2.1 of Chapter 4. Based on the workability, bond strength, compressive strength, and split tensile strength of the GPC mixes, suitable mixes of GPC are chosen and further modified by incorporating different volume fractions (V_f) of steel fiber, in developing the FRGC material. Different V_f of steel fiber whose effect has been investigated is given in Table. 4.2. under sub-section 4.2.2.2. of Chapter 4.

The selection of the FRGC material for the Jacketing purpose has been made mainly on the basis of workability, flexural strength and compressive strength. Based on the strength properties of the FRGC mixes, the mix MG9_13%, which is incorporated with 1.3 % V_f of steel fiber has been used for the Jacketing work. The mix proportion of the various raw material used in the FRGC mix is given in Table.6.2.

Table 6.2: Mix proportion of FRGC used for Jacketing

FRGC mix	UBFS (Kg/m^3)	FA (Kg/m^3)	Fine Agg (Kg/m^3)	Coarse Agg (Kg/m^3)	V_f (%)	Alkali (Kg/m^3)	Molarity (M)	w/s ratio	Water (Kg/m^3)	SP (%)
MG9_1.3	289.02	123.86	702	991.8	1.3	276.64	6	0.47	18.87	1.5

Note: Fine Agg- Fine Aggregate, Coarse Agg- Coarse Aggregate, w/s - Water to Total solid ratio.

To evaluate the properties of the FRGC mix various tests are conducted. The workability test for the FRGC mixes are evaluated by both Slump cone and the Vee-bee consistometer test as per IS 1199-1959 (2004) and IS 10510 (1983). The split tensile strength is determined as per IS 5816-1999 (2004). While the compressive strength test and the flexural strength test of FRGC has been evaluated as per IS 516-1959 (2006). The fresh and hardened properties of the mix MG9_1.3 % is given in the Table 6.3.

Table 6.3: Fresh and hardened test results of FRGC mix (MG9_1.3)

Test	Values
Slump Value	60 mm
Vee-bee time	14 Sec
Compressive strength (3^{rd} Day)	40.03 MPa
Compressive strength (28^{th} Day)	55.33 MPa
Tensile strength (3^{rd} Day)	3.43 MPa
Tensile strength (28^{th} Day)	4.84 MPa
Flexural strength (3^{rd} Day)	6.20 MPa
Flexural strength (28^{th} Day)	11.38 MPa

6.2.2.7 Fiber Reinforced Cement Concrete

FRCC is used as the alternate jacketing material that has been adopted for strengthening damaged beams. OPC 43 grade cement has been used as the binder in the FRCC. The properties of the OPC cement have been described in sub-section 2.2.1. of Chapter 2. Local river sand conforming to Zone III has been used as the fine aggregate. Similar to FRGC the angular-shaped aggregate of maximum size10 mm has been used as the coarse aggregate. The detailed properties of the fine aggregate and coarse aggregates have been given in the sub-section 2.2.5 of Chapter 2. The steel fiber used in the FRGC is also employed for the FRGC mix. An SP is also used to improve the fresh properties of the FRGC mix. The details of the SP used in the FRCC mix is given in the sub-section 2.2.6 of Chapter 2.

Table 6.4: Mix proportion of FRCC mix used for Jacketing

FRCC mix	Cement (Kg/m^3)	Fine Agg (Kg/m^3)	Coarse Agg (Kg/m^3)	w/c ratio	V_f (%)	SP (%)
CM3	450	860	826	0.47	1.3	0.15

The FRCC mix is opted to compare the performance of FRGC in jacketing; hence this mix is referred to as controlled mix, CM3, as discussed in the sub-section 4.2.2.3 of Chapter 4. The mix CM3 is designed with a water to cement ratio (w/c) of 0.47, which is similar to the water to total solid ratio (w/s) of the FRGC mix. Moreover, the percentage of V_f of the hooked end steel fiber is also kept the same. The mix proportion of CM3 is given in Table. 6.4. While the different test results obtained during the laboratory test of FRCC are presented in Table. 6.5.

Table 6.5: Fresh and hardened test results of FRCC mix (CM3)

Test	Values
Slump Value	20 mm
Vee-bee time	15 Sec
Compressive strength (3^{rd} Day)	14.28 MPa
Compressive strength (28^{th} Day)	38.22 MPa
Tensile strength (3^{rd} Day)	1.66 MPa
Tensile strength (28^{th} Day)	3.57 MPa
Flexural strength (3^{rd} Day)	2.70 MPa
Flexural strength (28^{th} Day)	7.32 MPa

6.2.2.8 Reinforcement

The main reinforcement in the controlled beam specimens consist of 2 numbers of 16 mm diameter tor steel bars at bottom and 2 numbers of 10 mm diameter bar at top. The shear reinforcement is provided using 2 legged 8 mm diameter tor steel bars. The details of the properties of the reinforcement are presented in the sub-section, 2.2.7 of Chapter 2.

6.2.3 Experimental setup and Instrument

The beams are tested under four-point loading as shown in the Fig. 6.2. All beams are tested under simply supported condition with an effective span of 1800 mm. The beams were subjected to static flexural load using MTS actuator, having a load capacity of 1000 kN and stroke length of 500 mm. Displacement based monotonic loading has been vertically applied

at the rate of 0.01 mm/s. All the specimens are loaded till the ultimate load is achieved and loading is continued till the load drops to 85 % of the ultimate load. The mid-span displacement was recorded using a linear variable differential transducer (LVDT) of 300 mm capacity, which is attached in the soffit of the beam with the help of an acrylic sheet.

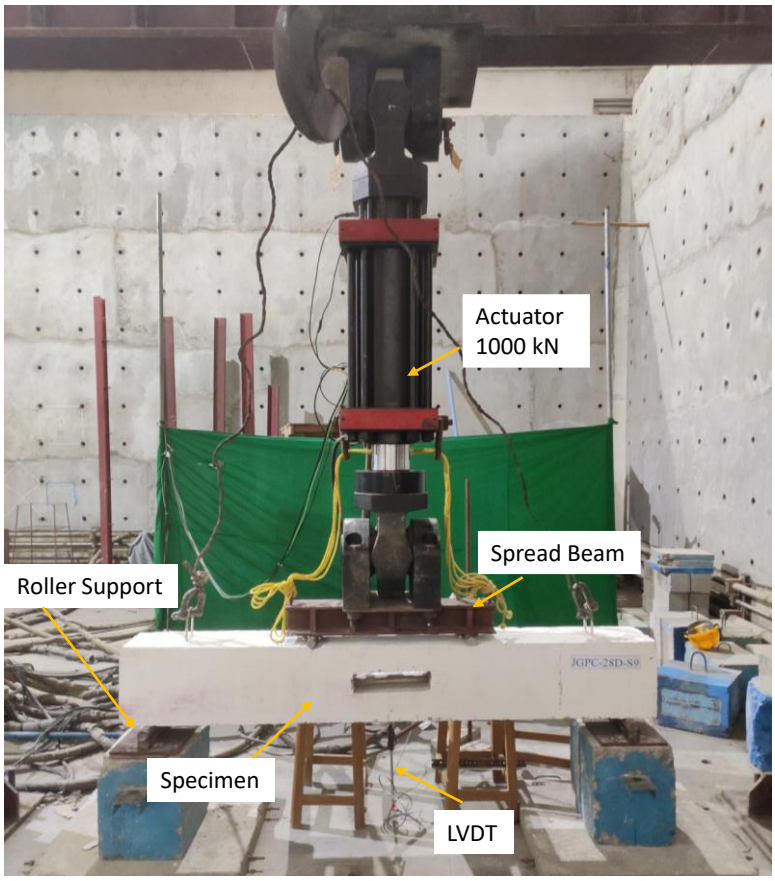

Figure 6.2: Test setup of Four-point bending for Jacketing work

6.2.4 Method of beam Jacketing

6.2.4.1 Repairing of Controlled beam

In order to study the effect of FRGC jacketing, eight numbers of the controlled specimen (RC Beam) are prepared. These beams are designed as doubly reinforced concrete beams, as per IS 456 2000, having a theoretical ultimate load carrying capacity of 145 kN. The design which was carried out to decide the beam size and reinforcement in case of preparing the RC beams is presented in Appendix B. The RC beams are of size 180 mm × 270 mm and length 2 m (see Fig. 6.1.).

All the beam specimens were cast with the same concrete mix CM1 of compressive strength 28.44 MPa. The detail of the casting process is explained in sub-section 5.2.3. of

Chapter 5. After casting, the beam specimens are subjected to curing using wet rags for 28 days and dry curing in the open air for another 28 days. As soon as the curing period is over a fine layer of whitewash was applied over the surface of the beams to facilitate the identification of cracks during testing. All these beams are tested under static monotonic load as described in the preceding sub-section 6.2.3. The beams are loaded up to the failure, and hence the tested beams are considered fully damaged beams. The damaged beams are then repaired and strengthened by the application jacketing with FRGC and FRCC.

6.2.4.2 Method of surface preparation and Jacketing

Before Jacketing the damaged specimen (controlled beam), the surface of the beams is prepared. The surface preparation includes chipping of the beam surface, enlarging cracks and removal of the crushed concrete and after that, filling the cracks with repairing paste and mortar. In this process, the major cracks that are visible on the surface of the beam are first identified and marked. For the ease of effective application of repairing material, the flexural cracks are enlarged up to an average depth of 50 mm and a width of 40 mm approximately. While crushed concrete portion in the top chord is entirely removed, up to the depth of the damage.

a) Removal of dust particles

b) Filling of cracks with GM

c) Filling of cracks with PCM

Figure 6.3: Repairing process of damaged beam

For better adhesion between the jacketing layer and the concrete, surface roughening was carried out by chipping manually with a hammer and chisel to expose the aggregates over the whole length of the beam on the three sides. The broken concrete particles that are loosely attached inside the beam surface are removed carefully with the help of a wire-brush such that no free particles remain attached to the surface of the cracks. The beams are then subjected to air blowing with the help of an air blower, as shown in Fig. 6.3. (a), to remove the dust and minute-free particles from the surface and ready it for further treatment. This method of crack cleaning and surface preparation is similar to that used by the field engineers and technical persons while repairing concrete structures with epoxy resin, cement grout, etc.

As soon as the surface of the bream is prepared, the repairing paste (GP or CP) is first applied to fill the cracks. Due to the high followability of the paste, it can penetrate inside the fine cracks, which are not wide enough to allow the accommodation of mortar. After applying the repairing paste, the larger cracks are then filled up by the repairing mortar (GM or PCM). The repairing mortar was placed inside the cracks with the help of a trowel, as shown in Fig. 6.3. (b)-(c). During this process, the repair material is also compacted with the tamping bar for better placement and removal of voids within. The mortar is continued to be filled inside the cracks till it fills the cracks up to the level of the beam surface. A repaired beam after filling of cracks can be seen in Fig. 6.4. On completion of the cracks filling process, the beams were kept un disturbed at an ambient temperature of 20 ± 2 ºC for one day. After one day of curing the specimen are again jacketed with the Jacketing agent (FRCC and FRGC).

Figure 6.4: Repaired beam with opening in the flexure zone

To carry out the strengthening of the repaired beam by FRGC jacketing technique, ‘U’ shaped jacketing scheme has been adopted. That is, the beams are jacketed only on the bottom and lateral sides and no jacking is provided at the top of the beam. The ‘U’ shaped jacketing is the

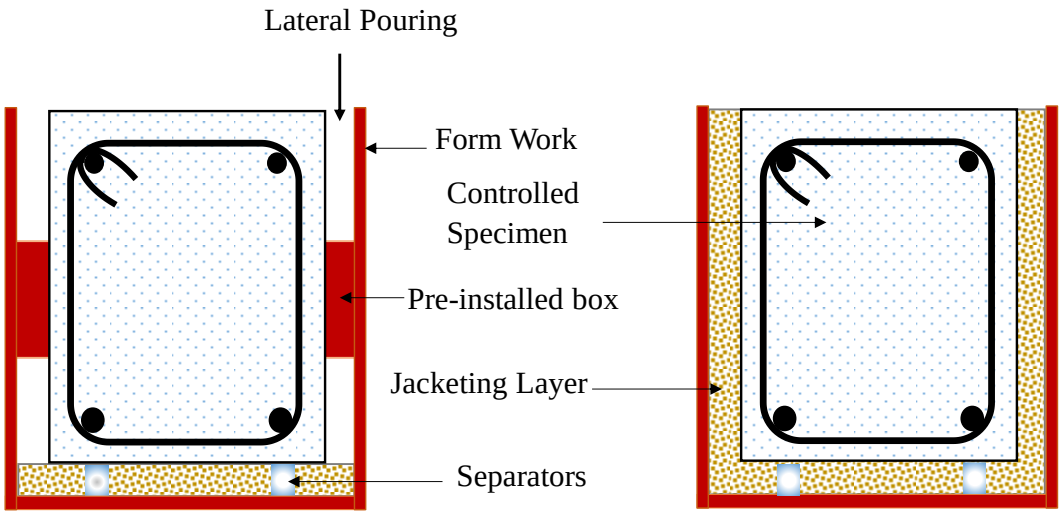

Figure 6.5. (a): Typical sectional details of the FRGC Jacketing

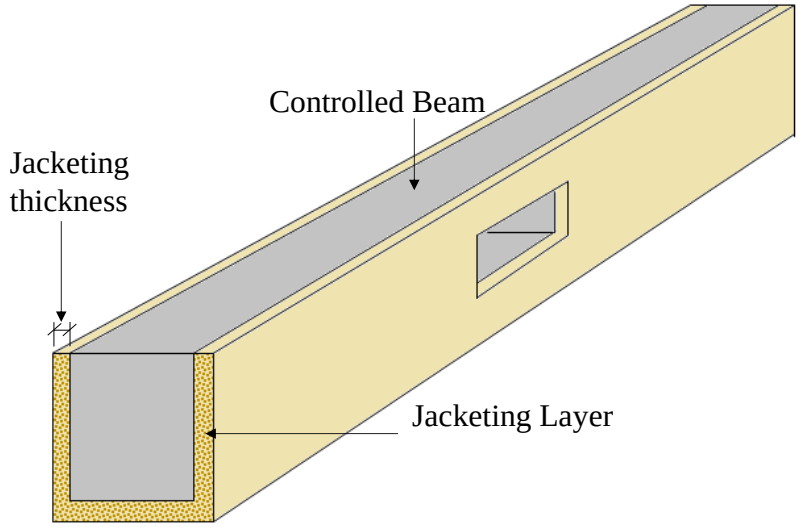

Figure 6.5. (b): Isometric view of the Jacketed beam

most effecting strengthening method, as reported by Al Osta et al. (2017), and is the most feasible way for field application. Fig. 6.5. shows the typical diagram of three-sided FRGC jacketing details adopted for strengthening of web opened beam. A 40 mm thickness jacketing layer is adopted for the study, which is kept constant for all three sides and in all the specimens. The original section of the beam is 180 × 270 mm, while after a thick jacketing layer of 40 mm, the section of the beam increases to 260 × 310 mm. Based on the section of the jacketed beam, form works have been initially prepared. In order to maintain a constant jacketing thickness of 40 mm along the length of the beam, 9 numbers of metallic separators of height 40 mm have been preinstalled at the bottom of the formwork, as shown in Fig. 6.6.

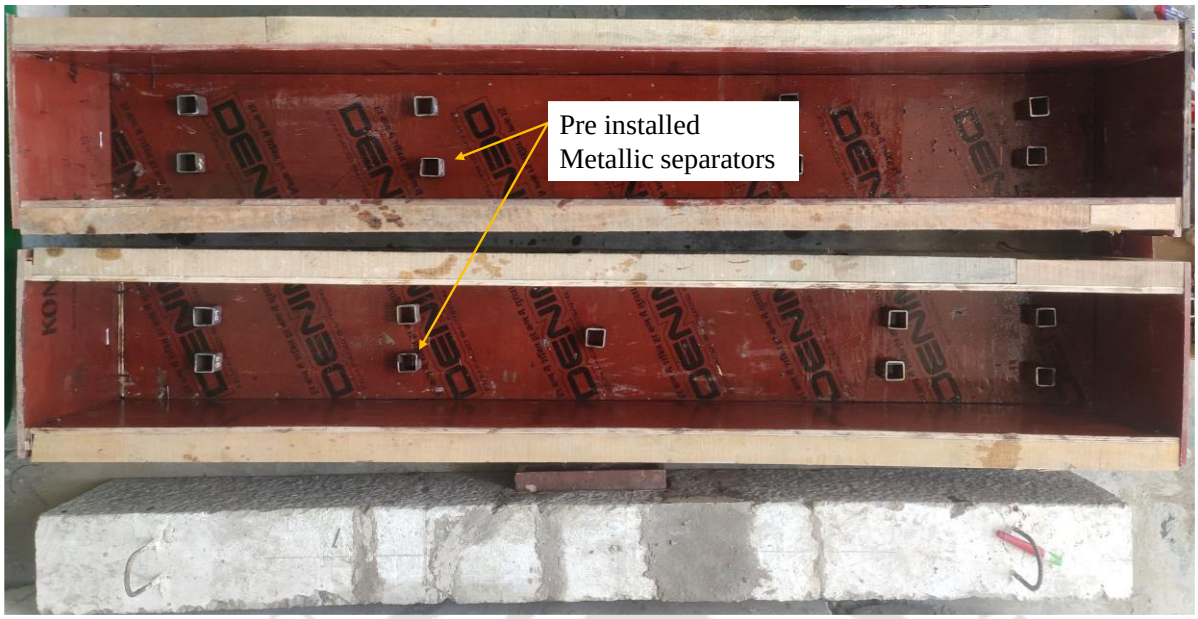

Figure 6.6: Form work for Jacketing

Figure 6.7: Pre-installed wooden box

The jacketing layer has been cast around the three sides of the beam, leaving the opening area. Thus a wooden box has been preinstalled in the opening. This has been done to prevent the FRGC concrete from occupying the opening area. Fig. 6.7. shows the pre-installation of wooden box in the opening zone of beam. The specimen is then lifted and carefully placed inside the form work in such a way that the beam rests uniformly on the metallic separator. During the process utmost care is taken so that a clear cover of 40 mm is maintained in the bottom as well as in both the lateral sides.

Therefore, just after the next day of repairing Jacketing of the repaired beams are carried out. Freshly prepared fiber reinforced concrete mix (FRGC and FRCC) is then poured laterally inside the jacketing layer in several layers. Fig. 6.8. (a) shows the casting process of the jacketed beam. In order to ensure uniform spreading and compaction of the concrete, electrically operated needle vibrator is used throughout the process.

a) Casting process of Jacketed specimen

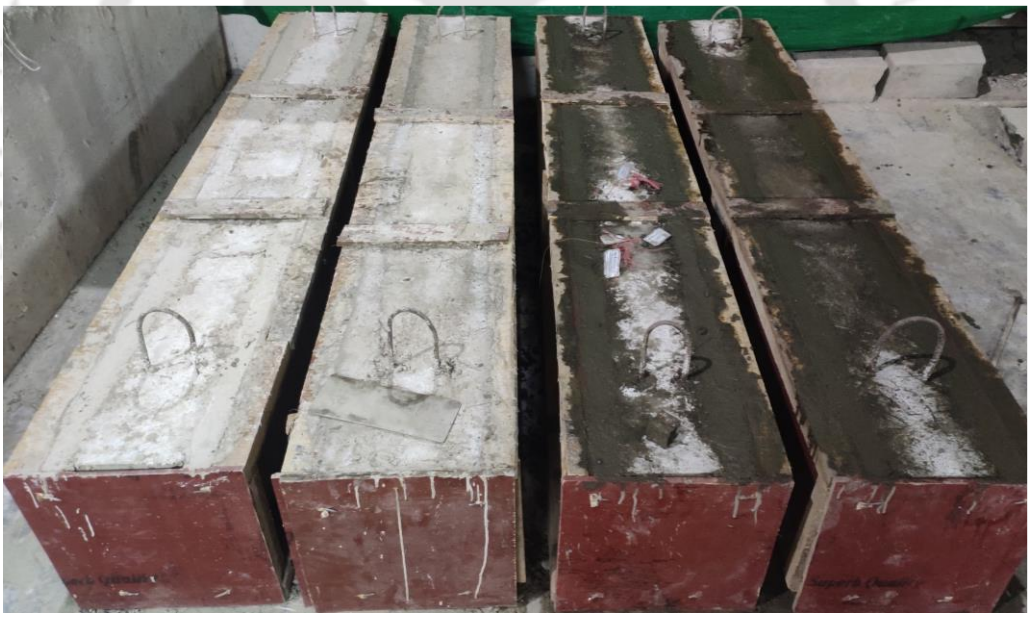

b) Cast Jacketed Specimen

Figure 6.8: Jacketing of specimen

As soon as the concrete is filled up to the level of the form work, the jacketing layer is properly finished at the level of the beam. The cast beams are then left undisturbed for 24 hours, as shown in the Fig. 6.8. (b). On the next day, the jacketed specimens are lifted and form work have been removed. The specimens are then cured with wet gunny bags maintaining a temperature of 20 ± 2 ºC. till the day of testing.

On the day of the testing, the specimens are taken out from the curing and kept in a dry place for air dying. Fig. 6.9. shows the section of the jacketed beam. A fine layer of white wash is then applied over the surface of the beams so that the cracks that were supposed to develop due to loading in the test are clearly visible.

a) Jacketing with FRCC b) Jacketing with FRGC

Figure 6.9: Section of Jacketed specimen

6.2.5 Preliminary investigation of Jacketing technique

A preliminary investigation has been carried out in order to define the procedure of FRGC strengthening layer application. To fulfil this aim, two RC prisms of size 150×150×700 mm, have been prepared and are named CS5 and CS6. All these specimens are prepared with two bottom bars and two top bars of 8 mm diameter. Nominal shear reinforcement with 8 mm bar is provided at a spacing of 300 mm center to center. The detail of the prismatic beam is given in Fig. 5.9, under the sub-section 5.2.6 of Chapter 5. These specimens are cast using PCC concrete CM1 of compressive strength 28.44 MPa. The details of the concrete mix CM1 are discussed in the preceding subsection 5.2.2. After casting, these specimens are initially cured for 28 days in water followed by 28 days in the open air. After completion of 56 days, the specimens are subjected to four-point loading in a UTM and are loaded up to their ultimate load.

The damaged specimens are then repaired and jacketed following the same procedure mentioned in the preceding subsection 6.2.4.2. Fig. 6.10 shows a typical description of the jacketing method. The thickness of the jacketing on the two lateral sides is taken as 40 mm,

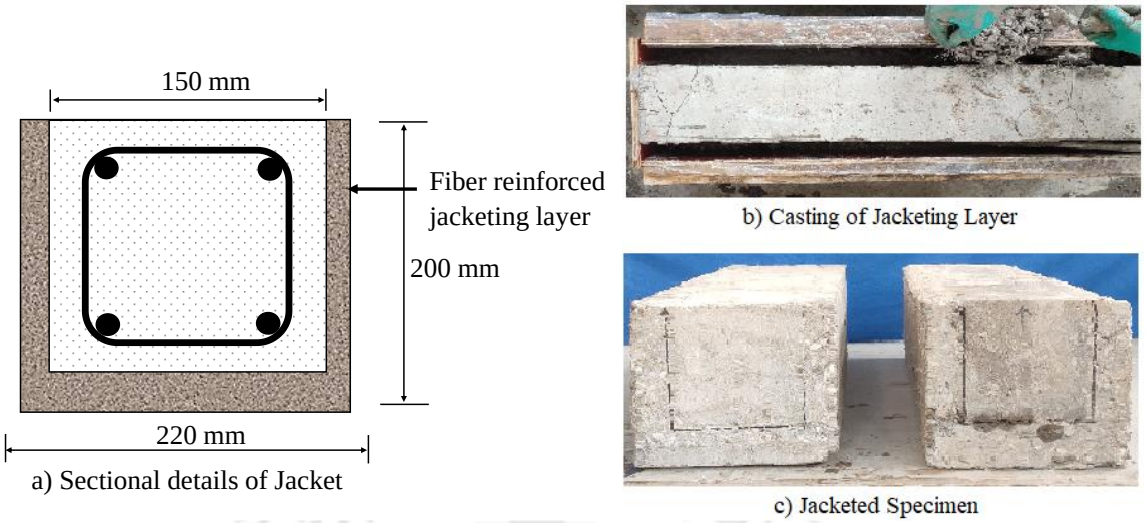

Figure 6.10: Jacketing of small prismatic beam

while the bottom layer consists of the jacketing thickness of 45 mm. These beams are the prototype beam; hence the thickness of the jacketing layer in the flexure is intentionally kept more to enhance the flexural strength of the beam (Guades et al., 2021). Moreover, this preliminary investigation is mainly conducted with the motive of finding the efficiency of FRGC by comparing it with FRCC. Hence, the main concern is to jacket both the specimen in an identical way and thereafter compare their strength. The specimen CS5 is jacketed with FRCC, and the specimen CS6 is jacketed with FRGC and are renamed JCS5 and JCS6. The mix proportion of the FRGC mix, GM9_1.3%, is given in Table. 6.2. under the sub-section 6.2.2.6, and that of FRCC is given in Table. 6.4 under the sub-section 6.2.2.7 of the preceding section. The compressive strength properties of the mixes attained on 7^{th} day and 28^{th} day is given in Table. 6.6. The jacketed specimen JCS5 and JCS6 are cast and cured for 7 days.

Table 6.6: Compressive strength properties of Jacketing Material

Type	Mix	Test	Values
FRGC	CM3	Compressive strength (7^{th} Day)	26.76 MPa
		Compressive strength (28^{th} Day)	38.22 MPa
FRCC	MG9_1.3%	Compressive strength (7^{th} Day)	41.81 MPa
		Compressive strength (28^{th} Day)	55.33 MPa

6.3 Result and Discussion

6.3.1 Test result of Jacketed prismatic beam

The preliminary investigation just after the 7th day of curing is done by retesting the small jacketed specimen in the UTM. These jacketed specimens are then loaded in UTM until the load reaches to the peak and stopped as soon as the load drops to 85 % of the peak load. Table 6.7. shows the test results of the jacketed beam. The original load attained by the specimen CS5 and CS6 are 134.12 kN and 137.85 kN, respectively. Both the beam exhibits outstanding performance in regaining the original strength. The beam JCS5 jacketed by FRCC controlled mix (CM3) exhibits a load carrying capacity of 137.11 kN, which is approximately 2 % higher than the original load. While the beam JCS6 jacketed by FRGC mix, MG9_1.3% exhibited a maximum load of 198.32, which is approximately 43 % higher than the original load attained by the controlled specimen CS6. The section enlargement in both the beam by application of

Table 6.7: Test result of the prismatic beam after Jacketing

Specimen	Jacketing agent	Mix	Ultimate Load before repairing (kN)	Ultimate Load after repairing (kN)	Strength Enhancement ratio (SER)
JCS5	FRCC	CM3	134.12	137.11	1.02
JCS6	FRGC	GM9_1.3%	137.85	198.32	1.43

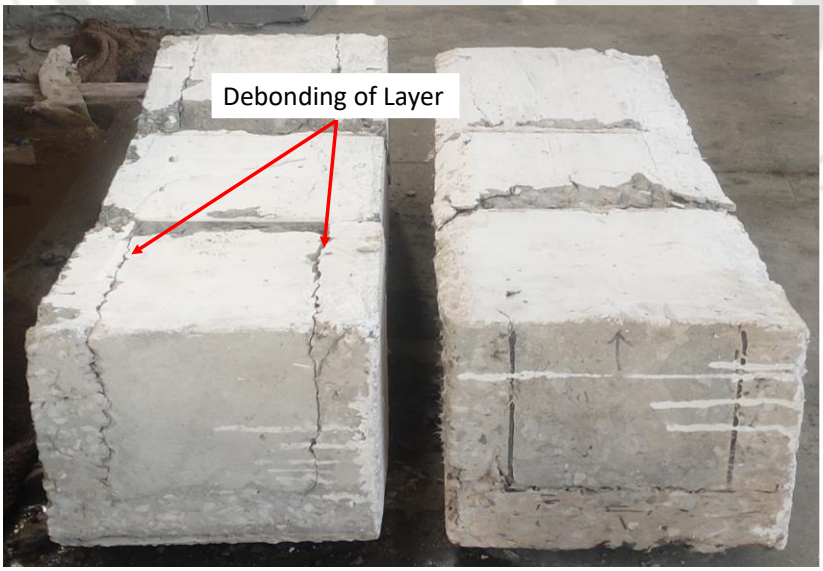

a) With FRCC b) With FRGC

Figure 6.11: Failed Jacketed prismatic beam specimen

fiber reinforced concrete exhibits an enhancement in the strength by more than 100 %. But the performance of geopolymer is much better than that of PCC based FRCC mix, which is attributed to better compressive strength and flexural properties of the FRGC. Furthermore, in JCS5 the FRCC de-bonds at an earlier stage of loading, as shown in the Fig. 6.11. Where as in the case of FRGC no sign of debonding can be noticed, even after the failure of the beam. This indicates a better monolithic action of FRGC material till its ultimate loading and hence possess a high potential in strengthening of damaged beam.

6.3.2 Experimental observation of Jacketed beam with web opening

The damaged beams that are strengthened using different Jacketing material (FRCC or FRGC) are renamed as J'specimen name'_'Jacketing material', as given in Table. 6.1. of subsection 6.2.1. The testing of the repaired specimen is conducted in the same way as done for the controlled specimen as mentioned in preceding sub-section 6.2.3.

6.3.2.1 Behaviour of Jacketed beam with web opening in the Flexure Zone

The crack pattern of the controlled beams and the strengthened beam tested on the 3rd day and 28th day are marked during the loading and the corresponding load for each individual cracks are also recorded. The results obtained from static flexural load test on the repaired beams with opening in the flexure zone are presented in Table 6.8.

Table 6.8: Test result of controlled and Jacketed beam with mid-span opening

Specimen	Test Day	Jacketing Agent	Yield Load (kN)	Deflection at Yield load (mm)	Peak load (kN)	MCC (kN.m)	Deflection at ultimate load (mm)	Load at 1st Crack (kN)	DR	SER
S16	56	_	144.00	11.25	164.79	49.44	26.23	24.17	2.33	_
S12	56	_	146.25	12.62	163.68	49.10	28.75	26.36	2.28	_
JS16_FRC	3	FRCC	112.05	10.20	133.26	39.98	13.80	32.96	1.35	0.81
JS12_FRGC	3	FRGC	163.12	10.88	189.35	56.81	42.30	34.65	3.89	1.16
S14	56	_	149.85	11.08	168.08	50.42	30.85	24.42	2.78	_
S9	56	_	145.76	11.17	170.78	51.23	27.40	18.02	2.45	_
JS14_FRC	28	FRCC	165.05	11.55	197.27	59.18	32.40	42.17	2.81	1.17
JS9_FRGC	28	FRGC	203.56	10.35	224.61	67.38	38.11	49.54	3.68	1.32

Note: MCC- Moment carrying capacity

3rd Day testing

Fig. 6.12 presents the crack pattern of the beams at the failure stage. The 1st crack in the controlled beam S16 and S12 appeared at a loading of 24.17 kN and 26.36 kN. While the 1st crack load appeared at the Jacketed beam, JS16_FRCC and JS12_FRGC appeared at a load of

32.96 kN and 34.65 kN. This increase in the crack load in the jacketed beam is contributed by the fibers present in the jacketing layer, which provided crack arresting features to the Jacketed specimen. However, the crack load of JS12_FRGC was relatively higher due to the better bonding of geopolymer with the fiber and the substrate. This statement is also supported by the better tensile strength and flexural property of FRGC as established in subsection 4.3.2.2 of Chapter 4. With the increase in load, more cracks start appearing both in the flexure and the shear zone. However, the pattern of the crack in the jacketed specimen, irrespective of FRCC or FRGC, was found nearly similar to the crack pattern exhibited by the controlled specimen, as seen in Fig. 6.12. (a) – (d).

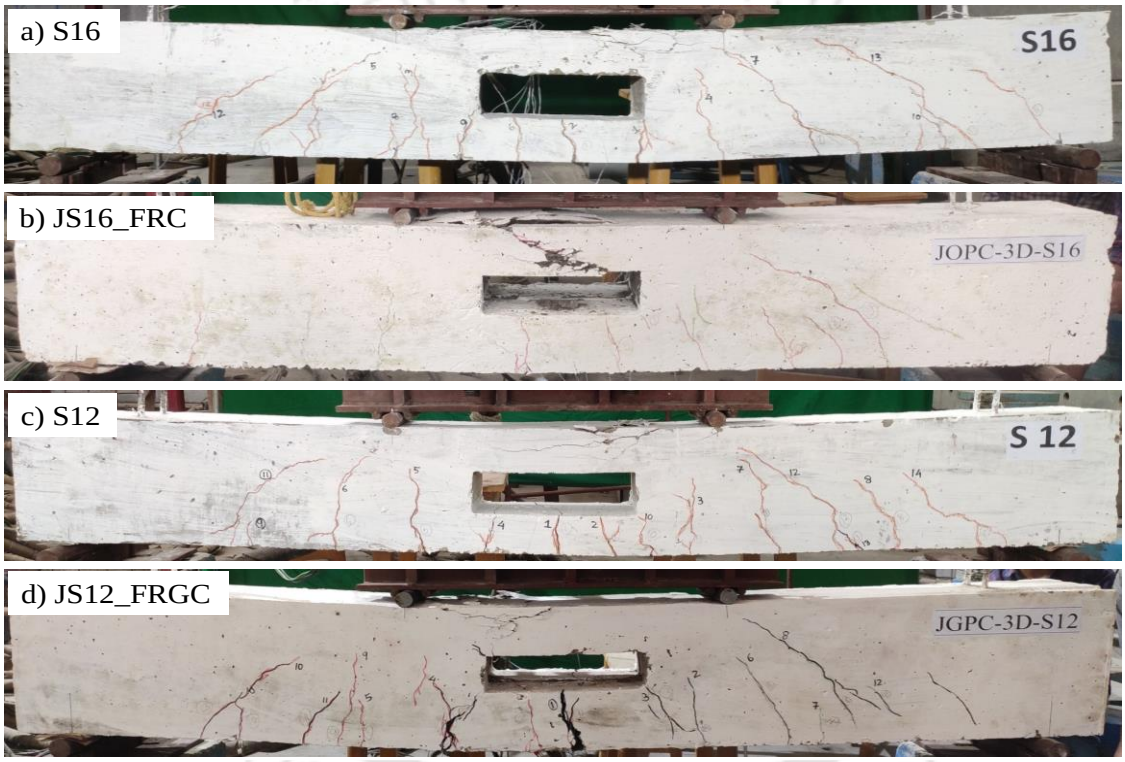

Figure 6.12: Crack patters of tested beam with opening in flexure (3rd Day)

But it can be noticed from Fig. 6.12. (b) that the cracks in JS16_FRC are much finer in comparison to those in JS12_FRGC as shown in Fig. 6.9. (d). This is due to the fact that the specimen JS16_FRC failed at a lower load due to the early crushing of the top chord. Early crushing of the top chord took place owing to lower compressive strength development of the repairing mortar (PCM) and the jacketing agent (FRCC) on the 3rd day, which was used to fill the damaged area in the top chord. This can be further understood from the early strength properties (3rd day) of PCM under subsection 3.3.2 of Chapter 3 and the early strength properties of FRCC under subsection 4.3.2.2 in Chapter 4.

Fig. 6.13. shows the load-deformation curve of the jacketed specimen and the controlled beam. It is observed that the jacketed specimen JS16_FRC exhibits a loss in elastic stiffness. This can be attributed to poor bonding between the FRCC layer and the beam, i.e. PCC to PCC layer, as established in subsection 4.3.1.4 of Chapter 4. The peak load attained by the beam (JS16_FRC) is 133.26 kN, which is only 80 % of the load attained by the original beam. The beam jacketed with FRCC could not attain the original load carrying capacity, thereby exhibiting a premature failure. As a result of this, the beam JS16_FRC showed a lower deformation capacity, as shown by the load-deformation curve in Fig. 6.13. Due to this low deformation capacity, the DR of the beam (JS16_FRC) reduced to 1.35, which is significantly lower than the DR (2.33) of the controlled specimen S16, as shown in Table 6.8.

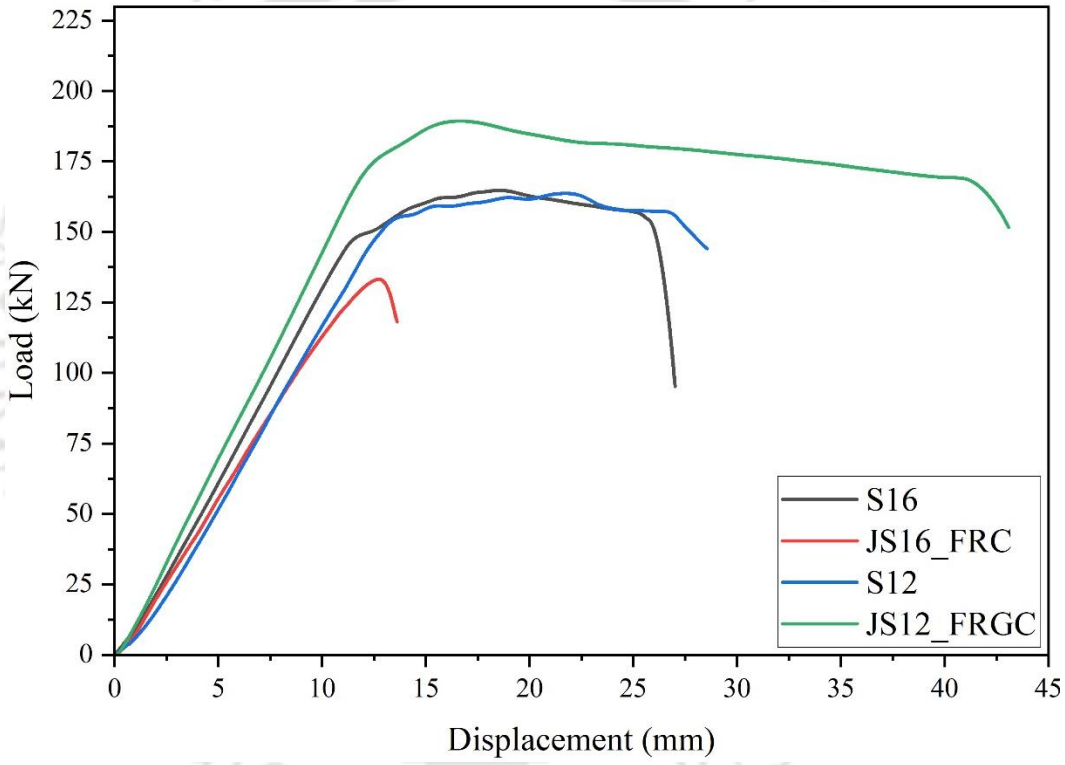

Figure 6.13: Load deflection curve of controlled and Jacketed beam with mid-span opening (3rd Day)

On the other hand, in the case of JS12_FRGC, repaired and strengthened by GM and FRGC. The beam is able to withstand a higher load and enhanced deformation capacity, as seen in Fig. 6.13. The better performance of JS12_FRGC is attributed to the better mechanical properties of the GM and FRGC, even on the 3rd day, as established in subsection 3.3.1 of Chapter 3 and subsections 4.3.1 and 4.3.2 of Chapter 4. The GM, which is used in filling the damaged portion of the top chord, and also the outer confinement provided by the FRGC jacketing layer

contributed to resisting higher compressive stress in the top chord, resulting in better performance than the controlled beam. Moreover, as the section of the jacketed beam has been enlarged, this leads to a higher moment of inertia of the specimen. The increased moment of inertia of the section contributed to the stiffness of the jacketed beam in comparison to that of the controlled specimen, shown in Fig. 6.13. The enhanced stiffness is also attributed to the cracks arresting features of the FRGC jacketing layer and the better composite action between the FRGC layer and the beam. This statement is supported by the excellent bond strength between the GPC and the PCC substrate, as established in subsection 4.3.1.4 of Chapter 4.

The maximum load attained by the beam JS12_FRGC is 15 % higher than that of the controlled beam S12. This leads to a higher strength enhancement ratio (SER) equal to 1.16. While the SER obtained for JS16_FRC jacketed by FRCC was only 0.81, as presented in Table 6.8. Further from Fig. 6.13, it can be seen that the load-deformation curve of the beam Jacketed by FRGC exhibits a large softening part after the peak load. As a result of which, the DR of the beam JS12_FRGC significantly improved to 3.89, which is approximately 70 % higher than the DR (2.28) of the controlled beam, S12. This improvement in ductility or the softening in the load-deformation curve can be attributed to better fiber matrix interaction mechanics at an early age on the 3rd day. The presence of hooked end steel fiber, resisted the rupture of the jacketing layer, thereby improving the ductility of the beam and finally failed at a displacement of 43.08 mm.

28th Day Testing

The crack pattern of the jacketed beam tested on the 28th day can be seen in Fig. 6.14. The 1st crack in the jacketed beams JS14_FRC and JS9_FRGC appears at a load of 42.17 kN and 49.54 kN, which is much higher than the 1st cracks of the controlled beam as presented in Table 6.8 and those tested on the 3rd day. The delay in the cracking of concrete is attributed to the better flexural properties of both FRCC and FRGC on the 28th day. With an increase in loading, more cracks appear and tend to widen but are significantly resisted by the crack bridging phenomena of the hooked end steel fiber. The sectional enlargement in the jacketed beam and crack bridging property of the FRCC and FRCG yields much better stiffness on the 28th day repaired beam as compared to the controlled specimen and the 3rd day jacketed specimen. However, the enhancement in the stiffness is much better in the beam JS9_FRGC jacketed by FRGC, which is due to the better bonding characteristics of geopolymer and better fiber matrix interaction of the FRGC material. As the load tends to reach its peak in the beam, the crack in the mid-span

significantly widens, as shown in Fig. 6.14. (b) and (d). On close observation, it was seen that such widening of these cracks is also accompanied by gradual pull out of the steel fiber, which leads to improvement in the deflection of the beam until the rupture of the jacketing layer.

The final failure of both the jacketed specimen is governed by rupture of the jacketing layer followed by crushing of the top chord. However, in the beam (JS14_FRC), local debonding of the jacketing layer at the top chord is also seen at the ultimate stage of loading. But in the case of JS9_FRGC, jacketed by FRGC, both the jacketing layer and the controlled beam act monolithically up to its ultimate loading. This behaviour can be attributed to the better bond strength of the PCC and the GPC. Whereas, inferior bond strength and mechanical properties of FRCC lead to lower load carrying capacity of the jacketed beam JS14_FRC.

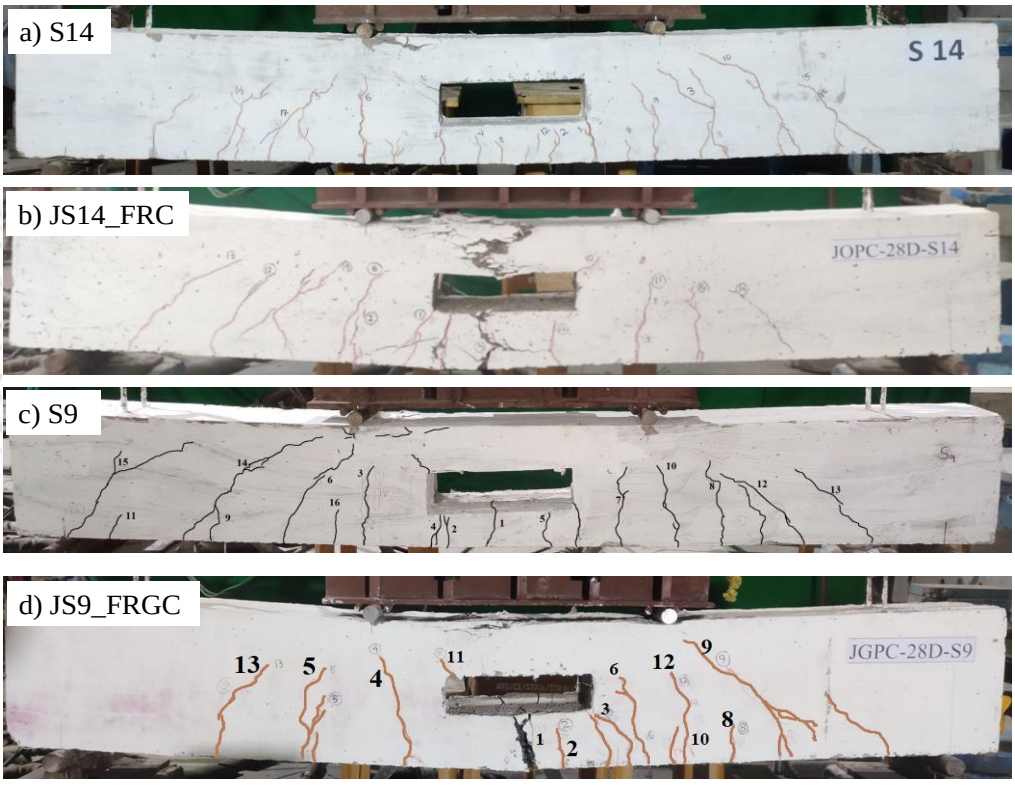

Figure 6.14: Crack patters of tested beam with opening in flexure (28th Days)

Fig. 6.15. shows the load-deflection curve of the jacketed and controlled beams. The maximum load withstands by JS14_FRC is 17 % higher than the load achieved by the controlled beam. This leads to a strength enhancement ratio (SER) of 1.17. While the maximum load withstands by JS9_FRGC is 32 % higher than the controlled beam, which implies an SER of 1.32. The higher load carrying capacity and/or SER of the JS9_FRGC is attributed to the better mechanical properties of the FRGC material. The beam JS14_FRC exhibits a ductility ratio

(DR) of 2.81, which is slightly higher (1 %) than that of the controlled beam. While DR exhibited by the beam JS9_FRGC is 3.68, which is 50 % higher than that of CB.

From the load-deflection curve in Fig. 6.15., it is also observed that both the jacketed beam exhibits a deflection hardening behaviour in the load-deformation curve on the 28th day. This phenomenon was also reported by Shaikh (2013) during his investigation of FA-based fiber reinforced concrete. This can be attributed to the fact then when the jacketed beam cracks, the bridging effect of the hooked end steel fiber comes into action, and partial load is transferred from the matrix to the steel fiber. Subsequently, the load is shared by the fiber and the interface, which leads to an increase in the load (Liu et al., 2020). However, better performance in the load-deformation is exhibited by the beam JS9_FRGC, which implies a better fiber matrix interaction in FRGC as compared to the FRCC on the 28th day. As a result of which, the beam JS9_FRGC showed better performance than JS14_FRC.

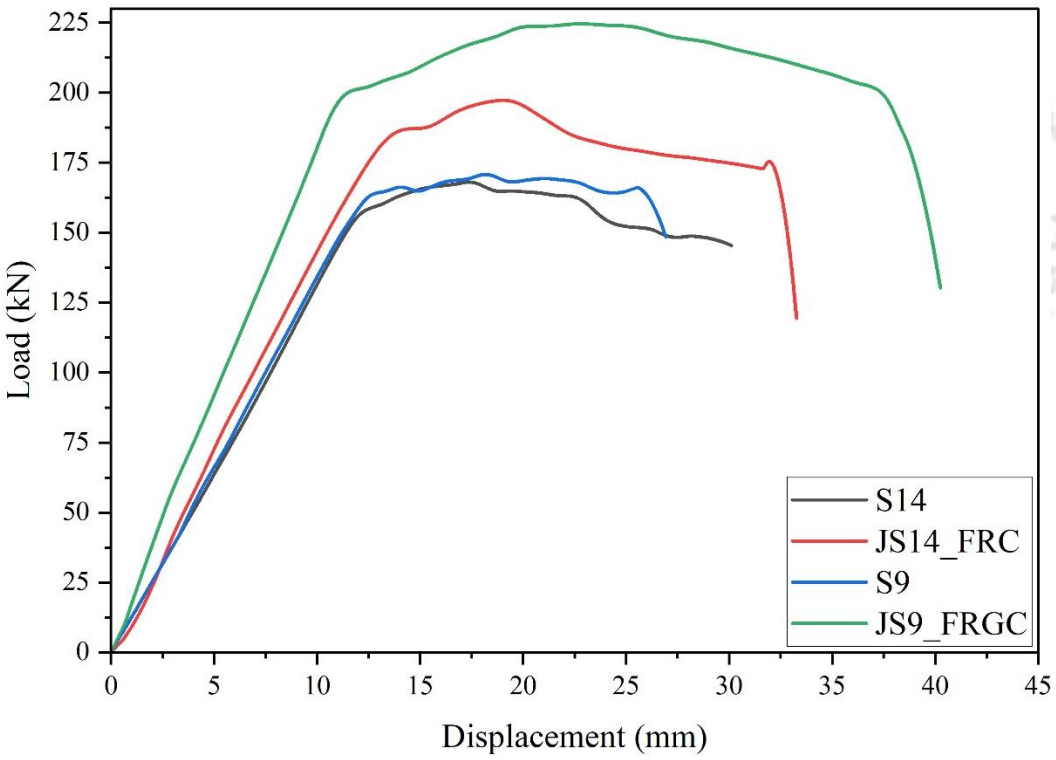

Figure 6.15: Load deflection curve of controlled and Jacketed beam with mid-span opening (28th Day)

6.3.2.2. Behaviour of Jacketed beam with web opening in the Shear Zone

The crack pattern of the controlled beams and the jacketed beam tested on the 3rd day and 28th day are marked during the loading and the corresponding load for each individual cracks are

also recorded during the test. The results obtained from static flexural load test on the jacketed RC beams with opening in the shear zone are presented in Table. 6.9.

3rd Day Testing

Fig. 6.16. shows the final crack pattern of the tested controlled beams and the jacketed beam with the shear opening. The presence of an opening in the shear span makes the beam weak in shear and fails at a much lower load than that of the beam with an opening in the flexure zone. The beam JS15_FRC jacketed by FRCC exhibits the 1st shear crack at a loading of 34.44 kN, which is approximately 80 % higher than the controlled specimen S15. Whereas the beam JS13_FRGC, exhibits the 1st crack in the shear zone at load 38.84 kN, which is 92 % higher than the 1st crack load in controlled specimen S13. This improved trend is the 1st crack load is also found in the previous specimens with a flexural opening, as shown in Table 6.9.

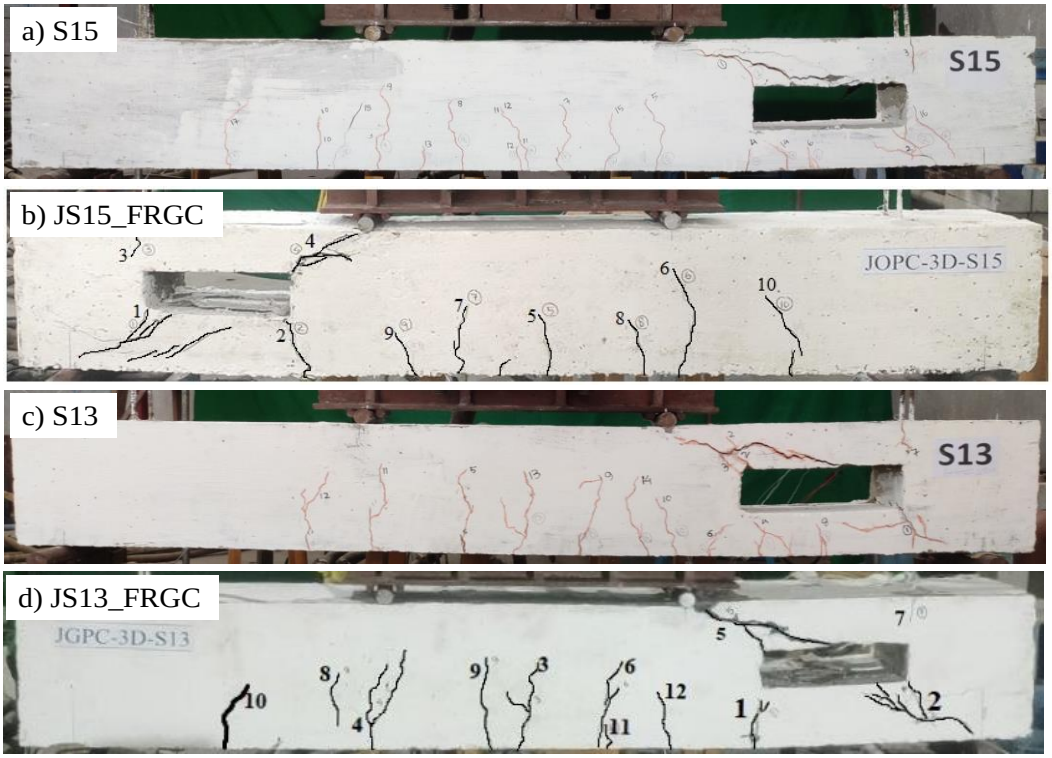

Figure 6.16: Crack patters of tested beam with shear-span opening (3rd Days)

As the load increases in JS15_FRC, the most critical crack, crack no 4, starts widening, and several branch cracks also appear, as shown in Fig. 6.16. (b). A similar trend is also noticed in the case of JS13_FRGC but at a higher loading level. As soon as the load tend to reach its peak, the shear cracks in the top chord start distributing with more branches of cracks, which start widening with simultaneous deformation in the beam. On close observation, it can be observed

that the distribution of the cracks and their widening is seen comparatively finer in the jacketed beam. While testing the controlled specimen, it was observed that an inclined crack initiates from the loading point, which propagates diagonally through the top chord. This crack was the most critical, which was responsible for the splitting of the top chord causing a brittle failure of the specimens. Similar cracks are also observed in the case of the jacketed beam that can be identified from Fig. 6.16 (b) and (d), denoted by cracks no 4 and 5, which propagated from the loading point. Nevertheless, these cracks do not proceed diagonally across the top chord but rather proceed towards the corner of the opening. This can be attributed to the FRCC and FRGC jacketing layer, which prevents the shearing of the top chord. Due to this resistance, the aforementioned cracks propagate towards the corner of the opening, thereby indicating a change in the load path due to the presence of jacketing layer. As the load reaches its peak, the aforementioned crack widens, followed by shear failure of the beam. However, the effect is slower due to the presence of hooked end steel fiber, which provides a better interlocking in the concrete matrix during pulling out in the shear crack, leading to a gradual failure.

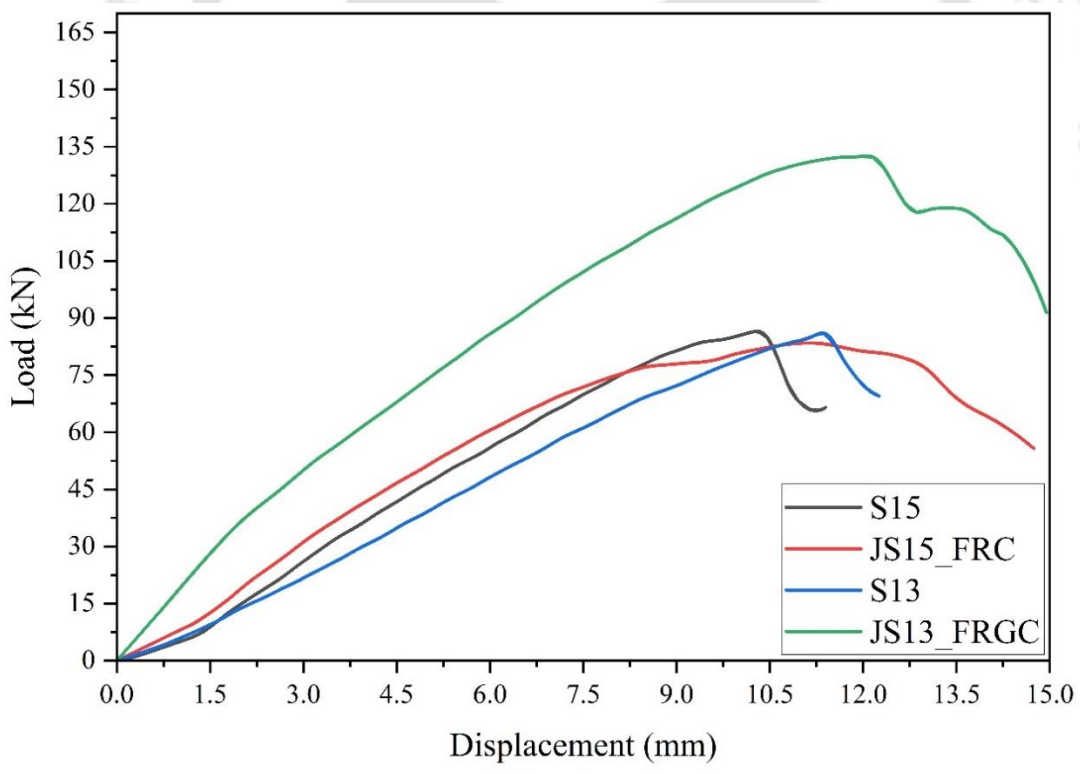

Figure 6.17: Load deflection curve of controlled and Jacketed beam with shear span opening (3rd Day)

The load-deformation curve of the tested beam on the 3rd day is presented in Fig. 6.17. Unlike the jacketed beam with an opening in the flexural zone, the failure of the jacketed beam with

an opening in the shear is relatively sudden. The beam JS15_FRC sustained a maximum load of 83.46 kN on the 3rd day, which is only 96 % of the peak load attained by the controlled beam, S15. On the other hand, the maximum load sustained by JS13_FRGC is 132.60 kN, which is 54 % higher than that of the controlled beam. The test result shows that jacketing scheme with FRCC and FRGC exhibits better strengthening in the damaged beams with the opening in shear, which is also understood by the SER value given in Table 6.9. This can be attributed to the fact that beams with a shear opening (BSS) are significantly weaker than those with a flexural opening (BMS) due to their reduced sectional area in the shear zone. However, as the beams are jacketed, it increases the sectional area, thus providing more concrete area to participate in bearing higher shear forces than the controlled specimen. This results in increasing the shear capacity of the BSS beam in comparison to BMS jacketed by FRCC and FRGC. However, better performance is observed by the beam JS13_FRGC jacketed by FRGC material.

Table 6.9: Test result of controlled and Jacketed beam with shear opening

Specimen	Test Day	Jacketing Agent	Yield Load (kN)	Deflection at Yield load (mm)	Peak load (kN)	MCC (kN.m)	Deflection at ultimate load (mm)	Load at 1st Crack (kN)	DR	SER
S15	56	_	73.65	7.38	86.53	25.96	10.77	19.11	1.46	_
S13	56	_	73.33	9.07	86.05	25.82	12.01	20.2	1.32	_
JS15_FRC	3	FRCC	66.67	6.98	83.46	25.04	13.01	34.44	1.86	0.96
JS13_FRGC	3	FRGC	100.65	7.24	132.6	39.78	14.32	38.84	1.98	1.54
S11	56	_	66.67	6.88	82.94	24.88	9.16	16.58	1.33	_
S10	56	_	74.66	7.16	88.42	26.53	9.43	18.09	1.32	_
JS11_FRC	28	FRCC	106.66	7.04	134.096	40.23	12.22	44.16	1.74	1.62
JS10_FRGC	28	FRGC	117.98	7.17	154.65	46.40	13.81	47.68	1.93	1.75

The application of FRCC and FRGC in the damaged beam also leads to a significant improvement in the ductility of the beam, as seen in Table 6.9. The beam JS13_FRGC, jacketed by FRGC, exhibits better improvement in the DR equal to 1.98, which is approximately 50 % higher than the controlled specimen. In comparison, the specimen JS15_FRC, jacketed by FRCC, exhibits an improvement in the DR by 27 %. This also reflects the better fiber matrix interaction in the FRGC than in the FRCC material, which is responsible for the better ductility of the beam. The load-deformation curve of the tested beams shows a smooth softening after the peak load. But above all, as the FRGC composite develops a better compressive strength even at an early age, this contributed to better SER (1.54) in the beam JS13_FRGC, as seen in Table 6.9.

28th Day Testing

The final crack pattern of the controlled beams and the Jacketed beam tested on the 28th day is shown in Fig. 6.18. The crack patterns of the jacketed beams are nearly identical to the cracks of the beam tested on the 3rd day. The beam JS11_FRC exhibits the 1st shear crack at a loading of 44.16 kN, whereas the 1st shear crack that appeared in the controlled beam, S11 is 16.58 kN. On the other hand, the 1st crack in the beam JS10_FRGC appeared at a loading of 47.68 kN, which is 62 % higher than the 1st crack load (18.09 kN) that appeared in the controlled specimen S10.

From Fig. 6.18. (a)-(d), it can be noticed that although the load sustained by both the jacketed beam are substantially high, the number of cracks in the jacketed beams are comparatively lesser. A similar trend has also been noticed in the jacketed beam with an opening in the flexural zone. Apparently, this is attributed to the high aspect ratio of the steel fiber used in the jacketing material. It can be observed that at the same stage of loading, the widening of the shear crack is relatively higher in the case of FRCC jacketed beam than those in FRGC jacketed beam. This is due to the better fiber matrix interaction of geopolymer and the steel fiber, leading to better resistance in crack widening.

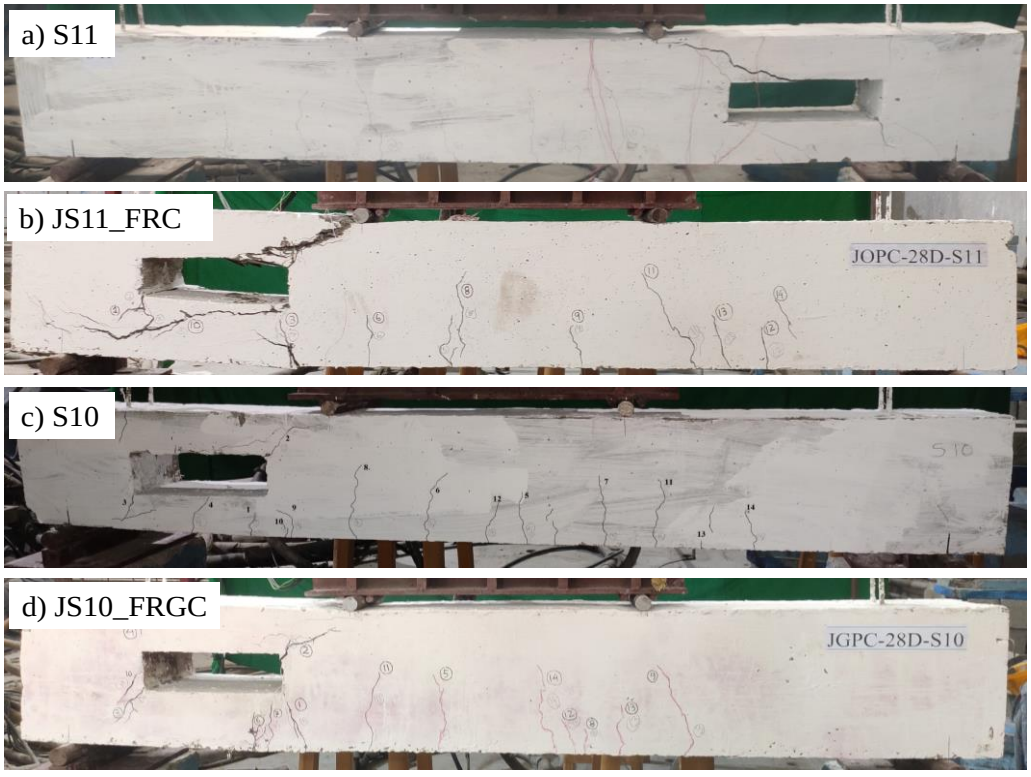

Figure 6.18: Crack patters of tested beam with shear-span opening (28th Day)

Fig. 6.19. shows the load-deflection curve of the controlled specimen and the jacketed specimen tested on the 28th day. It can be observed that both beam, jacketed by FRCC and FRGC, exhibits much better stiffness than those of the controlled beam. The higher stiffness can be attributed due to the enlarged section after jacketing. This behaviour is also noticed in the beam JS13_FRGC tested on the 3rd day. The test result shows that beam JS11_FRC withstands a load of 134.09 kN, which is approximately 62 % higher than the peak load achieved by the controlled specimen S11. On the other hand, the jacketed beam JS10_FRGC exhibits a peak load of 154.65 kN, which is 75 % higher than the peak load attained by the controlled specimen S10. This enhanced load carrying capacity of the beam JS10_FRGC is due to better mechanical properties of FRGC than that of FRCC on the 28th day. This also causes a better SER of the jacketed beam on the 28th day, as observed in Table 6.9. Furthermore, both the jacketed beam exhibited enhanced ductility on the 28th day, but better ductility was shown by the beam, JS10_FRGC, which exhibits a DR of 1.93. Whereas the DR exhibited by JS11_FRC was 1.74.

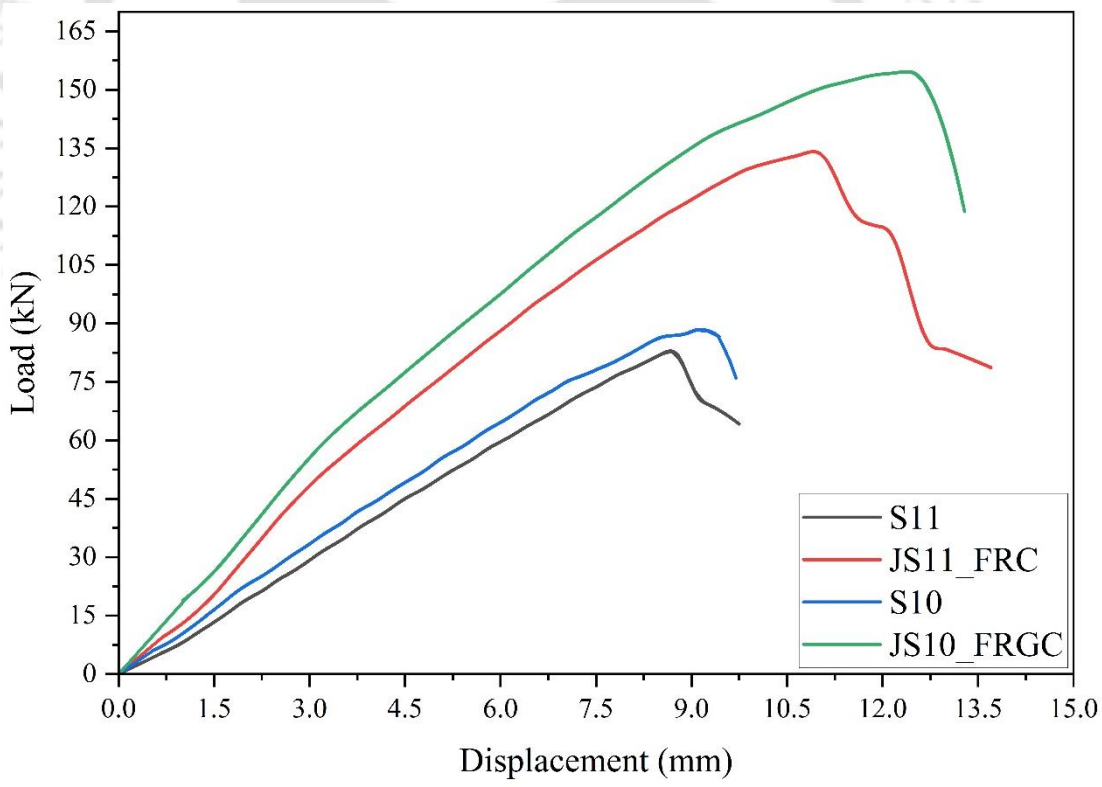

Figure 6.19. Load deflection curve of controlled and Jacketed beam with shear span opening (3rd Day)

From the above discussion it can be understood that the three side jacketing with FRGC can be used for effective restoration of damaged beam with web opening in flexure. The early strength

properties of FRGC leads to a full rehabilitation of the damaged beam even at the 3rd day. The increased section enhances the rigidity of the beam and found most effective in the case of beam with shear opening. The noble method of strengthening the damaged web opened beam not only improves the load bearing capacity of the beam but also improves the other structural integrity along with enhanced deformation capacity and prevents the beam from brittle failure.

6.4. Closure

A detailed study to understand the behaviour of damaged web opened beam repaired and strengthened with Fiber reinforced geopolymer concrete (FRGC) has been carried out in this chapter by performing a static flexural test in the laboratory. Total eight numbers of full-scale controlled beams with openings are cast for this purpose. Out of the eight beams, four beams are prepared with an opening in flexure, and four beams are prepared with an opening in the shear zone. These beams are tested using an MTS actuator by applying static monotonic load up to failure and are considered fully damaged beams. The damaged beams are initially repaired with repairing mortar (GM) and are jacketed on the three sides with FRGC concrete. A controlled mix, fiber reinforced cement concrete (FRCC) prepared with conventional cement (OPC 43 grade), is also prepared for the comparison of the jacketing with FRGC. The jacketed beam with then tested on the 3rd day and 28th day of curing.

The results of the study reveal that FRGC can be used effectively as a strengthening agent. Early strength achievement is the most important advantage of UBFS-based FRGC and hence can successfully be used for the restoration and strengthening of web opened beam. The application of FRGC significantly improves the load bearing capacity and the deformation capacity of both types of beam. The application of hooked end steel fiber restricts the crack widening, which ultimately improves the stiffness and ductility of the beam. The strengthening of beam with a web opening in the flexure exhibits even better performance than the solid beam (with no opening). Hence, it is recommended that repairing and strengthening the RC structural member at an early period with FRGC jacketing is an effective way of restoring the structure to its functional use at the earliest period possible. The findings of the present study may be useful for seismic retrofitting after an earthquake causes damage to RC members of different types.

Chapter 7

Summary and Conclusions

7.1 Introduction

In the present study, ultrafine ground granulated blast furnace slag (UBFS) based geopolymer mortar (GM), Geopolymer concrete (GPC) and Fiber reinforced geopolymer concrete (FRGC) are developed with the aim of investigating the efficiency of geopolymeric material in repairing and strengthening of damaged reinforced concrete (RC) structures. Thus RC beam with web opening has been selected for the investigation. The repairing of damaged web opening beam is conducted by a noble technique using GM and welded wire mesh, whereas for strengthening, three sides FRGC Jacketing has been adopted.

The study was directed toward two major directions firstly, the development of Geopolymeric material, which includes development of GM and FRGC and, thereafter, their application in retrofitting and strengthening of RC structures. To develop the GM, 28 numbers of UBFS-based GM mixes were developed, and detailed tests were carried out to evaluate the fresh and hardened state properties. Admixtures such as Fly ash (FA) and retarder (Borate) were added to the mixes, and their influence on setting time, workability and strength gain was assessed. Two different types of alkali activator are used in the preparation of GM, which includes sodium hydroxide solution (SH) and a combined mixture of SH and sodium silicate solution (SS). A controlled mortar mix is also prepared using Portland cement (PC), and similar tests as in the case of GM were conducted for comparison purposes.

In order to develop FRGC mix, GPC mix is initially prepared and investigated. A total 15 number of GPC mixes are prepared, and their fresh and hardened properties are evaluated. These mixes are activated only with SH solution. A mineral admixture, i.e. Fly ash, and a

superplasticizer (SP) are also used to enhance the workability of the GPC mixes. For comparison, controlled mix (PCC mixes) were also prepared using Portland cement. The GPC mixes that have been prepared are tested to evaluate the workability, compressive strength, split tensile strength and bond strength, and the results are compared with that of the PCC mixes. Based on the fresh and hardened properties, suitable mix proportions of GPC are selected and further modified by incorporating various volume fractions (V_f) of steel fiber to prepare the FRGC mixes. A total 10 number of FRGC mixes are studied along with a controlled mix FRCC, which is prepared by modifying the PCC mix with the addition of steel fiber. Hooked-end steel fiber of size 50 mm and diameter 0.75 mm is adopted for preparing the FRGC and FRCC composites. The properties of the FRGC and FRCC are evaluated by conducting several laboratory experiments such as slump test, vee-bee consistometer test, compressive strength test and flexural strength test.

Based on the test results of GM, a suitable mix was selected for the repairing of RC beams. Total 8 numbers of RC beams with web opening in the flexure zone and shear zone are studied, including one solid beam specimen for comparison. The section of beam specimens was 180 mm × 270 mm, with a clear span of 2 m. These specimens were subjected to damage by pre-loading the beams with static flexural four-point load. The damaged beams were repaired by filling the cracks with GM and PCM, while the opening area is additionally strengthened by wrapping of welded wire mesh and the repairing material similar to ferrocement laminates. The repaired beams are then retested by applying flexural four-point loading to observe the behaviour of the repaired beams due to static loading at different ages of curing.

For strengthening the damaged web opened beams, three-side fiber reinforced jacketing of 40 mm thickness is adopted. FRGC mix is used as jacketing agent, which is selected based on the results obtained from the workability and the strength test. Total 8 number of beam specimens are prepared. These beam specimens are divided in to two groups based on their location of opening. The beams are initially tested under static flexural load under four-point bending scheme. The damaged beams are then initially repaired using GM and PCM. The repaired beams are then jacketed with FRGC and FRCC mix. The beams were jacketed on the three sides, leaving the top face. The jacketed beams are then cured and then tested again under static flexural loading at different ages.

7.2 Major conclusions

The significant observations from the present study are outlined below under the following heads:

7.2.1 Properties of GM, GPC and FRGC

- G M containing a high volume of UBFS (70%), partially replaced by FA (30%), results in better production of geopolymeric gel (C-A-S-H gel), which greatly increases the strength characteristics of the mortar. The high fineness of the UBFS and its high calcium content contributed in rapid gain in strength of GM but substantially lowers the setting time and flowability of the GM mix.
- The addition of SS with the SH solution, used for the activation of geopolymeric precursor, increases the availability of silicate ions in the SHSS solution to participate in geopolymerization reaction, resulting in higher compressive and flexural strength than those activated by only SH solution.
- But at higher mass ratio of SHSS solution (SS/SH beyond 2), leads to an excess of silicate content during geopolymerization, which affects the structure of the geopolymeric products, resulting in a reduction in strength. The mass ratio within a range of 1.5 to 2 exhibits significant properties of GM.
- The compressive strength of UBFS based GM is directly dependent on the molar concentration of SH. A high molar concentration, up to 12 M, yields better compressive strength; however, molarity above 10 M has no significant effect on the flexural strength of GM.
- GM activated by low molar concentration of SHSS solution exhibits significant strength at an a/b ratio of 0.6. However, at a higher molar concentration, beyond 10 M, a higher a/b ratio of 0.65 improves homogeneity, resulting in a denser matrix exhibiting high compressive strength.
- The effect of SH and SHSS solution in the development of flexural strength of GM is nearly similar to that observed in the compressive strength. The flexural strength of GM linearly increases with compressive strength and possess a good correlation for a mass ratio of 1.5.
- The addition of borate dosage in the SHSS predominantly prolonged the setting property of geopolymer and improved the flowability of the mortar mixes by transforming the conventional O-Al-O-Si bond in geopolymer to B-O-Al-O-Si bond.

- Borate addition results in a more densely packed microstructure, which improves both compressive and flexural strength. A borate dosage of 2 % exhibits the maximum compressive strength (50.93 MPa).
- The flow characteristics of the UBFS based GPC with a high volume of UBFS are greatly enhanced by the constant dosage of naphthalene based SP. However, the slump value of GPC is significantly affected by the volume of sand. It is noted that slump values reduce by 6 % to 7 % for every 25 % increment in the volume of the sand. However, a considerable fluidity in each group of mixes (with different *s/a* ratio) can be retained up to an increase in the molar concentration of 8M.
- The variation in the *s/a* ratio significantly influences the thickness of the paste in GPC mix, which is directly related to the workability and the mechanical properties of the hardened concrete. The role of sand volume (or the s/a ratio) is found significant in controlling the bleeding and segregation of GPC mixes. An optimum value of *s/a* ratio (0.41) leads to a homogeneous distribution of aggregate thereby contributes to better packing leading to superior mechanical strength.
- The GPC mixes exhibited early compressive strength of 72 % and 83 % on the 3^{rd} day and 7^{th} day of the characteristic compressive strength achieved on 28^{th} day. A further improvement in strength within a range of 6 % - 7 % is also exhibited at the later age (56^{th} day).
- As high volume of UFBS is used in the GPC mix, it results into a very rapid hardening of the concrete. However, it is also observed that at a high molarity such mixes undergo fast geopolymerization, which gets precipitate at an early stage of reaction leading to poor microstructure and strength. Therefore, better strength properties have been achieved at a relatively lower molarity of 6M to 8M.
- All GPC mixes exhibit a superior bond with the PCC substrate both at an early stage of curing (3^{rd} day) and also at the 28^{th} day. The bond strength between the GPC and the old PCC concrete is significantly stronger than that between PCC to old PCC substrate.
- The tensile strength achieved by the GPC mixes is approximately 6.5 % of the compressive strength of GPC.
- The inclusion of hooked end steel fiber substantially effects the workability of the FRGC composites. But at the same time there is a significant improvement in the compressive strength and the flexural strength of the FRGC along with their post cracking behaviour.

- The improvement in the mechanical properties due to steel fiber is more significant in the flexural properties. Addition of 1.3 % V_f of steel fiber is found to be the optimum quantity, which leads to better mechanical properties in the FRGC mix.

7.2.2 Repairing of Web opened RC beam using GM

- The presence of an opening in mid-span causes no significant loss in the load carrying capacity unless the opening reduces the concrete above the neutral axis. However, such a beam exhibits early and wider cracks, which reduces the stiffness of the beam. Such beams also exhibit low deformation capacity at the post-peak subjected to high compressive stresses at the top chord, which leads to an early crushing of the top chord.
- The presence of an opening in the shear zone interrupts the load transfer path, which leads to a high accumulation of stresses around the corner of the opening. This leads to the early occurrence of diagonal cracks, which results in a drastic reduction in the stiffness of the beam. As opening in shear, span reduced the concrete area responsible for resisting the shear force hence such specimen (i.e. BSS type) leads to a reduction in the shear capacity of the beam by 54 % and also exhibited a sudden shear failure.
- Beams repaired by GM and the welded wire mesh exhibited a superior cracking behaviour in the form of a higher number of distributed cracks in the strengthened zone, which are finer than those in the controlled beam. This is attributed to the effectiveness of wire mesh in the repaired beam, which prevented the crack widening.
- Due to the early strength de,elopment and better bonding characteristics of GM, the repaired beam with GM exhibited a better adherence with the beam specimen, causing no debonding or spalling of the repair material, which was common in the beam repaired by PCM.
- The wrapping of wire mesh and the effective bonding between the GM and the wire mesh provides a better confinement to the strengthened area, which contributes to resisting the high compressive stresses developed in the top chord, resulting in enhanced load bearing capacity and post-peak deformation.
- The noble repairing techniques using GM and welded wire-mesh not only restore the structural integrity of the fully damaged beams but also enhances the strength even on the 3rd day of repairing. In contrast, the specimen repaired by PCM exhibits a premature failure, subjected to poor strength properties of PCM on the 3rd day.

- On the 28th day, both types of specimens, either repaired by GM or PCM, exhibited full restoration of strength. However, better performance is achieved by the beam of BMS types repair by GM, which exhibits significant strength enhancement and stiffness along with substantial improvement in the ductility of the repaired beam.

- However, in the case of BSS Type, although the repaired beams exhibit higher strength enhancement but no significant improvement in the ductility of beam could be achieved. On the 28th day, the BMS type specimen (i.e. R2_GM) repaired by GM attains a load carrying capacity of 18 % higher than the original beam, while that of BSS type (i.e. R4_GM) attains a 41 % higher load than the controlled specimen.

7.2.3 Jacketing of Web opened RC beam using FRGC

- The application of three-side FRGC jacketing significantly increased the cracking load, delayed crack propagation and the spread of cracks as compared to those jacketed by FRCC material and the original specimen. This can be attributed to the better crack-bridging action in the FRGC layer and the monolithic action between the FRGC jacket and the controlled beam.
- The effectiveness of hooked end steel fiber and the increase in the sectional area of the jacketed beam with FRCC and FRGC, leads to a significant improvement in the stiffness in both types of beams (BMS and BSS) as compared to the respective controlled beam specimen.
- Due to their superior early age strength properties of FRGC, the strengthening scheme with FRGC jacketing is successful in the rehabilitation of the damaged web opened beams both on the 3rd day and the 28th day. In contrast, the FRCC needs 28th day curing time for full restoration of the damaged beam, and hence such beam exhibits premature failure when tested on the 3rd day.
- On 28th day, the beam BMS jacketed with FRGC exhibited an enhanced load carrying capacity of 1.32 times higher than the controlled specimen. At the same time, the BSS-type beam jacketed by FRGC attained a load of 1.75 times higher than the controlled specimen. It can be established that enhancement in the structural integrity was significantly higher in the jacketed beam, especially with a shear opening. This is because of the enlarged section sectional, which contributed to enhance the shear capacity of the BSS.

- The jacketed beams also exhibit a deflection hardening behaviour and enhanced deformation capacity with improvement in the ductility of the beam. However, better performance and enhanced ductility were exhibited by the beam jacketed by FRGC.

7.3 Significant contribution

Firstly, the high volume of calcium rich binder (UBFS) used in the development of GM leads to early geopolymeric products and the strength. However, such mixes when activated by SHSS solution leads to a rapid setting due to the presence of calcium hydroxide. To control this setting property optimum proportion of a Type II retarder (as per ASTM) Borate has been introduced and studied based on their fresh and hardened property and the microstructural changes. Secondly, the technique of repairing using wire mesh and GM and the strengthening of the damaged beam using FRGC Jackets is a noble retrofitting method which enables a full restoration of the beam with a strength enhancement ratio of 1.03 with an improved DR ratio of 2.99, even on the 3rd day of testing."

7.4 Scope of Future work

From the present study, following future research works are recommended:

1. The repairing material can be prepared using other by-products such as rice husk, metakaolin, etc.
2. The welded wire mesh of different mesh size with change in orientation can be explored in retrofitting.
3. The Jacketing material can be prepared by utilisation of hybrid fiber and the durability aspect of the jacketed specimens can be studied.
4. The application of the repairing technique and the jacketing material can also be investigated in other structural members like beam column joints, column, pier etc.
5. The behaviour of the retrofitted specimen can also be explore under cyclic loading condition.

7.5 Closure

The investigation carried out in the thesis has been summarized and conclusions are listed in different sub section. The conclusions have been drawn from the result and discussions presented in the preceding chapters. The present method of repairing and strengthening of damaged web open beam with geopolymeric successfully restores the structural integrity of the damaged beam. The possible extension of the research work that can be carried out in the future is also listed in this chapter.

Appendix A

Mix Design for Portland Cement Concrete mix

The mix design of the Portland Cement Concrete (PCC) mixes is calculated as per IS 10262 2009. A total two number of controlled mixes were prepared for the purpose of conducting laboratory tests in this study. The Mix CM1 was designed with a target strength of 20 N/mm^2, and mix CM2 was designed adopting a water to cement (w/c) ratio equivalent to the water to solid (w/s) ratio of that of the geopolymer concrete mix (GPC). The minimum and maximum cement content and the w/c ratio for the controlled mix (CM1) was selected from Table 5 of IS 456 2000. Since the concrete in both cases was cast and tested in the laboratory, the standard deviation was taken as 0.

A.1 Mix CM1

Given,

1. Compressive strength of concrete: 20 N/mm^2
2. Maximum nominal size of aggregate: 20 mm
3. Minimum cement content: 320 kg/m^3 (Table 5, IS: 456-2000)
4. Maximum w/c ratio: 0.55 (Table 5, IS: 456-2000)
5. Workability: 100 mm (slump)
6. Grade of cement: OPC 43 grade
7. Specific gravity of -
    a. Cement (SG_C): 3.11
    b. Fine aggregate ($SG_{F.A}$): 2.60
    c. Coarse aggregate ($SG_{C.A}$): 2.66
8. Water absorption of -
    a. Fine Aggregate: 1.7 %
    b. Coarse aggregate: 0.7 %
9. Zone of Fine aggregate: Zone III

Target strength of for mix proportioning:

Target Strength of concrete at 28 days (f'_{ck}) = Compressive strength of concrete at 28 days (f_{ck}) + standard deviation (σ)

Here,

σ = 0 (Since, casting of concrete specimens were done in controlled condition in laboratory.)

Therefore, f'_{ck} = 20 + 0 = 20 N/mm^2

Selection of w/c ratio:

Maximum w/c ratio = 0.55 (Table 5, IS: 456-2000)

Adopted w/c ratio = 0.55

Calculation of water content:

Maximum water content for 20 mm size aggregate and for 25 - 50 mm slump range = 186 kg

(Table 2, IS: 10262-2009)

Therefore, estimated water content for 100 mm slump = $186 + 2 \times \frac{3}{100} \times 186 = 197.16$ kg

Mass of water (M_W) =197.16 kg

Calculation of cement content:

w/c = 0.55

Therefore, cement content/Mass of cement (M_C) $= \frac{\text{water}}{0.55}$ = 358.47 kg

Proportion of volume of Coarse Aggregate and Fine Aggregate:

Volume of CA corresponding to 20 mm size aggregate and FA (zone III)

for w/c of 0.50 = 0.64 (Table 3, IS: 10262-2009)

But since adopted w/c = 0.55

Therefore,

Adjustment in the volume of Coarse aggregate (V_{CA}) = 0.64 + (-1) × 0.01= 0.63

(Cl.- 4.4, IS 10262-2009)

Volume of Fine aggregate (V_{FA}) = 1 - 0.63 = 0.37

Mix calculation:

1. Volume of concrete, a = 1 m^3

2. Volume of cement, b = (M_C / SG_C) × (1/1000)

= 0.1152 m^3

3. Volume of water, c = (M_W / SG_W) × (1/1000)

$= 0.197\ m^3$

4. Volume of all in aggregate, d = a-(b+c) = $0.687\ m^3$

5. Mass of Coarse aggregate ($M_{C.A}$) = $d \times V_{CA} \times SG_{C.A} \times 1000$

$= 1152.62$ kg

6. Mass of Fine Aggregate ($M_{F.A}$) = $d \times V_{FA} \times SG_{F.A} \times 1000$

$= 661.67$ kg

Mix proportion for CM1:

1. Cement = 358 kg
2. Fine Aggregate = 661 kg
3. Coarse Aggregate = 1152 kg
4. Water = 197 kg
5. w/c = 0.55

A.2 Mix CM2

The mix is designed by considering a w/c ratio of 0.47 which is equivalent to the w/s ratio of the geopolymer concrete (GPC)

1. Maximum water/cement (w/c): 0.47
2. Nominal size of aggregate= 10 mm
3. Workability: 75 mm (slump)
4. Grade of cement: OPC 43 grade
5. Specific gravity of
    a. Cement (SG_C): 3.11
    b. Fine aggregate ($SG_{F.A}$): 2.60
    c. Coarse aggregate ($SG_{C.A}$): 2.66
6. Water absorption of
    c. Fine Aggregate: 1.7 %
    d. Coarse aggregate: 0.7 %
7. Zone of Fine aggregate: Zone III

Selection of w/c ratio:

Adopted w/c ratio = 0.47

(which is equivalent to w/s ratio of the mix MG9 and MG9_1.3 % used for the purpose of Jacketing)

Calculation of water content:

Maximum water content for 10 mm size aggregate and for 25 - 50 mm slump range = 208 kg

(Table 2, IS: 10262-2009)

Therefore, estimated water content for 75 mm slump = $208 + \frac{3}{100} \times 208 = 214.24 \simeq 214$ kg

Therefore Mass of water (M_W) = 214 kg

Calculation of cement content:

w/c = 0.47

Mass of cement (w/c = $\frac{214}{450}$) $= \frac{\text{water}}{0.47} = 455.83$ kg

But maximum cement quantity $\langle 450$ kg

Therefore Mass of cement (M_C) adopted = 450 kg

Check w/c = $\frac{214}{450} = 0.47$

Proportion of volume of Coarse Aggregate and Fine Aggregate:

Volume of CA corresponding to 10 mm size aggregate and FA (zone III)

for w/c of 0.50 = 0.48 (Table 3, IS: 10262-2009)

But since adopted w/c = 0.47

Therefore,

Adjustment in the volume of Coarse aggregate (V_{CA}) = 0.48+0.004 = 0.484

(Cl.- 4.4, IS 10262-2009)

Volume of Fine aggregate (V_{FA}) = 1 – 0.484 = 0.516

Mix calculation:

1. Volume of concrete, a = 1 m^3

2. Volume of cement, b = (M_C / SG_C) × (1/1000) = 0.145 m^3

3. Volume of water, c = (M_W / SG_W) × (1/1000) = 0.214 m^3

4. Volume of all in aggregate, d = a-(b+c) = 0.641 m^3

5. Mass of Coarse aggregate ($M_{C.A}$) = $d \times V_{CA} \times SG_{C.A} \times 1000$ = 825.24 kg

6. Mass of Fine Aggregate ($M_{F.A}$) = $d \times V_{FA} \times SG_{F.A} \times 1000$ = 859.67 kg

Mix proportion for CM2:

1. Cement = 450 kg
2. Fine Aggregate = 860 kg
3. Coarse Aggregate = 826 kg
4. Water = 214 kg
5. w/c = 0.47

Mix design of Geopolymer concrete

The mix design of the Geopolymer concrete (GPC) by taking the help of IS 10262 2009 and previous literature (Reddy et al. 2018). Several trial mixes are initially conducted to choose a suitable alkali to binder (a/b) required for the mix design. The mixes proportion are initially calculated by considering a molar concentration of 10M of the NaOH solution.

A.3 Mix MG1 (Trial mix)

Given,

1. Molar concentration of alkali: 10M
2. Binder: Ultrafine blast furnace slag (UBFS) and Fly Ash (FA)
3. Alkali to binder ratio (a/b): 0.67
4. Nominal size of aggregate: 50 mm
5. Workability: 100 mm (slump)
6. Specific gravity of
    a. UBFS (SG_S): 2.92
    b. FA (SG_F): 2.23
    c. Alkali activator (10M): 1.37
    d. Fine aggregate ($SG_{F.A}$): 2.60
    d. Coarse aggregate ($SG_{C.A}$): 2.66
8. Water absorption of
    e. Fine Aggregate: 1.7 %
    f. Coarse aggregate: 0.7 %

9. Zone of Fine aggregate: Zone III

Selection of w/s ratio:

Adopted a/b ratio = 0.67

Therefore, w/s ratio = 0.40

Calculation of Alkali content:

Maximum water content for 10 mm size aggregate and for 25 - 50 mm slump range = 208 kg

i.e. $M_W = 208$ kg (Table 2, IS: 10262-2009)

We know, 1.4 kg of 10M alkali content contains 1kg water and 0.4 kg solid (NaOH pallets)

And weight of alkali content = Weight of (NaOH pallets +Water)

Therefore, equivalent alkali content containing 208 kg of water = $1.4 \times 208 = 291.20$ kg

Mass of alkali content (M_a) = 291.20 kg

Mass of SH in 291.20 kg of Alkali solution (M_{SH}) = 83.20 kg

Calculation of Binder content:

Total binder = Mass of (FA +UBFS)

Now, a/b ratio = 0.67

Therefore Mass of total binder (M_{TB}) = $\frac{M_a}{0.67} = 434.63$ kg

Based on preliminary investigation, 70 % UBFS and 30% FA is considered.

Therefore,

Mass of FA (M_F) = $0.3 \times 434.63 = 130.38$ kg

Mass of UBFS (M_S) = $0.7 \times 434.63 = 304.24$ kg

Check w/s = $\frac{M_W}{M_F + M_s + M_{SH}} = 0.40$

Proportion of volume of Coarse Aggregate and Fine Aggregate:

The initial trials of mixes are conducted with a volume sand by total aggregate ratio (s/a) equivalent to 0.33. This is the initial trials are carried out with a volume of coarse aggregate corresponding to 20 mm size coarse aggregate and fine aggregate conforming to Zone III.

Therefore, Volume of coarse aggregate (V_{CA}) = 0.64 (Table 3, IS: 10262-2009)

But since, w/s = 0.4

Therefore, Adjustment in V_{CA} = 0.64 + 0.02 = 0.66

(Cl.- 4.4, IS 10262-2009)

Volume of Fine aggregate (V_{FA}) = 1 – 0.66 = 0.34

Mix calculation:

1. Volume of concrete, a = 1 m^3

2. Volume of FA, b = (M_F / SG_F) × (1/1000) = 0.058 m^3

3. Volume of UBFS , c = (M_s / SG_S) × (1/1000) = 0.104 m^3

4. Volume of Alkali solution, d = (M_a / SG_{SH}) × (1/1000) = 0.213 m^3

5. Volume of all in aggregate, e= a-(b+c+d) = 0.624 m^3

6. Mass of Coarse aggregate ($M_{C.A}$) = e× V_{CA} × $SG_{C.A}$ × 1000 = 1095.60 kg

6. Mass of Fine Aggregate ($M_{F.A}$) = e× V_{FA} × $SG_{F.A}$ ×1000 = 551.67 kg

Extra water:

7. Water = (1.7/100 × 551.67) + (0.7/100 ×1095.60) = 17.04 kg

Mix proportion for MG1:

1. Fly Ash = 130.39 kg
2. UBFS = 304.24 kg
3. Fine Aggregate = 551.67 kg
4. Coarse Aggregate = 1095.60 kg
5. Total alkali solution (10M) = 291.20 kg
6. Water = 17.04 kg

भारतीय प्रौद्योगिकी संस्थान गुवाहाटी
Indian Institute of Technology Guwahati

Appendix B

Design of Reinforced Concrete Beam

Controlled Beam Weak in Flexure

The beams were designed without considering material factor of safety of concrete and steel. All the beams were designed as doubly reinforced beams. The beams were designed targeting a total load carrying capacity of 145 kN from the actuator. The design of beam is as follows:

Let, it be assumed that 2-16 Ø bars to be provided at the bottom of the beam and 2-10 Ø at the top of the beam and 2-legged 8 Ø bars are used as stirrups.

Therefore,

Area of tension steel, A_{st} = 402.12 mm^2

Area of compression steel, A_{sc} = 157.07 mm^2

Area of shear reinforcement, A_{sv} = 100.53 mm^2

Breadth, b = 180 mm

Overall depth, D = 270 mm

Clear cover, d_c = 20 mm

Effective cover, d' = 33 mm

Effective depth, d = 234 mm

Span of the beam, L = 1800 mm

f_{ck} = 28.44 N/mm^2

Yield stress f_y = 566 N/mm^2 (8Ø rebar)

f_y = 505 N/mm^2 (10Ø rebar)

f_y = 507.35 N/mm^2 (16Ø rebar)

Analysis of Beam:

The equilibrium equation for a doubly reinforced RC beam is given by

$$C_{uc} + C_{us} = T_u \quad \text{(A)}$$

Where,

C_{uc} = Resultant compressive force in concrete

C_{us} = Resultant compressive force in the compressive steel

T_u = Resultant tensile force in tension steel

Let 'x' be the neutral axis depth of the beam

Now,

$$C_{uc} = 0.81 \times f_{ck} \times b \times x \text{ (Neglecting the safety factors)}$$

$$= 0.81 \times 28.44 \times 180 \times x$$

$$C_{uc} = 4146.55x \text{ N} \quad (1)$$

$$C_{us} = E_s \times \varepsilon_{s1} \times A_{sc}$$

(Where ε_{s1} is the strain in compression steel and E_s is the modulus of elasticity of steel)

$$= 2 \times 10^5 \times .0035 \times \frac{x-33}{x} \times 157.07$$

$$C_{us} = 109949 \times \frac{x-33}{x} \text{ N} \quad (2)$$

$$T_u = f_y \times A_{st}$$

$$T_u = 204015.58 \text{ N} \quad (3)$$

Substituting the values of (1), (2) and (3) in equation (A),

$$4146.55x + 109949\left(\frac{x-33}{x}\right) = 204015.58$$

Solving for x,

$$x = 43.02$$

Now, moment carrying capacity of the beam

$$M_u = C_{uc} \times (d - 0.42x) + C_{us}(d - d')$$

$$M_u = 43.67 \text{ kN.m}$$

Therefore, load producing moment, under two-point loading is W= 72.78 kN.

Total load carrying capacity of the beam $W_u = 2W = 145.56$ kN

Now,

Total load in the beam = $W_{DL} + W_{SIL}$

Where, W_{DL} is the deal load of the beam and W_{LL} is the super imposed load in the beam

$W_{DL} = 0.180 \times .270 \times 25 = 2.43$ kN

$W_{LL} = 145.56$ kN

Therefore, maximum Shear force $V_u = 73.99$ kN

Design of shear reinforcement

Here, percentage of steel in the tension side, $p_t = 0.95\%$

Using Table 19 of IS 456 2000, we obtain $\tau_c = 0.63\,\text{MPa}$

Again, $\tau_v = \dfrac{V_u}{bd}$ (CL -40.1, IS 456 2000)

$$\tau_v = \frac{73.99 \times 1000}{180 \times 234} = 1.75$$

Since $\tau_c \langle \tau_v$, hence shear reinforcement is required. (CL-40.4, IS 456 2000)

Now, shear to be resisted by the steel

$V_{us} = V_u - V_c = V_u - \tau_c bd$ (CL-40.4.c, IS 456 2000)

$V_{us} = 73.99 \times 1000 - 0.63 \times 180 \times 234 = 47.45\,\text{kN}$

Let, S_v be the spacing of stirrups and $f_y^{/} = \dfrac{f_y}{0.87} = 566/0.87$

$$V_{us} = \frac{0.87 f_y^{/} A_{sv} d}{S_v}$$ (CL-40.4.a, IS456 2000)

Putting the values in the above equation we get, $S_v = 280\,\text{mm}$

But maximum spacing should not be greater than 0.75d or 300 mm

Hence shear reinforcement of 2-legged 8 mm diameter stirrups are provided at a spacing of 100 mm center to center at a distance of 468 mm from both the end and rest of the part 1064 mm is provided with stirrups spacing of 150 mm and 170 mm center to center as shown in the Fig. B1.

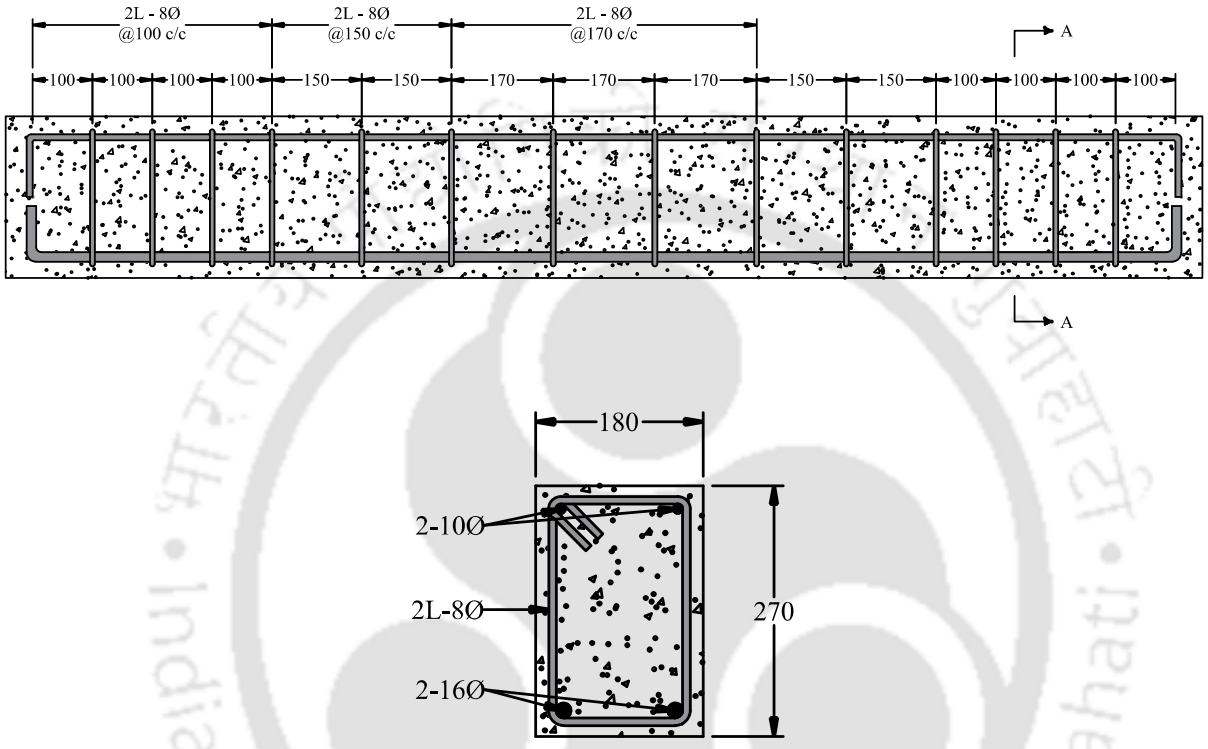

Figure B1: Reinforcement detailing of Beam specimen

References

Ahmad, S., Elahi, A., Barbhuiya, S. A., and Farid, Y. (2012). Use of polymer modified mortar in controlling cracks in reinforced concrete beams. Construction and building materials, 27(1), 91-96.

Ahmed A, A., Naganathan, S., Nasharuddin, K., and Fayyadh, M. M. (2015). Repair effectiveness of CFRP and steel plates in RC beams with web opening: effect of plate thickness. International Journal of Civil Engineering, 13(2), 234-244.

Ahmed, A., Fayyadh, M. M., Naganathan, S., and Nasharuddin, K. (2012). Reinforced concrete beams with web openings: A state of the art review. Materials and Design, 40, 90-102.

Alanazi, H., Yang, M., Zhang, D., and Gao, Z. J. (2016). Bond strength of PCC pavement repairs using metakaolin-based geopolymer mortar. Cement and Concrete Composites, 65, 75-82.

Alcocer, S. M., Flores, L., and Duran, R. (2006). Recent experimental evidence on the seismic performance of rehabilitation techniques in Mexico. In Advances in Earthquake Engineering for Urban Risk Reduction (pp. 261-274). Springer, Dordrecht.

Ali, S. R. M., and Saeed, J. A. (2022). Shear capacity and behavior of high-strength concrete beams with openings. Engineering Structures, 264, 114431.

Allam SM, “Strengthening of RC beams with large openings in the shear zone”. Alexandria Engineering Journal. 2005 Jan;44(1):59-78.

Al-Majidi, M. H., Lampropoulos, A., Cundy, A., and Meikle, S. (2016). Development of geopolymer mortar under ambient temperature for in situ applications. Construction and Building Materials, 120, 198-211.

Al-Osta, M. A., Isa, M. N., Baluch, M. H., and Rahman, M. K. (2017). Flexural behavior of reinforced concrete beams strengthened with ultra-high performance fiber reinforced concrete. Construction and Building Materials, 134, 279-296.

Altan, E., and Erdoğan, S. T. (2012). Alkali activation of a slag at ambient and elevated temperatures. Cement and Concrete Composites, 34(2), 131-139.

Altun, F. (2004). An experimental study of the jacketed reinforced-concrete beams under bending. Construction and Building Materials, 18(8), 611-618.

Andrews, G., and Sharma, A. K. (1988). Repaired reinforced concrete beams. Concrete International, 10(4), 47-51.

Assi, L. N., Carter, K., Deaver, E., and Ziehl, P. (2020). Review of availability of source materials for geopolymer/sustainable concrete. Journal of Cleaner Production, 263, 121477.

ASTM A 370-92 (2021). Standard test methods and definitions for mechanical testing of steel products. ASTM International, West Conshohocken, PA. www.astm.org

ASTM C109 / C109M-21 (2021). Standard Test Method for Compressive Strength of Hydraulic Cement Mortars, ASTM International, West Conshohocken, PA. www.astm.org

ASTM C1437-20 (2020). Standard Test Method for Flow of Hydraulic Cement Mortar, ASTM International, West Conshohocken, PA. www.astm.org

ASTM C230 / C230M-21 (2021). Standard Specification for Flow Table for Use in Tests of Hydraulic Cement, ASTM International, West Conshohocken, PA. www.astm.org

ASTM C311 / C311M-18 (2018). Standard Test Methods for Sampling and Testing Fly Ash or Natural Pozzolans for Use in Portland-Cement Concrete, ASTM International, West Conshohocken, PA. www.astm.org

ASTM C348-14 (2014). Standard Test Method for Flexural Strength of Hydraulic-Cement Mortars, ASTM International, West Conshohocken, PA. www.astm.org

ASTM C494 / C494M-19(2019). Standard Specification for Chemical Admixtures for Concrete, ASTM International, West Conshohocken, PA. www.astm.org

ASTM C618 - 17a (2013). Standard Specification for Coal Fly Ash and Raw or Calcined Natural Pozzolan for Use in Concrete, ASTM International, West Conshohocken, US. www.astm.org

ASTM C618-19 (2019). Standard Specification for Coal Fly Ash and Raw or Calcined Natural Pozzolan for Use in Concrete, ASTM International, West Conshohocken, PA. www.astm.org

ASTM C882/C882M – 13a (2005). Standard Test Method for Bond Strength of Epoxy-Resin Systems used with Concrete by Slant Shear, vol. 04.02, Annual Book of ASTM Standard, United States.

Aykac, B., Kalkan, I., Aykac, S., and Egriboz, Y. E. (2013). Flexural behavior of RC beams with regular square or circular web openings. Engineering Structures, 56, 2165-2174.

Babaee, M., and Castel, A. (2018). Chloride diffusivity, chloride threshold, and corrosion initiation in reinforced alkali-activated mortars: Role of calcium, alkali, and silicate content. Cement and Concrete Research, 111, 56-71.

Basunbul, I. A., Gubati, A. A., Al-Sulaimani, G. J., and Baluch, M. H. (1990). Repaired reinforced concrete beams. Materials Journal, 87(4), 348-354.

Bensted, J., Callaghan, I. C., and Lepre, A. (1991). Comparative study of the efficiency of various borate compounds as set-retarders of class G oilwell cement. Cement and concrete research, 21(4), 663-668.

Bernal, S. A., Provis, J. L., Walkley, B., San Nicolas, R., Gehman, J. D., Brice, D. G., and van Deventer, J. S. (2013). Gel nanostructure in alkali-activated binders based on slag and fly ash, and effects of accelerated carbonation. Cement and Concrete Research, 53, 127-144.

Bernal, S., De Gutierrez, R., Delvasto, S., and Rodriguez, E. (2010). Performance of an alkali-activated slag concrete reinforced with steel fibers. Construction and building Materials, 24(2), 208-214.

Bhutta, A., Borges, P. H., Zanotti, C., Farooq, M., and Banthia, N. (2017). Flexural behavior of geopolymer composites reinforced with steel and polypropylene macro fibers. Cement and Concrete Composites, 80, 31-40.

Castel, A., and Foster, S. J. (2015). Bond strength between blended slag and Class F fly ash geopolymer concrete with steel reinforcement. Cement and Concrete Research, 72, 48-53.

Chi, M., and Huang, R. (2013). Binding mechanism and properties of alkali-activated fly ash/slag mortars. Construction and building materials, 40, 291-298.

Chin, S. C., Shafiq, N., and Nuruddin, M. F. (2016). Behaviour of RC beams with CFRP-strengthened openings. Structural Concrete, 17(1), 32-43.

Chindaprasirt, P., De Silva, P., Sagoe-Crentsil, K., and Hanjitsuwan, S. (2012). Effect of SiO2 and Al2O3 on the setting and hardening of high calcium fly ash-based geopolymer systems. Journal of Materials Science, 47(12), 4876-4883.

Chithambaram, S. J., Kumar, S., and Prasad, M. M. (2019). Thermo-mechanical characteristics of geopolymer mortar. Construction and Building Materials, 213, 100-108.

Chu, S. H. (2019). Effect of paste volume on fresh and hardened properties of concrete. Construction and Building Materials, 218, 284-294.

Coo, M., and Pheeraphan, T. (2015). Effect of sand, fly ash, and coarse aggregate gradation on preplaced aggregate concrete studied through factorial design. Construction and Building Materials, 93, 812-821.

Criado, M., Palomo, A., Fernández-Jiménez, A., and Banfill, P. F. G. (2009). Alkali activated fly ash: effect of admixtures on paste rheology. Rheologica Acta, 48(4), 447-455.

Das, C. S., Dey, T., Dandapat, R., Mukharjee, B. B., and Kumar, J. (2018). Performance evaluation of polypropylene fibre reinforced recycled aggregate concrete. Construction and Building Materials, 189, 649-659.

Davidovits, J. (1982). "Mineral polymers and methods of making them." U.S. Patent No. 4,349,386.

Davidovits, J. (1991). Geopolymers: inorganic polymeric new materials. Journal of Thermal Analysis and calorimetry, 37(8), 1633-1656.

Davidovits, J. (1994, October). Properties of geopolymer cements. In First international conference on alkaline cements and concretes (Vol. 1, pp. 131-149). Kiev, Ukraine: Kiev State Technical University.

Deb, P. S., Nath, P., and Sarker, P. K. (2014). The effects of ground granulated blast-furnace slag blending with fly ash and activator content on the workability and strength properties of geopolymer concrete cured at ambient temperature. Materials and Design (1980-2015), 62, 32-39.

Diggikar, R., Mangalgi, S., and Harsoor, R. (2013, October). Behavior of RCC Beam with Rectangular opening Strengthened by CFRP and GFRP sheets. In International conference on recent innovations in civil engineering (pp. 25-27).

Douglas, E., Bilodeau, A., Brandstetr, J., and Malhotra, V. M. (1991). Alkali activated ground granulated blast-furnace slag concrete: preliminary investigation. Cement and concrete research, 21(1), 101-108.

Duxson, P., Fernández-Jiménez, A., Provis, J. L., Lukey, G. C., Palomo, A., and van Deventer, J. S. (2007). Geopolymer technology: the current state of the art. Journal of materials science, 42(9), 2917-2933.

Elansary, A. A., Aty, A. A. A., Abdalla, H. A., and Zawam, M. (2022, March). Shear behavior of reinforced concrete beams with web opening near supports. In Structures (Vol. 37, pp. 1033-1041). Elsevier.

Elchalakani, M., Dong, M., Karrech, A., Li, G., Mohamed Ali, M. S., Xie, T., and Yang, B. (2018). Development of fly ash-and slag-based geopolymer concrete with calcium carbonate or microsilica. Journal of Materials in Civil Engineering, 30(12), 04018325.

El-Maaddawy, T., and El-Ariss, B. (2012). Behavior of concrete beams with short shear span and web opening strengthened in shear with CFRP composites. Journal of Composites for Construction, 16(1), 47-59.

Elyamany, H. E., Abd Elmoaty, M., and Elshaboury, A. M. (2018). Setting time and 7-day strength of geopolymer mortar with various binders. Construction and Building Materials, 187, 974-983.

Fang, G., Ho, W. K., Tu, W., and Zhang, M. (2018). Workability and mechanical properties of alkali-activated fly ash-slag concrete cured at ambient temperature. Construction and Building Materials, 172, 476-487.

Farhan, N. A., Sheikh, M. N., and Hadi, M. N. (2018). Engineering properties of ambient cured alkali-activated fly ash–slag concrete reinforced with different types of steel fiber. Journal of Materials in Civil Engineering, 30(7), 04018142.

Fernández-Jiménez, A., and Palomo, A. (2005). Composition and microstructure of alkali activated fly ash binder: Effect of the activator. Cement and concrete research, 35(10), 1984-1992.

Fernández-Jiménez, A., García-Lodeiro, I., and Palomo, A. (2007). Durability of alkali-activated fly ash cementitious materials. Journal of Materials Science, 42(9), 3055-3065.

Ganesh, P., and Murthy, A. R. (2019). Repair, retrofitting and rehabilitation techniques for strengthening of reinforced concrete beams-A review. Adv. Concrete Constr, 8(2), 101-117.

Görhan, G., and Kürklü, G. (2014). The influence of the NaOH solution on the properties of the fly ash-based geopolymer mortar cured at different temperatures. Composites part b: engineering, 58, 371-377.

Guades, E. J., Stang, H., Schmidt, J. W., and Fischer, G. (2021). Flexural behavior of hybrid fibre-reinforced geopolymer composites (FRGC)-jacketed RC beams. Engineering Structures, 235, 112053.

Hardjito, D., Wallah, S. E., Sumajouw, D. M., and Rangan, B. V. (2004). On the development of fly ash-based geopolymer concrete. Materials Journal, 101(6), 467-472.

Hassan, A., Atta, A. M., and El-Shafiey, T. F. (2020, June). Restoration of the shear capacity for RC beams with web openings using precast SHCC plates. In Structures (Vol. 25, pp. 603-612). Elsevier.

Hassan, A., Shoeib, A. E. K., and Abd El-Magied, M. (2018). Use of carbon nanotubes in the retrofitting of reinforced concrete beams with an opening and the effect of direct fire on their behaviour. GEOMATE Journal, 14(44), 149-158.

He, J., Jie, Y., Zhang, J., Yu, Y., and Zhang, G. (2013). Synthesis and characterization of red mud and rice husk ash-based geopolymer composites. Cement and Concrete Composites, 37, 108-118.

Hossain, S. S., Mathur, L., and Roy, P. K. (2018). Rice husk/rice husk ash as an alternative source of silica in ceramics: A review. Journal of Asian Ceramic Societies, 6(4), 299-313.

Hu, S., Wang, H., Zhang, G., and Ding, Q. (2008). Bonding and abrasion resistance of geopolymeric repair material made with steel slag. Cement and concrete composites, 30(3), 239-244.

Humad, A. M., Kothari, A., Provis, J. L., and Cwirzen, A. (2019). The effect of blast furnace slag/fly ash ratio on setting, strength, and shrinkage of alkali-activated pastes and concretes. Frontiers in Materials, 6, 9.

Huseien, G. F., Mirza, J., Ismail, M., Ghoshal, S. K., and Hussein, A. A. (2017). Geopolymer mortars as sustainable repair material: A comprehensive review. Renewable and Sustainable Energy Reviews, 80, 54-74.

Huseien, G. F., Mirza, J., Ismail, M., Ghoshal, S. K., and Hussein, A. A. (2017). Geopolymer mortars as sustainable repair material: A comprehensive review. Renewable and Sustainable Energy Reviews, 80, 54-74.

IS 10262-2009 (2009). Concrete Mix Proportioning – Guidelines, Bureau of Indian Standard, New Delhi, India.

IS 10510-1983 (2004), Specification of Vee-Bee Consistometer, Bureau of Indian Standard, New Delhi, India.

IS 1608 2005 (2008). Metallic materials - tensile testing at ambient temperature, Bureau of Indian Standard, New Delhi, India.

IS 2386 (Part III)-1963 (2002). Methods of test for aggregates for concrete – Part 3: Specific gravity, density, voids, absorption and bulking, Bureau of Indian Standard, New Delhi, India

IS 383 1970 (2002). Specification for coarse and fine aggregates from natural sources for concrete, Bureau of Indian Standard, New Delhi, India.

IS 4031 (Part 11) – 1988 (2005). Methods of physical tests for hydraulic cement- Part 11: Determination of Density. Bureau of Indian Standard, New Delhi, India.

IS 4031 (Part 4) – 1988 (2005). Methods of physical tests for hydraulic cement- Part 4: Determination of consistency of standard cement paste. Bureau of Indian Standard, New Delhi, India.

IS 4031 (Part 5) – 1988 (2005). Methods of physical tests for hydraulic cement- Part 5: Determination of initial and final setting time. Bureau of Indian Standard, New Delhi, India.

IS 432 (Part I)-1982 (1992), Specification for mild steel and medium tensile steel bars and ard-drawn steel wire for concrete reinforcement – Part 1: mild steel and medium tensile steel bars, Bureau of Indian Standard, New Delhi, India.

IS 432 Part I 1982 (1992), Specification for mild steel and medium tensile steel bars and hard-drawn steel wire for concrete reinforcement – Part 1: mild steel and medium tensile steel bars, Bureau of Indian Standard, New Delhi, India

IS 456 - 2000 (2007). Plain and Reinforced concrete - Code of Practice. Bureau of Indian Standard, New Delhi, India.

IS 516 – 1959 (2006), Methods of Tests for Strength of Concrete, Bureau of Indian Standard, New Delhi, India, 2004.

IS 5816-1999 (2004), Splitting Tensile Strength of Concrete -Method of Test, Bureau of Indian Standard, New Delhi, India.

IS 8112-2013 (2013). Ordinary Portland cement 43 Grade- specification. Bureau of Indian Standard, New Delhi, India

IS: 1199 – 1959 (2004), Methods of Sampling and Analysis of Concrete, Bureau of Indian Standard, New Delhi, India.

IS: 1727-1967 (2004), Methods of Test for Pozzolanic Materials, Bureau of Indian Standard, New Delhi, India.

IS: 383-1970 (2002), Specification for Coarse and Fine Aggregates from Natural Sources for Concrete, Bureau of Indian Standard, New Delhi, India.

IS: 383-1970 (2002), Specification for Coarse and Fine Aggregates from Natural Sources for Concrete, Bureau of Indian Standard, New Delhi, India.

IS: 8112-1989 (2005), 43 Grade Ordinary Portland Cement – Specification, Bureau of Indian Standard, New Delhi, India.

IS:1727-1967 (2004), Methods of Test for Pozzolanic Materials, Bureau of Indian Standard, New Delhi, India.

IS:4031(Part 6) - 1988 (2006), Methods of physical tests for hydraulic cement, Indian Standard Code, New Delhi, India.

Islam, A., Alengaram, U. J., Jumaat, M. Z., and Bashar, I. I. (2014). The development of compressive strength of ground granulated blast furnace slag-palm oil fuel ash-fly ash based geopolymer mortar. Materials and Design (1980-2015), 56, 833-841.

Jabbar, S., Hejazi, F., and Mahmod, H. M. (2016). Effect of an opening on reinforced concrete hollow beam web under torsional, flexural, and cyclic loadings. Latin American Journal of Solids and Structures, 13, 1576-1595.

Jang, J. G., Lee, N. K., and Lee, H. K. (2014). Fresh and hardened properties of alkali-activated fly ash/slag pastes with superplasticizers. Construction and Building Materials, 50, 169-176.

Jauberthie, R., Rendell, F., Tamba, S., and Cisse, I. (2000). Origin of the pozzolanic effect of rice husks. Construction and Building Materials, 14(8), 419-423.

John, S. K., Nadir, Y., and Girija, K. (2021). Effect of source materials, additives on the mechanical properties and durability of fly ash and fly ash-slag geopolymer mortar: A review. Construction and Building Materials, 280, 122443.

Joseph, B., and Mathew, G. (2012). Influence of aggregate content on the behavior of fly ash based geopolymer concrete. Scientia Iranica, 19(5), 1188-1194.

Kong, D. L., and Sanjayan, J. G. (2010). Effect of elevated temperatures on geopolymer paste, mortar and concrete. Cement and concrete research, 40(2), 334-339.

Kumar, S., Das, C. S., Lao, J., Alrefaei, Y., and Dai, J. G. (2022). Effect of sand content on bond performance of engineered geopolymer composites (EGC) repair material. Construction and Building Materials, 328, 127080.

Laskar, S. M., and Talukdar, S. (2017). Preparation and tests for workability, compressive and bond strength of ultra-fine slag based geopolymer as concrete repairing agent. Construction and building materials, 154, 176-190.

Lee, N. K., Kim, E. M., and Lee, H. K. (2016). Mechanical properties and setting characteristics of geopolymer mortar using styrene-butadiene (SB) latex. Construction and Building Materials, 113, 264-272.

Lee, S. J., and Park, J. M. (2015, November). Shear strength and structural behaviours of HPRWO with web openings with circular steel tubes. In IOP Conference Series: Materials Science and Engineering (Vol. 103, No. 1, p. 012050). IOP Publishing.

Li, Z., You, H., Gao, Y., Wang, C., and Zhang, J. (2021). Effect of ultrafine red mud on the workability and microstructure of blast furnace slag-red mud based geopolymeric grouts. Powder Technology, 392, 610-618.

Liu, Y., Zhang, Z., Shi, C., Zhu, D., Li, N., and Deng, Y. (2020). Development of ultra-high performance geopolymer concrete (UHPGC): Influence of steel fiber on mechanical properties. Cement and Concrete Composites, 112, 103670.

Madhav, T. V., Reddy, I. R., Ghorpade, V. G., and Jyothirmai, S. (2018). Compressivestrength study of geopolymer mortar using quarry rock dust. Materials Letters, 231, 105-108.

Mallikarjuna Rao, G., and Gunneswara Rao, T. D. (2015). Final setting time and compressive strength of fly ash and GGBS-based geopolymer paste and mortar. Arabian Journal for Science and Engineering, 40(11), 3067-3074.

Manjunatha, G. S., Radhakrishna, Venugopal, K., and Maruthi, S. V. (2014). Strength characteristics of open air cured geopolymer concrete. Transactions of the indian ceramic society, 73(2), 149-156.

Mansur, M. A. (1998). Effect of openings on the behaviour and strength of R/C beams in shear. Cement and concrete composites, 20(6), 477-486.

Mansur, M. A., and Tan, K. H. (1999). Concrete beams with openings: analysis and design (Vol. 20). CRC Press.

Mansur, M. A., Tan, K. H., and Lee, S. L. (1984). Collapse loads of R/C beams with large openings. Journal of Structural Engineering, 110(11), 2602-2618.

Martinola, G., Meda, A., Plizzari, G. A., and Rinaldi, Z. (2010). Strengthening and repair of RC beams with fiber reinforced concrete. Cement and concrete composites, 32(9), 731-739.

Mehta, P. K. (2002). Greening of the concrete industry for sustainable development. Concrete international, 24(7), 23-28.

Ministry of coal, Government of India, https://coal.gov.in/en/major-statistics/production-and-supplies (accessed on 1st July 2022)

Mohammed, T. U., and Rahman, M. N. (2016). Effect of types of aggregate and sand-to-aggregate volume ratio on UPV in concrete. Construction and Building Materials, 125, 832-841.

Mohd, M. A. B., and I, K. N. (2011). Review on fly ash-based geopolymer concrete without Portland Cement. Journal of engineering and technology research, 3(1), 1-4.

Montgomery, D. C., and Runger, G. C. (1994). Applied statistics and probability for engineers.

Mora-Ruacho, J., Gettu, R., and Aguado, A. (2009). Influence of shrinkage-reducing admixtures on the reduction of plastic shrinkage cracking in concrete. Cement and Concrete Research, 39(3), 141-146.

Musaddiq Laskar, S., and Talukdar, S. (2017). Development of ultrafine slag-based geopolymer mortar for use as repairing mortar. Journal of Materials in Civil Engineering, 29(5), 04016292.

Nadoushan, M. J., and Ramezanianpour, A. A. (2016). The effect of type and concentration of activators on flowability and compressive strength of natural pozzolan and slag-based geopolymers. Construction and Building Materials, 111, 337-347.

Nanni, A. (2012). A new tool for concrete and masonry repair. Concr Int, 34(4), 1-7.

Nasser, K. W., Acavalos, A., and Daniel, H. R. (1967, January). Behavior and design of large openings in reinforced concrete beams. In Journal Proceedings (Vol. 64, No. 1, pp. 25-33).

Nath, P., and Sarker, P. K. (2014). Effect of GGBFS on setting, workability and early strength properties of fly ash geopolymer concrete cured in ambient condition. Construction and Building materials, 66, 163-171.

Nematollahi, B., and Sanjayan, J. (2014). Effect of different superplasticizers and activator combinations on workability and strength of fly ash based geopolymer. Materials and Design, 57, 667-672.

Neville, A. M. (1995). Properties of concrete (vol. 4): Longman london.

Nicholson, C. L., Murray, B. J., Fletcher, R. A., Brew, D. R. M., Mackenzie, K. J., and Schmücker, M. (2005, September). Novel geopolymer materials containing borate structural units. In World Congress Geopolymer (pp. 31-33).

Nicholson, C. L., Murray, B. J., Fletcher, R. A., Brew, D. R. M., Mackenzie, K. J., and Schmücker, M. (2005, September). Novel geopolymer materials containing borate structural units. In World Congress Geopolymer (pp. 31-33).

Nie, X. F., Zhang, S. S., Teng, J. G., and Chen, G. M. (2018). Experimental study on RC T-section beams with an FRP-strengthened web opening. Composite Structures, 185, 273-285.

Obaidat, Y. T., Heyden, S., Dahlblom, O., Abu-Farsakh, G., and Abdel-Jawad, Y. (2011). Retrofitting of reinforced concrete beams using composite laminates. Construction and Building Materials, 25(2), 591-597.

Oderji, S. Y., Chen, B., Shakya, C., Ahmad, M. R., and Shah, S. F. A. (2019). Influence of superplasticizers and retarders on the workability and strength of one-part alkali-activated fly ash/slag binders cured at room temperature. Construction and Building Materials, 229, 116891.

Oh, J. E., Monteiro, P. J., Jun, S. S., Choi, S., and Clark, S. M. (2010). The evolution of strength and crystalline phases for alkali-activated ground blast furnace slag and fly ash-based geopolymers. Cement and Concrete Research, 40(2), 189-196.

Ong, K. C. G., Paramasivam, P., and Lim, C. T. E. (1992). Flexural strengthening of reinforced concrete beams using ferrocement laminates. Journal of Ferrocement, 22, 331-331.

Özkılıç, Y. O., Aksoylu, C., Gemi, L., and Arslan, M. H. (2022, July). Behavior of CFRP-strengthened RC beams with circular web openings in shear zones: Numerical study. In Structures (Vol. 41, pp. 1369-1389). Elsevier.

Palomo, Á., Kavalerova, E., Fernández-Jiménez, A., Krivenko, P., García-Lodeiro, I., and Maltseva, O. (2015). A review on alkaline activation: new analytical perspectives.

Paramasivam, P., Lim, C. T. E., and Ong, K. C. G. (1998). Strengthening of RC beams with ferrocement laminates. Cement and Concrete Composites, 20(1), 53-65.

Part, W. K., Ramli, M., and Cheah, C. B. (2015). An overview on the influence of various factors on the properties of geopolymer concrete derived from industrial by-products. Construction and Building Materials, 77, 370-395.

Phoo-ngernkham, T., Maegawa, A., Mishima, N., Hatanaka, S., and Chindaprasirt, P. (2015). Effects of sodium hydroxide and sodium silicate solutions on compressive and shear bond strengths of FA–GBFS geopolymer. Construction and Building Materials, 91, 1-8.

Pimanmas, A. (2010). Strengthening R/C beams with opening by externally installed FRP rods: Behavior and analysis. Composite Structures, 92(8), 1957-1976.

Puligilla, S. (2011). Understanding the role of slag on geopolymer hardening and microstructural development.

Qian, J., and Song, M. (2015). Study on influence of limestone powder on the fresh and hardened properties of early age metakaolin based geopolymer. In Calcined clays for sustainable concrete (pp. 253-259). Springer, Dordrecht.

Racherla, U. S. (2002). U.S. Patent No. 6,440,908. Washington, DC: U.S. Patent and Trademark Office.

Rakhshanimehr, M., Esfahani, M. R., Kianoush, M. R., Mohammadzadeh, B. A., and Mousavi, S. R. (2014). Flexural ductility of reinforced concrete beams with lap-spliced bars. Canadian Journal of Civil Engineering, 41(7), 594-604.

Ranjbar, N., and Zhang, M. (2020). Fiber-reinforced geopolymer composites: A review. Cement and Concrete Composites, 107, 103498.

Rao, T. G., and Seshu, D. R. (2003). Torsion of steel fiber reinforced concrete members. Cement and concrete research, 33(11), 1783-1788.

Rashad, A. M. (2013). Metakaolin as cementitious material: History, scours, production and composition–A comprehensive overview. Construction and building materials, 41, 303-318.

Rashad, A. M. (2020). Effect of steel fibers on geopolymer properties–the best synopsis for civil engineer. Construction and Building Materials, 246, 118534.

Rattanasak, U., Pankhet, K., and Chindaprasirt, P. (2011). Effect of chemical admixtures on properties of high-calcium fly ash geopolymer. International Journal of Minerals, Metallurgy, and Materials, 18(3), 364-369.

Reddy, M. S., Dinakar, P., and Rao, B. H. (2018). Mix design development of fly ash and ground granulated blast furnace slag based geopolymer concrete. Journal of Building Engineering, 20, 712-722.

Ren, J., Zhang, L., and San Nicolas, R. (2020). Degradation process of alkali-activated slag/fly ash and Portland cement-based pastes exposed to phosphoric acid. Construction and Building Materials, 232, 117209.

Richard, P., and Cheyrezy, M. (1995). Composition of reactive powder concretes. Cement and concrete research, 25(7), 1501-1511.

Romualdi, J. P. (1987). Ferrocement for infrastructure rehabilitation. Concrete International, 9(9), 24-28.

Ruan, Y., Jamil, T., Hu, C., Gautam, B. P., and Yu, J. (2022). Microstructure and mechanical properties of sustainable cementitious materials with ultra-high substitution level of calcined clay and limestone powder. Construction and Building Materials, 314, 125416.

Ruano, G., Isla, F., Pedraza, R. I., Sfer, D., and Luccioni, B. (2014). Shear retrofitting of reinforced concrete beams with steel fiber reinforced concrete. Construction and Building Materials, 54, 646-658.

Ryu, G. S., Lee, Y. B., Koh, K. T., and Chung, Y. S. (2013). The mechanical properties of fly ash-based geopolymer concrete with alkaline activators. Construction and building materials, 47, 409-418.

Sagoe-Crentsil, K. K., Brown, T., and Taylor, A. H. (2001). Performance of concrete made with commercially produced coarse recycled concrete aggregate. Cement and concrete research, 31(5), 707-712.

Saha, S., and Rajasekaran, C. (2017). Enhancement of the properties of fly ash based geopolymer paste by incorporating ground granulated blast furnace slag. Construction and Building Materials, 146, 615-620.

Said, A., Elsayed, M., Abd El-Azim, A., Althoey, F., and Tayeh, B. A. (2022). Using ultra-high performance fiber reinforced concrete in improvement shear strength of reinforced concrete beams. Case Studies in Construction Materials, 16, e01009.

Salama, A. E., Kassem, M. E., and Mahmoud, A. A. (2018). Torsional behavior of T-shaped reinforced concrete beams with large web openings. Journal of Building Engineering, 18, 84-94.

Sarker, P. K. (2011). Bond strength of reinforcing steel embedded in fly ash-based geopolymer concrete. Materials and structures, 44(5), 1021-1030.

Sasaki, K., Kurumisawa, K., and Ibayashi, K. (2019). Effect of retarders on flow and strength development of alkali-activated fly ash/blast furnace slag composite. Construction and building materials, 216, 337-346.

Sengul, O., and Tasdemir, M. A. (2009). Compressive strength and rapid chloride permeability of concretes with ground fly ash and slag. Journal of materials in civil engineering, 21(9), 494-501.

Shaikh, F. U. A. (2013). Deflection hardening behaviour of short fibre reinforced fly ash based geopolymer composites. Materials and Design, 50, 674-682.

Sheikh, T. R., Khan, M. K., and Izhar, T. (2017). A review on Strengthening of RCC square columns with Reinforced Concrete Jacketing. International Research Journal of Engineering and Tecnology, 4(03), 1797-1799.

Singh, B., Ishwarya, G., Gupta, M., and Bhattacharyya, S. K. (2015). Geopolymer concrete: A review of some recent developments. Construction and building materials, 85, 78-90.

Soman, M., and Mohan, J. (2018). Rehabilitation of RC columns using ferrocement jacketing. Construction and Building materials, 181, 156-162.

Somes, N. F., and Corley, W. G. (1974). Circular openings in webs of continuous beams. Special Publication, 42, 359-398.

Somna, K., Jaturapitakkul, C., Kajitvichyanukul, P., and Chindaprasirt, P. (2011). NaOH-activated ground fly ash geopolymer cured at ambient temperature. Fuel, 90(6), 2118-2124.

Song, P. S., and Hwang, S. (2004). Mechanical properties of high-strength steel fiber-reinforced concrete. Construction and Building Materials, 18(9), 669-673.

Statista, the statistics portal, https://www.statista.com/statistics/267364/worldcement production-by-country/, 2018 (accessed on 1st July, 2022)

Statista, the statistics portal, https://www.statista.com/statistics/269322/cementconsumption in-india-since-2004/ , 2018 (accessed on 1st July, 2022).

Statista, the statistics portal, https://www.statista.com/statistics/667485/india-iron-ore-production-volume/, 2021 (assessed on 1st July,2022)

Suresh, D., and Nagaraju, K. (2015). Ground granulated blast slag (GGBS) in concrete–a review. IOSR journal of mechanical and civil engineering, 12(4), 76-82.

Suresh, J., and Prabhavathy, R. A. (2014). Behaviour of steel fibre reinforced concrete beams with duct openings strengthened by steel plates. International Journal of Advanced Information Science and Technology (IJAIST), 28(28).

Swamy, G. J., Sangamithra, A., and Chandrasekar, V. (2014). Response surface modeling and process optimization of aqueous extraction of natural pigments from Beta vulgaris using Box–Behnken design of experiments. Dyes and Pigments, 111, 64-74.

Tan, J., Dan, H., and Ma, Z. (2022). Metakaolin based geopolymer mortar as concrete repairs: Bond strength and degradation when subjected to aggressive environments. Ceramics International.

Tena-Colunga, A., Hernandez-Marquez, O., and Archundia-Aranda, H. I. (2020). Strengthening of reinforced concrete prismatic and haunched beams using light jacketing. Journal of Building Engineering, 32, 101757.

Teng, S., Lim, T. Y. D., and Divsholi, B. S. (2013). Durability and mechanical properties of high strength concrete incorporating ultra-fine ground granulated blast-furnace slag. Construction and Building Materials, 40, 875-881.

Thunuguntla, C. S., and Rao, T. G. (2018). Effect of mix design parameters on mechanical and durability properties of alkali activated slag concrete. Construction and Building Materials, 193, 173-188.

Ueng, T. H., Lyu, S. J., Chu, H. W., Lee, H. H., and Wang, T. T. (2012). Adhesion at interface of geopolymer and cement mortar under compression: An experimental study. Construction and Building Materials, 35, 204-210.

Verma, M., and Dev, N. (2021). Sodium hydroxide effect on the mechanical properties of flyash-slag based geopolymer concrete. Structural Concrete, 22, E368-E379.

Wang, J., Han, L., Liu, Z., and Wang, D. (2020). Setting controlling of lithium slag-based geopolymer by activator and sodium tetraborate as a retarder and its effects on mortar properties. Cement and Concrete Composites, 110, 103598.

Wang, J., Han, L., Liu, Z., and Wang, D. (2020). Setting controlling of lithium slag-based geopolymer by activator and sodium tetraborate as a retarder and its effects on mortar properties. Cement and Concrete Composites, 110, 103598.

Wang, W. C., Wang, H. Y., and Lo, M. H. (2015). The fresh and engineering properties of alkali activated slag as a function of fly ash replacement and alkali concentration. Construction and Building Materials, 84, 224-229.

Wang, Y. S., Peng, K. D., Alrefaei, Y., and Dai, J. G. (2021). The bond between geopolymer repair mortars and OPC concrete substrate: Strength and microscopic interactions. Cement and Concrete Composites, 119, 103991.

Yang, K. H., Eun, H. C., and Chung, H. S. (2006). The influence of web openings on the structural behavior of reinforced high-strength concrete deep beams. Engineering Structures, 28(13), 1825-1834.

Yang, T., Zhu, H., Zhang, Z., Gao, X., Zhang, C., and Wu, Q. (2018). Effect of fly ash microsphere on the rheology and microstructure of alkali-activated fly ash/slag pastes. Cement and Concrete Research, 109, 198-207.

Yazıcı, Ş., İnan, G., and Tabak, V. (2007). Effect of aspect ratio and volume fraction of steel fiber on the mechanical properties of SFRC. Construction and Building Materials, 21(6), 1250-1253.

Yip, C. K. B. (2004). The role of calcium in geopolymerisation (Doctoral dissertation, University of Melbourne).

Yousuf, A., Manzoor, S. O., Youssouf, M., Malik, Z. A., and Khawaja, K. S. (2020). Fly ash: production and utilization in India-an overview. J Mater Environ Sci, 11(6), 911-921.

Yu, R., Spiesz, P., and Brouwers, H. J. H. (2014). Mix design and properties assessment of ultra-high performance fibre reinforced concrete (UHPFRC). Cement and concrete research, 56, 29-39.

Zanotti, C., Borges, P. H., Bhutta, A., and Banthia, N. (2017). Bond strength between concrete substrate and metakaolin geopolymer repair mortar: Effect of curing regime and PVA fiber reinforcement. Cement and Concrete Composites, 80, 307-316.

Zhang, L., Ji, Y., Li, J., Gao, F., and Huang, G. (2019). Effect of retarders on the early hydration and mechanical properties of reactivated cementitious material. Construction and Building Materials, 212, 192-201.

Zhang, Y. S., Sun, W., and Li, J. Z. (2005). Hydration process of interfacial transition in potassium polysialate (K-PSDS) geopolymer concrete. Magazine of Concrete Research, 57(1), 33-38.

Zhao, J., Tong, L., Li, B., Chen, T., Wang, C., Yang, G., and Zheng, Y. (2021). Eco-friendly geopolymer materials: A review of performance improvement, potential application and sustainability assessment. Journal of Cleaner Production, 307, 127085.

List of Publications

International Journals

1. Sinha, A. K., and Talukdar, S. (2021). Enhancement of the properties of silicate activated ultrafine-slag based geopolymer mortar using retarder. Construction and Building Materials, 313, 125380. https://doi.org/10.1016/j.conbuildmat.2021.125380
2. Sinha, A. K., and Talukdar, S. (2022). Mechanical and Bond behaviour of high volume Ultrafine-slag blended Fly Ash based alkali activated concrete (Manuscript no. CONBUILDMAT-D-22-05845, Under review in Construction and Building Materials, Elsevier).
3. Arnab Kumar Sinha and Sudip Talukdar (2022). “Repairing of web opened RC beam with ferrocement laminates using Geopolymer mortar.” (Manuscript no. 7ff1f232-e400-40f8-947d-56de4ab40973, Journal of Building Pathology and Rehabilitation , Springer, Revision sent).
4. Arnab Kumar Sinha and Sudip Talukdar (2023). “Rehabilitation of Web opened RC beam with alkali activated fiber reinforced U-Jacket .” (Manuscript no. CFENG-4487, Under review in Journal of Performance of Constructed Facilities, ASCE)

International Conferences

1. Sinha, A. K., and Talukdar, S. (2021). "Retrofitting and Strengthening techniques applied on damage RCC prism using geopolymer ", Proceedings of the International Conference in Futuristic Technologies, January 22-24, 2021, Paper ID: FT21010, p-G271.